



VNIVERSITAT
DE VALÈNCIA

THE HIGGS ERA

Tesis Doctoral

Victor Ilisie

IFIC - Universidad de Valencia - CSIC
Departamento de Física Teórica

Director: Antonio Pich Zardoya

Valencia, 2016

*A mi familia, especialmente a Carmen y
Alicia*

ANTONIO PICH ZARDOYA,
catedrático de la Universidad de Valencia,

CERTIFICA:

Que la presente memoria "The Higgs Era" ha sido realizada bajo su dirección en el Instituto de Física Corpuscular, centro mixto de la Universidad de Valencia y del CSIC, por Victor Ilisie y constituye su Tesis para optar al grado de Doctor en Física.

Y para que así conste, en cumplimiento de la legislación vigente, presenta en el Departamento de Física Teórica de la Universidad de Valencia la referida Tesis Doctoral, y firma el presente certificado.

Valencia, a 08 de marzo de 2016.

Antonio Pich Zardoya

CONTENTS

Resumen de la Tesis	1
Introduction	5
1 The Standard Model	7
1.1 Local Gauge Invariance	8
1.2 Electroweak Sector	9
1.2.1 Higgs Mechanism	12
1.2.2 CP Violation in the SM	14
1.3 Strong Sector	16
1.3.1 SU(3) Algebra	17
2 The Two-Higgs-Doublet Model	21
2.1 The Aligned Two-Higgs-Doublet Model	21
2.1.1 Yukawa Alignment	23
2.1.2 Bosonic Couplings	25
2.2 Scalar Potential	26
2.2.1 Neutral scalar mass matrix to lowest order in CP violation	30
2.3 Scalar Couplings to the Gauge Bosons	32
2.3.1 Inert 2HDM	34
3 Motivation and Preliminaries	37
3.1 Paper I	37
3.2 Paper II	38
3.3 Paper III	39
3.4 Paper IV	40
3.5 Paper V	41
3.6 Updated fits from Run 1	43
4 QCD exotics versus a Standard Model Higgs	49
4.1 Exotic coloured fermions	50
4.2 Higgs production at LHC	54

4.3	Higgs search	56
4.4	Discussion	60
4.A	Anomaly cancellation	61
5	LHC constraints on two-Higgs-doublet models	69
5.1	Introduction	70
5.2	The Aligned Two-Higgs-Doublet Model	72
5.2.1	Yukawa Alignment	73
5.2.2	Bosonic Couplings	75
5.3	Higgs Signal Strengths	76
5.4	Phenomenological Analysis	79
5.4.1	The A2HDM in the CP-conserving limit	80
5.4.2	The CP-violating A2HDM	93
5.5	Summary	101
5.A	Scalar Potential	104
5.A.1	Neutral scalar mass matrix to lowest order in CP violation	106
5.B	Scalar Couplings to the Gauge Bosons	108
5.C	Statistical treatment and data	110
5.D	Perturbativity Constraints	111
5.E	Oblique Parameters	112
6	Towards a general analysis of LHC data within two-Higgs doublet models	125
6.1	Introduction	126
6.2	A2HDM fit in the CP-conserving limit	127
6.2.1	Implications of LHC and Tevatron data for the h(126) boson	129
6.2.2	SM-like gauge coupling, $\kappa_{\mathbf{V}}^{\mathbf{h}} \sim \mathbf{1}$, without decoupling	133
6.3	Searches for additional Higgs bosons	137
6.3.1	Charged Higgs searches	139
6.3.2	Neutral Higgs searches	143
6.4	The fermiophobic charged Higgs scenario	145
6.5	Comparison with other works	148
6.6	Summary	150
6.A	Useful formulae for a light charged Higgs	151
6.B	Statistical treatment and experimental data	153

7	Low-mass fermiophobic charged Higgs phenomenology in two-Higgs-doublet models	163
7.1	Introduction	164
7.2	The Aligned Two-Higgs-Doublet Model	165
7.3	Decay and Production modes	168
7.3.1	$\mathbf{H}^+ \rightarrow \mathbf{W}^+\gamma$	169
7.3.2	$\mathbf{H}^+ \rightarrow \mathbf{W}^+\varphi_i^0$	171
7.3.3	Charged-Higgs Production	173
7.4	Phenomenology	175
7.4.1	Decay rates and branching ratios	176
7.4.2	Production cross sections	184
7.5	Conclusions	189
7.A	Scalar Potential	190
7.A.1	Inert 2HDM	193
7.B	Heavy neutral Higgs decay rates	194
7.C	QCD corrections to $\mathbf{pp} \rightarrow \mathbf{H}^+\varphi_i^0$	196
7.D	QCD corrections to $\mathbf{pp} \rightarrow \mathbf{H}^+\mathbf{W}^-$	197
8	New Barr-Zee contributions to $(g-2)_\mu$ in two-Higgs-doublet models	209
8.1	Introduction	210
8.2	The Aligned Two-Higgs-Doublet Model	211
8.3	One-loop contribution	212
8.4	Two-loop contribution	214
8.4.1	Gauge invariant effective vertices	216
8.4.2	Contributions to Δa_μ	219
8.5	Phenomenology	221
8.5.1	Individual $\Delta \mathbf{a}_\mu^{(i)}$ contributions	222
8.5.2	Total contribution to $(\mathbf{g}-\mathbf{2})_\mu$	227
8.6	Conclusions	228
8.A	$WW\gamma$ effective vertex contribution to $(g-2)_\mu$	229
9	Updated fits from Run 1	245
	Conclusions	251
	Acknowledgements	255

RESUMEN DE LA TESIS

El descubrimiento de un bosón escalar con masa alrededor de 125 GeV abre ante nosotros la puerta a una nueva era. La última pieza del Modelo Estándar parece haber sido descubierta, pero esa no tiene por que ser la última palabra. El Modelo Estándar parece funcionar perfectamente, pero todavía hay mucho espacio (y necesidad) para nueva física. En este trabajo estudiamos dos tipos de extensiones del Modelo Estándar, las dos relacionadas con el sector escalar. Los primeros capítulos están dedicados a la introducción, una breve presentación del Modelo Estándar, una introducción al Modelo Alineado con dos Dobletes de Higgs y finalmente una breve motivación de este trabajo.

Sabemos que la Cromodinámica Cuántica se basa en el grupo de simetría $SU(3)_C$ de color. Los fermiones de la teoría pertenecen a la representación fundamental (de dimensión 3). En la primera parte de la tesis (Capítulo 4) estudiamos la posible existencia de fermiones pertenecientes a representaciones de orden superior. No hay ninguna simetría fundamental de la Naturaleza que prohíba la existencia de tales objetos, por tanto la existencia de estos fermiones es plausible. En este capítulo analizamos pues, el impacto que dichos quarks exóticos puedan tener sobre el *running* de la constante de acoplamiento fuerte α_s y las posibles implicaciones experimentales sobre la sección eficaz de producción del bosón de Higgs (suponiendo que estos fermiones obtienen masa mediante el mecanismo de Higgs).

La segunda parte está dedicada al estudio exhaustivo del Modelo Alineado de los dos Dobletes de Higgs teniendo en cuenta los datos experimentales de las colaboraciones del LHC, los análisis previos en el sector de sabor, física de precisión, el momento anómalo del muón, etc. En los dos primeros capítulos dedicados a este tema (Capítulos 5 y 6), estudiaremos las implicaciones de los datos de los dos experimentos del LHC y los resultados previos de sabor, sobre el espacio de parámetros del modelo. También estudiaremos las búsquedas experimentales de bosones adicionales de Higgs, especialmente un Higgs cargado decayendo a dos fermiones y a dos fermiones y un bosón W .

En el Capítulo 7 estudiamos la fenomenología de un Higgs cargado fermiofóbico (no se acopla a fermiones a nivel árbol). En este caso particular todas las restricciones experimentales obtenidas en el trabajo anterior son evadidas de forma

trivial. Analizaremos, por tanto, las nuevas vías de producción y también las formas de desintegración de dicha partícula. Incluiremos también las correcciones de QCD para la sección eficaz de producción y tendremos en cuenta todas las restricciones experimentales aplicables. Los resultados obtenidos deberían servir de motivación para que las colaboraciones experimentales inicien la búsqueda de este tipo de partículas.

En el penúltimo capítulo analizaremos el momento anómalo del muón a dos loops en teoría de perturbaciones. Veremos que los diagramas de tipo Barr-Zee analizados hasta ahora no son los únicos que pueden añadir contribuciones significativas y que, para una comprensión mas completa, es necesario un análisis de diagramas adicionales. Estos nuevos diagramas adquieren especial relevancia dentro de modelo alineado y pueden reducir e incluso llegar a explicar la discrepancia entre el valor medido experimentalmente y la predicción teórica del momento anómalo del muón.

Finalmente en el último capítulo actualizamos partes relevantes de los estudios realizados en los Capítulos 5 y 6 utilizando los últimos datos experimentales del LHC.

This thesis is based on the following publications:

1. V. Ilisie and A. Pich, *QCD exotics versus a Standard Model Higgs*, Phys. Rev. D **86**, 033001 (2012), arXiv:1202.3420.
2. A. Celis, V. Ilisie and A. Pich, *LHC constraints on two-Higgs doublet models*, JHEP **1307** (2013) 053, arXiv:1302.4022.
3. A. Celis, V. Ilisie and A. Pich, *Towards a general analysis of LHC data within two-Higgs-doublet models*, JHEP **1312** (2013) 095, arXiv:1310.7941.
4. V. Ilisie and A. Pich, *Low-mass fermiophobic charged Higgs phenomenology in two-Higgs-doublet models*, JHEP **1409** (2014) 089, arXiv:1405.6639.
5. V. Ilisie, *New Barr-Zee contributions to $(g - 2)_\mu$ in two-Higgs-doublet models*, JHEP **1504** (2015) 077, arXiv:1502.04199.

During my period as a PhD student I have also authored a book and two proceedings, namely:

B. V. Ilisie, *Concepts in Quantum Field Theory. A practitioner's toolkit*, ISBN: 978-3-319-22965-2 (Hardcover), 978-3-319-22966-9 (eBook), Springer International Publishing, <http://www.springer.com/us/book/9783319229652>.

P1. V. Ilisie, *Constraining the two-Higgs doublet models with the LHC data*, PoS EPS **-HEP2013** (2013) 286, arXiv:1310.0931.

P2. V. Ilisie, *Bounds on neutral and charged Higgs from the LHC*, doi:10.1016/j.nuclphysbps.2015.09.103, arXiv:1410.5164.

INTRODUCTION

Philosophiae Naturalis Principia Mathematica can be regarded as the first stone of the basis of modern physics. It constitutes the first (known) formal, mathematical, formulation of *physical laws*. Since then, all branches of physics (and science in general) have been growing and separating into numerous, specialized, sub-branches. All this at an exponential rate. Nowadays, physics, is formed by a huge number of disciplines, trying to describe our surrounding Universe from the microscopic to the macroscopic scale.

The realm of Quantum Field Theory (QFT) and particle physics was born from the successful marriage between Quantum Mechanics and Special Relativity in the second half of the last century, and it took almost half a century to mature. Quantum Filed Theory was only the first step, the theoretical framework; we still had to find out the symmetries of the Universe, symmetries that our QFT had to obey. Again, the perfect symbiosis, this time between theory and experiment, have led us to what we now call the Standad Model (SM) of particle physics.

It describes three of the fundamental interactions in Nature, the electromagnetic and the weak (the electroweak) and the strong force. It does not integrate gravity and its many aspects such as Dark Energy (DE) and Dark Matter (DM). However, many efforts have been and are currently being made in this direction, namely, trying to incorporate DM within particle physics. On the other hand, even if there are many well motivated theoretical models, DE and the *correct* quantum theory of gravity are still open issues.

Far from the energy scale, where quantum gravity effects are supposed to come into the game, we can nicely incorporate gravity to particle physics and work within the Quantum Field Theory in Curved Space-time framework. This framework predicts new interesting phenomena, such as particle production due to the expansion of the Universe, the black-hole (Hawking) radiation, anisotropies in the remnant background radiation, etc. However, all these phenomena, for now, lay just on the frontier of the current experimental precision.

Understanding QFT and its many aspects was not an easy task, as we already mentioned. Renormalization and renormalizability required a deep change of paradigm. One had to realize that in QFT, coupling constants were not constants

any more, and that all the parameters were energy-dependent. The proof of the renormalizability of the SM was itself a Nobel prize awarding task.

So, what next? The SM has been proven to be extremely successful and passed many experimental and precision tests, with the exception of a few *tensions* here and there, between theoretical predictions and experiment. In spite of this, it is firmly believed, that the SM does not have the final word. Gauge invariance has proven to be an excellent tool for building renormalizable models, and works perfectly in the SM. It does not, however, forbid us to extend the SM. A *more* fundamental principle, would be needed.

It seems that one has to incorporate more sources of CP violation (than the SM predicts) in order to explain the matter-antimatter asymmetry in the Universe. The last piece of the puzzle, needed to explain the presence of mass in the Universe, seems to have been found. It leaves, nevertheless, many open questions. Maybe the one that hurts the most, is the fine-tuning and the hierarchy problem. This is not a problem of the SM itself, but of its extensions. By trying to incorporate new heavy states (at higher energy scales) into the SM Lagrangian, quantum corrections would terribly modify the Higgs mass, and, in order to explain the observed resonance at 125 GeV, tremendous cancellations would have to occur among the different contributions to the mass loop corrections. Another closely related question is the quark-mass hierarchy problem. There is not even a hint in the SM of why the masses of the various fermions are so different (in many orders of magnitude).

From a theoretical point of view, one would also expect to be able to unify the electroweak force with the strong force and, if possible incorporate gravity, DM, etc. Again, nobody knows how the SM could be extended in order to accomplish this. These are just a few of the many open problems left by the SM.

We can thus conclude that the study of SM extensions is a very well motivated task, and deserves much attention from a theoretical point of view. Here we will study two types of such extensions, both of them related to the Higgs sector. More details along with the theoretical framework of the SM are presented in the next chapter.

1. THE STANDARD MODEL

Since the discovery of the β decay of neutrons, many efforts have been made to understand the nature of the weak interaction. The development of a formal consistent theory of this interaction had to pass through many stages and tests. The first model capable of describing successfully the experimental data at low energies was the effective interaction proposed by Fermi in 1934:

$$\mathcal{L}_{eff}(x) = -\frac{G_F}{\sqrt{2}} J_\mu^\dagger(x) J^\mu(x). \quad (1.1)$$

This is a current-current interaction with J^μ given by

$$J^\mu(x) = \sum_l \bar{\nu}_l(x) \gamma^\mu (1 - \gamma_5) l(x) + \bar{p}(x) \gamma^\mu (1 - \gamma_5) n(x). \quad (1.2)$$

The first part is the leptonic part and the second one was naively thought to be the part describing the interaction between nucleons. Nowadays we know that nucleons are not the fundamental constituents of matter, thus we have to replace them by quark fields. With this contact interaction Lagrangian, if one considers a simple scattering process like $\nu_\mu e^- \rightarrow \nu_e \mu^-$ one obtains a cross section that behaves badly at high energies

$$\sigma(\nu_\mu e^- \rightarrow \nu_e \mu^-) = \frac{G_F^2 s}{\pi} \sim s. \quad (1.3)$$

Obviously, this is just a *toy* model, or an *effective Lagrangian* that can only describe low energy phenomenology for simple processes. At high enough energies, it violates unitarity. Another issue is that this model is, obviously, non-renormalizable.

After many unfruitful attempts to find the correct, renormalizable model, that would accommodate both low and high energy phenomenology, finally, Weinberg, Salam and Glashow proposed an electroweak unified model [1–4] which successfully passed all the tests. This model is what we now call the Standard Model of Electroweak Interactions. When also adding the strong interaction sector, the model is simply called the Standard Model (SM). It is a gauge theory based on

the $SU(3)_C \otimes SU(2)_L \otimes U(1)_Y$ group. By means of the Spontaneous Symmetry Breaking (SSB) mechanism, the $SU(2)_L \otimes U(1)_Y$ electroweak group breaks into the electromagnetic subgroup $U(1)_{QED}$ and generates the appropriate mass terms for the particles. The SSB is generated by the non-zero expectation value of a $SU(2)_L$ doublet which is called Higgs doublet. This doublet also gives rise to a scalar particle, the Higgs boson, which couples (at tree-level) to all massive fields of the model.

So far, the SM¹ has been very successful and has passed many precision tests and the only missing ingredient seems to have been found. However, having found a Higgs-like scalar boson compatible with the SM predictions [7, 8] does not exclude the possibility of having an enlarged scalar sector, or some other type of new physics, that would mimic a SM Higgs.

1.1 Local Gauge Invariance

In order to consistently introduce the building blocks of the SM one must start from the beginning and introduce the basic *guideline* of its construction, which is, the *principle of local gauge invariance*. Consider for instance, the free Dirac equation with a mass term

$$\mathcal{L}(x) = \bar{\psi}(x) (i\gamma^\mu \partial_\mu - m) \psi(x). \quad (1.4)$$

It turns out that our Lagrangian is symmetric under a phase redefinition of the fermionic field $\psi(x) \rightarrow \psi(x) e^{iQ\theta}$, where Q (which, for now, is only introduced for convenience) and θ are just arbitrary real constants. The gauge principle promotes the global phase (constant) to a local phase (function of the space-time coordinates) $e^{iQ\theta} \rightarrow e^{iQ\theta(x)}$. Under this transformation, our previous Lagrangian is obviously, no longer invariant. As is normally done in tensor analysis over manifolds, one can define a *covariant* derivative $D_\mu \equiv \partial_\mu + i e Q A_\mu(x)$, in order to restore the invariance of the Lagrangian under this type of transformation; here e is for now, just another constant. Thus, one can deduce that under the *local gauge transformation* of the fermionic field $\psi(x) \rightarrow \psi(x) e^{iQ\theta(x)}$, the *affine connection* or the *gauge field* $A_\mu(x)$ must transform as $A_\mu(x) \rightarrow A_\mu(x) - e^{-1} \partial_\mu \theta(x)$. Thus, the Lagrangian given by

$$\mathcal{L} = \bar{\psi} (i\gamma^\mu D_\mu - m) \psi, \quad (1.5)$$

¹For a nice review of the SM read [5, 6].

is invariant under local gauge transformations. Adding a kinetic term (fixed by the requirement of gauge invariance) for the field A_μ , one immediately recognizes the Quantum Electrodynamics (QED) Lagrangian

$$\mathcal{L}_{QED} = -\frac{1}{4}F^{\mu\nu}F_{\mu\nu} + \bar{\psi} (i\gamma^\mu D_\mu - m) \psi, \quad (1.6)$$

with Q the electric charge of the fermion, e the electric coupling constant, and where we have defined $F^{\mu\nu} \equiv \partial^\mu A^\nu - \partial^\nu A^\mu$. Obviously a mass term for A^μ is forbidden as it would break gauge invariance. We shall now extend this analysis to the whole SM group in the next sections.

1.2 Electroweak Sector

In order to reproduce the precise, low energy experimental data on β decays, where only left-handed fermion and right-handed antifermion chiralities participate in the weak interaction, one must introduce the following left-handed doublets and right-handed singlets for a fermion family

$$\psi_1(x) = \begin{pmatrix} q_u \\ q_d \end{pmatrix}_L, \quad \psi_2(x) = q_{u,R}, \quad \psi_3(x) = q_{d,R}. \quad (1.7)$$

where $q(x)_{L,R} \equiv \mathcal{P}_{L,R} q(x) \equiv \frac{1 \mp \gamma_5}{2} q(x)$. Here we have used a family of quarks, however a similar analysis can be made for leptons i.e., by making the substitutions $q_u \rightarrow \nu_l$ and $q_d \rightarrow l^-$.

The gauge symmetry group that we will impose on our Lagrangian is $SU(2)_L \otimes U(1)_Y$, where L stands for left-handed and Y for hypercharge (we shall see it cannot be identified with the electric charge). Thus, under this transformation our fields will transform as

$$\begin{aligned} \psi_1 &\rightarrow e^{iy_1\beta} U_L \psi_1, \\ \psi_2 &\rightarrow e^{iy_2\beta} \psi_2, \\ \psi_3 &\rightarrow e^{iy_3\beta} \psi_3, \end{aligned} \quad (1.8)$$

where $e^{iy_i\beta}$ are $U(1)_Y$ transformations and where $U_L \equiv e^{i\vec{\sigma}\cdot\vec{\alpha}/2}$ is a $SU(2)_L$ transformation; y_i , β , $\vec{\alpha}$ are arbitrary real constants and $\vec{\sigma}$ are the Pauli matrices. The only free fermionic Lagrangian, invariant under $SU(2)_L \otimes U(1)_Y$, that we can write down must necessarily be massless (a mass terms would mix chiralities,

and therefore spoil our symmetries) i.e.,

$$\mathcal{L} = \sum_{i=1}^3 i \bar{\psi}_i \gamma^\mu \partial_\mu \psi_i. \quad (1.9)$$

Promoting these symmetries from global to local (as in the QED case) $\beta \rightarrow \beta(x)$ and $\vec{\alpha} \rightarrow \vec{\alpha}(x)$, one must introduce the following covariant derivatives, for each field, in order to maintain our local gauge invariance $\partial_\mu \psi_i \rightarrow D_{\mu,i} \psi_i$ (no summation over i) with

$$\begin{aligned} D_{\mu,1} &\equiv \partial_\mu + ig \frac{\sigma^j}{2} W_\mu^j + ig' y_1 B_\mu, \\ D_{\mu,2} &\equiv \partial_\mu + ig' y_2 B_\mu, \\ D_{\mu,3} &\equiv \partial_\mu + ig' y_3 B_\mu. \end{aligned} \quad (1.10)$$

One immediately deduces the transformation laws of the gauge fields

$$B_\mu \rightarrow B_\mu - (g')^{-1} \partial_\mu \beta(x), \quad (1.11)$$

$$\frac{\sigma^j}{2} W_\mu^j \rightarrow U_L \left(\frac{\sigma^j}{2} W_\mu^j \right) U_L^\dagger + ig^{-1} (\partial_\mu U_L) U_L^\dagger. \quad (1.12)$$

Adding the proper gauge invariant kinetic terms corresponding to the gauge fields one obtains

$$\mathcal{L}' = -\frac{1}{4} W_i^{\mu\nu} W_{\mu\nu}^i - \frac{1}{4} B^{\mu\nu} B_{\mu\nu} + \sum_{i=1}^3 i \bar{\psi}_i \gamma^\mu D_{\mu,i} \psi_i \quad (1.13)$$

where $B_{\mu\nu} \equiv \partial_\mu B_\nu - \partial_\nu B_\mu$ and $W_{\mu\nu}^i \equiv \partial_\mu W_\nu^i - \partial_\nu W_\mu^i - g \epsilon^{ijk} W_\mu^j W_\nu^k$. The gauge-fermion interaction term generated by the covariant derivative $D_{\mu,i}$ can be separated into a charged current interaction and a neutral current interaction. Defining appropriately the charged W boson field as $W^\mu = (W_1^\mu + iW_2^\mu)/\sqrt{2}$ and re-parametrizing the neutral part as

$$\begin{pmatrix} W_3^\mu \\ B^\mu \end{pmatrix} = \begin{pmatrix} \cos \theta_W & \sin \theta_W \\ -\sin \theta_W & \cos \theta_W \end{pmatrix} \begin{pmatrix} Z^\mu \\ A^\mu \end{pmatrix} \quad (1.14)$$

one easily obtains

$$\sum_{i=1}^3 i \bar{\psi}_i \gamma^\mu D_{\mu,i} \psi_i = \sum_{i=1}^3 i \bar{\psi}_i \gamma^\mu \partial_\mu \psi_i + \mathcal{L}_{QED}^{int} + \mathcal{L}_Z^{int} + \mathcal{L}_W^{int} \quad (1.15)$$

where *int* stands for interaction term. These interaction Lagrangians are explicitly given by

$$\mathcal{L}_{QED}^{int} = -e A_\mu \sum_f Q_f \bar{f} \gamma^\mu f, \quad (1.16)$$

$$\mathcal{L}_Z^{int} = -\frac{e}{2 \cos \theta_W \sin \theta_W} Z_\mu \sum_f \bar{f} \gamma^\mu (v_f - a_f \gamma_5) f, \quad (1.17)$$

$$\mathcal{L}_W^{int} = -\frac{g}{2\sqrt{2}} W_\mu \left(\bar{q}_d \gamma^\mu (1 - \gamma_5) q_u + \bar{l} \gamma^\mu (1 - \gamma_5) \nu_l \right) + \text{h.c.}, \quad (1.18)$$

where $f = q_u, q_d, l, \nu_l$ (we have also introduced the leptonic part) with $e \equiv g \sin \theta_W = g' \cos \theta_W$ and where:

	q_u	q_d	ν_l	l
v_f	$\frac{1}{2} - \frac{4}{3} \sin^2 \theta_W$	$-\frac{1}{2} + \frac{2}{3} \sin^2 \theta_W$	$\frac{1}{2}$	$-\frac{1}{2} + 2 \sin^2 \theta_W$
a_f	$\frac{1}{2}$	$-\frac{1}{2}$	$\frac{1}{2}$	$-\frac{1}{2}$
Q_f	$\frac{2}{3}$	$-\frac{1}{3}$	0	-1

The kinetic part of the Lagrangian \mathcal{L}' , written in terms of the physical fields W, Z and A , gives rise to the kinetic terms of the previously mentioned fields and cubic and quartic interactions among them:

$$-\frac{1}{4} W_i^{\mu\nu} W_{\mu\nu}^i - \frac{1}{4} B^{\mu\nu} B_{\mu\nu} = \mathcal{L}_{kin}^{W,Z,A} + \mathcal{L}_3 + \mathcal{L}_4 \quad (1.19)$$

where

$$\mathcal{L}_{kin}^{W,Z,A} = -\frac{1}{2}F_W^{\mu\nu}F_{\mu\nu}^W - \frac{1}{4}F_Z^{\mu\nu}F_{\mu\nu}^Z - \frac{1}{4}F_A^{\mu\nu}F_{\mu\nu}^A, \quad (1.20)$$

$$\begin{aligned} \mathcal{L}_3 = & ie \cot \theta_W \left\{ (\partial^\mu W^\nu - \partial^\nu W^\mu) W_\mu^\dagger Z_\nu - (\partial^\mu W^{\nu\dagger} - \partial^\nu W^{\mu\dagger}) W_\mu Z_\nu \right. \\ & \left. + W_\mu W_\nu^\dagger (\partial^\mu Z^\nu - \partial^\nu Z^\mu) \right\} + ie \left\{ (\partial^\mu W^\nu - \partial^\nu W^\mu) W_\mu^\dagger A_\nu \right. \\ & \left. - (\partial^\mu W^{\nu\dagger} - \partial^\nu W^{\mu\dagger}) W_\mu A_\nu + W_\mu W_\nu^\dagger (\partial^\mu A^\nu - \partial^\nu A^\mu) \right\}, \quad (1.21) \end{aligned}$$

$$\begin{aligned} \mathcal{L}_4 = & -\frac{e^2}{2\sin^2 \theta_W} \left\{ (W_\mu^\dagger W^\mu)^2 - W_\mu^\dagger W^{\mu\dagger} W_\nu W^\nu \right\} \\ & - e^2 \cot \theta_W \left\{ 2W_\mu^\dagger W^\mu Z_\nu A^\nu - W_\mu^\dagger Z^\mu W_\nu A^\nu - W_\mu^\dagger A^\mu W_\nu Z^\nu \right\} \\ & - e^2 \cot^2 \theta_W \left\{ W_\mu^\dagger W^\mu Z_\nu Z^\nu - W_\mu^\dagger Z^\mu W_\nu Z^\nu \right\} \\ & - e^2 \left\{ W_\mu^\dagger W^\mu A_\nu A^\nu - W_\mu^\dagger A^\mu W_\nu A^\nu \right\}, \quad (1.22) \end{aligned}$$

and where, as in the QED case we have defined $F_X^{\mu\nu} \equiv \partial^\mu X^\nu - \partial^\nu X^\mu$, ($X = W, Z, A$).

1.2.1 Higgs Mechanism

So far we have been able to generate the correct interaction terms and the correct number of vector bosons observed by experiments. However, we have not been able to introduce the needed mass terms for the fermions nor for the Z and W vector gauge bosons. As in the QED case, adding (by hand) a mass term would spoil our gauge symmetry.

Let's consider an additional complex scalar $SU(2)_L$ doublet of the form

$$\Phi(x) \equiv \begin{pmatrix} \phi^{(+)}(x) \\ \phi^{(0)}(x) \end{pmatrix} \equiv \begin{pmatrix} G^+(x) \\ \frac{1}{\sqrt{2}}(v + h(x) + iG^0(x)) \end{pmatrix}, \quad (1.23)$$

so that it has a positive, non-zero vacuum expectation value (vev), i.e.,

$$\langle 0|\Phi(x)|0\rangle = v/\sqrt{2} > 0. \quad (1.24)$$

The most generic Lagrangian, associated to the Φ scalar doublet, invariant under the electroweak gauge group can be written as

$$\mathcal{L}_\Phi = \left(D_\mu^S \Phi \right)^\dagger D_\mu^S \Phi - \mu_S^2 \Phi^\dagger \Phi - h_S \left(\Phi^\dagger \Phi \right)^2, \quad (1.25)$$

with $h_S > 0$, $\mu_S^2 < 0$ and with the covariant derivative given by

$$D_\mu^S = \partial_\mu + i g \frac{\sigma^j}{2} W_\mu^j + i g' \frac{1}{2} B^\mu. \quad (1.26)$$

and where G^+ and G^0 correspond to the the so-called Goldstone bosons. Due to the $SU(2)_L$ invariance, one can re-parametrize the scalar field $\Phi(x)$ as

$$\Phi(x) = e^{i\vec{\sigma}\cdot\vec{\theta}(x)/2} \frac{1}{\sqrt{2}} \begin{pmatrix} 0 \\ v + h(x) \end{pmatrix}. \quad (1.27)$$

The unitary gauge (where the Goldstone bosons are absent) is then given by $\vec{\theta}(x) = 0$.

The non-zero vev of the scalar field generates mass terms for the Z and W bosons. Choosing the unitary gauge (for simplicity) we can write \mathcal{L}_S as

$$\begin{aligned} \mathcal{L}_S = & \frac{1}{4} h_S v^4 + \frac{1}{2} \partial_\mu h \partial^\mu h - \frac{1}{2} M_h^2 h^2 - \frac{M_h^2}{2v} h^3 - \frac{M_h^2}{8v^2} h^4 \\ & + M_W^2 W_\mu^\dagger W^\mu \left\{ 1 + \frac{2}{v} h + \frac{h^2}{v^2} \right\} + \frac{1}{2} M_Z^2 Z_\mu Z^\mu \left\{ 1 + \frac{2}{v} h + \frac{h^2}{v^2} \right\}, \end{aligned} \quad (1.28)$$

with the mass terms given by $M_W = M_Z \cos \theta_W = v g/2$ and $M_h = \sqrt{-2\mu_S^2} = \sqrt{2h_S} v$. Similar considerations can be made for the fermion sector.

Consider the three (experimentally observed) quark and lepton families, given in the form of electroweak fermion doublets and singlets as in (1.7):

$$Q'_L = \begin{pmatrix} q'_u \\ q'_d \end{pmatrix}_L, \quad q'_{u,R}, \quad q'_{d,R}, \quad (1.29)$$

$$L'_L = \begin{pmatrix} \nu'_l \\ l' \end{pmatrix}_L, \quad \nu'_{l,R}, \quad l'_{R}, \quad (1.30)$$

where, this time, we have introduced the primed notation in order to differentiate between the mass eigenstates (non-primed) and non-mass eigenstates (primed).

The most generic Yukawa Lagrangian, invariant under our electroweak gauge group, can be written in the form

$$\mathcal{L}_Y = -\frac{\sqrt{2}}{v} \left\{ \bar{Q}'_L M'_d \Phi d'_R + \bar{Q}'_L M'_u \tilde{\Phi} u'_R + \bar{L}'_L M'_l \Phi l'_R \right\}. \quad (1.31)$$

where $\tilde{\Phi} \equiv i\sigma_2 \Phi^*$ is the charge conjugate Higgs doublet. Choosing again the unitary gauge, and diagonalizing the mass matrices, one find that the previous Lagrangian takes the simple form

$$\mathcal{L}_Y = -\left(1 + \frac{H}{v}\right) \left\{ \bar{\mathbf{q}}_d \mathcal{M}_d \mathbf{q}_d + \bar{\mathbf{q}}_u \mathcal{M}_u \mathbf{q}_u + \bar{\mathbf{l}} \mathcal{M}_l \mathbf{l} \right\}, \quad (1.32)$$

where the fermion vectors are $\mathbf{q}_u^T = (u, c, t)$, $\mathbf{q}_d^T = (d, s, b)$, $\mathbf{l}^T = (e, \mu, \tau)$ and the diagonal mass matrices are given by $\mathcal{M}_u = \text{diag}\{m_u, m_c, m_t\}$, $\mathcal{M}_d = \text{diag}\{m_d, m_s, m_b\}$, $\mathcal{M}_l = \text{diag}\{m_e, m_\mu, m_\tau\}$. One can check that $\bar{\mathbf{f}}'_L \mathbf{f}'_L = \bar{\mathbf{f}}_L \mathbf{f}_L$ and $\bar{\mathbf{f}}'_R \mathbf{f}'_R = \bar{\mathbf{f}}_R \mathbf{f}_R$, thus the previously introduced (neutral current) interaction Lagrangians \mathcal{L}_{QED}^{int} and \mathcal{L}_Z^{int} do not change when expressed in terms of the fermion mass eigenstate fields. However, this is not true for the charged current interaction Lagrangian \mathcal{L}_W^{int} . Defining the Cabibbo-Kobayashi-Maskawa (CKM) unitary matrix as $\bar{\mathbf{q}}'_{u,L} \mathbf{q}'_{d,L} \equiv \bar{\mathbf{q}}_{u,L} \mathbf{V} \mathbf{q}_{d,L}$, considering massless neutrinos and summing over all fermion families one obtains

$$\mathcal{L}_W^{int} = -\frac{g}{2\sqrt{2}} W_\mu \left(\sum_{u,d} V_{ud}^* \bar{q}_d \gamma^\mu (1 - \gamma_5) q_u + \sum_l \bar{l} \gamma^\mu (1 - \gamma_5) \nu_l \right) + \text{h.c.}, \quad (1.33)$$

The SM is able to also accommodate non-zero neutrino masses by introducing right-handed neutrino fields ν_R and an additional Yukawa term in \mathcal{L}_Y that would give rise to an analogous (to the CKM mixing matrix \mathbf{V}) mixing matrix \mathbf{V}_l .

1.2.2 CP Violation in the SM

The previously introduced CKM mixing matrix \mathbf{V} is able to accommodate successfully all the available experimental data. It is able to describe the quark mixing phenomenology with both high accuracy and high precision. It can be

parametrized in many ways [9–11], i.e.,

$$\begin{aligned}
\mathbf{V} &= \begin{bmatrix} V_{ud} & V_{us} & V_{ub} \\ V_{cd} & V_{cs} & V_{cb} \\ V_{td} & V_{ts} & V_{tb} \end{bmatrix} \\
&= \begin{bmatrix} c_{12} c_{13} & s_{12} c_{13} & s_{13} e^{-i\delta_{13}} \\ -s_{12} c_{23} - c_{12} s_{23} s_{13} e^{i\delta_{13}} & c_{12} c_{23} - s_{12} s_{23} s_{13} e^{i\delta_{13}} & s_{23} c_{13} \\ s_{12} s_{23} - c_{12} c_{23} s_{13} e^{i\delta_{13}} & -c_{12} s_{23} - s_{12} c_{23} s_{13} e^{i\delta_{13}} & c_{23} c_{13} \end{bmatrix} \\
&= \begin{bmatrix} 1 - \frac{\lambda^2}{2} & \lambda & A\lambda^3(\rho - i\eta) \\ -\lambda & 1 - \frac{\lambda^2}{2} & A\lambda^2 \\ A\lambda^3(1 - \rho - i\eta) & -A\lambda^2 & 1 \end{bmatrix} + O(\lambda^4). \quad (1.34)
\end{aligned}$$

Defining $s_{12} \equiv \lambda$, $s_{23} \equiv A\lambda^2$ and $s_{13}e^{-i\delta_{13}} \equiv A\lambda^3(\rho - i\eta)$, this last parametrization, due to Wolfenstein, exploits the strong hierarchy among the matrix elements, and it is just a Taylor expansion in powers of λ . The latest fit by the CKMfitter group [12] is shown in Fig. 1.1, with $(\bar{\rho}, \bar{\eta}) \equiv (1 - \lambda^2/2)(\rho, \eta)$ and where the α , β and γ angles are given by

$$\alpha \equiv -\arg\left(\frac{V_{td}V_{tb}^*}{V_{ud}V_{ub}^*}\right), \quad \beta \equiv -\arg\left(\frac{V_{cd}V_{cb}^*}{V_{td}V_{tb}^*}\right), \quad \gamma \equiv -\arg\left(\frac{V_{ud}V_{ub}^*}{V_{cd}V_{cb}^*}\right). \quad (1.35)$$

The only complex phase in the SM Lagrangian is δ_{13} , which is the only source of CP violation. Thus, the SM can only describe this phenomenon in a very limited way. It can only occur in processes where all three generations appear, for example. CP violation is very suppressed, thus, in the SM, and it seems not to be enough to explain the huge matter-antimatter asymmetry observed in the Universe. A SM extension with extra sources of CP violation, would therefore, be more than welcome.

An extension of the SM that contains an extra scalar doublet, namely the Two-Higgs doublet model (2HDM), with extra sources of CP violation, will be introduced in Chapter 2 and extensively analysed in Chapters 5 to 8.

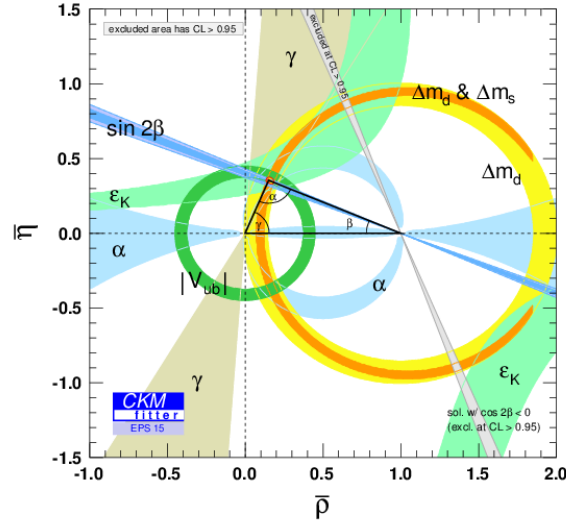


Figure 1.1: Latest constraints on the $(\bar{\rho}, \bar{\eta})$ plane from the CKMfitter group.

1.3 Strong Sector

In order to accommodate the strong interaction into the SM we have to enlarge the broken $SU(2)_L \otimes U(1)_Y$ electroweak gauge group with the colour $SU(3)_C$ group [13,14], i.e., the complete SM group is given by $SU(2)_L \otimes U(1)_Y \otimes SU(3)_C$. Let's consider thus the massive Dirac Lagrangian invariant under $SU(3)_C$ global transformations. It can be written as

$$\mathcal{L}(x) = \sum_{f,\alpha} \left\{ \bar{q}_f^\alpha(x) i \gamma^\mu \partial_\mu q_f^\alpha(x) - m_f \bar{q}_f^\alpha(x) q_f^\alpha(x) \right\}, \quad (1.36)$$

where f stands for the quark index $f = u, c, t, d, s, b$, and α stands for the colour index $\alpha = 1, 2, 3$. Under a global $SU(3)$ transformation the quark fields transform as

$$q_f^\alpha \rightarrow U_{\alpha\beta} q_f^\beta \quad (1.37)$$

where the operator U is given by

$$U = e^{-i g_s \lambda^a \theta^a / 2}, \quad (1.38)$$

and where summation over all repeated indices is understood. The λ^a matrices are the group generators and θ^a are real arbitrary constants. Promoting, as usual, the gauge symmetry from global to local i.e., $\theta^a = \theta^a(x)$, one must introduce the covariant derivative

$$(D_\mu)_{\alpha\beta} \equiv \delta_{\alpha\beta} \partial_\mu - ig_s \left(\frac{\lambda^a}{2} \right)_{\alpha\beta} G_\mu^a. \quad (1.39)$$

with the gauge fields transforming as

$$\left(\frac{\lambda^a}{2} \right) G_\mu^a \rightarrow U \left(\frac{\lambda^a}{2} \right) G_\mu^a U^\dagger - ig_s^{-1} (\partial_\mu U) U^\dagger. \quad (1.40)$$

Thus, the Quantum Chromodynamics (QCD) Lagrangian is finally given by

$$\mathcal{L}_{QCD} = -\frac{1}{4} G_a^{\mu\nu} G_{\mu\nu}^a + \sum_{f,\alpha} \left\{ \bar{q}_f^\alpha i \gamma^\mu (D_\mu)_{\alpha\beta} q_f^\beta - m_f \bar{q}_f^\alpha q_f^\alpha \right\}, \quad (1.41)$$

where we have introduced the gauge invariant kinetic term corresponding to the gluon fields G_μ^a given by $G_a^{\mu\nu} = \partial^\mu G_a^\nu - \partial^\nu G_a^\mu + g_s f^{abc} G_b^\mu G_c^\nu$ (summation over all repeated indices is, again, understood). The quantities f^{abc} are the totally antisymmetric $SU(3)$ structure constants defined by the Lie algebra

$$[\lambda^a, \lambda^b] = 2i f^{abc} \lambda^c. \quad (1.42)$$

1.3.1 $SU(3)$ Algebra

Introducing the shorthand notation $T^a \equiv \lambda^a/2$, the previous Lie algebra simplifies to

$$[T^a, T^b] = i f^{abc} T^c. \quad (1.43)$$

Given the f^{abc} structure constants of the $SU(3)$ group, we call a *group representation* a set of $d_R \times d_R$ hermitian matrices that obey the same Lie algebra as the group generators i.e.,

$$[T_R^a, T_R^b] = i f^{abc} T_R^c, \quad (1.44)$$

where d_R is called the *dimension of the representation*. A representation is called *reducible* if there exists a unitary transformation U so that $U^{-1} T_R^a U$ puts all the non-zero entries in the same diagonal blocks for each a ; if not it is called

irreducible. An $SU(3)$ irreducible representation can be in general labelled by two indices $R \equiv (\lambda_1, \lambda_2)$. The dimension of the representation is then given by:

$$d_R = \frac{1}{2}(\lambda_1 + 1)(\lambda_2 + 1)(\lambda_1 + \lambda_2 + 2) \quad (1.45)$$

Another important quantity can be found by taking the following trace:

$$\text{Tr} \left\{ T_R^a T_R^b \right\} = T_R \delta^{ab}. \quad (1.46)$$

T_R can be related to the quadratic Casimir operator eigenvalue

$$T_R \cdot d_A = C_R \cdot d_R \quad (1.47)$$

where $d_A = 3^2 - 1 = 8$, the dimension of the adjoint representation and C_R is the d_R -degenerate Casimir operator eigenvalue. The quadratic Casimir operator has the form:

$$\mathbb{C}_R \equiv T_R^a T_R^a = C_R \mathbb{I}_{d_R}, \quad (1.48)$$

with \mathbb{I}_{d_R} the $d_R \times d_R$ identity matrix.

For the two fundamental representations $(1, 0)$ and $(0, 1)$ we have $d_R = 3$ (3 colours of quarks and anti-quarks). Gluons obviously belong to the adjoint representation. QCD, however, does not forbid the existence of multiplets belonging to higher $SU(3)_C$ group representations. These exotic fields could therefore exist in nature. As they have not been experimentally observed we can only set bounds on their masses. This analysis is performed in Chapter 4.

BIBLIOGRAPHY

- [1] S.L. Glashow, *Nucl. Phys.* **22** (1961) 579.
- [2] S. Weinberg, *Phys. Rev. Lett.* **19** (1967) 1264.
- [3] A. Salam, in *Elementary Particle Theory*, ed. N. Svartholm (Almqvist and Wiksells, Stockholm, 1969), p. 367.
- [4] S.L. Glashow, J. Iliopoulos and L. Maiani, *Phys. Rev.* **D2** (1970) 1285.
- [5] A. Pich, *The Standard Model of Electroweak Interactions*, arXiv:1201.0537 [hep-ph].
- [6] A. Pich, *Aspects of Quantum Chromodynamics*, arXiv:hep-ph/0001118.
- [7] G. Aad *et al.* [ATLAS Collaboration], *Phys. Lett. B* **716** (2012) 1 doi:10.1016/j.physletb.2012.08.020 [arXiv:1207.7214 [hep-ex]].
- [8] S. Chatrchyan *et al.* [CMS Collaboration], *Phys. Lett. B* **716** (2012) 30 doi:10.1016/j.physletb.2012.08.021 [arXiv:1207.7235 [hep-ex]].
- [9] K.A. Olive *et al.* (Particle Data Group), *Chin. Phys. C*, **38**, 090001 (2014) and 2015 update, <http://pdg.lbl.gov>.
- [10] L. Wolfenstein, *Phys. Rev. Lett.* **51** (1983) 1945.
- [11] A.J. Buras, M.E. Lautenbacher and G. Ostermaier, *Phys. Rev.* **D50** (1994) 3433.
- [12] J. Charles *et al.*, *Current status of the Standard Model CKM fit and constraints on $\Delta F = 2$ New Physics*, *Phys. Rev. D* **91** (2015) 7, 073007 doi:10.1103/PhysRevD.91.073007, arXiv:1501.05013 [hep-ph].
- [13] H. Fritzsch and M. Gell-Mann, Proc. XVI International Conference on High Energy Physics, eds. J.D. Jackson and A. Roberts (Fermilab, 1972), Vol. 2, p. 135.
- [14] H. Fritzsch, M. Gell-Mann and H. Leutwyler, *Phys. Lett.* **B47** (365) 1973.

2. THE TWO-HIGGS-DOUBLET MODEL

So far, we have introduced the SM which contains a scalar $SU(2)_L$ Higgs doublet with a non-zero vacuum expectation value, responsible for the electroweak symmetry breaking. One of the consequences is that the fermions and W and Z bosons acquire mass while preserving gauge invariance. Another consequence is that, the physical particle spectrum is enlarged with a scalar particle, the Higgs boson. However, there is no fundamental motivation that forbids the presence of more than one doublet. Moreover, there are many open questions that the SM leaves unanswered. As we have already mentioned, it seems that more sources of CP violation are needed in order to explain the huge matter-antimatter asymmetry observed in the Universe; there is also lack for a dark matter candidate, to cite just a few of them. Thus, there are many theoretical and observational motivations for enlarging the scalar sector of the SM. Next we shall present one of these models, namely the two-Higgs-doublet model (2HDM).

2.1 The Aligned Two-Higgs-Doublet Model

The 2HDM extends the SM with a second scalar doublet of hypercharge $Y = \frac{1}{2}$. The neutral components of the scalar doublets $\phi_a(x)$ ($a = 1, 2$) acquire vacuum expectation values that are, in general, complex:

$$\langle 0 | \phi_a^T(x) | 0 \rangle = \frac{1}{\sqrt{2}} (0, v_a e^{i\theta_a}) . \quad (2.1)$$

Through an appropriate $U(1)_Y$ transformation one can enforce $\theta_1 = 0$, since only the relative phase $\theta \equiv \theta_2 - \theta_1$ is observable. It is convenient to perform a global $SU(2)$ transformation on the scalar doublets (ϕ_1, ϕ_2) and work in the so-called Higgs basis (Φ_1, Φ_2) , where only one of them acquires a vacuum expectation value:

$$\begin{pmatrix} \Phi_1 \\ -\Phi_2 \end{pmatrix} \equiv \begin{bmatrix} \cos \beta & \sin \beta \\ \sin \beta & -\cos \beta \end{bmatrix} \begin{pmatrix} \phi_1 \\ e^{-i\theta} \phi_2 \end{pmatrix} , \quad (2.2)$$

and where we have defined $\tan \beta \equiv v_2/v_1$. In this basis, the two doublets are parametrized as

$$\Phi_1 = \begin{bmatrix} G^+ \\ \frac{1}{\sqrt{2}}(v + S_1 + iG^0) \end{bmatrix}, \quad \Phi_2 = \begin{bmatrix} H^+ \\ \frac{1}{\sqrt{2}}(S_2 + iS_3) \end{bmatrix}, \quad (2.3)$$

where G^\pm and G^0 denote the Goldstone fields and where $\langle 0|H^+|0\rangle = \langle 0|G^+|0\rangle = \langle 0|G^0|0\rangle = \langle 0|S_i|0\rangle = 0$. Thus, Φ_1 plays the role of the SM scalar doublet with its vacuum expectation value given by $v \equiv \sqrt{v_1^2 + v_2^2} \simeq (\sqrt{2}G_F)^{-1/2} = 246$ GeV.

The physical scalar spectrum contains five degrees of freedom: the two charged Higgs fields $H^\pm(x)$ and three neutral scalars $\varphi_i^0(x) = \{h(x), H(x), A(x)\}$. These last are related to the original S_i fields through an orthogonal transformation \mathcal{R} given by $\varphi_i^0(x) = \mathcal{R}_{ij}S_j(x)$. The form of the \mathcal{R} matrix is fixed by the scalar potential, which determines the neutral scalar mass matrix and the corresponding mass eigenstates. A detailed discussion will be given later on. In general, the CP-odd component S_3 mixes with the CP-even fields $S_{1,2}$ and the resulting mass eigenstates do not have a definite CP quantum number. If the scalar potential is CP conserving this admixture disappears. In this particular case, $A(x) = S_3(x)$ and¹

$$\begin{pmatrix} h \\ H \end{pmatrix} = \begin{bmatrix} \cos \tilde{\alpha} & \sin \tilde{\alpha} \\ -\sin \tilde{\alpha} & \cos \tilde{\alpha} \end{bmatrix} \begin{pmatrix} S_1 \\ S_2 \end{pmatrix}. \quad (2.4)$$

Performing a phase redefinition of the neutral CP-even fields, we can fix the sign of $\sin \tilde{\alpha}$. In this work we adopt the conventions $M_h \leq M_H$ and $0 \leq \tilde{\alpha} \leq \pi$, so that $\sin \tilde{\alpha}$ is always positive.

¹ In the usually adopted notation $\tilde{\alpha} = \alpha - \beta$, where α is the rotation angle expressing the two mass eigenstates h and H in terms of the CP-even neutral fields of the original scalar basis $\phi_1(x)$ and $\phi_2(x)$. Since the choice of initial basis is arbitrary, the parameters α and β are in general unphysical; their values can be changed at will through SU(2) rotations. These angles only become meaningful in particular models where a specific basis is singled out (through a symmetry for instance).

2.1.1 Yukawa Alignment

The most generic Yukawa Lagrangian with the SM fermionic content can be written in the Higgs basis as:

$$\begin{aligned} \mathcal{L}_Y = -\frac{\sqrt{2}}{v} \left\{ \bar{Q}'_L (M'_d \Phi_1 + Y'_d \Phi_2) d'_R + \bar{Q}'_L (M'_u \tilde{\Phi}_1 + Y'_u \tilde{\Phi}_2) u'_R \right. \\ \left. + \bar{L}'_L (M'_l \Phi_1 + Y'_l \Phi_2) l'_R \right\} \end{aligned} \quad (2.5)$$

where Q'_L, L'_L are the left-handed quark and lepton doublets (just as in the SM). M'_f and Y'_f ($f = u, d, l$) are the non diagonal mass and Yukawa matrices which are in general complex and independent; therefore these two matrices are not simultaneously diagonalizable in flavour space. This gives rise to dangerous tree level flavour changing neutral currents (FCNCs) which are phenomenologically highly suppressed. In order to get rid of them one usually imposes a discrete \mathcal{Z}_2 symmetry on the Higgs doublets i.e., $\phi_1 \rightarrow \phi_1, \phi_2 \rightarrow -\phi_2$ (in a generic basis), etc. However, a more general approach is to impose alignment in the flavour space $Y'_f \sim M'_f$ [1]. In terms of the the mass-eigenstate mass matrix we obtain

$$Y_{d,l} = \varsigma_{d,l} M_{d,l}, \quad Y_u = \varsigma_u^* M_u, \quad (2.6)$$

where ς_f ($f = u, d, l$) are called the alignment parameters. These three parameters are independent, flavour universal, scalar basis independent and in general complex. Their phases introduce new sources of CP-violation. The usual models based on \mathcal{Z}_2 symmetries are recovered for particular (real) values of the couplings ς_f [1], as indicated in Table 2.1. We can now write our Yukawa Lagrangian in terms of the mass-eigenstate fields:

$$\begin{aligned} \mathcal{L}_Y = -\frac{\sqrt{2}}{v} H^+ \left\{ \bar{u} \left[\varsigma_d V M_d \mathcal{P}_R - \varsigma_u M_u^\dagger V \mathcal{P}_L \right] d + \varsigma_l \bar{\nu} M_l \mathcal{P}_R l \right\} \\ - \frac{1}{v} \sum_{\varphi_i^0, f} y_f^{\varphi_i^0} \varphi_i^0 \left[\bar{f} M_f \mathcal{P}_R f \right] + \text{h.c.} \end{aligned}$$

here $\mathcal{P}_{R,L} \equiv \frac{1 \pm \gamma_5}{2}$ are the right-handed and left-handed chirality projectors and the couplings of the neutral scalar fields are given by:

$$y_{d,l}^{\varphi_i^0} = \mathcal{R}_{i1} + (\mathcal{R}_{i2} + i \mathcal{R}_{i3}) \varsigma_{d,l}, \quad y_u^{\varphi_i^0} = \mathcal{R}_{i1} + (\mathcal{R}_{i2} - i \mathcal{R}_{i3}) \varsigma_u^*. \quad (2.7)$$

Table 2.1: *CP-conserving 2HDMs based on discrete Z_2 symmetries.*

Model	ς_d	ς_u	ς_l
Type I	$\cot \beta$	$\cot \beta$	$\cot \beta$
Type II	$-\tan \beta$	$\cot \beta$	$-\tan \beta$
Type X	$\cot \beta$	$\cot \beta$	$-\tan \beta$
Type Y	$-\tan \beta$	$\cot \beta$	$\cot \beta$
Inert	0	0	0

As in the SM, all scalar-fermion couplings are proportional to the corresponding fermion masses. This linear dependence on the fermion mass is characteristic of the Aligned two-Higgs-doublet model (A2HDM) framework and does not hold in non-aligned 2HDMs with FCNCs. The only source of flavour-changing interactions is the Cabibbo-Kobayashi-Maskawa (CKM) quark mixing matrix V [2]. All possible freedom allowed by the alignment conditions is determined by the three family-universal complex parameters ς_f .

Quantum corrections induce a misalignment of the Yukawa matrices, generating small FCNC effects suppressed by the corresponding loop factors [1, 3–6]. However, the flavour symmetries of the A2HDM tightly constraint the possible FCNC structures, keeping their effects well below the present experimental bounds [1, 3, 4, 7–9].²

² The only FCNC structures induced at one loop take the form [3, 4]:

$$\begin{aligned}
\mathcal{L}_{\text{FCNC}} = & \frac{C(\mu)}{4\pi^2 v^3} (1 + \varsigma_u^* \varsigma_d) \sum_i \varphi_i^0(x) \\
& \times \left\{ (\mathcal{R}_{i2} + i \mathcal{R}_{i3}) (\varsigma_d - \varsigma_u) \left[\bar{d}_L V^\dagger M_u M_u^\dagger V M_d d_R \right] \right. \\
& \left. - (\mathcal{R}_{i2} - i \mathcal{R}_{i3}) (\varsigma_d^* - \varsigma_u^*) \left[\bar{u}_L V M_d M_d^\dagger V^\dagger M_u u_R \right] \right\} + \text{h.c.}, \tag{2.8}
\end{aligned}$$

with $C(\mu) = C(\mu_0) - \log(\mu/\mu_0)$. These FCNC effects vanish identically in the Z_2 models where the alignment condition is protected by a discrete symmetry. In the most general case, assuming the alignment to be exact at some scale μ_0 , i.e. $C(\mu_0) = 0$, a non-zero value for the FCNC coupling is generated when running to a different scale. However, the numerical effect is suppressed by $m_q m_d^2/v^3$ and quark-mixing factors, avoiding the stringent experimental constraints for light-quark systems. Explicit examples of symmetry-protected underlying theories leading to a low-energy A2HDM structure have been discussed in Refs. [10–12].

The orthogonality of the rotation matrix \mathcal{R} , implies the following relations among the Yukawa couplings of the three neutral scalars:

$$\begin{aligned} \sum_{i=1}^3 (y_f^{\varphi_i^0})^2 &= 1, & \sum_{i=1}^3 |y_f^{\varphi_i^0}|^2 &= 1 + 2|\zeta_f|^2, & \sum_{i=1}^3 y_f^{\varphi_i^0} \mathcal{R}_{i1} &= 1, \\ \sum_{i=1}^3 y_{d,l}^{\varphi_i^0} \mathcal{R}_{i2} &= \zeta_{d,l}, & \sum_{i=1}^3 y_u^{\varphi_i^0} \mathcal{R}_{i2} &= \zeta_u^*, \\ \sum_{i=1}^3 y_{d,l}^{\varphi_i^0} \mathcal{R}_{i3} &= i \zeta_{d,l}, & \sum_{i=1}^3 y_u^{\varphi_i^0} \mathcal{R}_{i3} &= -i \zeta_u^*. \end{aligned} \quad (2.9)$$

2.1.2 Bosonic Couplings

The full set of interactions among the gauge and scalar bosons is given in Section 2.3. The relevant vertices for our analysis are the ones coupling a single neutral scalar with a pair of gauge bosons. As shown in Eq. (2.50), they are identical to their SM counterpart, with the field S_1 taking the role of the SM Higgs. Therefore ($VV = W^+W^-$, ZZ),

$$g_{\varphi_i^0 VV} = \mathcal{R}_{i1} g_{hVV}^{\text{SM}}, \quad (2.10)$$

which implies

$$g_{hVV}^2 + g_{HVV}^2 + g_{AVV}^2 = \left(g_{hVV}^{\text{SM}}\right)^2. \quad (2.11)$$

The strength of the SM Higgs interaction is shared by the three 2HDM neutral bosons. In the CP-conserving limit, the CP-odd field decouples while the strength of the h and H interactions is governed by the corresponding $\cos \tilde{\alpha}$ and $\sin \tilde{\alpha}$ factors. Thus, a general feature of 2HDMs is that, at tree level, the couplings of the neutral scalars to vector bosons cannot be enhanced over the SM value and obey the custodial symmetry relation $g_{\varphi_i^0 ZZ} = g_{\varphi_i^0 WW}$. Observing a scalar boson with a somewhat enhanced coupling to vector bosons or a deviation from custodial symmetry [13] would therefore be in clear contradiction with the predictions of this class of models. The relations (2.9) and (2.11) establish a connection between the couplings of the observed 125 GeV resonance and searches for other neutral and charged scalars within the A2HDM.

For the phenomenological analysis, in order to compute two-photon decays of neutral scalars, one will need their couplings to a pair of charged scalars, generated through the scalar potential discussed further on. Since these couplings

depend on still unknown parameters, we will normally parametrize the corresponding interactions as

$$\mathcal{L}_{\varphi^0 H^+ H^-} = -v \sum_{\varphi_i^0} \lambda_{\varphi_i^0 H^+ H^-} \varphi_i^0 H^+ H^-. \quad (2.12)$$

Explicit expressions for the cubic couplings $\lambda_{\varphi_i^0 H^+ H^-}$ in terms of the Higgs potential parameters can be found next. If CP is assumed to be an exact symmetry, then, $\lambda_{AH^+ H^-} = 0$.

2.2 Scalar Potential

In the Higgs basis, the most general scalar potential takes the form [14]

$$\begin{aligned} V = & \mu_1 \Phi_1^\dagger \Phi_1 + \mu_2 \Phi_2^\dagger \Phi_2 + [\mu_3 \Phi_1^\dagger \Phi_2 + \mu_3^* \Phi_2^\dagger \Phi_1] + \lambda_1 (\Phi_1^\dagger \Phi_1)^2 \\ & + \lambda_2 (\Phi_2^\dagger \Phi_2)^2 + \lambda_3 (\Phi_1^\dagger \Phi_1) (\Phi_2^\dagger \Phi_2) + \lambda_4 (\Phi_1^\dagger \Phi_2) (\Phi_2^\dagger \Phi_1) \\ & + [(\lambda_5 \Phi_1^\dagger \Phi_2 + \lambda_6 \Phi_1^\dagger \Phi_1 + \lambda_7 \Phi_2^\dagger \Phi_2) (\Phi_1^\dagger \Phi_2) + \text{h.c.}]. \end{aligned} \quad (2.13)$$

The Hermiticity of the potential requires all parameters to be real except μ_3 , λ_5 , λ_6 and λ_7 ; thus, there are 14 real parameters.

The minimization conditions $\langle 0 | \Phi_1^T(x) | 0 \rangle = \frac{1}{\sqrt{2}} (0, v)$ and $\langle 0 | \Phi_2^T(x) | 0 \rangle = \frac{1}{\sqrt{2}} (0, 0)$ impose the relations

$$\mu_1 = -\lambda_1 v^2, \quad \mu_3 = -\frac{1}{2} \lambda_6 v^2. \quad (2.14)$$

The potential can then be decomposed into a quadratic term plus cubic and quartic interactions

$$V = -\frac{1}{4} \lambda_1 v^4 + V_2 + V_3 + V_4. \quad (2.15)$$

The mass terms take the form

$$\begin{aligned} V_2 = & M_{H^\pm}^2 H^+ H^- + \frac{1}{2} (S_1, S_2, S_3) \mathcal{M} \begin{pmatrix} S_1 \\ S_2 \\ S_3 \end{pmatrix} \\ = & M_{H^\pm}^2 H^+ H^- + \frac{1}{2} M_h^2 h^2 + \frac{1}{2} M_H^2 H^2 + \frac{1}{2} M_A^2 A^2, \end{aligned} \quad (2.16)$$

with

$$M_{H^\pm}^2 = \mu_2 + \frac{1}{2} \lambda_3 v^2 \quad (2.17)$$

and

$$\mathcal{M} = \begin{pmatrix} 2\lambda_1 v^2 & v^2 \lambda_6^{\text{R}} & -v^2 \lambda_6^{\text{I}} \\ v^2 \lambda_6^{\text{R}} & M_{H^\pm}^2 + v^2 \left(\frac{\lambda_4}{2} + \lambda_5^{\text{R}} \right) & -v^2 \lambda_5^{\text{I}} \\ -v^2 \lambda_6^{\text{I}} & -v^2 \lambda_5^{\text{I}} & M_{H^\pm}^2 + v^2 \left(\frac{\lambda_4}{2} - \lambda_5^{\text{R}} \right) \end{pmatrix}, \quad (2.18)$$

where $\lambda_i^{\text{R}} \equiv \text{Re}(\lambda_i)$ and $\lambda_i^{\text{I}} \equiv \text{Im}(\lambda_i)$. The symmetric mass matrix \mathcal{M} is diagonalized by an orthogonal matrix \mathcal{R} , which defines the neutral mass eigenstates:

$$\mathcal{M} = \mathcal{R}^T \begin{pmatrix} M_h^2 & 0 & 0 \\ 0 & M_H^2 & 0 \\ 0 & 0 & M_A^2 \end{pmatrix} \mathcal{R}, \quad \begin{pmatrix} h \\ H \\ A \end{pmatrix} = \mathcal{R} \begin{pmatrix} S_1 \\ S_2 \\ S_3 \end{pmatrix}. \quad (2.19)$$

Since the trace remains invariant, the masses satisfy the relation

$$M_h^2 + M_H^2 + M_A^2 = 2 M_{H^\pm}^2 + v^2 (2 \lambda_1 + \lambda_4). \quad (2.20)$$

The minimization conditions allow us to trade the parameters μ_1 and μ_3 by v and λ_6 . The freedom to rephase the field Φ_2 implies, moreover, that only the relative phases among λ_5 , λ_6 and λ_7 are physical; but only two of them are independent. Therefore, we can fully characterize the potential with 11 parameters: v , μ_2 , $|\lambda_{1,\dots,7}|$, $\arg(\lambda_5 \lambda_6^*)$ and $\arg(\lambda_5 \lambda_7^*)$. Four parameters can be determined through the physical scalar masses. The matrix equation [15]

$$(\mathcal{M} \mathcal{R}^T - \mathcal{R}^T \mathcal{M}_D) = 0 \quad (2.21)$$

(where \mathcal{M}_D is the diagonal mass matrix from (2.19)) relates the scalar masses and mixings. Summing the second row with $(-i)$ times the third row, one obtains the identity (imaginary parts included):

$$v^2 \lambda_6 \mathcal{R}_{i1} + \left[M_{H^\pm}^2 - M_{\varphi_i^0}^2 + v^2 \left(\frac{\lambda_4}{2} + \lambda_5 \right) \right] (\mathcal{R}_{i2} - i \mathcal{R}_{i3}) + 2i v^2 \lambda_5 \mathcal{R}_{i3} = 0. \quad (2.22)$$

This proves in full generality that

$$\begin{aligned} (\mathcal{R}_{i2} - i\mathcal{R}_{i3}) \frac{M_{\varphi_i^0}^2 - M_{H^\pm}^2}{v^2} &= (\mathcal{R}_{i2} - i\mathcal{R}_{i3}) \left(\frac{\lambda_4}{2} + \lambda_5 \right) + 2i\mathcal{R}_{i3}\lambda_5 + \mathcal{R}_{i1}\lambda_6 \\ &= \lambda_{H^+G^-\varphi_i^0}. \end{aligned} \quad (2.23)$$

Taking instead the first row, one gets:

$$(2\lambda_1 v^2 - M_{\varphi_i^0}^2) \mathcal{R}_{i1} + v^2 \lambda_6^R \mathcal{R}_{i2} - v^2 \lambda_6^I \mathcal{R}_{i3} = 0, \quad (2.24)$$

which generalizes the usual relation determining $\tan \tilde{\alpha}$ in the CP-conserving limit ($\mathcal{R}_{13} = \mathcal{R}_{23} = 0$). It also proves that the following identity holds in general

$$\frac{M_{\varphi_i^0}^2}{v^2} \mathcal{R}_{i1} = 2\mathcal{R}_{i1}\lambda_1 + i\mathcal{R}_{i3}\lambda_6 + (\mathcal{R}_{i2} - i\mathcal{R}_{i3})\lambda_6^R = \lambda_{G^+G^-\varphi_i^0}. \quad (2.25)$$

Here, similarly to Eq. (2.12), we have parametrized the Goldstone terms of V_3 in the form

$$\left(v \lambda_{H^+G^-\varphi_i^0} H^+ G^- \varphi_i^0 + \text{h.c.} \right) + v \lambda_{G^+G^-\varphi_i^0} G^+ G^- \varphi_i^0 \subset V_3. \quad (2.26)$$

These identities generalize the ones from [16], that are valid only in the CP-conserving limit of the scalar potential. They turn out to be very useful if one works in R_ξ gauges with a fully general potential.

Using again Eq. (2.24), the orthogonality of \mathcal{R} implies:

$$\begin{aligned} \sum_i \mathcal{R}_{i1}^2 M_{\varphi_i^0}^2 &= 2\lambda_1 v^2, & \sum_i \mathcal{R}_{i1} \mathcal{R}_{i2} M_{\varphi_i^0}^2 &= \lambda_6^R v^2, \\ \sum_i \mathcal{R}_{i1} \mathcal{R}_{i3} M_{\varphi_i^0}^2 &= -\lambda_6^I v^2. \end{aligned} \quad (2.27)$$

Eq. (2.22) gives the additional orthogonality relations.

$$\sum_i \mathcal{R}_{i1} (\mathcal{R}_{i2} - i\mathcal{R}_{i3}) M_{\varphi_i^0}^2 = \lambda_6 v^2, \quad (2.28)$$

$$\sum_i \mathcal{R}_{i2} (\mathcal{R}_{i2} - i\mathcal{R}_{i3}) M_{\varphi_i^0}^2 = M_{H^\pm}^2 + v^2 \left(\frac{\lambda_4}{2} + \lambda_5 \right), \quad (2.29)$$

$$i \sum_i \mathcal{R}_{i3} (\mathcal{R}_{i2} - i\mathcal{R}_{i3}) M_{\varphi_i^0}^2 = M_{H^\pm}^2 + v^2 \left(\frac{\lambda_4}{2} - \lambda_5 \right). \quad (2.30)$$

The first identity reproduces in complex form the last two real equations in (2.27). Separating the real and imaginary parts of the last two relations, one gets:

$$\sum_i \mathcal{R}_{i2}^2 M_{\varphi_i^0}^2 = M_{H^\pm}^2 + v^2 \left(\frac{\lambda_4}{2} + \lambda_5^{\text{R}} \right), \quad (2.31)$$

$$\sum_i \mathcal{R}_{i3}^2 M_{\varphi_i^0}^2 = M_{H^\pm}^2 + v^2 \left(\frac{\lambda_4}{2} - \lambda_5^{\text{R}} \right), \quad (2.32)$$

$$\sum_i \mathcal{R}_{i2} \mathcal{R}_{i3} M_{\varphi_i^0}^2 = -v^2 \lambda_5^{\text{I}}. \quad (2.33)$$

In the CP conserving limit $\lambda_5^{\text{I}} = \lambda_6^{\text{I}} = \lambda_7^{\text{I}} = 0$ and S_3 does not mix with the other neutral fields. The scalar spectrum contains then a CP-odd field $A = S_3$ and two CP-even scalars h and H which mix through the rotation matrix (2.4). In this case, the scalar masses are given by

$$\begin{aligned} \bar{M}_h^2 &= \frac{1}{2} (\Sigma - \Delta), & \bar{M}_H^2 &= \frac{1}{2} (\Sigma + \Delta), \\ \bar{M}_A^2 &= M_{H^\pm}^2 + v^2 \left(\frac{\lambda_4}{2} - \lambda_5^{\text{R}} \right), \end{aligned} \quad (2.34)$$

where Σ and Δ are given by

$$\Sigma = M_{H^\pm}^2 + v^2 \left(2\lambda_1 + \frac{\lambda_4}{2} + \lambda_5^{\text{R}} \right), \quad (2.35)$$

$$\Delta = \sqrt{\left[M_{H^\pm}^2 + v^2 \left(-2\lambda_1 + \frac{\lambda_4}{2} + \lambda_5^{\text{R}} \right) \right]^2 + 4v^4 (\lambda_6^{\text{R}})^2}, \quad (2.36)$$

and where the mixing angle is determined through

$$\tan \tilde{\alpha} = \frac{\bar{M}_h^2 - 2\lambda_1 v^2}{v^2 \lambda_6^{\text{R}}}. \quad (2.37)$$

Here, we have used the notation $\bar{M}_{\varphi_i^0}$ to emphasize that these are the neutral scalar masses in the CP-conserving limit. The cubic and quartic Higgs couplings involving the charged and the neutral physical scalars (without Goldstone boson

couplings) take the form,

$$\begin{aligned}
V_3 = & v H^+ H^- \left(\lambda_3 S_1 + \lambda_7^R S_2 - \lambda_7^I S_3 \right) + \frac{1}{2} v \left(2\lambda_5^R + \lambda_3 + \lambda_4 \right) S_1 S_2^2 \\
& + \lambda_1 v S_1^3 + \frac{1}{2} v \lambda_7^R S_2^3 + \frac{3}{2} v \lambda_6^R S_1^2 S_2 - \frac{1}{2} v \lambda_7^I S_3^3 - \frac{1}{2} v \lambda_7^I S_2^2 S_3 \\
& - \frac{1}{2} v \left(2\lambda_5^R - \lambda_3 - \lambda_4 \right) S_1 S_3^2 + \frac{1}{2} v \lambda_7^R S_2 S_3^2 - 2 v \lambda_5^I S_1 S_2 S_3 \\
& - \frac{3}{2} v \lambda_6^I S_1^2 S_3, \tag{2.38}
\end{aligned}$$

$$\begin{aligned}
V_4 = & H^+ H^- \left(\lambda_2 H^+ H^- + \frac{\lambda_3}{2} S_1^2 + \lambda_2 S_3^2 + \lambda_2 S_2^2 - \lambda_7^I S_1 S_3 + \lambda_7^R S_1 S_2 \right) \\
& + \frac{1}{4} \left(\lambda_3 + \lambda_4 + 2\lambda_5^R \right) (S_1 S_2)^2 + \frac{1}{4} \left(\lambda_3 + \lambda_4 - 2\lambda_5^R \right) (S_1 S_3)^2 \\
& - \frac{1}{2} \lambda_6^I S_1^3 S_3 - \lambda_5^I S_1^2 S_2 S_3 - \frac{\lambda_7^I}{2} S_1 S_2^2 S_3 - \frac{\lambda_7^I}{2} S_1 S_3^3 \\
& + \frac{\lambda_1}{4} S_1^4 + \frac{\lambda_2}{4} S_2^4 + \frac{\lambda_2}{4} S_3^4 + \frac{\lambda_2}{2} (S_2 S_3)^2 \\
& + \frac{\lambda_6^R}{2} S_1^3 S_2 + \frac{\lambda_7^R}{2} S_1 S_2^3 + \frac{\lambda_7^R}{2} S_1 S_2 S_3^2. \tag{2.39}
\end{aligned}$$

In the CP-conserving limit all vertices involving an odd number of S_3 fields vanish. A basis-independent discussion of the 2HDM scalar sector can be found in Ref. [17].

2.2.1 Neutral scalar mass matrix to lowest order in CP violation

Assuming that λ_5^I and λ_6^I are small, we can diagonalize the mass matrix (2.18) perturbatively as an expansion in powers of these CP-violating parameters. The leading corrections to the neutral scalar masses are quadratic in $\lambda_{5,6}^I$:

$$M_{\varphi_i^0}^2 = \bar{M}_{\varphi_i^0}^2 + \alpha_1^{\varphi_i^0} (\lambda_5^I)^2 + \alpha_2^{\varphi_i^0} (\lambda_6^I)^2 + \alpha_3^{\varphi_i^0} (\lambda_5^I \lambda_6^I), \tag{2.40}$$

where $\bar{M}_{\varphi_i^0}$ denote the corresponding masses in the CP-conserving limit given in (2.34) and

$$\begin{aligned}\alpha_1^{\varphi_i^0} &= \frac{v^4 \left(\bar{M}_{\varphi_i^0}^2 - 2\lambda_1 v^2 \right)}{\prod_{j \neq i} \left(\bar{M}_{\varphi_j^0}^2 - \bar{M}_{\varphi_i^0}^2 \right)}, \\ \alpha_2^{\varphi_i^0} &= \frac{v^4 \left(2\lambda_1 v^2 + \bar{M}_{\varphi_i^0}^2 - \bar{M}_H^2 - \bar{M}_h^2 \right)}{\prod_{j \neq i} \left(\bar{M}_{\varphi_j^0}^2 - \bar{M}_{\varphi_i^0}^2 \right)}, \\ \alpha_3^{\varphi_i^0} &= \frac{2v^6 \lambda_6^R}{\prod_{j \neq i} \left(\bar{M}_{\varphi_j^0}^2 - \bar{M}_{\varphi_i^0}^2 \right)}.\end{aligned}\tag{2.41}$$

The physical states $\varphi_i^0 = \{h, H, A\}$ receive corrections at first order in $\lambda_{5,6}^I$, which are given by

$$\begin{pmatrix} h \\ H \\ A \end{pmatrix} = \begin{pmatrix} \cos \tilde{\alpha} & \sin \tilde{\alpha} & \epsilon_{13} \\ -\sin \tilde{\alpha} & \cos \tilde{\alpha} & \epsilon_{23} \\ \epsilon_{31} & \epsilon_{32} & 1 \end{pmatrix} \begin{pmatrix} S_1 \\ S_2 \\ S_3 \end{pmatrix},\tag{2.42}$$

where

$$\begin{aligned}\epsilon_{13} &= \frac{v^2}{\left(\bar{M}_A^2 - \bar{M}_h^2 \right)} \left(\sin \tilde{\alpha} \lambda_5^I + \cos \tilde{\alpha} \lambda_6^I \right), \\ \epsilon_{23} &= \frac{v^2}{\left(\bar{M}_A^2 - \bar{M}_H^2 \right)} \left(\cos \tilde{\alpha} \lambda_5^I - \sin \tilde{\alpha} \lambda_6^I \right), \\ \epsilon_{31} &= -\frac{1}{2v^2} \left(\alpha_3^A \lambda_5^I + 2\alpha_2^A \lambda_6^I \right), \\ \epsilon_{32} &= -\frac{1}{2v^2} \left(2\alpha_1^A \lambda_5^I + \alpha_3^A \lambda_6^I \right).\end{aligned}\tag{2.43}$$

Note that for the case of a scalar potential with a softly-broken \mathcal{Z}_2 symmetry in the Higgs basis we have $\lambda_6 = \lambda_7 = 0$ and, therefore, $\epsilon_{31} = 0$.

2.3 Scalar Couplings to the Gauge Bosons

The scalar doublets couple to the gauge bosons through the covariant derivative and gauge-fixing terms:

$$\mathcal{L}_K + \sum_{i=1}^2 (D_\mu \Phi_a)^\dagger D^\mu \Phi_a + \mathcal{L}_{\text{GF}} = \mathcal{L}_{V^2} + \mathcal{L}_{\phi^2} + \mathcal{L}_{\phi V} + \mathcal{L}_{\phi^2 V} + \mathcal{L}_{\phi V^2} + \mathcal{L}_{\phi^2 V^2}, \quad (2.44)$$

where \mathcal{L}_K is the usual gauge-boson kinetic term and the covariant derivative is given by³

$$D_\mu = \partial_\mu + ieQA_\mu + i\frac{g}{\cos\theta_W} Z_\mu(T_3 - Q\sin^2\theta_W) + ig\left[T_+W_\mu^\dagger + T_-W_\mu\right]. \quad (2.45)$$

It is convenient to adopt the following R_ξ gauge-fixing term ($\xi = 1$),

$$\begin{aligned} \mathcal{L}_{\text{GF}} = & -\frac{1}{2}(\partial_\mu A^\mu)^2 - (\partial^\mu W_\mu^\dagger + iM_W G^+) (\partial_\nu W^\nu - iM_W G^-) \\ & -\frac{1}{2}(\partial_\mu Z^\mu + M_Z G^0)^2, \end{aligned} \quad (2.46)$$

which cancels exactly the quadratic mixing terms between the gauge and Goldstone bosons generated by the covariant derivatives, so that $\mathcal{L}_{\phi V} = 0$, and provides the Goldstone bosons with the masses $M_{G^\pm} = M_W = gv/2$ and $M_{G^0} = M_Z = M_W/\cos\theta_W$. Then,

$$\begin{aligned} \mathcal{L}_{V^2} = & -\frac{1}{2}(\partial_\mu A^\mu)^2 - \frac{1}{2}(\partial_\mu Z^\mu)^2 + \frac{1}{2}M_Z^2 Z_\mu Z^\mu \\ & - (\partial^\mu W_\mu^\dagger)(\partial_\nu W^\nu) + M_W^2 W_\mu^\dagger W^\mu, \end{aligned} \quad (2.47)$$

while

$$\begin{aligned} \mathcal{L}_{\phi^2} = & \frac{1}{2}[\partial_\mu h \partial^\mu h + \partial_\mu H \partial^\mu H + \partial_\mu A \partial^\mu A] + \partial_\mu H^+ \partial^\mu H^- \\ & + \frac{1}{2}\partial_\mu G^0 \partial^\mu G^0 - \frac{1}{2}M_Z^2 (G^0)^2 \\ & + \partial_\mu G^+ \partial^\mu G^- - M_W^2 G^+ G^-. \end{aligned} \quad (2.48)$$

³The weak mixing angle θ_W is defined through the relation $g \sin\theta_W = g' \cos\theta_W = e$. The operators $T_\pm = \frac{1}{\sqrt{2}}(T_1 \pm T_2)$ and T_3 can be expressed in terms of the Pauli matrices by $T_i = \frac{\sigma_i}{2}$.

The interaction terms between the scalar and gauge bosons are given by:

$$\begin{aligned}
\mathcal{L}_{\phi^2 V} &= ie \left[A^\mu + \cot(2\theta_W) Z^\mu \right] \left[(H^+ \overleftrightarrow{\partial}_\mu H^-) + (G^+ \overleftrightarrow{\partial}_\mu G^-) \right] \\
&\quad + \frac{e}{\sin(2\theta_W)} Z^\mu \left[(G^0 \overleftrightarrow{\partial}_\mu S_1) + (S_3 \overleftrightarrow{\partial}_\mu S_2) \right] \\
&\quad + \frac{g}{2} W^{\mu\dagger} \left[(H^- \overleftrightarrow{\partial}_\mu S_3) - i (H^- \overleftrightarrow{\partial}_\mu S_2) \right. \\
&\quad\quad\quad \left. + (G^- \overleftrightarrow{\partial}_\mu G^0) - i (G^- \overleftrightarrow{\partial}_\mu S_1) \right] \\
&\quad + \frac{g}{2} W^\mu \left[(H^+ \overleftrightarrow{\partial}_\mu S_3) + i (H^+ \overleftrightarrow{\partial}_\mu S_2) \right. \\
&\quad\quad\quad \left. + (G^+ \overleftrightarrow{\partial}_\mu G^0) + i (G^+ \overleftrightarrow{\partial}_\mu S_1) \right], \tag{2.49}
\end{aligned}$$

$$\begin{aligned}
\mathcal{L}_{\phi V^2} &= \frac{2}{v} S_1 \left[\frac{1}{2} M_Z^2 Z_\mu Z^\mu + M_W^2 W_\mu^\dagger W^\mu \right] \\
&\quad + \left(e M_W A^\mu - g M_Z \sin^2 \theta_W Z^\mu \right) \left(G^+ W_\mu + G^- W_\mu^\dagger \right), \tag{2.50}
\end{aligned}$$

$$\begin{aligned}
\mathcal{L}_{\phi^2 V^2} &= \frac{1}{v^2} \left[\frac{1}{2} M_Z^2 Z_\mu Z^\mu + M_W^2 W_\mu^\dagger W^\mu \right] \left[H^2 + h^2 + A^2 + (G^0)^2 \right] \\
&\quad + \left\{ e^2 [A^\mu + \cot(2\theta_W) Z^\mu]^2 + \frac{g^2}{2} W_\mu^\dagger W^\mu \right\} (G^+ G^- + H^+ H^-) \\
&\quad + \frac{eg}{2} (A^\mu - \tan \theta_W Z^\mu) \left[S_1 (G^+ W_\mu + G^- W_\mu^\dagger) \right. \\
&\quad\quad\quad + S_2 (H^+ W_\mu + H^- W_\mu^\dagger) + i S_3 (H^- W_\mu^\dagger - H^+ W_\mu) \\
&\quad\quad\quad \left. + i G^0 (G^- W_\mu^\dagger - G^+ W_\mu) \right], \tag{2.51}
\end{aligned}$$

with $S_i = \mathcal{R}_{ji} \varphi_j^0$ ($\varphi_j^0 = \{h, H, A\}$) and where we have introduced the usual notation $A \overleftrightarrow{\partial}_\mu B \equiv A(\partial_\mu B) - (\partial_\mu A)B$.

2.3.1 Inert 2HDM

Imposing a discrete \mathcal{Z}_2 symmetry such that all SM fields remain invariant under a \mathcal{Z}_2 transformation, while

$$\Phi_1 \rightarrow \Phi_1, \quad \Phi_2 \rightarrow -\Phi_2, \quad (2.52)$$

one makes the second scalar doublet *inert*: linear interactions of Φ_2 with the SM fields are odd under a \mathcal{Z}_2 transformation, and thus forbidden [18, 19]. In particular, Φ_2 is fermiophobic. This inert scalar doublet can only interact with the other fields through quadratic couplings. The lightest neutral component of Φ_2 is then a very good candidate for dark matter.

The \mathcal{Z}_2 symmetry implies a significant simplification of the scalar potential, because all terms with an odd number of Φ_2 fields vanish: $\mu_3 = \lambda_6 = \lambda_7 = 0$. Moreover, making an appropriate rephasing of Φ_2 , λ_5 can be taken real. Therefore, the neutral mass matrix (2.18) becomes diagonal and there is no mixing among the neutral scalars ($\mathcal{R} = I$). The neutral scalar masses are given by:

$$\begin{aligned} M_h^2 &= 2\lambda_1 v^2, & M_H^2 &= M_{H^\pm}^2 + \left(\frac{\lambda_4}{2} + \lambda_5\right) v^2, \\ M_A^2 &= M_{H^\pm}^2 + \left(\frac{\lambda_4}{2} - \lambda_5\right) v^2. \end{aligned} \quad (2.53)$$

A generalization of the *inert* model, in which, in particular, the charged Higgs and the neutral scalar A are fermiophobic will be analysed later on, in Chapter 7.

BIBLIOGRAPHY

- [1] A. Pich and P. Tuzón, Phys. Rev. D **80** (2009) 091702 [arXiv:0908.1554 [hep-ph]].
- [2] N. Cabibbo, Phys. Rev. Lett. **10** (1963) 531; M. Kobayashi, T. Maskawa, Prog. Theor. Phys. **49** (1973) 652.
- [3] A. Pich, Nucl. Phys. Proc. Suppl. **209** (2010) 182 [arXiv:1010.5217 [hep-ph]].
- [4] M. Jung, A. Pich and P. Tuzón, JHEP **1011** (2010) 003 [arXiv:1006.0470 [hep-ph]].
- [5] P. M. Ferreira, L. Lavoura and J. P. Silva, Phys. Lett. B **688** (2010) 341 [arXiv:1001.2561 [hep-ph]].
- [6] C. B. Braeuninger, A. Ibarra and C. Simonetto, Phys. Lett. B **692** (2010) 189 [arXiv:1005.5706 [hep-ph]].
- [7] M. Jung, A. Pich and P. Tuzón, Phys. Rev. D **83** (2011) 074011 [arXiv:1011.5154 [hep-ph]].
- [8] M. Jung, X. -Q. Li and A. Pich, JHEP **1210** (2012) 063 [arXiv:1208.1251 [hep-ph]].
- [9] A. Celis, M. Jung, X. -Q. Li and A. Pich, JHEP **1301** (2013) 054 [arXiv:1210.8443 [hep-ph]].
- [10] H. Serodio, Phys. Lett. B **700** (2011) 133 [arXiv:1104.2545 [hep-ph]].
- [11] I. de Medeiros Varzielas, Phys. Lett. B **701** (2011) 597 [arXiv:1104.2601 [hep-ph]].
- [12] G. Cree and H. E. Logan, Phys. Rev. D **84** (2011) 055021 [arXiv:1106.4039 [hep-ph]].
- [13] M. Farina, C. Grojean and E. Salvioni, JHEP **1207** (2012) 012 [arXiv:1205.0011 [hep-ph]].

- [14] A. Celis, V. Ilisie and A. Pich, JHEP **1307** (2013) 053 [arXiv:1302.4022 [hep-ph]].
- [15] V. Ilisie and A. Pich, JHEP **1409** (2014) 089 [arXiv:1405.6639 [hep-ph]].
- [16] J. F. Gunion and H. E. Haber, *The CP-conserving two-Higgs-doublet model: the approach to the decoupling limit*, Phys. Rev. D **67** 075019 [hep-ph/0207010].
- [17] H. E. Haber and D. O'Neil, Phys. Rev. D **74** (2006) 015018 [hep-ph/0602242].
- [18] E. Ma, *Utility of a Special Second Scalar Doublet*, Mod. Phys. Lett. A **23** (2008) 647 [arXiv:0802.2917 [hep-ph]];
- [19] E. Ma, *Verifiable radiative seesaw mechanism of neutrino mass and dark matter*, Phys. Rev. D **73** (2006) 077301 [hep-ph/0601225].

3. MOTIVATION AND PRELIMINARIES

The SM is so far, one of the most successful and predictive models in the whole realm of physics. The last piece of the SM puzzle was the Higgs boson. For many decades, this scalar particle has eluded the experimental discovery, however, nowadays, this seems no longer to be the case. In 2012 the ATLAS and CMS collaborations announced the discovery of a scalar boson compatible with the SM predictions [1, 2]. However, having found a Higgs-like scalar boson compatible with the SM predictions does not exclude the possibility of having an enlarged scalar sector, or some other type of new physics (even strongly interacting), that would mimic a Higgs-like boson, as we have already insisted in previous chapters. In general, there is no fundamental *guiding* symmetry or principle that forbids us to extend the SM by adding more scalar doublets for example, or by enlarging the model with new particles or interactions in general. All of these extensions, must of course, pass all the available experimental constraints and precision fits and (should) make new predictions that could be tested by future experiments.

In this work, we analyse two of these types of extensions. First, we shall consider particles that belong to higher order representations of the QCD group (Paper I, Chapter 4). As for the second part (Papers II-V, Chapters 5 to 8), we will extensively treat the many aspects of the rich phenomenology of the two-Higgs-doublet model.

3.1 Paper I

Exotic quark-like fermions that belong to higher representations of the $SU(3)_C$ colour group are an interesting possibility which was previously considered [3–7]. We can search for the presence of such exotic quarks in direct and indirect ways. Since not a single exotic QCD particle has been directly observed so far, their masses should be heavy enough to avoid the present experimental constraints from direct searches. However, new fermions from higher QCD representations would contribute to the QCD β -function and, therefore, their existence is highly constrained by the very successful experimental tests of asymptotic freedom. Also, if those exotic quarks get their masses through the Standard Model Higgs mech-

anism, they would strongly enhance the Higgs production at LHC, which seems not to be the case with the present collider data.

At the two-loop level the β function is given by [8, 9]

$$\begin{aligned}\beta_1 &= -\frac{11}{6} C_A + \frac{2}{3} \sum_R n_R T_R, \\ \beta_2 &= -\frac{17}{12} C_A^2 + \frac{1}{6} \sum_R n_R T_R (5 C_A + 3 C_R),\end{aligned}\tag{3.1}$$

with n_R the number of active fermions in the representation R , T_R is the normalization trace factor and C_R the Casimir operator eigenvalue. More details are given in Section 1.3.1 of Chapter 1. The values of the various trace factor for different representations are given by $T_3 = \frac{1}{2}$, $T_6 = \frac{5}{2}$, $T_A = 3$, $T_{10} = \frac{15}{2}$, $T_{15} = 10$, etc. Due to the large algebraic contribution of these higher colour representations asymptotic freedom is rapidly lost.

The same large algebraic factors would contribute to the dominant (gluon fusion) Higgs production cross section. By the time this project was finished, the mass of Higgs boson was still unknown. However we were able to exclude a large region of Higgs mass parameter space. After the discovery of the scalar boson at the LHC, this work gains in relevance. Supposing that it is indeed the SM Higgs, the existence of all exotic quarks is excluded (given, of course, that this exotic matter acquires mass through the SM Higgs mechanism).

3.2 Paper II

The discovery of a Standard Model-like boson with mass of about 125 GeV seems to be the first direct information on the electroweak symmetry breaking mechanism. It brings us to a whole new horizon of possibilities regarding its nature and origin. Many theoretical models (SM extensions) are able to reproduce the properties of this particle. The simplest extension that gives rise to a richer scalar sector and to new interesting phenomenology in the flavour sector is the Two-Higgs-Doublet Model.

In this work we study the phenomenology of the scalar sector and see how the new LHC data constrains its parameter space. The main feature of the 2HDM is the presence of three neutral and one charged Higgs bosons, thus we study all possible interpretations for the discovered scalar boson as one of the three neutral scalars of the model. The electroweak precision fits are used to constrain the mass scalar spectrum for the remaining bosons. We assume the generic Yukawa texture

of the Aligned Two-Higgs Doublet Model. We also study the implication for the particular models with discrete \mathcal{Z}_2 symmetries.

Using the first relevant data released by the LHC collaborations as well as Tevatron [10–12], one finds a slight excess for the center value of the two-photon decay channel both in gluon-fusion and vector boson fusion production. This excess is highly interesting because it might be the origin of new interesting physics. It could signal the presence of a charged Higgs (by adding an extra loop of a charged Higgs to the $h \rightarrow \gamma\gamma$ decay) or it might originate in a different (than the SM), perhaps complex, Yukawa structure. All these possibilities are also extensively analysed.

3.3 Paper III

In this work we extend the previous analysis and update the bounds that the new LHC and Tevatron data impose on the CP-conserving A2HDM. We discuss the role of electroweak precision observables and include previously studied flavour constraints (such as $Z \rightarrow b\bar{b}$ and $B \rightarrow X_s\gamma$), in order to further restrict the parameter space. We also consider searches for additional neutral Higgs bosons at the LHC.

Last, we analyse the possibility of a light charged Higgs produced via top quark decays i.e., $t \rightarrow H^+b$, and its relevant decay channels $H^+ \rightarrow \tau^+\nu_\tau$, $H^+ \rightarrow c\bar{s}$ and $H^+ \rightarrow c\bar{b}$. This last channel, usually ignored in both experimental and theoretical analyses due to a strong CKM suppression, can be of relevance in the A2HDM. Writing down the following approximate formula

$$\begin{aligned} \frac{\Gamma(H^+ \rightarrow c\bar{b})}{\Gamma(H^+ \rightarrow c\bar{s})} &\simeq \frac{|V_{cb}|^2 (|\zeta_d|^2 m_b^2 + |\zeta_u|^2 m_c^2)}{|V_{cs}|^2 (|\zeta_d|^2 m_s^2 + |\zeta_u|^2 m_c^2)}, \\ \frac{\Gamma(H^+ \rightarrow c\bar{b})}{\Gamma(H^+ \rightarrow \tau^+\nu_\tau)} &\simeq \frac{N_C |V_{cb}|^2 (|\zeta_d|^2 m_b^2 + |\zeta_u|^2 m_c^2)}{m_\tau^2 |\zeta_l|^2}. \end{aligned} \quad (3.2)$$

we can observe that the decay channel $H^+ \rightarrow c\bar{b}$ can be important, compared with $H^+ \rightarrow c\bar{s}$, $\tau^+\nu_\tau$, for $|\zeta_d| \gg |\zeta_u|, |\zeta_l|$. This does not usually occur in the 2HDMs with \mathcal{Z}_2 symmetries due to correlations among the ζ_f parameters. Another channel that is also, usually ignored by most analyses, is the three body decay $H^+ \rightarrow t^*\bar{b} \rightarrow W^+b\bar{b}$. This channel will be found to be relevant in a quite large region of the parameter space of our model. It is also worth mentioning that, combining flavour constraints and bounds from the direct searches for a

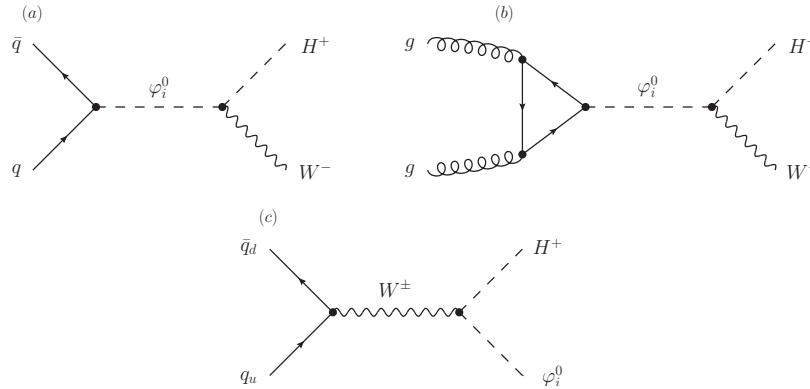


Figure 3.1: *Charged-Higgs associated production with a W boson (diagrams a, b) or a neutral scalar (diagram c), in the fermiophobic scenario.*

charged Higgs at the LHC, one can further eliminate some regions of the allowed parameter space of the model.

3.4 Paper IV

In this analysis we study the phenomenology associated with a fermiophobic charged Higgs (it does not couple to fermions at tree level), in two-Higgs-doublet models. Experimental searches for charged scalars have been already performed with negative results by the ATLAS [13,14] and CMS collaborations [15]. They both assume that the charged Higgs is produced from a top-quark decay ($t \rightarrow H^+b$) and that it decays dominantly into fermions; *i.e.*, $H^+ \rightarrow q_u\bar{q}_d, l^+\nu_l$. However, if the charged Higgs is fermiophobic, all experimental bounds are evaded trivially. One needs to perform in this case a different analysis. One has to consider other decay and production channels. Here, we study the associated production of a charged Higgs with either a W or a neutral scalar boson (see Fig 3.1), and the relevant decays for a light fermiophobic charged Higgs with mass in the range $M_{H^\pm} \in [M_W, M_W + M_Z]$. The kinematically open relevant decay modes are shown in Fig 3.2. For the loop-induced $H^+ \rightarrow W\gamma$, using the gauge symmetry of the process, one can extremely simplify the calculations and obtain simple, compact, analytical results. The calculation technique is also extensively presented.

Due to their similarity with the SM Higgs production channels, one expects the charged Higgs production cross sections to be experimentally accessible at

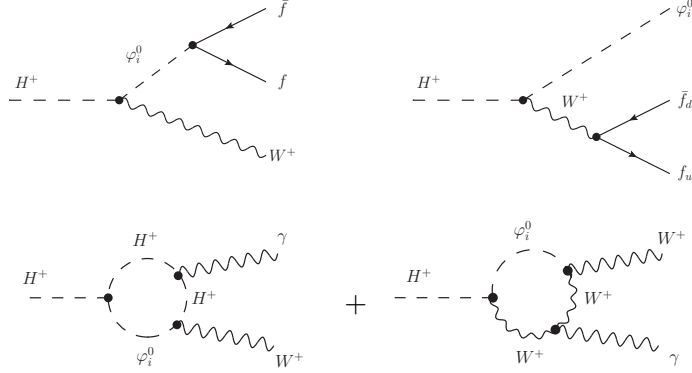


Figure 3.2: *Three-body decay $H^+ \rightarrow W^+ f \bar{f}$ mediated by the virtual neutral scalars φ_i^0 (top,left) and $H^+ \rightarrow \varphi_i^0 f_u \bar{f}_d$ mediated by a virtual W^+ (top,right). Loop induced $H^+ \rightarrow W^+ \gamma$ decay (bottom).*

LHC energies. Next-to-leading order QCD corrections will be included for both cross sections, and the bounds on the various parameters of the model from the LHC data (from our previous work) will also be taken into account.

The interesting features of this scenario should result encouraging for the LHC collaborations to perform searches for such a particle.

3.5 Paper V

In this analysis we use the anomalous magnetic moment of the muon as a probe for new physics and study new contributions to this observable within the 2HDM framework. The latest result for the discrepancy between the SM prediction and the experimental measured value is given by [16–38]

$$\Delta a_\mu^{exp} \equiv a_\mu^{exp} - a_\mu^{SM} = 262(85) \times 10^{-11}. \quad (3.3)$$

The $(g-2)_\mu$ has been extensively analysed within the SM and its various extensions. Even if the SM prediction still suffers from large theoretical uncertainties (mostly hadronic) it is a nice place to look for new physics. It's a known fact that the two-loop Bar-Zee type diagrams dominate over the one-loop contributions. The two-loop contributions have a loop suppression factor of (α/π) but also have an enhancement factor of (M^2/m_μ^2) , where M stands for the mass of heavy particles running in one of the loops: M_{H^\pm} , m_t , $M_{\varphi_i^0}$, etc. This last factor usually dominates over the first one.

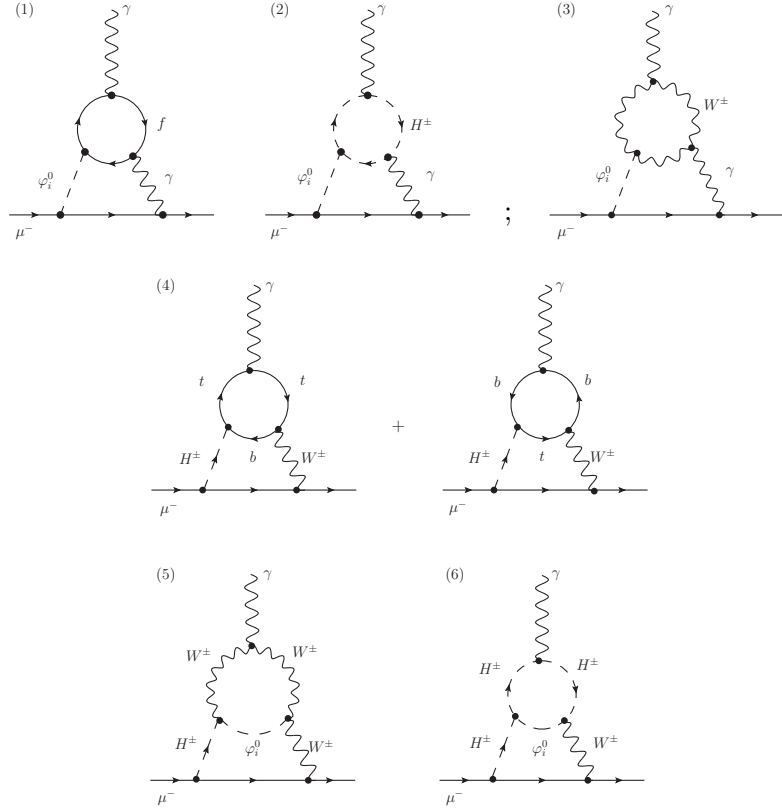


Figure 3.3: *Two-loop Barr-Zee type contributions to Δa_μ in two-Higgs-doublet models .*

Here we study the two-loop Barr-Zee type [39] contributions to Δa_μ that have not been analysed previously within the 2HDMs. Using the same calculation technique as in the previous analysis (Paper V) we can, again, simplify our result and present all the expression in a compact analytical form.

It is a common belief that only a restrained number of diagrams can significantly contribute to Δa_μ in 2HDMs at the two-loop level, namely diagrams (1) and (2) from Fig. 3.3. We show that this is not true, and that some of the new calculated diagrams (3-6, same figure), due to the extra degrees of freedom of the A2HDM given by the ζ_f parameters, can bring rather sizeable contributions for a quite large region of the parameter space and therefore can reduce, and in some cases even explain, the value of the difference between the SM prediction and experiment. A highly interesting scenario, deferred for future work, is to

also consider CP-violating effects. The imaginary part of the parameters of the potential and especially of the Yukawa sector might be able to bring somewhat extra sizeable effects.

3.6 Updated fits from Run 1

Finally, the last chapter, Chapter 9, is dedicated to the update of some relevant parts of the studies performed in Chapters 5 and 6, using the latest LHC combined data (at 7 and 8 TeV) from the Atlas and CMS collaborations [40]. As the experimental data are getting more precise, their impact on the parameter space of the 2HDM is somewhat sizeable when compared to the previous results. While the main conclusions from the previously performed analyses remain roughly the same, the allowed regions for the model parameters will be visibly modified. On the other hand, as the analyses performed in Chapters 7 and 8 are based upon very generic assumptions, the results presented therein are minimally (or not at all) affected by the new LHC results.

BIBLIOGRAPHY

- [1] G. Aad *et al.* [ATLAS Collaboration], *Phys. Lett. B* **716** (2012) 1
doi:10.1016/j.physletb.2012.08.020 [arXiv:1207.7214 [hep-ex]].
- [2] S. Chatrchyan *et al.* [CMS Collaboration], *Phys. Lett. B* **716** (2012) 30
doi:10.1016/j.physletb.2012.08.021 [arXiv:1207.7235 [hep-ex]].
- [3] E. Ma, *Phys. Lett.* **58B** (1975) 442.
- [4] G. Karl, *Phys. Rev.* **D14** (1976) 2374.
- [5] F. Wilczek and A. Zee, *Phys. Rev.* **D16** (1977) 860.
- [6] Y. Ng and S.-H. Tye, *Phys. Rev. Lett.* **41** (1978) 6.
- [7] H. Georgi and S. Glashow, *Nucl. Phys.* **B159** (1979) 29.
- [8] W.E. Caswell, *Phys. Rev. Lett.* **33** (1974) 244.
- [9] D.R.T. Jones, *Nucl. Phys. Rev.* **B75** (1974) 531.
- [10] G. Aad *et al.* [ATLAS Collaboration], *Phys. Lett. B* **716** (2012) 1
[arXiv:1207.7214 [hep-ex]]; ATLAS-CONF-2012-170 (December 13, 2012).
- [11] S. Chatrchyan *et al.* [CMS Collaboration], *Phys. Lett. B* **716** (2012) 30
[arXiv:1207.7235 [hep-ex]]; CMS-PAS-HIG-12-045 (November 16, 2012).
- [12] T. Aaltonen *et al.* [CDF and D0 Collaborations], *Phys. Rev. Lett.* **109**
(2012) 071804 [arXiv:1207.6436 [hep-ex]].
- [13] ATLAS Collaboration, *Search for charged Higgs bosons decaying via $H^+ \rightarrow \tau\nu$ in top quark pair events using pp collision data at $\sqrt{s} = 7$ TeV with the ATLAS detector*, *JHEP* **1206** (2012) 039 [arXiv:1204.2760 [hep-ex]]; ATLAS-CONF-2013-090 (August 25, 2013).
- [14] ATLAS Collaboration, *Search for a light charged Higgs boson in the decay channel $H^+ \rightarrow c\bar{s}$ in $t\bar{t}$ events using pp collisions at $\sqrt{s} = 7$ TeV with the ATLAS detector*, *Eur. Phys. J. C* **73** (2013) 2465 [arXiv:1302.3694 [hep-ex]].

-
- [15] CMS Collaboration, *Search for a light charged Higgs boson in top quark decays in pp collisions at $\sqrt{s} = 7$ TeV*, JHEP **1207** (2012) 143 [arXiv:1205.5736 [hep-ex]].
- [16] A. Broggio, E. J. Chun, M. Passera, K. M. Patel and S. K. Vempati, JHEP **1411** (2014) 058 [arXiv:1409.3199 [hep-ph]].
- [17] L. Wang and X. F. Han, arXiv:1412.4874 [hep-ph].
- [18] T. Aoyama, M. Hayakawa, T. Kinoshita and M. Nio, Phys. Rev. Lett. **109** (2012) 111808 [arXiv:1205.5370 [hep-ph]].
- [19] A. Czarnecki, B. Krause and W. J. Marciano, Phys. Rev. D **52** (1995) 2619 [hep-ph/9506256].
- [20] A. Czarnecki, B. Krause and W. J. Marciano, Phys. Rev. Lett. **76** (1996) 3267 [hep-ph/9512369].
- [21] C. Gnendiger, D. Stöckinger and H. Stöckinger-Kim, Phys. Rev. D **88** (2013) 5, 053005 [arXiv:1306.5546 [hep-ph]].
- [22] F. Jegerlehner and A. Nyffeler, Phys. Rept. **477** (2009) 1 [arXiv:0902.3360 [hep-ph]].
- [23] M. Davier, A. Hoecker, B. Malaescu and Z. Zhang, Eur. Phys. J. C **71** (2011) 1515 [Erratum-ibid. C **72** (2012) 1874] [arXiv:1010.4180 [hep-ph]].
- [24] B. Krause, Phys. Lett. B **390** (1997) 392 [hep-ph/9607259].
- [25] J. Prades, E. de Rafael and A. Vainshtein, (Advanced series on directions in high energy physics. 20) [arXiv:0901.0306 [hep-ph]].
- [26] G. Colangelo, M. Hoferichter, M. Procura and P. Stoffer, JHEP **1409** (2014) 091 [arXiv:1402.7081 [hep-ph]].
- [27] G. Colangelo, M. Hoferichter, B. Kubis, M. Procura and P. Stoffer, Phys. Lett. B **738** (2014) 6 [arXiv:1408.2517 [hep-ph]].
- [28] T. Blum, S. Chowdhury, M. Hayakawa and T. Izubuchi, Phys. Rev. Lett. **114** (2015) 012001 [arXiv:1407.2923 [hep-lat]].
- [29] V. Pauk and M. Vanderhaeghen, Phys. Rev. D **90** (2014) 11, 113012 [arXiv:1409.0819 [hep-ph]].

-
- [30] A. Kurz, T. Liu, P. Marquard and M. Steinhauser, Phys. Lett. B **734** (2014) 144 [arXiv:1403.6400 [hep-ph]].
- [31] G. Colangelo, M. Hoferichter, A. Nyffeler, M. Passera and P. Stoffer, Phys. Lett. B **735** (2014) 90 [arXiv:1403.7512 [hep-ph]].
- [32] T. Blum, A. Denig, I. Logashenko, E. de Rafael, B. Lee Roberts, T. Teubner and G. Venanzoni, arXiv:1311.2198 [hep-ph].
- [33] K. Melnikov and A. Vainshtein, Springer Tracts Mod. Phys. **216** (2006) 1.
- [34] M. Davier and W. J. Marciano, Ann. Rev. Nucl. Part. Sci. **54** (2004) 115.
- [35] M. Passera, J. Phys. G **31** (2005) R75 [hep-ph/0411168].
- [36] M. Knecht, Lect. Notes Phys. **629** (2004) 37 [hep-ph/0307239].
- [37] G. W. Bennett *et al.* [Muon G-2 Collaboration], Phys. Rev. D **73** (2006) 072003 [hep-ex/0602035].
- [38] K. A. Olive *et al.* [Particle Data Group Collaboration], Chin. Phys. C **38** (2014) 090001.
- [39] S. M. Barr and A. Zee, Phys. Rev. Lett. **65** (1990) 21 [Erratum-ibid. **65** (1990) 2920].
- [40] ATLAS-CONF-2015-044; CMS-PAS-HIG-15-002

4. QCD EXOTICS VERSUS A STANDARD MODEL HIGGS

Victor Ilisie and Antonio Pich

IFIC, Universitat de València – CSIC, Apt. Correus 22085, E-46071 València, Spain

Physical Review D: Phys.Rev. D 86(2012)033001, arXiv: 1202.3420

Abstract: The present collider data put severe constraints on any type of new strongly-interacting particle coupling to the Higgs boson. We analyze the phenomenological limits on exotic quarks belonging to non-triplet $SU(3)_C$ representations and their implications on Higgs searches. The discovery of the Standard Model Higgs, in the experimentally allowed mass range, would exclude the presence of exotic quarks coupling to it. Thus, such QCD particles could only exist provided that their masses do not originate in the SM Higgs mechanism.

4.1 Exotic coloured fermions

Exotic matter in higher representations of the $SU(3)_C$ colour group is an appealing possibility which was already considered in the early times of QCD [1–5]. In particular, the sextet representation has been extensively analyzed as a possible source of dynamical electroweak symmetry breaking [6–13]. It is well known that such exotic quarks modify very sizeably the running of the strong coupling and, therefore, their hypothetical existence is strongly constrained by the very successful experimental tests of asymptotic freedom [14].

Since not a single exotic QCD particle has been observed so far, their masses should be heavy enough to avoid the present experimental constraints from direct searches. However, even with very large masses, if those exotic quarks get their masses through the Standard Model Higgs mechanism, they would strongly enhance the production of Higgs bosons at LHC. The non-decoupling character of the Higgs couplings, being proportional to the coupled-object mass, implies sizeable effects from any strongly-interacting heavy mass scale generated by the Higgs mechanism. Therefore, the present collider limits on the production cross section $\sigma(gg \rightarrow H)$ put a very severe constraint on the possible existence of such objects.

Let us consider an exotic spin- $\frac{1}{2}$ fermion X_R , with mass M_X , belonging to the irreducible representation $\underline{R} \equiv (\lambda_1, \lambda_2)$ of $SU(3)_C$. The dimension of the representation is given by $d_R = \frac{1}{2}(\lambda_1 + 1)(\lambda_2 + 1)(\lambda_1 + \lambda_2 + 2)$; the fundamental $\underline{3} = (1, 0)$ [$\underline{3}^* = (0, 1)$] and adjoint $\underline{8} = (1, 1)$ representations have dimensions $d_F = 3$ and $d_A = 8$, respectively. The gluonic couplings of X_R are fixed by the generators t_R^a ($a = 1, \dots, d_A$), satisfying $[t_R^a, t_R^b] = if^{abc} t_R^c$. The quadratic Casimir operator,

$$\sum_{a=1}^{d_A} t_R^a t_R^a = C_R \mathbb{I}_{d_R},$$

$$C_R = \frac{1}{3} \left(\lambda_1^2 + \lambda_2^2 + \lambda_1 \lambda_2 + 3\lambda_1 + 3\lambda_2 \right), \quad (4.1)$$

determines the trace normalization factor for the representation \underline{R} :

$$\text{Tr} \left(t_R^a t_R^b \right) = T_R \delta^{ab}, \quad T_R = \frac{C_R d_R}{d_A}. \quad (4.2)$$

This trace factor grows rapidly with increasing dimensions d_R , implying larger contributions of the exotic object X_R to the relevant QCD cross sections: $T_F = \frac{1}{2}$,

$T_6 = \frac{5}{2}$, $T_A = 3$, $T_{10} = \frac{15}{2}$, $T_{15} = 10 \dots$, where $\underline{6} = (2, 0)$, $\underline{10} = (3, 0)$, $\underline{15} = (2, 1)$ \dots

If kinematically allowed, charged exotic quarks would be copiously produced in e^+e^- annihilation. For a charged X_R the ratio

$$R_{e^+e^-} \equiv \sigma(e^+e^- \rightarrow \text{hadrons})/\sigma(e^+e^- \rightarrow \mu^+\mu^-)$$

would rise dramatically at the production threshold $s = 4M_X^2$ with an additive contribution $\Delta R_{e^+e^-} = d_R Q_X^2 \delta_{\text{QCD}}$. A neutral exotic X_R^0 would be pair-produced at $\mathcal{O}(\alpha_s^2)$ through gluon emission, i.e. $e^+e^- \rightarrow q\bar{q}g \rightarrow q\bar{q}X_R^0\bar{X}_R^0$. Independently of their electric charge, exotic quarks would imply large modifications of the hadronic cross sections at pp and $p\bar{p}$ colliders and a proliferation of new hadrons containing X_R constituents (unless the X_R lifetime is too small to hadronize). The absence of any exotic signal in the present data puts the lower limit on the mass M_X well above 100 or 200 GeV.

New fermions in higher QCD representations would contribute to the QCD β function

$$\mu \frac{d\alpha_s}{d\mu} = \alpha_s \beta(\alpha_s), \quad \beta(\alpha_s) = \sum_{n=1} \beta_n \left(\frac{\alpha_s}{\pi}\right)^n. \quad (4.3)$$

At the two loop level [15, 16],

$$\begin{aligned} \beta_1 &= -\frac{11}{6} C_A + \frac{2}{3} \sum_R n_R T_R, \\ \beta_2 &= -\frac{17}{12} C_A^2 + \frac{1}{6} \sum_R n_R T_R (5 C_A + 3 C_R), \end{aligned} \quad (4.4)$$

where n_R is the number of fermion flavours in the representation \underline{R} . In the three-generation Standard Model ($n_F = 6$) both β_1 and β_2 are negative. In order to flip the sign of β_1 (β_2), $n_F > 16$ (8) triplet quarks would be needed. However, the larger algebraic contribution of a higher colour representation implies a much faster loss of asymptotic freedom. Keeping $n_F = 6$, the only possible additions preserving $\beta_1 < 0$ are at most two sextet or one octet fermion representations; but even a single sextet flips already the sign of β_2 . Since the running of α_s has been successfully tested with high precision (at the four loop level) from the τ mass scale [17, 18] up to energies above 200 GeV [14], exotic quarks in higher QCD representations are clearly excluded in this energy domain [19–23].

Higher energy scales are presently being explored at the LHC, where the main production mechanism of exotic QCD fermions is $gg \rightarrow X_R \bar{X}_R$, with a subdominant contribution from $q\bar{q} \rightarrow X_R \bar{X}_R$. The calculation of the corresponding

partonic cross sections is straightforward at tree level; we obtain

$$\begin{aligned}\sigma(gg \rightarrow X_R \bar{X}_R) &= \frac{\pi\alpha_s^2}{16s} C_R d_R \mathcal{G}\left(\frac{4M_X^2}{s}\right), \\ \sigma(q\bar{q} \rightarrow X_R \bar{X}_R) &= \frac{2\pi\alpha_s^2}{27s} C_R d_R \left(1 + \frac{2M_X^2}{s}\right) \sqrt{1 - \frac{4M_X^2}{s}},\end{aligned}\tag{4.5}$$

where

$$\begin{aligned}\mathcal{G}(x) &= \left[\left(1 + x - \frac{x^2}{2}\right) C_R + \frac{3}{4}x^2 \right] \ln\left(\frac{1 + \sqrt{1-x}}{1 - \sqrt{1-x}}\right) \\ &\quad - \left[(1+x)C_R + 1 + \frac{5}{4}x \right] \sqrt{1-x},\end{aligned}\tag{4.6}$$

in agreement with Ref. [24]. Particularizing to the fundamental representation, one gets the well-known results for quark-antiquark production [25]. The production of exotic fermions in higher representations is enhanced by the global algebraic factor $\xi_R = C_R d_R / (C_F d_F)$ [$\xi_6 = 5$, $\xi_8 = 6$, $\xi_{10} = 15$, $\xi_{15} = 20$, ...], which is further reinforced by another factor C_R/C_F in the leading parts of the 2-gluon contribution. Figure 4.1 shows the ratio $\sigma(pp \rightarrow X_R \bar{X}_R)/\sigma(pp \rightarrow q\bar{q})$ at $\sqrt{s} = 7$ TeV, as a function of M_X , for the representations with lower dimensions. We have convoluted the partonic cross sections with standard parton distribution functions and have assumed a common K factor for all representations; i.e., we have taken the same QCD corrections as for triplet quark production. This is a very conservative assumption because, given the larger algebraic factors, gluonic corrections should be larger for higher colour representations. Thus, the curves in Fig. 4.1 are actually lower bounds on the expected production ratios. The enhancement factors are predicted to be larger than 10 for sextet and octet fields and much higher values are obtained for higher-dimensional representations.

Once produced, the exotic X_R particles should decay strongly generating an excess of (multi) jet events. Fermionic objects in the triplet, sextet and 15 representations could couple to a qg ($\bar{q}g$) operator and are thus expected to produce 2-jet events, while fermionic octets and decuplets have qqq ($\bar{q}\bar{q}\bar{q}$) quantum numbers and should be looked for in 3-jet events [24]. The generic 2-jet searches performed at the LHC [26, 27] have not found any evidence for new particle production, severely constraining narrow resonances decaying into qq , qg or gg final states. The lower limits on different types of strongly-interacting particles have been pushed up beyond the 1 TeV scale; for instance the data excludes

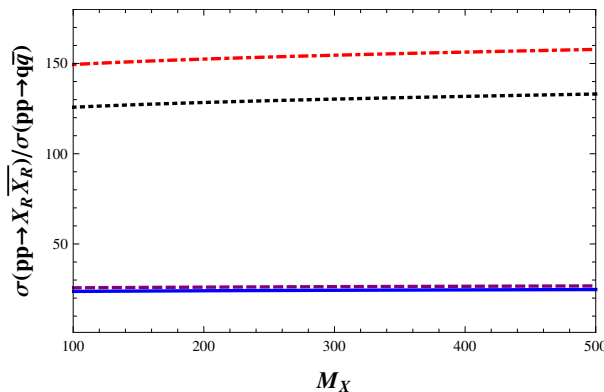


Figure 4.1: Ratio $\sigma(pp \rightarrow X_R \bar{X}_R) / \sigma(pp \rightarrow q\bar{q})$ at $\sqrt{s} = 7\text{TeV}$, as a function of M_X . The different curves correspond to the exotic fermion X_R in the sextet (continuous, blue), octet (dashed, violet), decuplet (dotted, black) and $\underline{15}$ (dash-dotted, red) representations.

at 95% CL excited quarks with mass below 2.64 TeV or coloured octet scalars with mass below 1.92 TeV. Searches with 3 jets have been already performed by CMS [28] and CDF [29]; no significant excess has been found, excluding gluino masses up to 280 GeV¹.

A dedicated search for stable quarks in higher colour representations was performed a long time ago by CDF [34]. No such particles were found in 26.2nb^{-1} of data; at 95% CL, the resulting lower limits for M_X were 98 (84) GeV for color sextets, 99 (86) GeV for octets, and 137 (121) GeV for decuplets, assuming that X_R carries charge one (either one or zero). A recent CMS search for heavy stable charged particles produced at LHC has put a lower limit of 808 GeV (95% CL) on a stable gluino, under the conservative hypothesis that any hadron containing this particle becomes neutral before reaching the muon detectors (relaxing this hypothesis, the limit improves to 899 GeV) [35]. Slightly weaker bounds have been set by ATLAS through a search for slow-moving gluino-based R-hadrons [36].

The present 95% CL limits on fourth-generation quarks, $m_{Q'} > 350\text{GeV}$ [37], $m_{b'} > 372\text{GeV}$ [38] and $m_{t'} > 404\text{GeV}$ [39–41] assume the decays (with 100% branching fraction) $Q' \rightarrow Wq$, $b' \rightarrow Wt$ and $t' \rightarrow Wb$, respectively. While these direct limits are set on new triplet quarks, the (absence of) experimental signature, $W + \text{Jets}$, is also sensitive to other strongly-interacting exotic particles

¹Stronger bounds on gluino masses are obtained through searches for jet events with large missing energy or transverse momentum [30–33]. The excluded region depends on the assumed supersymmetric model, reaching in some cases the 1 TeV scale.

in weak $SU(2)_L$ representations, as we are going to consider next, provided they decay within the detector through $X_R \rightarrow W X'_R \rightarrow W + \text{Jets}$.

4.2 Higgs production at LHC

In the Standard Model, the Higgs mechanism is responsible for all particle masses. If the mass of the exotic colour object X_R is also generated through its coupling to the Higgs boson, the Higgs properties are modified through quantum loops involving the fermion X_R . Let us consider the consequences of a generic Higgs coupling

$$\mathcal{L}_H = -\frac{M_X}{v} H(x) \left[\bar{X}_R(x) X_R(x) \right], \quad (4.7)$$

with $v = (\sqrt{2}G_F)^{-1/2} = 246$ GeV the Higgs vacuum expectation value. The usual Standard Model mechanism for fermion masses requires X_R to be an electroweak doublet. More specifically, X_R contains two fermion fields, differing by one unit of electric charge, with their left-handed chiralities forming a $SU(2)_L$ doublet while their right-handed chiralities are singlets. We neglect their mass difference since the two fields should be degenerated enough to satisfy the electroweak precision tests. One should also implement the cancelation of the electroweak anomalies generated by the new $SU(2)_L$ doublet; we will assume for the moment that this is achieved through the addition of new exotic leptons. We will comment later on the implications of arranging instead the anomaly cancelation with additional coloured objects. The anomaly constraints are discussed in the appendix for completeness.

Since X_R couples strongly to gluons, the vertex in Eq. (4.7) generates a very sizeable contribution to the main Higgs production channel at LHC, through an intermediate $X_R \bar{X}_R$ virtual pair: $gg \rightarrow X_R \bar{X}_R \rightarrow H$. The resulting amplitude can be easily obtained from the standard quark-loop result, accounting for the different colour factors:

$$\begin{aligned} \sigma(gg \rightarrow H) &= \frac{M_H^2 \alpha_s^2}{256\pi v^2} \left| \sum_q T_F \mathcal{F} \left(\frac{4m_q^2}{M_H^2} \right) \right. \\ &\quad \left. + 2 T_R \mathcal{F} \left(\frac{4M_X^2}{M_H^2} \right) \right|^2 \delta(s - M_H^2), \end{aligned} \quad (4.8)$$

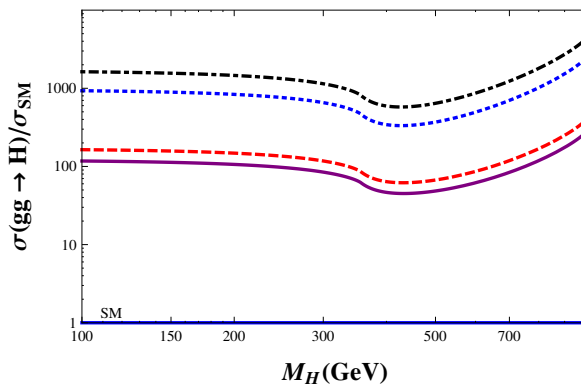


Figure 4.2: Ratio $\sigma(gg \rightarrow H)/\sigma_{\text{SM}}$ at $\sqrt{s} = 7$ TeV and $M_X = 500$ GeV, as a function of M_H . The different curves correspond to an exotic fermion multiplet X_R in the sextet (continuous), octet (dashed), decuplet (dotted) and $\underline{15}$ (dash-dotted) representations.

where

$$\mathcal{F}(x) = \frac{x}{2} [4 + (x-1)f(x)],$$

$$f(x) = \begin{cases} -4 \arcsin^2(1/\sqrt{x}), & x \geq 1 \\ \left[\ln \left(\frac{1+\sqrt{1-x}}{1-\sqrt{1-x}} \right) - i\pi \right]^2, & x < 1 \end{cases}. \quad (4.9)$$

The first term in (4.8) is the usual triplet-quark contribution; it is completely dominated by the top loop because the function $\mathcal{F}(x)$ vanishes in the massless limit ($x \rightarrow 0$). The second term stands for the additional contribution from the exotic coloured fermion multiplet X_R . Given the experimental constraints on M_X discussed before, $M_H^2 < 4M_X^2$ in the interesting kinematical regime and the corresponding loop function does not have any absorptive part. Moreover, the numerical result is not sensitive to the exact value of M_X because $\mathcal{F}(x)$ is a very smooth function for $x \geq 1$, decreasing gently from $\mathcal{F}(1) = 2$ to $\mathcal{F}(\infty) = 4/3$.

Owing to the relative colour enhancement factor T_R/T_F , the X_R contribution generates a large increase of the Higgs production cross section. The ratio $\sigma(gg \rightarrow H)/\sigma_{\text{SM}}$ for different colour representations is shown in Fig. 4.2, as a function of M_H , taking $\sqrt{s} = 7$ TeV and $M_X = 500$ GeV. The normalization $\sigma_{\text{SM}} \equiv \sigma(gg \rightarrow H)_{\text{SM}}$ is the Standard Model cross section with three quark families. Again, we have assumed the same QCD corrections as for triplet quarks, which underestimates the actual cross section. Very large enhancement factors are

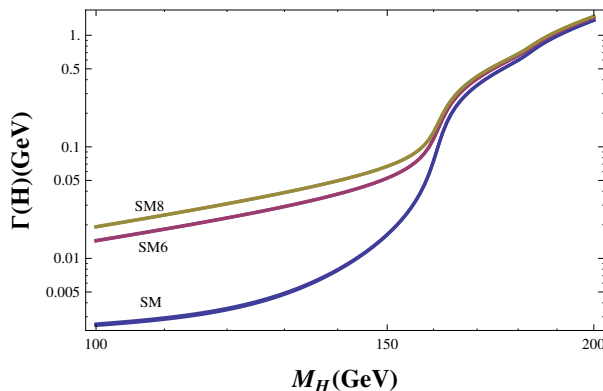


Figure 4.3: Higgs total decay width in the 3-generation Standard Model (SM), and with the addition of colour sextet (SM6) or octet (SM8) multiplets.

obtained for all non-triplet representations. In the sextet and octet cases, the Higgs production cross section is larger than the SM one by a factor between 40 or 300, depending on M_H . The enhancement surpasses the three orders of magnitude for the 15 and higher colour representations.

4.3 Higgs search

Since the decay $H \rightarrow X_R \bar{X}_R$ is not kinematically allowed for $M_H < 2M_X$, a heavy Higgs would decay into WW , ZZ and $t\bar{t}$ with approximately the same branching fractions as in the absence of the fermion X_R . The Standard Model Higgs has already been experimentally excluded for Higgs masses between $2M_W$ and 600 (525) GeV, at 95% CL (99% CL) [42,43]. The existence of an additional coloured fermion would only make the exclusion much stronger. More care has to be taken below the WW threshold, because the same enhancement present in the Higgs production cross section also appears in the $H \rightarrow gg$ decay width, modifying all branching ratios. Figure 4.3 shows the total Higgs decay width Γ_H , as a function of M_H , for the Standard Model with three families of triplet quarks, and with the addition of one (electroweak doublet) colour sextet or octet multiplet. The exotic contributions are small for $M_H > 2M_W$, but at lower Higgs masses they generate a big enhancement of Γ_H . Figures 4.4, 4.5 and 4.6 plot the corresponding branching ratios in the different channels.

The strong enhancement of the two-gluon decay channel at low Higgs masses, affects in a very sizeable way the suppressed (one loop) 2γ and γZ decay modes,

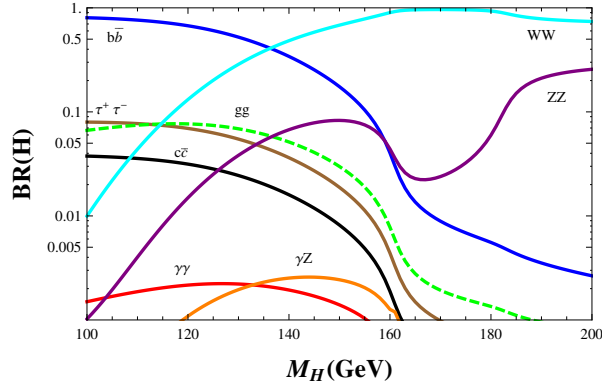


Figure 4.4: Higgs decay branching ratios in the 3-generation Standard Model.

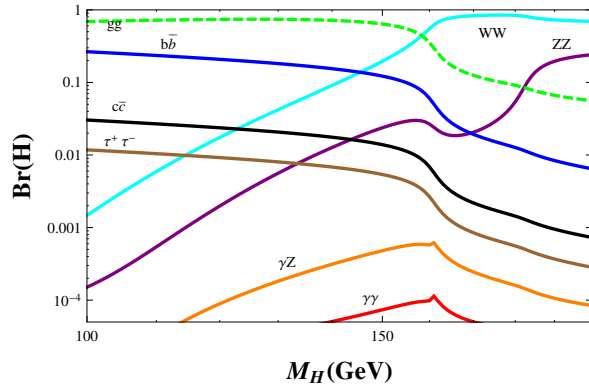


Figure 4.5: Higgs branching ratios with the addition of a colour sextet multiplet.

making them insignificant. However, in the WW and ZZ modes the branching fraction suppression cannot compensate the large enhancement of the production rate. In order to compare with the LHC experimental data, the relevant ratio is

$$R_{VV} = \frac{\sigma(pp \rightarrow H) \text{Br}(H \rightarrow VV)}{\sigma(pp \rightarrow H)_{\text{SM}} \text{Br}(H \rightarrow VV)_{\text{SM}}}, \quad (4.10)$$

where SM refers again to the Standard Model with three quark families and $V = W, Z$. This is plotted in Fig. 4.7, for sextet and octet colour representations, showing that, at $\sqrt{s} = 7$ TeV, $R_{VV} > 15$ in the relevant range of Higgs masses. Much larger values of R_{VV} would be obtained with higher-dimensional

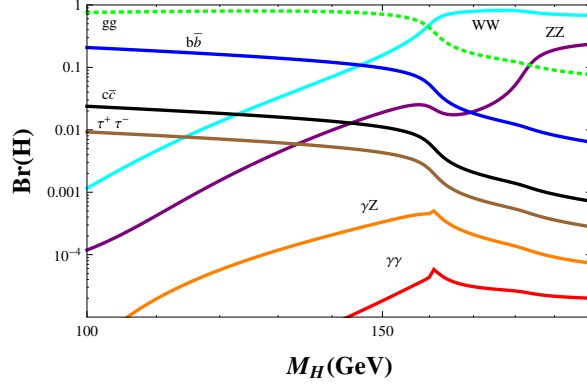


Figure 4.6: Higgs branching ratios with the addition of a colour octet multiplet.

representations or additional coloured fermion multiplets. Therefore, the present ATLAS [42] and CMS [43] searches in the WW and ZZ channels, already exclude a Standard Model Higgs boson coupled to exotic colour multiplets, in the whole range between 110 and 600 GeV.

The combined CDF and D0 data [44] exclude Higgs masses between 100 and 108 GeV (95% CL), within the three-generation Standard Model. Although $gg \rightarrow H$ accounts for 76% of the Higgs production cross section in this mass region, the Tevatron constraints are mainly extracted from $q\bar{q} \rightarrow WH/ZH$, with a small contribution from $q\bar{q} \rightarrow q'\bar{q}'H$. These production mechanisms are not enhanced by the exotic colour-multiplet contributions. In this mass range the main Higgs signature is $H \rightarrow b\bar{b}$; therefore, the Tevatron information translates into 95% CL upper bounds for $\mathcal{R}_{b\bar{b}} \equiv \text{Br}(H \rightarrow b\bar{b})/\text{Br}(H \rightarrow b\bar{b})_{\text{SM}}$ ranging from 0.45 at 100 GeV to 1.1 at 110 GeV [44]. The addition of a sextet (octet) multiplet implies $\mathcal{R}_{b\bar{b}}$ values ranging from 0.33 (0.26) at 100 GeV to 0.31 (0.24) at 110 GeV, which are slightly below the present Tevatron bounds. A mild improvement of the Tevatron constraints could exclude sextet or octet contributions for M_H between 100 and 110 GeV.

The LEP exclusion limit below 114.5 GeV [45] needs also to be re-analyzed in view of the strong enhancement of $\text{Br}(H \rightarrow gg)$. While the production mechanism $e^+e^- \rightarrow Z^* \rightarrow ZH$ remains unchanged in the presence of exotic quarks, there is a large suppression of the Higgs branching fractions into $b\bar{b}$ and $\tau^+\tau^-$ and, therefore, of the sought experimental signal. OPAL performed a generic search for neutral scalars decaying into an arbitrary combination of hadrons, leptons, photons and invisible particles, covering as well the possibility of a stable scalar

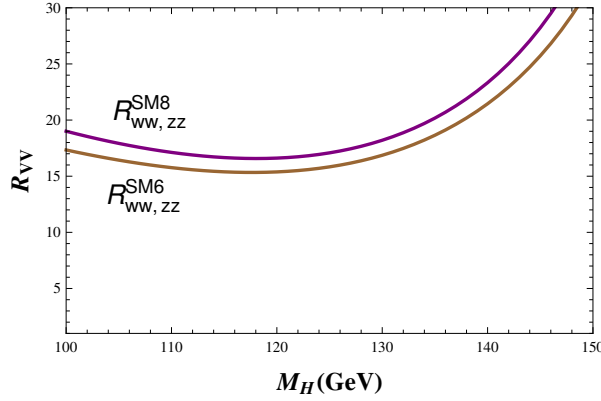


Figure 4.7: $R_{WW,ZZ}$ at $\sqrt{s} = 7$ TeV, as a function of M_H , with the addition of colour sextet (SM6) or octet (SM8) multiplets.

[46]. Thus, the OPAL bound, $M_H > 81$ GeV (95% CL) [46], remains valid in the presence of exotic colour multiplets. For larger masses, the combined LEP analysis relies in the $H \rightarrow b\bar{b}$ decay mode. Figure 4.8 compares the LEP bounds on $\text{Br}(H \rightarrow b\bar{b})$ [45], with the expected values with one (electroweak doublet) sextet (top red curve) or octet (bottom blue curve) multiplet. Higgs masses below 96 (92) GeV are then excluded in the sextet (octet) case.

The triplet case of a fourth quark generation has been already discussed before [47–59]. The enhancement of $\sigma(gg \rightarrow H)$ is milder, about a factor of 9, but enough to exclude Higgs masses above 110 GeV from the LHC constraints on R_{VV} . The corresponding weaker enhancement of $\text{Br}(H \rightarrow gg)$ implies a much smaller suppression of the remaining channels; in particular, for Higgs masses smaller than 110 GeV, the $b\bar{b}$ branching fraction is predicted to be above the LEP bound in Fig. 4.8. Therefore, in the presence of an additional (electroweak doublet) colour quark triplet, the Higgs boson is excluded in the whole mass range up to 600 GeV.

Note, however, that additional exotic multiplets or higher colour representations would imply a larger suppression of $\text{Br}(H \rightarrow b\bar{b})$, weakening the LEP and Tevatron constraints. That would be the case, for instance, if the anomaly matching condition is fulfilled with (at least two) coloured exotic multiplets, instead of leptons. Thus, in the region of Higgs masses between 81 and 110 GeV the constraints are sensitive to the assumed exotic spectrum. This is not the case for lower or higher values of M_H ; Higgs masses between 110 and 600 GeV, or

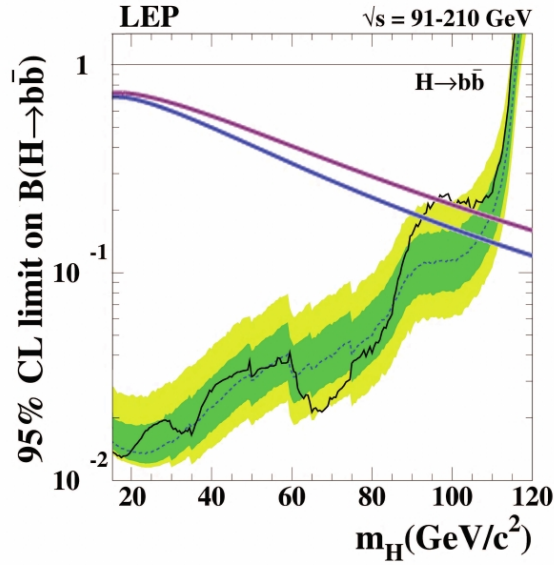


Figure 4.8: The LEP exclusion limits on $\text{Br}(H \rightarrow b\bar{b})$ [45], as a function of M_H , are compared with the expected signals in the presence of one exotic (electroweak doublet) sextet (top red curve) or octet (bottom blue curve) multiplets.

smaller than 81 GeV, are excluded in the presence of any exotic colour multiplets coupled to the Higgs boson.

4.4 Discussion

Present LHC data imply that a Standard Model Higgs cannot exist in the presence of new coloured fermions coupled to it, in exotic QCD representations, except for a small M_H region between 92 (81 with several exotic multiplets) and 110 GeV which could be soon excluded. Exotic quarks in higher-dimension colour representations generate a very large enhancement of $\sigma(gg \rightarrow H)$, in contradiction with the available experimental bounds. Strong limits have been already put before in the case of a fourth quark generation, where the enhancement of the Higgs production cross section is milder [49–51].

One could certainly try to evade the experimental constraints, enlarging the Standard Model in appropriate ways to compensate the enhancement from exotic quarks. For instance, introducing additional coloured scalars with couplings to the Higgs adjusted to suppress the $gg \rightarrow H$ amplitude [60–64]. Another

possibility is “hiding” the Higgs; i.e., opening new decay channels into invisible modes without strong interactions [53, 54, 65–71], in order to suppress the visible branching fractions. While well-motivated arguments, such as dark matter, exist to do it, we feel that this hides the main reason behind such strong exclusion: the intrinsic non-decoupling of the Yukawa vertex (4.7) makes the Higgs boson sensitive to arbitrary high mass scales.

The Higgs vacuum expectation value is linked to the electroweak scale, i.e., to the gauge boson masses M_W and M_Z . In the Standard Model this scale is also used to generate all fermion masses through the Yukawa couplings. The known pattern of lepton and quark masses, with very different mass scales, implies a large variety of Yukawa couplings with magnitudes ranging from $m_\nu/v \sim 10^{-13}$ to $m_t/v \sim 0.7$. This wide range of couplings/scales is not yet understood. Introducing additional fermions with even higher masses, would bring much larger Yukawa couplings inducing a non-perturbative dynamical regime in the electroweak sector. In fact, the Higgs production and decay amplitudes used in our analysis are subject to potentially large electroweak corrections [59].

If a light neutral scalar boson is finally discovered, one should study very carefully its properties in order to clarify the true pattern of electroweak symmetry breaking. The Standard Model is certainly a very plausible possibility, but heavier mass scales should not couple to the Higgs boson, i.e., they should have a different origin. Multi-Higgs models offer a much more flexible framework to accommodate future data, but soon or later they would also face the characteristic non-decoupling of the Higgs mechanism in (parts of) their extended Yukawa couplings. A perhaps more interesting possibility is that fermion masses could be generated through a mechanism different than the one responsible for the gauge boson masses. Another alternative, of course, is that the Higgs boson does not exist (dynamical symmetry breaking) or it is a composite object with rather different properties. The forthcoming LHC data should soon show us the option chosen by Nature to break the electroweak symmetry and hopefully provide some hints on the dynamics behind the observed pattern of fermion masses and mixings.

4.A Anomaly cancellation

The cancellation of the triangular gauge anomalies requires [72]

$$\mathrm{Tr} \left(\{T^a, T^b\} T^c \right)_L - \mathrm{Tr} \left(\{T^a, T^b\} T^c \right)_R = 0, \quad (4.11)$$

where T^a are the Standard Model group generators and the traces sum over all possible left- and right-handed fermions. Owing to the algebraic properties of the $SU(2)$ and $SU(3)$ generators, the only non-trivial anomalies involve one or three $U(1)_Y$ bosons, giving conditions on traces of Y and Y^3 , respectively, where the hypercharge is related to the electric charge through $Y = Q - T^3$. These relations imply that the sum of all fermion electric charges should be zero:

$$\sum_f Q_f = \text{Tr}(Y)_L = \text{Tr}(Y)_R = 0. \quad (4.12)$$

Let us consider N $SU(2)_L$ fermion doublets ψ_i with $Y(\psi_{i,L}) = y_i$, and their corresponding right-handed singlets with $Y(\psi_{i,R}) = Q_i = y_i + \frac{1}{2}$ and $Y(\psi'_{i,R}) = Q'_i = y_i - \frac{1}{2}$. In order to cancel the Standard Model gauge anomalies, one needs to satisfy

$$2 \sum_i^N d_i y_i = \sum_i^N d_i (2Q_i - 1) = 0, \quad (4.13)$$

where d_i denotes the multiplicity of the $SU(3)_C$ representation of ψ_i . The number of left-handed fermion doublets, $\sum_i^N d_i$, should be even in order to avoid a global (non-perturbative) $SU(2)$ chiral gauge anomaly [73]. The normal Standard Model generations fulfil these conditions with one quark ($d_q = 3$, $y_q = \frac{1}{6}$) and one lepton ($d_l = 1$, $y_l = -\frac{1}{2}$) multiplets.

Thus, there are many possible ways of adding exotic coloured fermions to the 3-generation Standard Model, while preserving the anomaly cancellation conditions. A single exotic representation with even dimension and $y = 0$ ($Q = \frac{1}{2}$, $Q' = -\frac{1}{2}$) would of course be anomaly free, but it would be stable (it cannot decay into ordinary quarks and gluons). The simplest solution to the anomaly constraint involves two exotic multiplets with the same $SU(3)_C$ multiplicity and opposite hypercharge.

The most general solution with two additional multiplets of different dimensionalities is $y_2 = -y_1 d_1 / d_2$, with $d_1 + d_2$ even. For odd-dimensional exotic representations ($d_1 = 15, 27 \dots$), it is then possible to cancel the anomaly with a new lepton multiplet of hypercharge $y_2 = -y_1 d_1$. Two lepton multiplets with $y_2 + y_3 = -y_1 d_1$ would be needed to cancel the anomaly of an exotic representation with even multiplicity ($d_1 = 6, 8, 10 \dots$). For any exotic colour representation of dimension d and hypercharge y , the anomaly could of course be canceled with d lepton multiplets of hypercharge $y_l = -y$.

The figures shown in the paper refer to the simplest case of a single (electroweak doublet) exotic quark multiplet, with the anomaly cancelled by exotic

lepton multiplets. If one considers instead models where the anomaly is cancelled through additional coloured fermions, the LHC constraints become much stronger in the whole mass range analyzed. For instance two exotic quark multiplets with the same $SU(3)_C$ multiplicity and opposite hypercharge, would increase the ratio R_{VV} (Fig. 7) by a factor close to two. Therefore the range of Higgs masses between 110 and 600 GeV is completely excluded in any exotic model. However, since additional coloured fermions imply a suppression of $\text{Br}(H \rightarrow b\bar{b})$, weakening the LEP and Tevatron constraints, an open window of allowed Higgs masses between 81 and 110 GeV remains in this type of models.

Acknowledgements

This work has been supported in part by MICINN, Spain [Grants FPA2007-60323, FPA2011-23778 and Consolider-Ingenio 2010 Program CSD2007-00042 (CPAN)] and by Generalitat Valenciana under Grant No. Prometeo/2008/069.

BIBLIOGRAPHY

- [1] E. Ma, *Phys. Lett.* **58B** (1975) 442.
- [2] G. Karl, *Phys. Rev.* **D14** (1976) 2374.
- [3] F. Wilczek and A. Zee, *Phys. Rev.* **D16** (1977) 860.
- [4] Y. Ng and S.-H. Tye, *Phys. Rev. Lett.* **41** (1978) 6.
- [5] H. Georgi and S. Glashow, *Nucl. Phys.* **B159** (1979) 29.
- [6] W.J. Marciano, *Phys. Rev.* **D21** (1980) 2425.
- [7] B. Holdom and M.E. Peskin, *Nucl. Phys.* **B208** (1982) 397.
- [8] K. Konishi and R. Tripicciono, *Phys. Lett.* **B121** (1983) 403.
- [9] D. Lüst et al., *Nucl. Phys.* **B268** (1986) 49.
- [10] E. Braaten, A.R. White and C.R. Willcox, *Intern. J. Mod. Phys.* **A1** (1986) 693.
- [11] T.E. Clark et al., *Phys. Lett.* **B177** (1986) 413.
- [12] A.R. White, *Mod. Phys. Lett.* **A2** (1987) 945.
- [13] K. Fukazawa et al., *Prog. Theor. Phys.* **85** (1991) 111.
- [14] S. Bethke et al., arXiv:1110.0016 [hep-ph].
- [15] W.E. Caswell, *Phys. Rev. Lett.* **33** (1974) 244.
- [16] D.R.T. Jones, *Nucl. Phys. Rev.* **B75** (1974) 531.
- [17] A. Pich, arXiv:1107.1123 [hep-ph].
- [18] E. Braaten, S. Narison and A. Pich, *Nucl. Phys.* **B373** (1992) 581.
- [19] S. Bethke, *Phys. Rept.* **403-404** (2004) 203; *Eur. Phys. J.* **C64** (2009) 689.

-
- [20] F. Csikor and Z. Fodor, *Phys. Rev. Lett.* **78** (1997) 4335.
- [21] ALEPH Collaboration, *Eur. Phys. J.* **C35** (2004) 457; **C27** (2003) 1; *Z. Phys.* **C76** (1997) 1; *Phys. Rept.* **294** (1998).
- [22] OPAL Collaboration, *Eur. Phys. J.* **C71** (2011) 1733; **C20** (2001) 601; **C16** (2000) 185.
- [23] JADE and OPAL Collaborations, *Eur. Phys. J.* **C17** (2000) 19.
- [24] J. Kumar, A. Rajaraman and B. Thomas, *Phys. Rev.* **D84** (2011) 115005.
- [25] R.K. Ellis, W.J. Stirling and B.R. Webber, *QCD and Collider Physics*, Cambridge Monographs in Particle Physics, Nuclear Physics and Cosmology (Cambridge University Press, 2003).
- [26] ATLAS Collaboration, *New J. Phys.* **13** (2011) 053044; *Phys. Lett.* **B** 708 (2012) 37.
- [27] CMS Collaboration, *Phys. Lett.* **B704** (2011) 123; *Phys. Rev. Lett.* **105** (2010) 211801.
- [28] CMS Collaboration, *Phys. Rev. Lett.* **107** (2011) 101801.
- [29] CDF Collaboration, *Phys. Rev. Lett.* **107** (2011) 042001.
- [30] ATLAS Collaboration, *Phys. Lett.* **B710** (2012) 67; **B701** (2011) 186, 398; *Phys. Rev. Lett.* **106** (2011) 131802; *Eur. Phys. J.* **C71** (2011) 1682.
- [31] CMS Collaboration, *Phys. Lett.* **B698** (2011) 196; *JHEP* **1108** (2011) 155; *Phys. Rev.* **D85** (2012) 012004; *Phys. Rev. Lett.* **107** (2011) 221804; **106** (2011) 211802; *JHEP* **07** (2011) 113.
- [32] CDF Collaboration, *Phys. Rev. Lett.* **101** (2008) 251801; **102** (2009) 121801.
- [33] D0 Collaboration, *Phys. Lett.* **B660** (2008) 449; **B680** (2009) 34.
- [34] CDF Collaboration, *Phys. Rev. Lett.* **63** (1989) 1447.
- [35] CMS Collaboration, CMS PAS EXO-11-022 (2011); *JHEP* **1103** (2011) 024; *Phys. Rev. Lett.* **106** (2011) 011801.
- [36] ATLAS Collaboration, *Phys. Lett.* **B701** (2011) 1; **B703** (2011) 428; *Eur. Phys. J.* **C72** (2012) 1965.

-
- [37] ATLAS Collaboration, arXiv:1202.3389 [hep-ex].
- [38] CDF Collaboration, *Phys. Rev. Lett.* **106** (2011) 141803.
- [39] ATLAS Collaboration, *Phys. Rev. Lett.* **108** (2012) 261802.
- [40] CDF Collaboration, *Phys. Rev. Lett.* **107** (2011) 261801.
- [41] D0 Collaboration, *Phys. Rev. Lett.* **107** (2011) 082001.
- [42] ATLAS Collaboration, *Phys. Lett.* **B710** (2012) 49, 383; *Phys. Rev. Lett.* **108** (2012) 111802, 111803.
- [43] CMS Collaboration, *Phys. Lett.* **B710** (2012) 26, 91, 284, 403; **B713** (2012) 68; *JHEP* **1203** (2012) 040, 081; **1204** (2012) 036; *Phys. Rev. Lett.* **108** (2012) 111804.
- [44] TEVNP (Tevatron New Phenomena and Higgs Working Group) and CDF and D0 Collaborations, arXiv:1107.5518 [hep-ex].
- [45] ALEPH, DELPHI, L3 and OPAL Collaborations, The LEP Working Group for Higgs Boson Searches, *Phys. Lett.* **B565** (2003) 61.
- [46] OPAL Collaboration, *Eur. Phys. J.* **C27** (2003) 311.
- [47] G.D. Kribs, T. Plehn, M. Spannowsky and T.M.P. Tait, *Phys. Rev.* **D76** (2007) 075016.
- [48] N. Becerici Schmidt, S.A. Çetin, S. İştin and S. Sultansoy, *Eur. Phys. J.* **C66** (2010) 119.
- [49] CDF and D0 Collaborations, *Phys. Rev.* **D82** (2010) 011102.
- [50] CMS Collaboration, *Phys. Lett.* **B699** (2011) 25; CMS-PAS-HIG-11-011.
- [51] ATLAS Collaboration, *Eur. Phys. J.* **C71** (2011) 1728.
- [52] A.N. Rozanov and M.I. Vysotsky, *Phys. Lett.* **B700** (2011) 313.
- [53] K. Belotsky et al., *Phys. Rev.* **D68** (2003) 054027.
- [54] W.-Y. Keung and P. Schwaller, *JHEP* **1106** (2011) 054.
- [55] C. Anastasiou, R. Boughezal and E. Furlan, *JHEP* **1006** (2010) 101.
- [56] C. Anastasiou et al., *Phys. Lett.* **B702** (2011) 224.

-
- [57] X. Ruan and Z. Zhang, arXiv:1105.1634 [hep-ph].
- [58] J.F. Gunion, arXiv:1105.3965 [hep-ph].
- [59] A. Denner et al., *Eur. Phys. J.* **C72** (2012) 1992.
- [60] B.A. Dobrescu, G.D. Kribs and A. Martin, *Phys. Rev.* **D85** (2012) 074031.
- [61] X.-G. He and G. Valencia, *Phys. Lett.* **B707** (2012) 381.
- [62] A.V. Manohar and M.B. Wise, *Phys. Rev.* **D74** (2006) 035009.
- [63] A. Djouadi, *Phys. Lett.* **B435** (1998).
- [64] Y. Bai, J.J. Fan, J.L. Hewett, arXiv:1112.1964 [hep-ph].
- [65] R.E. Shrock and M. Suzuki, *Phys. Lett.* **B110** (1982) 250.
- [66] X.-G. He, S.-Y. Ho, J. Tandean and H.-C. Tsai, *Phys. Rev.* **D82** (2010) 035016.
- [67] M. Raidal and A. Strumia, *Phys. Rev.* **D84** (2011) 077701.
- [68] E. Ma, *Phys. Lett.* **B706** (2012) 350; *Int. J. Mod. Phys.* **A27** (2012) 1250059.
- [69] S. Chang, R. Dermisek, J.F. Gunion and N. Weiner, *Ann. Rev. Nucl. Part. Sci.* **58** (2008) 75.
- [70] S. Bock et al., *Phys. Lett.* **B694** (2010).
- [71] C. Englert et al., *Phys. Rev.* **D85** (2012) 035008.
- [72] A. Pich, “The Standard Model of Electroweak Interactions”, Proc. 2010 European School of High-Energy Physics, CERN-2012-001, p. 1, arXiv:1201.0537 [hep-ph].
- [73] E. Witten, *Phys. Lett.* **B117** (1982) 324.

5. LHC CONSTRAINTS ON TWO-HIGGS- DOUBLET MODELS

Alejandro Celis, Victor Ilisie and Antonio Pich

IFIC, Universitat de València – CSIC, Apt. Correus 22085, E-46071 València, Spain

Journal of High Energy Physics: JHEP 07(2013)053, arXiv: 1302.4022

Abstract: A new Higgs-like boson with mass around 126 GeV has recently been discovered at the LHC. The available data on this new particle is analyzed within the context of two-Higgs doublet models without tree-level flavour-changing neutral currents. Keeping the generic Yukawa structure of the Aligned Two-Higgs Doublet Model framework, we study the implications of the LHC data on the allowed scalar spectrum. We analyze both the CP-violating and CP-conserving cases, and a few particular limits with a reduced number of free parameters, such as the usual models based on discrete \mathcal{Z}_2 symmetries.

5.1 Introduction

The ATLAS and CMS collaborations have recently announced the discovery of a new neutral boson, with a measured mass of $125.2 \pm 0.3 \pm 0.6$ GeV [1] and $125.8 \pm 0.4 \pm 0.4$ GeV [2], respectively. The LHC data is compatible with the expected production and decay of the Standard Model (SM) Higgs boson, the most significant decay modes being $H \rightarrow \gamma\gamma$ and $H \rightarrow ZZ^{(*)} \rightarrow \ell^+\ell^-$. The excess of events observed by ATLAS (CMS) has a (local) statistical significance of 6.1σ (6.9σ). Although the spin of the new particle has not been measured yet, the observed diphoton decay channel shows clearly that it is a boson with $J \neq 1$, making very plausible the scalar hypothesis. Preliminary analyses of $H \rightarrow ZZ \rightarrow 4\ell$ [3, 4] and $H \rightarrow \gamma\gamma$ [5, 6] events suggest indeed the assignment $J^P = 0^+$, though more statistics is still needed to give a definite answer.

Additional (but less significant) evidence has been reported by the CDF and $D\bar{O}$ collaborations [7], which observe an excess of events in the mass range between 120 and 135 GeV (the largest local significance is 3.3σ). The excess seems consistent with a SM Higgs produced in association with a W^\pm or Z boson and decaying to a bottom-antibottom quark pair.

While more experimental analyses are needed to assess the actual nature of this boson, the present data give already very important clues, constraining its couplings in a quite significant way. The stringent exclusion limits set previously on a broad range of masses provide also complementary information which is very useful to establish allowed domains for alternative new-physics scenarios. A SM Higgs boson has been already excluded at 95% CL in the mass ranges 0–122.5 and 127–600 GeV [5, 8–14].

The new boson appears to couple to the known gauge bosons (W^\pm , Z , γ , g) with the strength expected for the SM Higgs [15–24], although a slight excess of events in the 2γ decay channel, compared with the SM expectation, is observed by ATLAS and CMS [1, 2]. Moreover, its fermionic couplings seem compatible with a linear dependence with the fermion mass, scaled by the electroweak scale $v \approx 246$ GeV [23]. Thus, it has the properties expected for a Higgs-like particle, related with the spontaneous breaking of the electroweak symmetry. An obvious question to address is whether it corresponds to the unique Higgs boson incorporated in the SM, or it is just the first signal of a much richer scalar sector.

The simplest modification of the SM Higgs mechanism consists in incorporating additional scalar doublets, respecting the custodial symmetry, which can easily satisfy the electroweak precision tests. This leads to a rich spectrum of neutral and charged scalars, providing a broad range of dynamical possibilities

with very interesting phenomenological implications. The minimal extension of the scalar sector with only one additional doublet contains five physical scalars: two charged fields H^\pm and three neutral ones h , H and A ; thus, there are three possible candidates for the recently discovered neutral boson. If the scalar potential preserves the CP symmetry, h and H are CP-even, while A is CP-odd; in this case there are no AW^+W^- and AZZ couplings at tree level, which makes the A possibility quite unlikely.

Generic multi-Higgs doublet models give rise to unwanted flavour-changing neutral current (FCNC) interactions through non-diagonal couplings of neutral scalars to fermions. The tree-level FCNCs can be eliminated requiring the alignment in flavour space of the Yukawa matrices coupling to a given right-handed fermion [25]. The Aligned Two-Higgs Doublet Model (A2HDM) [26] results in a very specific structure, with all fermion-scalar interactions being proportional to the corresponding fermion masses. This leads to a rich and viable phenomenology [25–30] with an interesting hierarchy of FCNC effects, suppressing them in light-quark systems while allowing potentially relevant signals in heavy-quark transitions. The A2HDM constitutes a very general framework which includes, for particular values of its parameters, all previously considered two-Higgs doublet models (2HDMs) without FCNCs [31, 32], and incorporates in addition new sources of CP violation.

In the following, we will analyze the recent discovery of a Higgs-like object within the A2HDM. We will study the different possible interpretations of the new boson, the corresponding experimental constraints on its couplings, and the implications for the remaining scalar spectrum. Previous analyses [33–43] have only considered more specific scenarios based on discrete \mathcal{Z}_2 symmetries [44], *i.e.*, the so called 2HDMs of types I [45, 46], II [46, 47], X (leptophilic or lepton specific), Y (flipped) [48–51] and inert [52]. The more general A2HDM framework opens a wide range of additional possibilities, which we will try to characterize keeping in mind the high-statistics data samples that the LHC is expected to deliver in the future, at higher energies. Two very recent works have already employed the A2HDM, in the limit of CP conservation, to analyze the Higgs data [53, 54]. Another previous work has considered the CP-conserving A2HDM with a custodial symmetry imposed on the Higgs potential [55]. We will compare our results in that limit and will also explore the consequences of allowing CP-violating phases, either in the scalar potential (mixing of the three neutral scalars) or in the Yukawa couplings. While parts of our analysis remain valid in more general 2HDM settings, the flavour constraints would necessarily be dif-

ferent in models with tree-level FCNCs [56–58] and, therefore, the appropriate modifications should be taken into account.

Our paper is organized as follows: In section 5.2, we describe the theoretical framework adopted in our analysis, indicating the relevant couplings of the A2HDM scalars. In section 3 we define the Higgs signal strengths, which are used to make contact with the experimental measurements. Section 5.4 presents our results and shows the scalar parameter ranges needed to explain the present data. Our conclusions are given in section 5.5. The appendices include a compilation of useful formulae as well as the statistical treatment and data used in this work.

5.2 The Aligned Two-Higgs-Doublet Model

The 2HDM extends the SM with a second scalar doublet of hypercharge $Y = \frac{1}{2}$. The neutral components of the scalar doublets $\phi_a(x)$ ($a = 1, 2$) acquire vacuum expectation values that are, in general, complex: $\langle 0 | \phi_a^T(x) | 0 \rangle = \frac{1}{\sqrt{2}} (0, v_a e^{i\theta_a})$. Through an appropriate $U(1)_Y$ transformation we can enforce $\theta_1 = 0$, since only the relative phase $\theta \equiv \theta_2 - \theta_1$ is observable. It is convenient to perform a global $SU(2)$ transformation in the scalar space (ϕ_1, ϕ_2) and work in the so-called Higgs basis (Φ_1, Φ_2) , where only one doublet acquires a vacuum expectation value:

$$\begin{pmatrix} \Phi_1 \\ -\Phi_2 \end{pmatrix} \equiv \begin{bmatrix} \cos \beta & \sin \beta \\ \sin \beta & -\cos \beta \end{bmatrix} \begin{pmatrix} \phi_1 \\ e^{-i\theta} \phi_2 \end{pmatrix}, \quad (5.1)$$

with $\tan \beta = v_2/v_1$. In this basis, the two doublets are parametrized as

$$\Phi_1 = \begin{bmatrix} G^+ \\ \frac{1}{\sqrt{2}}(v + S_1 + iG^0) \end{bmatrix}, \quad \Phi_2 = \begin{bmatrix} H^+ \\ \frac{1}{\sqrt{2}}(S_2 + iS_3) \end{bmatrix}, \quad (5.2)$$

where G^\pm and G^0 denote the Goldstone fields and $\langle 0 | H^+ | 0 \rangle = \langle 0 | G^+ | 0 \rangle = \langle 0 | G^0 | 0 \rangle = \langle 0 | S_i | 0 \rangle = 0$. Thus, Φ_1 plays the role of the SM scalar doublet with $v \equiv \sqrt{v_1^2 + v_2^2} \simeq (\sqrt{2} G_F)^{-1/2} = 246$ GeV.

The physical scalar spectrum contains five degrees of freedom: the two charged fields $H^\pm(x)$ and three neutral scalars $\varphi_i^0(x) = \{h(x), H(x), A(x)\}$, which are related with the S_i fields through an orthogonal transformation $\varphi_i^0(x) = \mathcal{R}_{ij} S_j(x)$. The form of the \mathcal{R} matrix is fixed by the scalar potential, which determines the neutral scalar mass matrix and the corresponding mass eigenstates. A detailed discussion is given in appendix 5.A. In general, the CP-odd component S_3 mixes with the CP-even fields $S_{1,2}$ and the resulting mass eigenstates do not have a defi-

nite CP quantum number. If the scalar potential is CP symmetric this admixture disappears; in this particular case, $A(x) = S_3(x)$ and¹

$$\begin{pmatrix} h \\ H \end{pmatrix} = \begin{bmatrix} \cos \tilde{\alpha} & \sin \tilde{\alpha} \\ -\sin \tilde{\alpha} & \cos \tilde{\alpha} \end{bmatrix} \begin{pmatrix} S_1 \\ S_2 \end{pmatrix}. \quad (5.3)$$

Performing a phase redefinition of the neutral CP-even fields, we can fix the sign of $\sin \tilde{\alpha}$. In this work we adopt the conventions $M_h \leq M_H$ and $0 \leq \tilde{\alpha} \leq \pi$, so that $\sin \tilde{\alpha}$ is positive.

5.2.1 Yukawa Alignment

The most generic Yukawa Lagrangian with the SM fermionic content gives rise to FCNCs because the fermionic couplings of the two scalar doublets cannot be simultaneously diagonalized in flavour space. The non-diagonal neutral couplings can be eliminated by requiring the alignment in flavour space of the Yukawa matrices [26]; *i.e.*, the two Yukawa matrices coupling to a given type of right-handed fermions are assumed to be proportional to each other and can, therefore, be diagonalized simultaneously. The three proportionality parameters ς_f ($f = u, d, l$) are arbitrary complex numbers and introduce new sources of CP violation.

In terms of the fermion mass-eigenstate fields, the Yukawa interactions of the A2HDM read [26]

$$\begin{aligned} \mathcal{L}_Y = & -\frac{\sqrt{2}}{v} H^+ \left\{ \bar{u} \left[\varsigma_d V M_d \mathcal{P}_R - \varsigma_u M_u^\dagger V \mathcal{P}_L \right] d + \varsigma_l \bar{\nu} M_l \mathcal{P}_R l \right\} \\ & - \frac{1}{v} \sum_{\varphi_i^0, f} y_f^{\varphi_i^0} \varphi_i^0 \left[\bar{f} M_f \mathcal{P}_R f \right] + \text{h.c.}, \end{aligned} \quad (5.4)$$

where $\mathcal{P}_{R,L} \equiv \frac{1 \pm \gamma_5}{2}$ are the right-handed and left-handed chirality projectors, M_f the diagonal fermion mass matrices and the couplings of the neutral scalar fields are given by:

$$y_{d,l}^{\varphi_i^0} = \mathcal{R}_{i1} + (\mathcal{R}_{i2} + i \mathcal{R}_{i3}) \varsigma_{d,l}, \quad y_u^{\varphi_i^0} = \mathcal{R}_{i1} + (\mathcal{R}_{i2} - i \mathcal{R}_{i3}) \varsigma_u^*. \quad (5.5)$$

¹ In the usually adopted notation $\tilde{\alpha} = \alpha - \beta$, where α is the rotation angle expressing the two mass eigenstates h and H in terms of the CP-even neutral fields of the original scalar basis $\phi_1(x)$ and $\phi_2(x)$. Since the choice of initial basis is arbitrary, the parameters α and β are in general unphysical; their values can be changed at will through $SU(2)$ rotations. These angles only become meaningful in particular models where a specific basis is singled out (through a symmetry for instance).

Table 5.1: *CP-conserving 2HDMs based on discrete \mathcal{Z}_2 symmetries.*

Model	ς_d	ς_u	ς_l
Type I	$\cot \beta$	$\cot \beta$	$\cot \beta$
Type II	$-\tan \beta$	$\cot \beta$	$-\tan \beta$
Type X	$\cot \beta$	$\cot \beta$	$-\tan \beta$
Type Y	$-\tan \beta$	$\cot \beta$	$\cot \beta$
Inert	0	0	0

As in the SM, all scalar-fermion couplings are proportional to the corresponding fermion masses. This linear dependence on the fermion mass is characteristic of the A2HDM framework and does not hold in non-aligned 2HDMs with FCNCs. The only source of flavour-changing interactions is the Cabibbo-Kobayashi-Maskawa (CKM) quark mixing matrix V [59]. All possible freedom allowed by the alignment conditions is determined by the three family-universal complex parameters ς_f , which provide new sources of CP violation without tree-level FCNCs [26]. The usual models with natural flavour conservation, based on discrete \mathcal{Z}_2 symmetries, are recovered for particular (real) values of the couplings ς_f , as indicated in Table 5.1.

Quantum corrections induce a misalignment of the Yukawa matrices, generating small FCNC effects suppressed by the corresponding loop factors [25–27, 60, 61]. However, the flavour symmetries of the A2HDM tightly constraint the possible FCNC structures, keeping their effects well below the present experimental bounds [25–30].²

² The only FCNC structures induced at one loop take the form [25, 27]:

$$\begin{aligned}
\mathcal{L}_{\text{FCNC}} = & \frac{C(\mu)}{4\pi^2 v^3} (1 + \varsigma_u^* \varsigma_d) \sum_i \varphi_i^0(x) \\
& \times \left\{ (\mathcal{R}_{i2} + i \mathcal{R}_{i3}) (\varsigma_d - \varsigma_u) [\bar{d}_L V^\dagger M_u M_u^\dagger V M_d d_R] \right. \\
& \left. - (\mathcal{R}_{i2} - i \mathcal{R}_{i3}) (\varsigma_d^* - \varsigma_u^*) [\bar{u}_L V M_d M_d^\dagger V^\dagger M_u u_R] \right\} + \text{h.c.}
\end{aligned} \tag{5.6}$$

with $C(\mu) = C(\mu_0) - \log(\mu/\mu_0)$. These FCNC effects vanish identically in the \mathcal{Z}_2 models where the alignment condition is protected by a discrete symmetry. In the most general case, assuming the alignment to be exact at some scale μ_0 , i.e. $C(\mu_0) = 0$, a non-zero value for the FCNC coupling is generated when running to a different scale. However, the numerical effect is suppressed by $m_q m_q^2/v^3$ and quark-mixing factors, avoiding the stringent experimental constraints

The orthogonality of the rotation matrix \mathcal{R} , implies the following relations among the Yukawa couplings of the three neutral scalars:

$$\begin{aligned} \sum_{i=1}^3 (y_f^{\varphi_i^0})^2 &= 1, & \sum_{i=1}^3 |y_f^{\varphi_i^0}|^2 &= 1 + 2|\zeta_f|^2, & \sum_{i=1}^3 y_f^{\varphi_i^0} \mathcal{R}_{i1} &= 1, \\ \sum_{i=1}^3 y_{d,l}^{\varphi_i^0} \mathcal{R}_{i2} &= \zeta_{d,l}, & \sum_{i=1}^3 y_u^{\varphi_i^0} \mathcal{R}_{i2} &= \zeta_u^*, \\ \sum_{i=1}^3 y_{d,l}^{\varphi_i^0} \mathcal{R}_{i3} &= i \zeta_{d,l}, & \sum_{i=1}^3 y_u^{\varphi_i^0} \mathcal{R}_{i3} &= -i \zeta_u^*. \end{aligned} \quad (5.7)$$

5.2.2 Bosonic Couplings

The full set of interactions among the gauge and scalar bosons is given in appendix 5.B. The relevant vertices for our analysis are the ones coupling a single neutral scalar with a pair of gauge bosons. As shown in Eq. (5.55), they are identical to their SM counterpart, with the field S_1 taking the role of the SM Higgs. Therefore ($VV = W^+W^-$, ZZ),

$$g_{\varphi_i^0 VV} = \mathcal{R}_{i1} g_{hVV}^{\text{SM}}, \quad (5.8)$$

which implies

$$g_{hVV}^2 + g_{HVV}^2 + g_{AVV}^2 = \left(g_{hVV}^{\text{SM}}\right)^2. \quad (5.9)$$

The strength of the SM Higgs interaction is shared by the three 2HDM neutral bosons. In the CP-conserving limit, the CP-odd field decouples while the strength of the h and H interactions is governed by the corresponding $\cos \tilde{\alpha}$ and $\sin \tilde{\alpha}$ factors. Thus, a general feature of 2HDMs is that, at tree level, the couplings of the neutral scalars to vector bosons cannot be enhanced over the SM value and obey the custodial symmetry relation $g_{\varphi_i^0 ZZ} = g_{\varphi_i^0 WW}$. Observing a scalar boson with a somewhat enhanced coupling to vector bosons or a deviation from custodial symmetry [65] would therefore be in clear contradiction with the predictions of this class of models. The relations (5.7) and (5.9) establish a connection between the couplings of the observed 126 GeV resonance and searches for other neutral and charged scalars within the A2HDM.

for light-quark systems. Explicit examples of symmetry-protected underlying theories leading to a low-energy A2HDM structure have been discussed in Refs. [62–64].

In order to compute the two-photon decay widths of the neutral scalars, one also needs their couplings to a pair of charged scalars, generated through the scalar potential discussed in appendix 5.A. Since these couplings depend on still unknown parameters, we will parametrize the corresponding interaction as

$$\mathcal{L}_{\varphi^0 H^+ H^-} = -v \sum_{\varphi_i^0} \lambda_{\varphi_i^0 H^+ H^-} \varphi_i^0 H^+ H^-. \quad (5.10)$$

Explicit expressions for the cubic couplings $\lambda_{\varphi_i^0 H^+ H^-}$, in terms of the Higgs potential parameters, can be found in appendix 5.A. If CP is assumed to be an exact symmetry, $\lambda_{AH^+ H^-} = 0$.

5.3 Higgs Signal Strengths

The experimental data on Higgs searches is given in terms of the so-called signal strengths, measuring the observable cross sections in units of the corresponding SM expectations. At the LHC, the relevant production mechanisms for a SM-like Higgs particle are gluon fusion ($gg \rightarrow H$), vector boson fusion ($qq' \rightarrow qq'VV \rightarrow qq'H$), associated production with a vector boson ($q\bar{q}' \rightarrow WH/ZH$) and the associated production with a $t\bar{t}$ pair ($q\bar{q}/gg \rightarrow t\bar{t}H$). The Higgs decay channels explored so far are $\gamma\gamma$, $ZZ^{(*)}$, $WW^{(*)}$, $b\bar{b}$ and $\tau^+\tau^-$.

In order to fit the experimental measurements, we consider the ratios :

$$\begin{aligned} \mu_{\gamma\gamma}^{\varphi_i^0} &\equiv \frac{\sigma(pp \rightarrow \varphi_i^0) \text{Br}(\varphi_i^0 \rightarrow \gamma\gamma)}{\sigma(pp \rightarrow h)_{\text{SM}} \text{Br}(h \rightarrow \gamma\gamma)_{\text{SM}}} \\ \mu_{\tau\tau}^{\varphi_i^0} &\equiv \frac{\sigma(pp \rightarrow \varphi_i^0) \text{Br}(\varphi_i^0 \rightarrow \tau\tau)}{\sigma(pp \rightarrow h)_{\text{SM}} \text{Br}(h \rightarrow \tau\tau)_{\text{SM}}}, \\ \mu_{b\bar{b}V}^{\varphi_i^0} &\equiv \frac{\sigma(pp \rightarrow V\varphi_i^0) \text{Br}(\varphi_i^0 \rightarrow b\bar{b})}{\sigma(pp \rightarrow Vh)_{\text{SM}} \text{Br}(h \rightarrow b\bar{b})_{\text{SM}}}, \\ \mu_{VV}^{\varphi_i^0} &\equiv \frac{\sigma(pp \rightarrow \varphi_i^0) \text{Br}(\varphi_i^0 \rightarrow VV)}{\sigma(pp \rightarrow h)_{\text{SM}} \text{Br}(h \rightarrow VV)_{\text{SM}}}, \\ \mu_{\gamma\gamma jj}^{\varphi_i^0} &\equiv \frac{\sigma(pp \rightarrow jj\varphi_i^0) \text{Br}(\varphi_i^0 \rightarrow \gamma\gamma)}{\sigma(pp \rightarrow jjh)_{\text{SM}} \text{Br}(h \rightarrow \gamma\gamma)_{\text{SM}}}, \\ \mu_{WWjj}^{\varphi_i^0} &\equiv \frac{\sigma(pp \rightarrow jj\varphi_i^0) \text{Br}(\varphi_i^0 \rightarrow WW)}{\sigma(pp \rightarrow jjh)_{\text{SM}} \text{Br}(h \rightarrow WW)_{\text{SM}}}, \end{aligned} \quad (5.11)$$

where $V = W, Z$ and j stands for jet. QCD corrections cancel to a large extent in these ratios, provided that a single production mechanism dominates. This certainly applies to $\mu_{\gamma\gamma}^{\varphi_i^0}$, $\mu_{VV}^{\varphi_i^0}$ and $\mu_{\tau\tau}^{\varphi_i^0}$ which are governed by the dominant production channel through gluon fusion. The same would be true for $\mu_{WWjj}^{\varphi_i^0}$ and $\mu_{\gamma\gamma jj}^{\varphi_i^0}$ (gauge-boson fusion), and $\mu_{bbV}^{\varphi_i^0}$ (associated production), assuming that there is no contamination from other channels. It is convenient to express the ratio of the branching fractions as:

$$\frac{\text{Br}(\varphi_i^0 \rightarrow X)}{\text{Br}(h \rightarrow X)_{\text{SM}}} = \frac{1}{\rho(\varphi_i^0)} \frac{\Gamma(\varphi_i^0 \rightarrow X)}{\Gamma(h \rightarrow X)_{\text{SM}}}, \quad (5.12)$$

where $\rho(\varphi_i^0)$ measures the total decay width of the scalar φ_i^0 in units of the SM Higgs width,

$$\Gamma(\varphi_i^0) = \rho(\varphi_i^0) \Gamma_{\text{SM}}(h). \quad (5.13)$$

Particularizing to the A2HDM and assuming only one dominant production channel in each case,³ one finds:

$$\begin{aligned} \mu_{bbV}^{\varphi_i^0} &= (\mathcal{R}_{i1})^2 \left[\text{Re}(y_d^{\varphi_i^0})^2 + \text{Im}(y_d^{\varphi_i^0})^2 \beta_b^{-2} \right] \rho(\varphi_i^0)^{-1}, \\ \mu_{\tau\tau}^{\varphi_i^0} &= C_{gg}^{\varphi_i^0} \left[\text{Re}(y_l^{\varphi_i^0})^2 + \text{Im}(y_l^{\varphi_i^0})^2 \beta_\tau^{-2} \right] \rho(\varphi_i^0)^{-1}, \\ \mu_{\gamma\gamma}^{\varphi_i^0} &= C_{gg}^{\varphi_i^0} C_{\gamma\gamma}^{\varphi_i^0} \rho(\varphi_i^0)^{-1}, \\ \mu_{VV}^{\varphi_i^0} &= C_{gg}^{\varphi_i^0} (\mathcal{R}_{i1})^2 \rho(\varphi_i^0)^{-1}, \\ \mu_{\gamma\gamma jj}^{\varphi_i^0} &= (\mathcal{R}_{i1})^2 C_{\gamma\gamma}^{\varphi_i^0} \rho(\varphi_i^0)^{-1}, \\ \mu_{WWjj}^{\varphi_i^0} &= (\mathcal{R}_{i1})^4 \rho(\varphi_i^0)^{-1}, \end{aligned} \quad (5.14)$$

where $\beta_f = (1 - 4m_f^2/M_{\varphi_i^0}^2)^{1/2}$. The one-loop functions are given by

$$C_{gg}^{\varphi_i^0} = \frac{\sigma(gg \rightarrow \varphi_i^0)}{\sigma(gg \rightarrow h)_{\text{SM}}} = \frac{\left| \sum_q \text{Re}(y_q^{\varphi_i^0}) \mathcal{F}(x_q) \right|^2 + \left| \sum_q \text{Im}(y_q^{\varphi_i^0}) \mathcal{K}(x_q) \right|^2}{\left| \sum_q \mathcal{F}(x_q) \right|^2} \quad (5.15)$$

³ The contamination of the different Higgs production mechanisms in $h \rightarrow \gamma\gamma(jj)$ is discussed in appendix 5.C.

and

$$\begin{aligned}
C_{\gamma\gamma}^{\varphi_i^0} &= \frac{\Gamma(\varphi_i^0 \rightarrow \gamma\gamma)}{\Gamma(h \rightarrow \gamma\gamma)_{\text{SM}}} \\
&= \frac{1}{\left| \sum_f N_C^f Q_f^2 \mathcal{F}(x_f) + \mathcal{G}(x_W) \right|^2} \\
&\quad \times \left\{ \left| \sum_f \text{Re}(y_f^{\varphi_i^0}) N_C^f Q_f^2 \mathcal{F}(x_f) + \mathcal{G}(x_W) \mathcal{R}_{i1} + C_{H^\pm}^{\varphi_i^0} \right|^2 \right. \\
&\quad \left. + \left| \sum_f \text{Im}(y_f^{\varphi_i^0}) N_C^f Q_f^2 \mathcal{K}(x_f) \right|^2 \right\}
\end{aligned} \tag{5.16}$$

with N_C^f and Q_f the number of colours and the electric charge of the fermion f , $x_f = 4m_f^2/M_{\varphi_i^0}^2$ and $x_W = 4M_W^2/M_{\varphi_i^0}^2$. Notice that the ratios (5.11) are defined for $M_{\varphi_i^0} = M_{h_{\text{SM}}}$. The two separate terms in the numerators of Eqs. (5.15) and (5.16) correspond to the CP-even and CP-odd structures $\varphi_i^0 X_{\mu\nu} X^{\mu\nu}$ and $\varphi_i^0 X_{\mu\nu} \tilde{X}^{\mu\nu}$, with $X_{\mu\nu} = G_{\mu\nu}$ ($F_{\mu\nu}$) in the gluon (photon) case and $\tilde{X}^{\mu\nu} = \epsilon^{\mu\nu\sigma\rho} X_{\sigma\rho}$. The functions $\mathcal{F}(x_f)$, $\mathcal{K}(x_f)$ and $\mathcal{G}(x_W)$ contain the triangular 1-loop contributions from fermions and W^\pm bosons. We will neglect the masses of the first two fermion generations. Since $\mathcal{F}(x_f)$ and $\mathcal{K}(x_f)$ vanish for massless fermions, we only need to consider the top, bottom and tau contributions; the last two are negligible in the SM, but in the A2HDM could be enhanced by the alignment factors ς_d and ς_l . In $C_{\gamma\gamma}^{\varphi_i^0}$ we have also considered the contribution from a charged-scalar loop parametrized by

$$C_{H^\pm}^{\varphi_i^0} = \frac{v^2}{2M_{H^\pm}^2} \lambda_{\varphi_i^0 H^+ H^-} \mathcal{A}(x_{H^\pm}), \tag{5.17}$$

with $x_{H^\pm} = 4M_{H^\pm}^2/M_{\varphi_i^0}^2$. The explicit expressions of the different loop functions are:

$$\begin{aligned}
\mathcal{F}(x) &= \frac{x}{2} [4 + (x-1)f(x)], & \mathcal{G}(x) &= -2 - 3x + \left(\frac{3}{2}x - \frac{3}{4}x^2\right)f(x), \\
\mathcal{A}(x) &= -x - \frac{x^2}{4}f(x), & \mathcal{K}(x) &= -\frac{x}{2}f(x),
\end{aligned} \tag{5.18}$$

with

$$f(x) = \begin{cases} -4 \arcsin^2(1/\sqrt{x}), & x \geq 1 \\ \left[\ln \left(\frac{1+\sqrt{1-x}}{1-\sqrt{1-x}} \right) - i\pi \right]^2, & x < 1 \end{cases}. \quad (5.19)$$

5.4 Phenomenological Analysis

We are interested in analyzing the current LHC and Tevatron data within the A2HDM. The experimental information on the new neutral boson is certainly in early stages; some decay channels have very big uncertainties while some others have not even been seen yet. Nevertheless, while more precise information on all possible production and decay channels is necessary in order to make a detailed study, present data already allow us to extract significant constraints on the parameter space of the model.

The deviations from the SM expectations originate from several sources. The three neutral scalars of the A2HDM have couplings to the gauge bosons which are different (smaller in absolute value) than the ones of the SM Higgs: in SM units they are given by \mathcal{R}_{i1} . The Yukawa couplings get also multiplied by the factors $y_f^{\varphi_i^0}$, which are functions of \mathcal{R}_{ij} and the parameters ς_f . Moreover, the presence of a charged scalar manifests in one additional one-loop contribution to the $\varphi_i^0 \rightarrow 2\gamma$ decay amplitudes, parametrized through the constants $C_{H^\pm}^{\varphi_i^0}$. In the limit of CP conservation, there are two clear candidates for the new scalar, the CP-even fields h and H (we will nevertheless analyze later the unlikely A possibility). The A2HDM allows in addition for physical CP-violating phases, both in the scalar potential and the Yukawa couplings, generating mixings among the three neutral scalars and CP-odd contributions to the Higgs-like signal strength parameters. Being quadratic in the CP-violating parameters, this last type of corrections could be expected to be small. However, the current bounds on the A2HDM couplings still allow for sizeable effects [25–30].

Sensitivity to the top-quark Yukawa coupling and to a lesser extent to the bottom coupling appears through the one-loop production mechanism of gluon fusion and in the $\gamma\gamma$ decay channel. Neutral scalar production via $pp \rightarrow t\varphi_i^0 j(b)$ could provide complementary information on the top Yukawa coupling when more data becomes available [66, 67]. The most important constraints on the bottom Yukawa coupling come indirectly from the total decay width, which is in general dominated by $\varphi_i^0 \rightarrow b\bar{b}$, and the measurement of scalar production with an associated vector boson ($q\bar{q}' \rightarrow \varphi_i^0 V \rightarrow (b\bar{b})V$). Neutral boson production via top-quark fusion with subsequent decay into a pair of b quarks, $q\bar{q}/gg \rightarrow t\bar{t}\varphi_i^0 \rightarrow t\bar{t}(b\bar{b})$, in

which the bottom and top Yukawa couplings appear at tree level will also play an important role; the current experimental sensitivities in this channel are still low [68, 69]. The τ Yukawa coupling is directly tested through $\varphi_i^0 \rightarrow \tau^+\tau^-$, the most accessible production mechanisms at the LHC being in this case vector-boson fusion, associated production with a vector boson and gluon fusion.

For a given choice of neutral scalar-field candidate φ_i^0 and its couplings, we define the χ^2 function as

$$\chi^2(\varphi_i^0) = \sum_k \frac{\left(\mu_k^{\varphi_i^0} - \hat{\mu}_k\right)^2}{\sigma_k^2}, \quad (5.20)$$

where k runs over the different production/decay channels considered, $\hat{\mu}_k$ and σ_k are the measured Higgs signal strengths and their one-sigma errors, respectively, and $\mu_k^{\varphi_i^0}$ the corresponding theoretical predictions in terms of the A2HDM parameters, as given in Eqs. (5.11) and (5.14). Scanning over the allowed parameter space, we then look for those sets of couplings minimizing the χ^2 and their corresponding uncertainties. The details about the statistical treatment and data used in this work are presented in appendix 5.C.

We will first analyze the CP-conserving limit in section 5.4.1, where we will also study some particular scenarios often adopted in previous works. In section 5.4.2 we will discuss the most general case, without making any assumption about the scalar potential, and analyze the present constraints on the complex Yukawa couplings of the assumed 126 GeV scalar boson.

5.4.1 The A2HDM in the CP-conserving limit

Assuming that the Lagrangian preserves the CP symmetry, the two CP-even neutral scalars h and H couple to the gauge bosons with reduced couplings $\mathcal{R}_{11} = \cos \tilde{\alpha}$ and $\mathcal{R}_{21} = -\sin \tilde{\alpha}$, respectively, and their Yukawa couplings are real:

$$y_f^h = \cos \tilde{\alpha} + \varsigma_f \sin \tilde{\alpha}, \quad y_f^H = -\sin \tilde{\alpha} + \varsigma_f \cos \tilde{\alpha}. \quad (5.21)$$

The CP-odd boson A does not couple at tree-level to W^+W^- and ZZ ($\mathcal{R}_{31} = 0$), while its fermionic couplings are purely imaginary (pseudoscalar interaction):

$$y_{d,l}^A = i \varsigma_{d,l}, \quad y_u^A = -i \varsigma_u. \quad (5.22)$$

5.4.1.1 A light CP-even Higgs at 126 GeV

We will first focus in the most plausible possibility that the lightest scalar h corresponds to the observed neutral boson with $M_h = 126$ GeV. The alternative choice of the heavier field H can be easily recovered through an appropriate change of the mixing angle, $\tilde{\alpha} \rightarrow \tilde{\alpha} - \pi/2$, and will be further discussed in section 5.4.1.5. We will also consider later, in section 5.4.1.6, the more exotic case of a CP-odd Higgs A . In this first analysis we assume that the charged scalar is either very heavy or its coupling to the neutral Higgs is very small, so that its contribution $C_{H^\pm}^h$ to the $h \rightarrow \gamma\gamma$ decay width is negligible. We also assume that the bounds from flavour physics are naturally evaded, as it is the case at large values of the charged scalar mass. The H^\pm contribution to the diphoton decay width as well as the flavour constraints will be considered later in section 5.4.1.3.

The minimization of $\chi^2(h)$ leads to two different solutions, differing in the sign of the top Yukawa coupling. The central values of the corresponding A2HDM parameters and their statistical one-sigma errors obtained from the global fit are:

$$\begin{aligned} \cos \tilde{\alpha} &= 0.99_{-0.06}^{+0.01}, & y_u^h &= 0.8_{-0.2}^{+0.1}, \\ |y_d^h| &= 0.7 \pm 0.3, & |y_l^h| &= 0.8 \pm 0.5, \end{aligned} \quad (5.23)$$

and

$$\begin{aligned} \cos \tilde{\alpha} &= 0.99_{-0.04}^{+0.01}, & y_u^h &= -0.8_{-0.3}^{+0.1}, \\ |y_d^h| &= 1.1 \pm 0.3, & |y_l^h| &= 0.9 \pm 0.5. \end{aligned} \quad (5.24)$$

In both cases, the gauge coupling g_{hVV} is very close to the SM one. Changing simultaneously the signs of $\cos \tilde{\alpha}$ and y_f^h leads obviously to identical Higgs signal strengths and, therefore, to two equivalent solutions.

In the first solution the W^\pm and top-quark loops contribute with different signs to the $h \rightarrow \gamma\gamma$ amplitude, giving a destructive interference as in the SM. The needed enhancement of the 2γ branching ratio is obtained through a smaller total decay width, $\rho(h) \approx 0.6$. This pushes upward the ratios $\mu_{\gamma\gamma}^h$ and $\mu_{\gamma\gamma jj}^h$, allowing to explain part of the excess experimentally observed in these two channels. However, the gluon-fusion production channel has a smaller cross section than in the SM. The combined effect results in a small increase of the $\gamma\gamma$ channel, $\mu_{\gamma\gamma}^h \approx 1.1$, while a much larger enhancement remains in the $\gamma\gamma jj$ case, $\mu_{\gamma\gamma jj}^h \approx 1.5$.

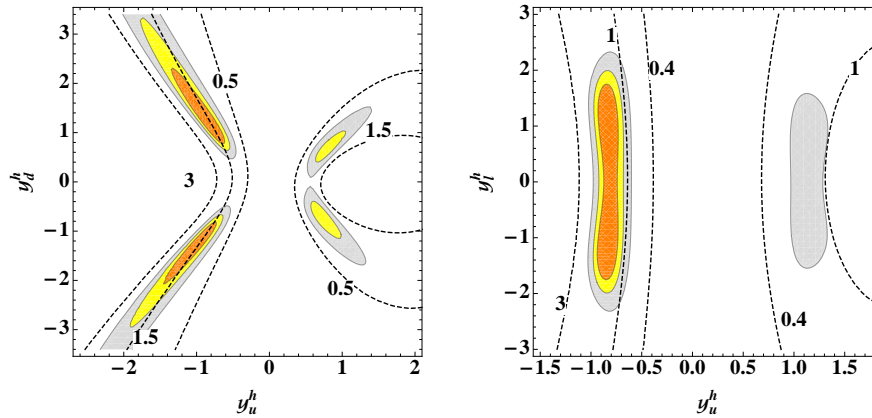


Figure 5.1: Global fit to the A2HDM, in the CP-conserving case, in the planes $y_u^h - y_d^h$ (left) and $y_u^h - y_l^h$ (right). The parameters not shown in each case are fixed to the best global-fit point. The orange, yellow and gray areas denote 68%, 90% and 99% CL regions. The dashed lines correspond to fixed values of $\mu_{\gamma\gamma}^h$.

The second solution corresponds to a top-quark contribution to $h \rightarrow \gamma\gamma$ with the opposite sign, so that it interferes constructively with the W^\pm amplitude. This allows one to explain the 2γ excess without hardly modifying the total decay rate, $\rho(h) \approx 1.1$ and providing a slightly better fit.

In both solutions there is a sign degeneracy in the bottom and tau Yukawa couplings. Although the tree-level decays $h \rightarrow \bar{b}b$ and $h \rightarrow \tau^+\tau^-$ are insensitive to these signs, the loop-induced processes $gg \rightarrow h$ and $h \rightarrow \gamma\gamma$ receive contributions from the bottom and tau (only the $\gamma\gamma$ process) Yukawas, which interfere with the leading top and W^\pm (in the $\gamma\gamma$ decay) amplitudes as shown in (5.15) and (5.16). In the SM the bottom and tau contributions are negligible, but their effect could be relevant in the A2HDM if the top Yukawa coupling is considerably suppressed or if the parameters $\varsigma_{d,l}$ are large. However, this is not the case for the fitted Yukawa values in (5.23) and (5.24), which are of $\mathcal{O}(1)$ for both solutions, leaving the sign of the bottom and tau Yukawas undetermined. The relevance of the $\tau^+\tau^-$ and $\bar{b}b$ channels to determine possible deviations from the SM and within the different \mathcal{Z}_2 versions of the 2HDM, which could be pointing to a more general Yukawa structure as provided by the A2HDM, has been emphasized recently in Ref. [53].

In Fig. 5.1 we show graphically the results of this global fit, giving the allowed regions in the $y_u^h - y_d^h$ (left) and $y_u^h - y_l^h$ (right) planes at 68%, 90% and 99% CL. The parameters that are not shown are, in each case, set to the best global-fit

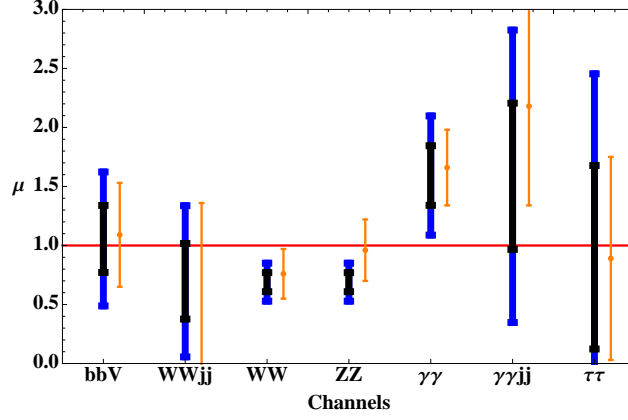


Figure 5.2: Allowed ranges for the Higgs signal strengths obtained from the fit (5.24) at 1σ (black, dark) and 2σ (blue, dark), together with the averaged experimental data from the ATLAS, CMS, CDF and DØ collaborations with the corresponding 1σ errors (orange, light).

point. The sign degeneracy in the τ and b Yukawa couplings is clearly observed. Moreover, the right panel shows a somewhat reduced sensitivity to the leptonic coupling y_l^h . The SM-like solution $(y_u^h, y_{d,l}^h) = (1, 1)$ lies inside the 90% CL allowed region; however, at 68% CL the top Yukawa has the sign flipped with respect to the SM, *i.e.*, only the solution (5.24) remains. Similar results have also been obtained in Ref. [24, 53].

The allowed ranges, at the 1σ and 2σ level, for the different Higgs signal strengths in the fit (5.24) are compared in Fig. 5.2 with the experimental values. A good agreement with data is obtained in all cases. Previous analyses within the CP-conserving A2HDM have been performed in Refs. [53, 54], using a different notation, also finding good agreement with the data.

Using the sum rules in Eqs. (5.7) and (5.9), we can extract constraints on the heavy CP-even Higgs couplings from our global fit with $M_h = 126$ GeV. For the solution (5.24) we find at 68% CL that the coupling of H to vector bosons is suppressed, $\sin \tilde{\alpha} < 0.37$, while its coupling to top quarks is very large, $|y_u^H| > 4.6$. This region of parameter space requires a very large value of $|\zeta_u|$ in order to flip the sign of y_u^h , which is the top Yukawa of h . Such large values of $|\zeta_u|$ would then imply a significant enhancement of the production of H via gluon fusion and can give rise to non-perturbative $H^+ \bar{t}b$, $H \bar{t}t$ and $A \bar{t}t$ couplings. This was noted previously within the same context in Ref. [53].

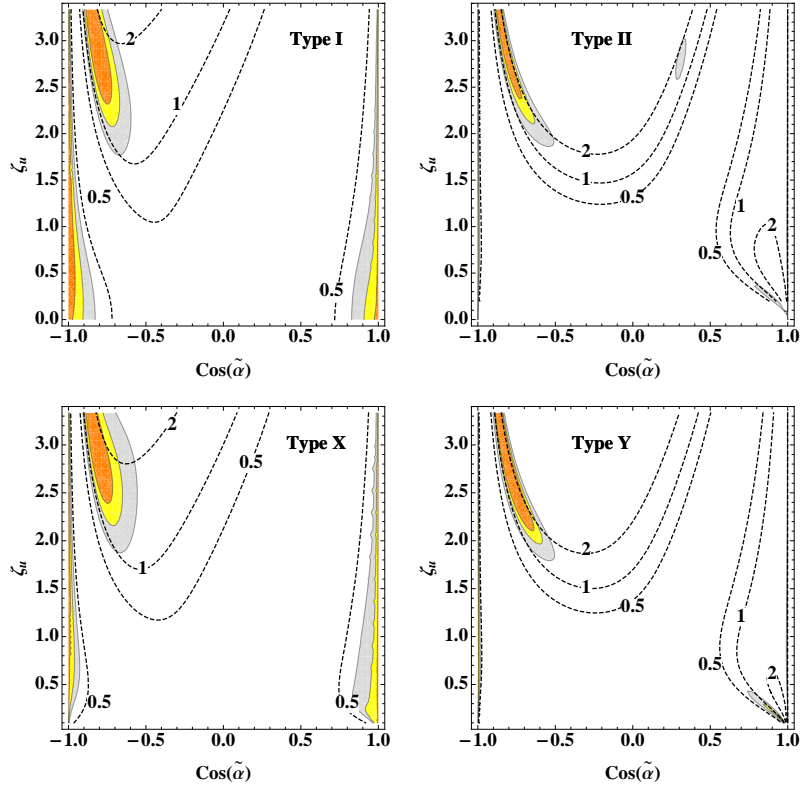


Figure 5.3: Global fit within 2HDMs of types I (upper left), II (upper right), X (lower left) and Y (lower right), at 68% (orange), 90% (yellow) and 99% (gray) CL. The dashed lines correspond to constant values of $\mu_{\gamma\gamma}^h$.

5.4.1.2 Global fit within \mathcal{Z}_2 models

The usual 2HDMs with natural flavour conservation, based on discrete \mathcal{Z}_2 symmetries, are particular cases of the CP-conserving A2HDM, with ζ_f taking the values given in Table 5.1. Thus, the three alignment factors are determined by a single parameter through the constraints $\zeta_u = \zeta_d = \zeta_l = \cot \beta$ (type I), $\zeta_u = -\zeta_d^{-1} = -\zeta_l^{-1} = \cot \beta$ (type II), $\zeta_u = \zeta_d = -\zeta_l^{-1} = \cot \beta$ (type X) and $\zeta_u = -\zeta_d^{-1} = \zeta_l = \cot \beta$ (type Y), with $\cot \beta = v_1/v_2 \geq 0$. This leads to specific relations among the production cross sections and decay rates for the Higgs bosons that can be tested with the LHC data. The separate measurement of the various Higgs signal strengths should allow to disentangle the different scalings of the three Yukawa couplings. In particular, exclusive Higgs production measurements

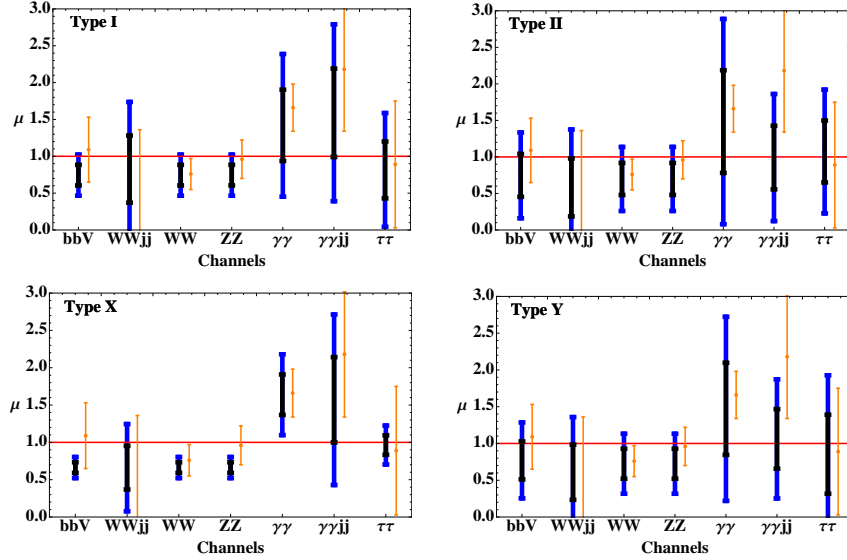


Figure 5.4: Allowed ranges for the Higgs signal strengths in 2HDMs of type I, II, X and Y, at 1σ (black, dark) and 2σ (blue, dark). Other captions as in Fig. 5.2.

in the final states $\tau^+\tau^-$ and $b\bar{b}$ will be crucial to test the different \mathcal{Z}_2 versions of the 2HDM [33, 43, 53].

Figure 5.3 shows the results of the global fit for the 2HDMs of types I, II, X and Y, assuming that the lightest neutral Higgs h is the boson observed around 126 GeV. Allowed regions at 68%, 90% and 99% CL are shown, together with lines of constant $\mu_{\gamma\gamma}^h$. The relevance of the diphoton channel is evident from the figure. In models I and X, an allowed region around $\cos\tilde{\alpha} \approx 1$ appears, where there is no sensitivity to ζ_u since its contribution to the neutral Yukawa couplings is suppressed by $\sin\tilde{\alpha}$; in this region the couplings of h to vector bosons and fermions are close to the SM ones. Another allowed region appears for negative values of $\cos\tilde{\alpha}$, in which the W^\pm and top-quark loops contribute with the same sign to the $h \rightarrow \gamma\gamma$ decay amplitude, thus allowing for a constructive interference. Both solutions with $\cos\tilde{\alpha} \approx \pm 1$ are present for the inert model (type I with $\zeta_u = 0$). There is a third allowed region at large values of the top Yukawa and negative $\cos\tilde{\alpha}$, which approaches $\cos\tilde{\alpha} = -1$ as ζ_u increases.

In models II and Y the solutions around $\cos\tilde{\alpha} \approx \pm 1$ reduce to two extremely narrow vertical lines and one small region at low ζ_u and positive $\cos\tilde{\alpha}$, which remain allowed at 99% CL but are not present at 90%. The solution at large

values of the top Yukawa and negative $\cos \tilde{\alpha}$ is also present, but in a region much smaller than in models I and X.

Figure 5.4 shows the allowed ranges for the Higgs signal strengths obtained in these four types of 2HDMs (I, II, X and Y). The agreement with the data is good; however, as already noted in Ref. [43], the preferred region has large values of $|\zeta_u|$, which are ruled out from flavour physics constraints for a charged Higgs boson below the TeV scale. Large values of $|\zeta_u|$ can also make some top-quark Yukawa couplings non-perturbative, as commented in the previous section.

5.4.1.3 A charged Higgs and the diphoton excess

One of the most distinctive features of 2HDMs with respect to other alternative scenarios of electroweak symmetry breaking is the presence of a charged scalar boson in the spectrum. The present experimental lower bound on the H^\pm mass is $M_{H^\pm} \gtrsim 80$ GeV (95% CL) [70], assuming that the charged scalar H^+ only decays into the fermionic channels $H^+ \rightarrow c\bar{s}$ and $H^+ \rightarrow \tau^+\nu_\tau$. A slightly softer limit $M_{H^\pm} \gtrsim 72.5$ GeV is obtained, allowing for the decay $H^+ \rightarrow W^+A \rightarrow W^+b\bar{b}$, with $M_A > 12$ GeV, and assuming a type-I fermionic structure [70]. A model-independent bound can be extracted from the measured Z width which constrains the Z decays into non-SM modes, and in particular $Z \rightarrow H^+H^-$, to be below $\Gamma_Z^{\text{non-SM}} < 2.9$ MeV (95% CL); this implies $M_{H^\pm} \gtrsim 39.6$ GeV (95% CL) [70].

Direct searches for charged Higgs bosons at the Tevatron [71] and the LHC [72] have also been performed with null results so far.

Current LHC data are sensitive to such charged scalar through the $h \rightarrow \gamma\gamma$ decay channel. The one-loop H^\pm contribution can interfere with the W^\pm and fermionic amplitudes, thus being able to enhance or suppress the decay rate. The exact value of the charged Higgs contribution $C_{H^\pm}^h$ depends on the cubic Higgs coupling $\lambda_{hH^+H^-}$ and the charged Higgs mass M_{H^\pm} . One expects however that $|C_{H^\pm}^h| \lesssim O(1)$ based on perturbativity arguments (see appendix 5.D).

When considering a relatively light charged Higgs boson, one must take into account constraints from electroweak precision tests and the flavour sector; a light H^\pm would contribute sizably to loop-induced processes, such as $Z \rightarrow \bar{b}b$, $b \rightarrow s\gamma$ or $B^0-\bar{B}^0$ mixing. These phenomenological constraints have been analyzed in detail within the framework of the A2HDM in Refs. [27–30], where it has been found that a charged Higgs below the TeV scale would require $|\zeta_u| \lesssim 2$ to be compatible with present data. This rules out the hypothetical scenario of a top Yukawa coupling with flipped sign, as found in (5.24) and also favoured by the fits shown in Fig. 5.3 within the four types of \mathcal{Z}_2 models. The reason is that

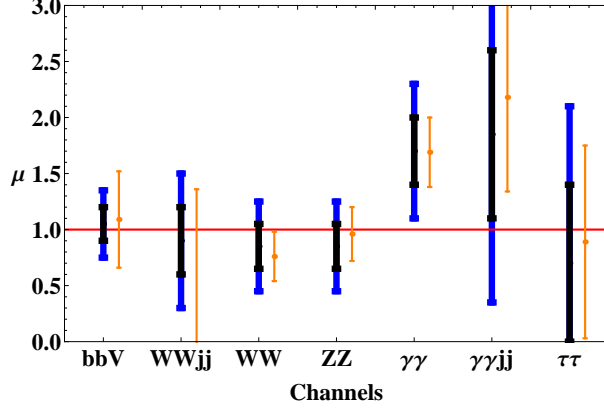


Figure 5.5: Allowed ranges for the Higgs signal strengths from the global fit within the CP-conserving A2HDM, including the charged Higgs contribution to $h \rightarrow \gamma\gamma$, at 1σ (black, dark) and 2σ (blue, dark). Other captions as in Figure 5.2.

current $h \rightarrow WW, ZZ, \gamma\gamma(jj)$ data require $|\cos \tilde{\alpha}| \sim 1$ (*i.e.*, the gauge coupling of the new neutral scalar should be close to the SM one). Since the top Yukawa coupling is given by $y_u^h = \cos \tilde{\alpha} + \varsigma_u \sin \tilde{\alpha}$, in order to flip the sign of y_u^h one needs then a large value for $|\varsigma_u|$, which is excluded by the previous bound.

Including the charged-Higgs contribution, it is no longer necessary to flip the sign of the top Yukawa in order to enhance the $h \rightarrow \gamma\gamma$ decay width. The best fit region is now obtained for Yukawa and gauge couplings close to the SM limit:

$$\begin{aligned} \cos \tilde{\alpha} &= 0.98_{-0.06}^{+0.02}, & C_{H^\pm}^h &= (-2.8 \pm 1.3) \cup (16.0 \pm 1.3), \\ y_u^h &= 1.0 \pm 0.2, & |y_d^h| &= 1.1 \pm 0.3, & |y_l^h| &= 0.8 \pm 0.5. \end{aligned} \quad (5.25)$$

The two disjoint $C_{H^\pm}^h$ solutions correspond to either a constructive interference of the H^\pm and W^\pm amplitudes or a destructive one but with a charged-Higgs contribution so large that it reverses the sign of the total $h \rightarrow 2\gamma$ amplitude. In both cases, one obtains a better fit than in the SM and also better than the previous A2HDM fits (except for (5.24) which is comparable to this one). The presence of the charged Higgs allows one to easily explain the $h \rightarrow \gamma\gamma(jj)$ excess without large modifications of the total decay rate (*i.e.*, $\rho(h) \approx 1.1$). The fit predictions for the μ_k ratios and their one and two-sigma statistical errors are shown in Fig. 5.5. In all cases, good agreement with the data is obtained.

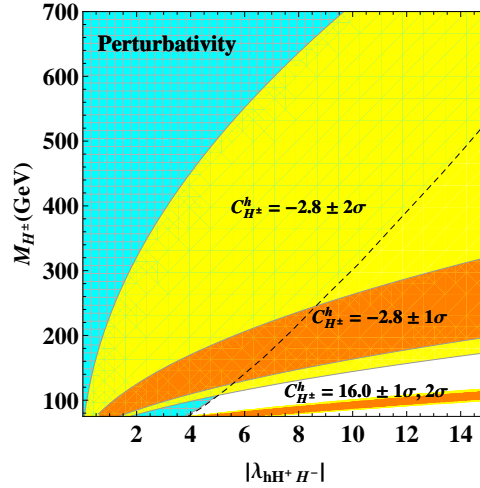


Figure 5.6: Allowed regions of the $(|\lambda_{hH^+H^-}|, M_{H^\pm})$ plane, corresponding to the two possible fitted values of $C_{H^\pm}^h$, at 68% (orange, dark) and 90% CL (yellow, light). The blue (hashed) area, between the left vertical axis and the dashed line, is the domain where the theory remains perturbative.

In Fig. 5.6 we show the allowed regions of the $(|\lambda_{hH^+H^-}|, M_{H^\pm})$ plane, corresponding to the two possible fitted values of $C_{H^\pm}^h$, at 68% and 90% CL, together with the perturbativity bounds discussed in appendix 5.D. Clearly, the solution with a very large contribution to $h \rightarrow \gamma\gamma$ from the charged Higgs ($C_{H^\pm}^h \approx 16$) is excluded if one requires the theory to be perturbative. We obtain an upper bound for the mass of the charged Higgs around 300 GeV, at the one-sigma level. However, the bound disappears at the two-sigma level because the charged-Higgs contribution becomes compatible with zero.

5.4.1.4 Inert 2HDM

In the inert 2HDM a \mathcal{Z}_2 symmetry is imposed, in the Higgs basis (5.2), under which all SM fields and Φ_1 are even while $\Phi_2 \rightarrow -\Phi_2$. Terms with an odd number of Φ_2 fields in the scalar potential (5.31) are then forbidden by the \mathcal{Z}_2 symmetry, therefore $\mu_3 = \lambda_6 = \lambda_7 = 0$. In this case there is no mixing between the CP-even neutral states h and H , and the scalars H , A and H^\pm decouple from the fermions. The couplings of the remaining Higgs field h to fermions and to vector bosons are the same than in the SM (*i.e.*, $\cos \tilde{\alpha} = 1$ and $y_f^h = 1$). Thus, only the diphoton channels can show a deviation from the SM prediction (assuming that there are no open decay channels other than the SM ones). From the global fit

of this scenario, we find a charged-Higgs contribution to the $h \rightarrow \gamma\gamma$ amplitude in the range $C_{H^\pm}^h \in [-1.7, -0.89]$ at 68% CL and $C_{H^\pm}^h \in [-2.4, -0.1]$ at 90% CL. We have assumed that M_{H^\pm} is greater than $M_h/2 \approx 63$ GeV so that $C_{H^\pm}^h$ is real; for lower charged-Higgs masses, it would develop an imaginary absorptive part. The fitted negative sign of $C_{H^\pm}^h$ causes a constructive interference with the W^\pm amplitude in the $h \rightarrow \gamma\gamma$ decay width.

Note that in the limit $\varsigma_f = 0$, the charged Higgs does not couple to fermions independently of any assumption on the scalar potential, see Eq. (5.4). The implications of this more general case for the neutral Higgs boson phenomenology as well as the possibility of a very light charged Higgs boson are discussed in section 5.4.2.2. Detailed analyses of the inert 2HDM and the possibility of a Dark Matter candidate within this model, in light of the LHC data, can be found in Refs. [39, 73]. An enhancement of the $h \rightarrow \gamma\gamma$ decay rate has also been discussed in Ref. [74] within the Quasi-Inert 2HDM in connection with the top forward-backward asymmetry observed at the Tevatron; the limit on $C_{H^\pm}^h$ obtained in this section also applies to this scenario.

5.4.1.5 A heavy CP-even Higgs at 126 GeV

We have discussed so far the phenomenology of the lightest Higgs boson, but there is nothing a priori preventing the boson discovered by ATLAS and CMS to be identified with the heaviest CP-even state H or with the CP-odd Higgs A . These possibilities have been already discussed in Refs. [35, 37, 53]. An analysis in terms of the more general CP-violating scalar potential, setting limits on the scalar-pseudoscalar mixing, has been done in Ref. [36].

Using the previous fits for h , it is straightforward to analyze the possibility of having a heavy Higgs with $M_H = 126$ GeV. Assuming that non-SM decays like $H \rightarrow hh$ are kinematically forbidden or very suppressed, the constraints on the heavy Higgs boson couplings can be easily obtained from those of h through an appropriate change of the mixing angle: $\tilde{\alpha} \rightarrow \tilde{\alpha} - \pi/2$. In this case the coupling of the heavy Higgs to vector bosons is close to the SM limit ($\sin \tilde{\alpha} \approx 1$), while the light-scalar g_{hVV} couplings are suppressed by $\cos \tilde{\alpha} \approx 0$. The absolute values of the Yukawa couplings and all the other parameters remain unchanged. A solution analogous to the one in Eq. (5.24), where a large value of $|\varsigma_u|$ is required to flip the sign of the top Yukawa coupling, is excluded by low energy flavour constraints for a charged Higgs below the TeV scale ($Z \rightarrow \bar{b}b$, $B^0 - \bar{B}^0$ mixing and neutral Kaon mixing [27]).

The LEP searches for neutral Higgs particles could have missed the light scalar h , since the associated production with a vector boson would be strongly

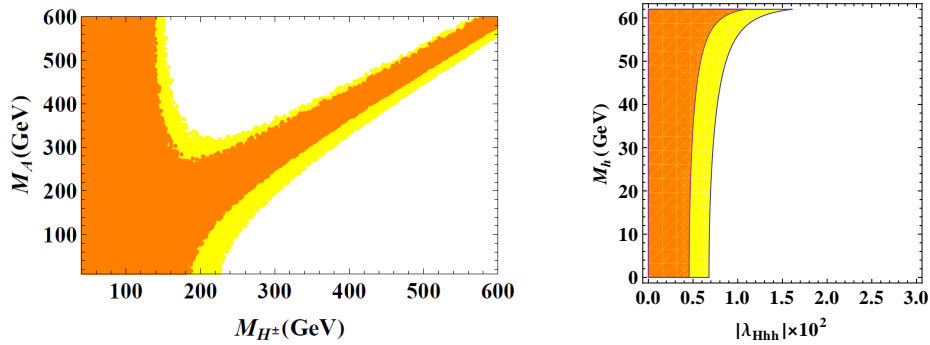


Figure 5.7: *Left-panel: Constraint in the (M_{H^\pm}, M_A) plane from the oblique parameters S , T and U . Right-panel: Constraints from the invisible Higgs decay width in the $(|\lambda_{Hhh}|, M_h)$ plane, assuming SM couplings of H to fermions and vector bosons. The orange (dark) and yellow (light) regions are allowed at 68% and 90% CL.*

suppressed. Moreover, $|y_d^h| \sim |\varsigma_d|$ could be small enough to avoid the constraints from the usual $h \rightarrow b\bar{b}$ search mode. The OPAL collaboration performed a decay-mode-independent search for a light neutral scalar and found upper limits for the Higgs-strahlung cross section in units of the SM: $(\mathcal{R}_{11})^2 \equiv (g_{hVV}/g_{hVV}^{\text{SM}})^2 < 0.1$ for $M_h < 19$ GeV, and $(\mathcal{R}_{11})^2 < 1$ for $M_h < 81$ GeV [75]. Together with the constraints from electroweak precision tests at the Z peak, this provides useful information on the allowed mass spectrum for the remaining scalars. Using the current bounds from the oblique parameters S , T and U [76, 77] (the corresponding A2HDM formulae are given in appendix 5.E), we show in the left panel of Fig. 5.7 the allowed regions in the (M_{H^\pm}, M_A) plane. We have set $M_H = 126$ GeV and $\sin \tilde{\alpha} \in [0.7, 1]$. The constraints shown in the figure turn out to be determined by the T parameter, since S and U give weaker restrictions. The charged scalar mass is of course constrained by the direct experimental lower bound discussed before, but its exact value depends on the assumed decay channels. The region where both M_{H^\pm} and M_A become very heavy corresponds to uncomfortably large values of the quartic couplings λ_i of the scalar potential and the theory is no longer perturbative.

A light neutral boson h or A below the kinematical threshold of $M_H/2 \approx 63$ GeV would have important phenomenological consequences, because the 126 GeV Higgs could decay into lighter scalars. These decay channels can be included in our fit in terms of an invisible decay width as long as we neglect possible contri-

butions from cascade decays into the observed final states.⁴ In general one would expect in this case a suppression of the measured Higgs decay rates compared with the SM, due to the larger total width of the scalar H . Current data for the $\gamma\gamma$ channel, however, shows a slight enhancement over the SM prediction, thus placing strong bounds on possible invisible decays of the 126 GeV Higgs boson. Assuming that the heavy-Higgs couplings to fermions and vector bosons are SM-like (*i.e.*, $y_f^H = 1$ and $\sin \tilde{\alpha} = 1$), the best fit point is obtained for a null invisible H decay width; at 68% CL (90% CL) we obtain an upper bound of 9% (20%) on the invisible H decay width (in units of the SM total decay width).

Considering the scenario of a very light CP-even Higgs h , the decay width of the heavier CP-even scalar into hh is given by

$$\Gamma(H \rightarrow hh) = \frac{v^2 \lambda_{Hhh}^2}{8\pi M_H} \left(1 - \frac{4M_h^2}{M_H^2}\right)^{1/2}, \quad (5.26)$$

where the cubic scalar coupling λ_{Hhh} is expressed in units of v and can be obtained from Eq. (5.43). In the right panel of Fig. 5.7 we show the constraints from our $\Gamma(H \rightarrow hh)$ fit in the $(|\lambda_{Hhh}|, M_h)$ plane. Strong bounds are obtained for the cubic Higgs coupling, $|\lambda_{Hhh}| \lesssim 10^{-2}$, as expected.

Recent updates from the ATLAS collaboration in the high-resolution channels report a significant difference in the mass of the neutral boson as determined from $H \rightarrow ZZ^{(*)} \rightarrow 4\ell$ ($123.5 \pm 0.8 \pm 0.3$ GeV) and $H \rightarrow \gamma\gamma$ ($126.6 \pm 0.3 \pm 0.7$ GeV) events [1]. Here we do not consider as a possible explanation for this discrepancy, the possibility of having two quasi-degenerate Higgs bosons, since the current mass value in the $H \rightarrow ZZ^{(*)} \rightarrow 4\ell$ channel obtained by CMS, $126.2 \pm 0.6 \pm 0.2$ GeV [3], does not support this hypothesis.

5.4.1.6 Degenerate CP-even and CP-odd Higgs bosons at 126 GeV

A CP-odd scalar does not couple at tree level to two vector bosons; its decay to gauge bosons starts at the one-loop level and it is therefore very suppressed. For this reason, a pure CP-odd Higgs boson is already strongly disfavoured by present data as a candidate for the 126 GeV boson. However, the observed signal could result from two Higgs bosons with quasi-degenerate masses; this could explain the excess of $\gamma\gamma$ events observed by ATLAS and CMS. This possibility was proposed in Ref. [79] within the non-minimal supersymmetric extension of

⁴These effects are beyond the scope of the present work, but they could be relevant. For example, $H \rightarrow AA \rightarrow \gamma\gamma + \gamma\gamma$ could be mistaken by a two-photon signal when the photon pairs are very collimated [78]

the SM, and has also been considered within the context of 2HDMs, both for \mathcal{Z}_2 versions [80–82] and with a more general Yukawa structure [53, 55]. Model-independent methods to test experimentally for such possibility have also been proposed recently in Refs. [83, 84].

We consider in this section the possibility of two Higgs bosons with quasi-degenerate masses around 126 GeV, one of them being CP-even and the other one CP-odd. We perform a global fit of the data with $M_h = M_A \approx 126$ GeV, and comment on the alternative possibility of quasi-degenerate H and A . The observed Higgs signals strengths will then receive contributions from both particles:

$$\mu_k^{(h+A)} = \mu_k^h + \mu_k^A. \quad (5.27)$$

Given the presently large experimental uncertainties, we neglect the small AVV coupling generated at one loop. Therefore, among all the channels considered in this work, the CP-odd Higgs will only contribute to $A \rightarrow \tau\tau$ and $A \rightarrow \gamma\gamma$. In both cases the dominant production channel is the gluon-fusion one. The loop-induced decay $A \rightarrow \gamma\gamma$ is only mediated by fermions. In Fig. 5.8 (left) we show the constraints on M_{H^\pm} and M_H obtained from the oblique parameters. These masses are varied in the ranges $M_{H^\pm} \in [50, 600]$ GeV and $M_H \in [126, 600]$ GeV, while the coupling of h to vector bosons is kept close to the SM limit (*i.e.*, $|\cos \tilde{\alpha}| \in [0.8, 1]$), as suggested by the current experimental data. In the right panel of Fig. 5.8 we show similar bounds on the plane (M_{H^\pm}, M_h) , keeping the light scalar mass below $M_H = M_A = 126$ GeV and taking $\sin \tilde{\alpha} \in [0.8, 1]$; in this case the oblique parameters require the existence of a charged Higgs below the electroweak symmetry breaking scale $v = 246$ GeV.

In the scenario $M_h = M_A = 126$ GeV, the best fit region in the A2HDM parameter space, assuming the charged Higgs contribution to the 2γ channel to be negligible, is given by:

$$\begin{aligned} \cos \tilde{\alpha} &= 0.98 \pm 0.2, & \varsigma_u &= -1.1^{+0.5}_{-0.4}, \\ |\varsigma_d| &= 1.2 \pm 1.2, & \varsigma_l &= -0.2^{+0.6}_{-0.4}. \end{aligned} \quad (5.28)$$

The corresponding allowed ranges for the Higgs signal strengths, at 1σ and 2σ , are shown in Fig. 5.9. We obtain a smaller total decay width of the CP-even boson, $\rho(h) \approx 0.7$, which produces a sizeable enhancement of the $\mu_{\gamma\gamma jj}^h$ signal strength (the CP-odd boson A does not contribute to this channel). On the other hand, the excess in the two photon channel comes from the decays of both A and h , which give contributions of similar size ($\mu_{\gamma\gamma}^h \approx \mu_{\gamma\gamma}^A \approx 0.7$). The remaining contribution of A is to the $\tau^+\tau^-$ decay channel, which is small (ς_l is small). We

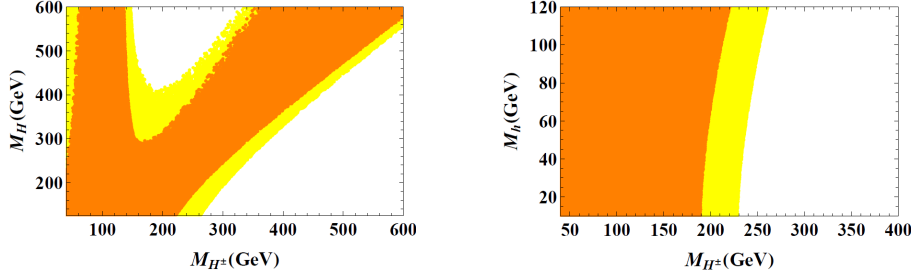


Figure 5.8: Constraints in the (M_{H^\pm}, M_H) plane for the case $M_h = M_A = 126$ GeV (left) and in the (M_{H^\pm}, M_h) plane for the case $M_H = M_A = 126$ GeV (right), from the oblique parameters S , T and U . The orange (dark) and yellow (light) regions are allowed at 68% and 90% CL.

must also notice that solutions with a flipped relative sign between the W and top contributions to $h \rightarrow \gamma\gamma$ are not allowed because they would require large values of ς_u ; this would increase C_{gg}^A and $C_{\gamma\gamma}^A$ generating a large excess in the $\tau^+\tau^-$ and $\gamma\gamma$ channels, exceeding the current experimental bounds.

It is important to note that for a light charged Higgs boson, very strong flavour constraints in the $\varsigma_u - \varsigma_d$ plane can be obtained from $\bar{B} \rightarrow X_s \gamma$ [27]. The allowed ranges at 68% CL shown in Eq. (5.28) were obtained assuming that the charged Higgs contribution to the diphoton channel is negligible (this is true even for a light charged Higgs if $\lambda_{hH^+H^-} \simeq 0$). Including the charged Higgs contribution to the 2γ channel in the fit one obtains at 68% CL that $C_{H^\pm}^h = -3.0 \pm 1.4$, while the alignment parameters ς_f remain weakly constrained and compatible with zero. In the limit $\varsigma_f = 0$, the stringent flavour constraints for a light charged Higgs, in particular $\bar{B} \rightarrow X_s \gamma$, are avoided since the charged Higgs decouples from the fermions. These constraints would be particularly relevant in the scenario $M_H = M_A = 126$ GeV for which the charged Higgs mass is bounded to lie below the electroweak scale, see Figure 5.8 (right).

5.4.2 The CP-violating A2HDM

In the A2HDM the up and down-quark as well as the leptonic Yukawa couplings are all independent complex parameters. Thus, one can expect a very rich phenomenology associated to the Higgs sector responsible for the breaking of the electroweak symmetry. Moreover, if one considers the most general scalar potential, the neutral scalars h , H and A are not CP eigenstates but rather a mixture

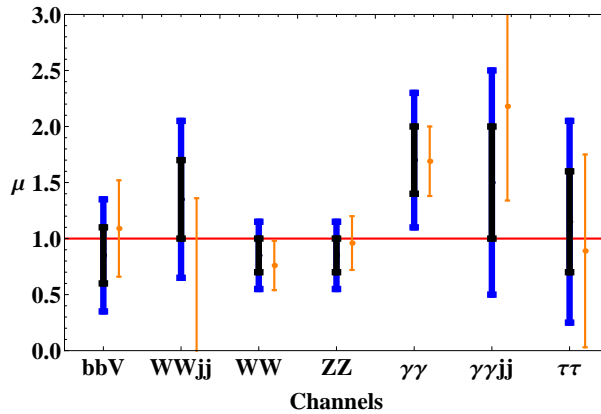


Figure 5.9: Allowed ranges for the Higgs signal strengths from the global fit within the CP-conserving $A2HDM$ for the case of degenerate Higgs bosons with $M_h = M_A = 126$ GeV, at 1σ (black, dark) and 2σ (blue, dark). Other captions as in Figure 5.2.

of CP-even and CP-odd fields, parametrized by the general orthogonal matrix \mathcal{R} introduced in section 5.2. Thus, there are new sources of CP violation, both from the Yukawa sector and the scalar potential, which could lead to interesting phenomenological predictions.

The study of CP-violating observables is beyond the scope of the present work and we will defer it to future publications.⁵ Nevertheless, we shall investigate next, the sensitivity of the different (CP-conserving) Higgs signal strengths to the CP-violating phases. Since the present data are consistent with the SM within rather large uncertainties, we will consider separately the different CP-odd possibilities, by fitting some complex coupling constants to the Higgs-signal-strength data while setting the remaining parameters to their SM-like values. A similar analysis has also been performed within a model independent framework in Ref. [24].

5.4.2.1 Complex Yukawa couplings

Let us consider φ_i^0 to be the observed boson with a mass of 126 GeV. We will analyze three simple scenarios that will serve to determine the sensitivity to its complex Yukawa couplings and to what extent the SM limit is preferred by

⁵ For theoretical studies about the CP-properties of extended Higgs sectors at the LHC and in possible future colliders see Ref. [85] and references therein.

present data. We will set two Yukawa couplings to their SM values ($y_f^{\varphi_i^0} = 1$), and find the preferred values for the remaining Yukawa coupling by minimizing the χ^2 function. Figure 5.10 shows the resulting allowed regions for the top, bottom and tau Yukawa couplings when the coupling of φ_i^0 to vector bosons is fixed to $\mathcal{R}_{i1} = 0.95$; this value lies well within the 90% CL allowed band obtained from our previous fits.

Since all the observables considered are CP-even, the bounds obtained are symmetric under $\text{Im}(y_f^{\varphi_i^0}) \rightarrow -\text{Im}(y_f^{\varphi_i^0})$. Moreover, the real and imaginary parts of the Yukawa couplings do not interfere. The sensitivity to $\text{Im}(y_f^{\varphi_i^0})$ is similar to that obtained previously, when considering only real couplings. For tree-level decays this is obvious from Eq. (5.14), given that the parameter β_f is very close to one for $f = b, \tau$. For loop-induced decays this can be understood by observing that the loop functions (5.18) are closely related, $\mathcal{F}(\tau) = 2\tau + \frac{\tau^2}{2}f(\tau) + \mathcal{K}(\tau)$. For b quarks and τ leptons, $\mathcal{F}(\tau_f) \approx \mathcal{K}(\tau_f)$; for the top quark there is a small but sizable difference between the contributions of its real and imaginary Yukawa parts. Note that in the limit $\mathcal{R}_{i1} = 1$ the Yukawa couplings of φ_i^0 become SM-like ($y_f^{\varphi_i^0} = 1$) due to the orthogonality of \mathcal{R} ; thus, there is no sensitivity to the ς_f parameters when considering the neutral Higgs couplings. The charged Higgs couplings on the other hand are proportional to ς_f and do not depend on the mixing matrix \mathcal{R} .

In the left upper panel of Fig. 5.10 we show the results of the fit for a complex top Yukawa coupling, while setting $y_d^{\varphi_i^0} = y_l^{\varphi_i^0} = 1$. The dashed lines show contours of constant value for $\mu_{\gamma\gamma}^{\varphi_i^0}$. The SM-like point $(\text{Re}(y_u^{\varphi_i^0}), \text{Im}(y_u^{\varphi_i^0})) = (1, 0)$ lies outside the 90% CL region, but becomes allowed at 99% CL. It can be seen that the allowed region at 90% CL accommodates an enhanced $\gamma\gamma$ rate between one and two times that of the SM. Within this 90% CL region, $\rho(\varphi_i^0) = 1.00 \pm 0.03$ as expected, since the dominant decay channel is $\bar{b}b$; the gluon fusion cross section is slightly reduced compared with the SM ($C_{gg}^{\varphi_i^0} = 0.87 \pm 0.28$), while the $\gamma\gamma$ partial decay width is enhanced ($C_{\gamma\gamma}^{\varphi_i^0} = 1.67 \pm 0.56$). The preferred allowed region is that for which the top Yukawa coupling has opposite sign to \mathcal{R}_{i1} , thus, creating a constructive interference with the vector boson contribution for the $\varphi_i^0 \rightarrow \gamma\gamma$ amplitude. The other option would be to have a significant imaginary component $\text{Im}(y_u^{\varphi_i^0})$, which would also enhance the $\gamma\gamma$ rate. Similar results were obtained in Ref. [24].

The right upper panel of Fig. 5.10 shows the fitted values for the complex bottom coupling, with the top and tau Yukawa couplings set to their SM values.

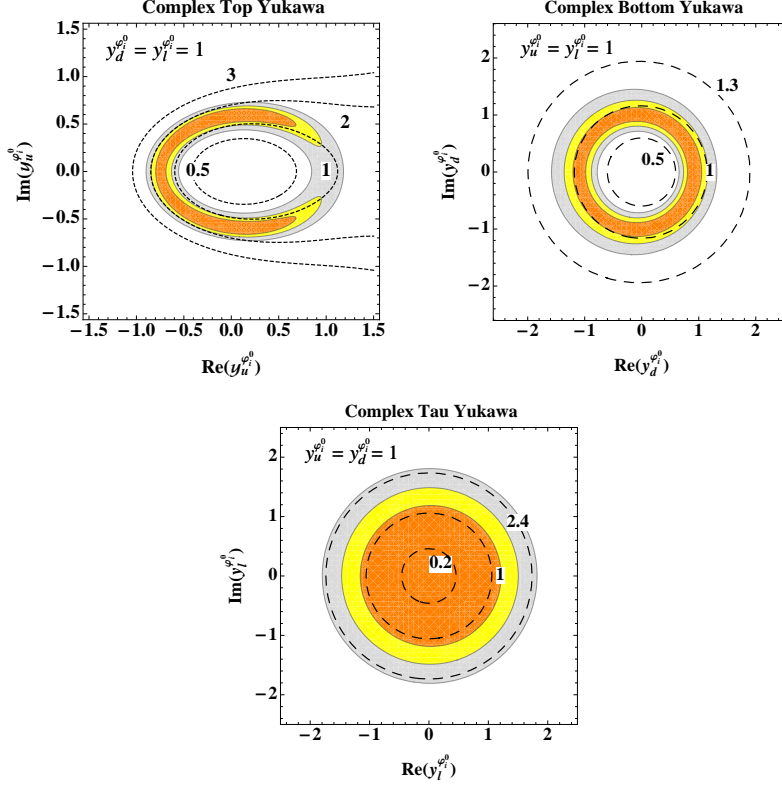


Figure 5.10: Allowed regions at 68% (orange), 90% (yellow) and 99% (grey) CL for the complex top (upper-left), bottom (upper-right) and tau (lower) Yukawa couplings. In each plot the two Yukawa couplings not shown are set to their SM value and the coupling to vector bosons is taken to be $\mathcal{R}_{i1} = 0.95$. The dashed lines show contours of constant values for $\mu_{\gamma\gamma}^0$ (top plot), μ_{bbV}^0 (bottom plot) and $\mu_{\tau\tau V}^0$ (tau plot).

The dashed lines indicate contours of constant value for μ_{bbV}^0 . In this case the SM limit $(\text{Re}(y_d^0), \text{Im}(y_d^0)) = (1, 0)$ lies inside the 90% CL allowed region, which accommodates $0.7 < \mu_{bbV}^0 < 1.2$. In this 90% CL region, the total decay width is rescaled by $\rho(\varphi_i^0) = 1.11 \pm 0.67$; the gluon-fusion cross section ratio is $C_{gg}^{\varphi_i^0} = 1.15 \pm 0.10$, while the $\gamma\gamma$ partial decay width turns out to be slightly suppressed with respect to the SM, $C_{\gamma\gamma}^{\varphi_i^0} = 0.89 \pm 0.10$. Since the total decay width depends strongly on the value of $|y_d^0|^2$, a large variation range is obtained for $\rho(\varphi_i^0)$.

In the lower panel of Fig. 5.10, we show the fitted values of the complex τ Yukawa coupling assuming $y_u^{\varphi_i^0} = y_d^{\varphi_i^0} = 1$. Contours of constant value for $\mu_{\tau\tau V}^{\varphi_i^0}$ are also shown as dashed lines. We obtain that the signal strength $\mu_{\tau\tau V}^{\varphi_i^0} < 1.5$ lies within the 68% CL allowed region. The total Higgs decay width and the gluon-fusion cross section are equal in this case to the SM ones, while some suppression is observed in the $\gamma\gamma$ partial decay width: at 90% CL, $C_{\gamma\gamma}^{\varphi_i^0} = 0.90 \pm 0.11$ is obtained. This scenario is therefore disfavoured by the observed excess in the two-photon channel.

5.4.2.2 A fermiophobic charged Higgs

In the limit $\zeta_f \rightarrow 0$ the charged Higgs does not couple to fermions, independently of any assumption about the scalar potential. Such *fermiophobic* charged Higgs could have avoided detection at LEP while being very light. Current LHC searches, as well as searches at the Tevatron, would have also missed such particle since it can neither be produced via top decay nor decay into fermions. Flavour constraints on this charged Higgs are also avoided trivially. Detecting such particle in an experiment is therefore quite challenging, since it can only be produced in processes involving vector bosons and/or neutral Higgs particles; the same occurs for its decay channels.

The case of a fermiophobic charged Higgs is however highly predictive in the neutral Higgs sector, since all the channels which do not involve the $\gamma\gamma$ (γZ) final state only depend on one free parameter, \mathcal{R}_{i1} . The rescaling of the Higgs coupling to vector bosons in this case is the same as that of the neutral Yukawa ones, $y_f^{\varphi_i^0} = g_{\varphi_i^0 VV} / g_{\varphi_i^0 VV}^{\text{SM}} = \mathcal{R}_{i1}$, which implies that all Higgs signal strengths are rescaled by a factor \mathcal{R}_{i1}^2 with respect to the SM, meaning that $\mu_{bb}^{\varphi_i^0} = \mu_{\tau\tau}^{\varphi_i^0} = \mu_{WW,ZZ}^{\varphi_i^0} = \rho(\varphi_i^0)^{-1} \mathcal{R}_{i1}^4 = \mathcal{R}_{i1}^2$, in any of the relevant production mechanisms. Therefore, in this scenario the signal strengths of the three neutral scalars are correlated:

$$\sum_{\varphi_i^0=h,H,A} \mu_{ff}^{\varphi_i^0} = \sum_{\varphi_i^0=h,H,A} \mu_{WW,ZZ}^{\varphi_i^0} = 1. \quad (5.29)$$

Present data on the neutral Higgs boson are sensitive to a fermiophobic charged Higgs through the loop-induced decay $\varphi_i^0 \rightarrow \gamma\gamma$. The charged-scalar contribution to this decay can be sizeable for a light H^\pm , and this is a quite interesting situation in view of the possibility to detect such particle in the future. Assuming that the scalar with a mass of 126 GeV does not decay into

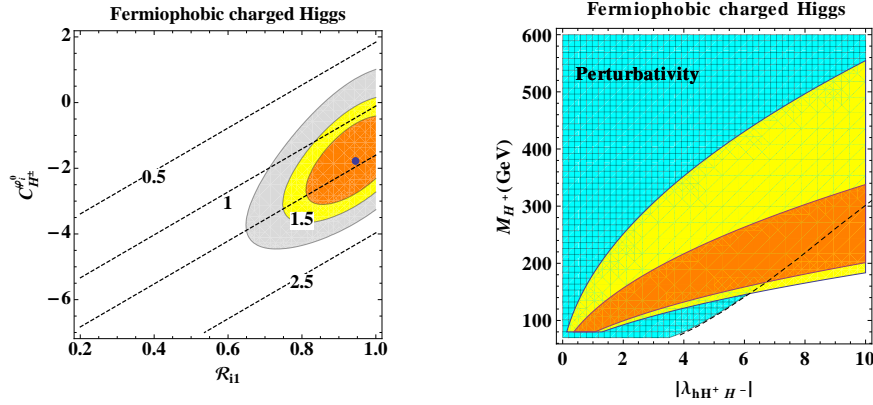


Figure 5.11: Allowed regions at 68% (orange), 90% (yellow) and 99% CL (gray) for a fermiophobic charged Higgs on the parameter space $(\mathcal{R}_{i1}, C_{H^\pm}^{\varphi_i^0})$; dashed lines denote contours of constant $\mu_{\gamma\gamma}^{\varphi_i^0}$ (left). The right plot shows the corresponding 68% and 90% CL regions in the parameters $\lambda_{\varphi_i^0 H^+ H^-}$ and M_{H^\pm} , setting the value of \mathcal{R}_{i1} at its best fit point. The region where perturbation theory remains valid is indicated in blue (hashed).

lighter scalars, we show in Fig. 5.11 the allowed region in the parameter space $(\mathcal{R}_{i1}, C_{H^\pm}^{\varphi_i^0})$. For the χ^2 fit we have only considered real values of $C_{H^\pm}^{\varphi_i^0}$, which is true above the kinematical threshold $M_{H^\pm} > M_{\varphi_i^0}/2 \approx 63$ GeV, as we have mentioned before. In the figure we also show dashed contour lines of constant $\mu_{\gamma\gamma}^{\varphi_i^0}$. It can be observed that the preferred relative sign between the charged Higgs and the W^\pm contributions to the $\gamma\gamma$ decay rate is such that it causes a constructive interference, thus enhancing slightly the $\gamma\gamma$ decay rate. The fit prefers a gauge coupling close to the SM one (χ_{\min}^2 is obtained for $\mathcal{R}_{i1} \approx 0.95$) and puts the 90% CL lower bound $|\mathcal{R}_{i1}| > 0.79$. The SM-like point $(\mathcal{R}_{i1}, C_{H^\pm}^{\varphi_i^0}) = (1, 0)$ lies outside the 68% CL region, but is allowed at 90% CL (although close to the boundary). The presence of a non-zero (and negative) $C_{H^\pm}^{\varphi_i^0}$ contribution is clearly favoured, while the preference for a slightly reduced gauge coupling implies a small suppression of the total decay width compared with the SM (*i.e.*, $\rho(\varphi_i^0) = 0.85 \pm 0.19$, at 90% CL). From the global fit, $\mu_{\gamma\gamma}^{\varphi_i^0} = \mu_{\gamma\gamma jj}^{\varphi_i^0} = 1.45 \pm 0.49$ is obtained at 90% CL; all the other Higgs signal strengths that are not affected by the charged Higgs contribution are equal to $\mu = 0.8 \pm 0.2$.

The right panel in Fig. 5.11 shows the corresponding allowed regions in terms of the variables $\lambda_{\varphi_i^0 H^+ H^-}$ and M_{H^\pm} . The value of \mathcal{R}_{i1} has been set to its best

fit point. Also shown in the figure, is the region satisfying the perturbativity constraints discussed in appendix 5.D.

For the previous discussion we have not made any assumptions on the quantum numbers of the scalar field φ_i^0 ; we have only assumed that $M_{\varphi_i^0} = 126$ GeV and that its decay into lighter scalars is not allowed. Thus, the obtained results are general and apply both to a CP-conserving and to a CP-violating scalar potential. It must be noted that in the limit $|\mathcal{R}_{i1}| = 1$ the phenomenology of φ_i^0 becomes identical to that of the SM in every channel, except for $\gamma\gamma$ and γZ which are affected by the H^\pm contribution. For a fermiophobic charged Higgs lighter than $M_{\varphi_i^0}/2 \approx 63$ GeV, $\mathcal{C}_{H^\pm}^{\varphi_i^0}$ develops an imaginary absorptive part. If kinematically open, the channel $\varphi_i^0 \rightarrow H^+H^-$ would increase the total width of the Higgs boson; furthermore, in this scenario the production cross section is always less or equal to the SM. Therefore, the signal strengths would be reduced in every channel, with respect to the SM. This is in clear contradiction with the data, specially with the measurements for the two-photon channel.

5.4.2.3 CP-even and CP-odd neutral scalar mixing

A CP-violating scalar potential generates mixings among the three neutral scalars, which are no longer CP eigenstates. Here, we are interested in exploring the possibility that the observed 126 GeV state could be the CP-odd scalar with a small CP admixture of the CP-even ones. A similar analysis within 2HDMs of types I and II, with explicit CP violation and soft breaking of the \mathcal{Z}_2 symmetry has been done in Ref. [36], placing numerical bounds on the size of a possible CP-odd component for the scalar particle with 126 GeV of mass.

In the presence of CP violation, the admixture between the three neutral scalar fields is described by the 3-dimensional orthogonal matrix \mathcal{R} which diagonalizes their mass matrix. This diagonalization can be done numerically, once the parameters of the scalar potential are known, but a simple analytical solution is not available for the most general case. It is well known, on the other hand, that in the CP-conserving limit the mass-matrix simplifies and it is possible to give explicit expressions for the masses and physical states in terms of the scalar potential parameters. A reasonable assumption when dealing with the general 2HDM scalar potential, is that the CP-violating terms are small; this makes a perturbative expansion in these parameters a valid approximation in principle. In appendix 5.A we provide explicit analytical expressions for the neutral scalar masses and the corresponding eigenstates to leading order in the CP-violating parameters of the scalar potential $\lambda_{5,6}^I$. The corrections to the masses are quadratic

in $\lambda_{5,6}^I$, while the mixing between the CP-even and CP-odd states is only suppressed by one power of $\lambda_{5,6}^I$, making this effect the dominant one.

Let us assume that the discovered boson is the state $A = S_3 + \mathcal{R}_{31}S_1 + \mathcal{R}_{32}S_2$, with \mathcal{R}_{31} and \mathcal{R}_{32} the small CP-even admixture coefficients. To simplify the discussion, we consider a simple scenario in which we set the parameters $\varsigma_{u,d,l} = 0$. The Yukawa couplings, as well as the coupling to vector bosons, are equal in this case, $y_f^A = \mathcal{R}_{31}$. From a global fit to the data, we find a lower bound on the admixture coefficient: $\mathcal{R}_{31} > 0.83$, at 99% CL. This result is mainly driven by the measurements in the W^+W^- , ZZ and $\gamma\gamma$ channels, which are SM-like to a good degree.

We can analyze whether such large values for the correction \mathcal{R}_{31} can be obtained for natural values of the scalar potential parameters. From Eq. (5.48), one has:

$$\mathcal{R}_{31} \approx \frac{v^4 \left(2\lambda_5^R \lambda_6^I - \lambda_6^R \lambda_5^I \right)}{\left(\bar{M}_A^2 - \bar{M}_h^2 \right) \left(\bar{M}_A^2 - \bar{M}_H^2 \right)}. \quad (5.30)$$

Thus, large mass differences between the scalar states suppress the effect of mixing due to CP violation in the scalar potential; on the other hand if the scalar bosons have very similar masses these effects could be considerably enhanced. Assuming that $|\lambda_{5,6}^{I,R}| \lesssim 10^{-1}$ we obtain

$$R_{31} \lesssim \left[\left(\bar{M}_A^2 - \bar{M}_H^2 \right) \left(\bar{M}_A^2 - \bar{M}_h^2 \right) \right]^{-1} 10^8 \text{ GeV}^4,$$

which implies that $|\mathcal{R}_{31}| \lesssim 10^{-2}$ for $\bar{M}_H > \bar{M}_h \gtrsim 300 \text{ GeV}$. Of course, when either $\bar{M}_h \sim \bar{M}_A$ or $\bar{M}_H \sim \bar{M}_A$ the coefficient \mathcal{R}_{31} diverges and the approximations used in appendix 5.A are no longer valid. The general formalism to describe the dynamics of CP violation near degenerate neutral Higgs bosons has been developed in Refs. [86, 87]. In Ref. [88] the effect of resonant enhancement of H and A mixing was studied for the CP-violating 2HDM in the decoupling limit, $\bar{M}_A^2 \gg |\lambda_i| v^2$. In this case the heavy states H , H^\pm and A are nearly mass degenerate and decouple from the light state h .

In Fig. 5.12 we show the allowed values at 90% CL for $(\mathcal{R}_{i1}, \mathcal{R}_{i2}, \mathcal{R}_{i3})$ for a general scalar state φ_i^0 with $m_{\varphi_i^0} = 126 \text{ GeV}$, assuming that the alignment parameters ς_f ($f = u, d, l$) are real. We have imposed $|\varsigma_u| < 2$, in order to satisfy the flavour constraints for a charged Higgs below the TeV scale, and moreover we have set $|\varsigma_{d,l}| < 10$. It is seen that the CP-odd admixture in the 126 GeV state has an upper bound $\mathcal{R}_{i3} \lesssim 0.7$, similar to that obtained in Ref. [36] within

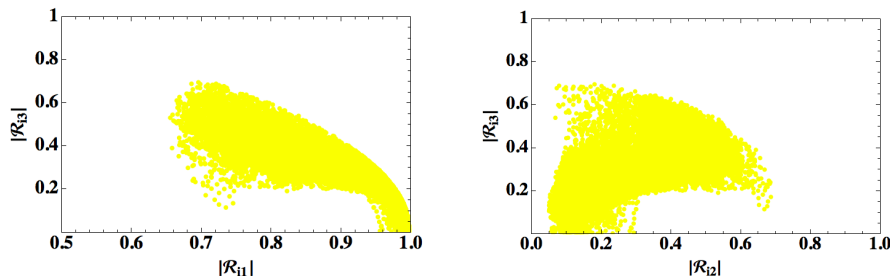


Figure 5.12: Allowed regions at 90% CL (yellow) on the parameter space $(\mathcal{R}_{i1}, \mathcal{R}_{i3})$, for real alignment parameters in the ranges $|\varsigma_u| < 2$ and $|\varsigma_{d,i}| < 10$ (left). The right plot shows the corresponding 90% CL region for the parameters $(\mathcal{R}_{i2}, \mathcal{R}_{i3})$.

2HDMs of types I and II, with explicit CP violation and soft breaking of the \mathcal{Z}_2 symmetry.

5.5 Summary

The recent LHC discovery of a new neutral boson, with mass close to 126 GeV, provides for the first time direct information on the electroweak symmetry breaking mechanism. The current data are so far compatible with the SM Higgs hypothesis, although a slight excess in the diphoton channel has been observed by the ATLAS and CMS collaborations. This channel is particularly interesting since the decay of the Higgs into two photons occurs at the one-loop level and is therefore sensitive to new charged particles that couple directly to the Higgs.

As new and more precise data become available, we shall test whether the properties of the 126 GeV particle correspond indeed to the SM Higgs boson or they manifest evidences for new phenomena, perhaps signalling the existence of a much richer scalar sector. Present experimental errors are still large but, nevertheless, they already allow us to extract useful constraints on alternative scenarios of electroweak symmetry breaking.

2HDMs constitute the simplest extension of the SM scalar sector, satisfying the electroweak precision tests, and give rise to interesting new phenomena through their enlarged scalar spectrum containing five physical scalars. In order to avoid dangerous FCNCs, the 2HDM phenomenology has been usually particularized to a few specific implementations, based on discrete \mathcal{Z}_2 symmetries, which severely restrict the fermionic couplings of the scalar bosons. The most widely used scenario is the so-called type II 2HDM, since it corresponds to the

tree-level scalar sector of the minimal supersymmetric SM. However, the phenomenological FCNC requirements can be easily satisfied imposing a much softer alignment condition on the Yukawa couplings. The resulting A2HDM provides a general framework to describe an extended scalar sector with two Higgs doublets and no FCNCs at tree level, which includes as particular cases all previously considered 2HDM variants. It has a much larger parameter space with plenty of new phenomenological possibilities, such as new sources of CP violation and tunable strengths of the (family universal) Yukawas. Thus, it is the appropriate framework to perform an unbiased phenomenological analysis of the Higgs data.

In this paper, we have analyzed the present data on the Higgs signal strengths from the ATLAS, CMS, CDF and DØ collaborations, within the framework of the A2HDM. Even with the currently large experimental uncertainties, interesting conclusions can be obtained regarding the preferred regions in the parameter space of the model. We have considered a variety of possible departures from the SM predictions, within this framework, including the effects from new CP-violating phases. In particular, we have searched for possible ways to enhance the diphoton channel while being compatible with the rest of the data.

The measured WW , ZZ and $\gamma\gamma$ decay channels of the new boson suggest that its coupling to the weak vector bosons (W^+W^- , ZZ) is close to the SM one. This rules out the possibility of a pure CP-odd assignment for the quantum numbers of the new Higgs-like boson. A CP-even scalar, either pure or with a CP-odd admixture arising from CP-violating terms in the scalar potential, however, can accommodate the data rather well.

By flipping the relative sign of the top Yukawa coupling, the top-quark contribution to the Higgs decay amplitude into 2γ interferes constructively with the dominant W^\pm contribution. This can only be realized in the A2HDM for large values of $|\zeta_u|$, given that $g_{\varphi_i^0 VV} \approx g_{hVV}^{\text{SM}}$. However, flavour constraints on a charged Higgs below the TeV scale (from $Z \rightarrow \bar{b}b$, $b \rightarrow s\gamma$ and $B^0-\bar{B}^0$ mixing) require that $|\zeta_u| < 2$, even in the most general CP-violating A2HDM. Thus, a 2γ enhancement through a constructive interference of the top and W^\pm contributions could only be possible in a decoupling scenario with an enormously large H^\pm mass.

Including the charged scalar contribution to the Higgs decay amplitude into two photons, one can explain the observed excess without significant deviations of the neutral scalar couplings from the SM limit, and satisfying at the same time the flavour constraints. This appears to be the most natural and likely possibility to accommodate current data within the A2HDM framework. The confirmation by future data of a significantly enhanced 2γ decay width could

be a strong indication that a light charged scalar is around the corner, within the LHC reach.

The possibility that a CP-even and a CP-odd Higgs bosons have quasi-degenerate masses near 126 GeV was also analyzed. An excess in the $\gamma\gamma$ channel can occur in this case due to the contributions from both scalars (when signal strengths are added incoherently). We have also considered the most general A2HDM with complex Yukawa couplings. Since the Higgs signal strengths are CP-even observables, there is no interference between the contributions from the real and imaginary parts of the Yukawa couplings. It is then possible to enhance the $\gamma\gamma$ decay rate with a complex Yukawa coupling which has its real part close to the SM-like limit.

Future improvements of the present bounds on neutral and charged Higgs bosons, or perhaps their direct discovery, as well as more precise measurements of the current Higgs signal strengths are expected from the LHC in the next years. The complementarity between flavour constraints and collider searches for new scalar resonances will be crucial for the understanding of the mechanism of electroweak symmetry breaking. We have shown different alternative scenarios within the A2HDM that can accommodate present data very well, placing bounds on the relevant parameter space and discussing possible consequences that could be tested in the near future.

Note added: After the submission of this work for publication, updated experimental analyses of the LHC data have been made public [89, 90]. While an enhanced diphoton rate is still present in the ATLAS results, the CMS collaboration finds now a 2γ rate compatible with the SM prediction. The new CMS results would favour a SM-like scenario, similar to that obtained in Eq. (5.23), without any need for a charged scalar contribution to the 2γ decay mode. More data are needed to clarify this issue.

Acknowledgements

We are grateful to Luca Fiorini for discussions about the experimental data. This work has been supported in part by the Spanish Government and ERDF funds from the EU Commission [grants FPA2007-60323, FPA2011-23778 and CSD2007-00042 (Consolider Project CPAN)]. The work of A. C. is funded through an FPU grant (AP2010-0308, MINECO, Spain).

5.A Scalar Potential

In the Higgs basis, the most general scalar potential takes the form

$$\begin{aligned}
V = & \mu_1 \Phi_1^\dagger \Phi_1 + \mu_2 \Phi_2^\dagger \Phi_2 + \left[\mu_3 \Phi_1^\dagger \Phi_2 + \mu_3^* \Phi_2^\dagger \Phi_1 \right] + \lambda_1 \left(\Phi_1^\dagger \Phi_1 \right)^2 \\
& + \lambda_2 \left(\Phi_2^\dagger \Phi_2 \right)^2 + \lambda_3 \left(\Phi_1^\dagger \Phi_1 \right) \left(\Phi_2^\dagger \Phi_2 \right) + \lambda_4 \left(\Phi_1^\dagger \Phi_2 \right) \left(\Phi_2^\dagger \Phi_1 \right) \\
& + \left[\left(\lambda_5 \Phi_1^\dagger \Phi_2 + \lambda_6 \Phi_1^\dagger \Phi_1 + \lambda_7 \Phi_2^\dagger \Phi_2 \right) \left(\Phi_1^\dagger \Phi_2 \right) + \text{h.c.} \right]. \quad (5.31)
\end{aligned}$$

The Hermiticity of the potential requires all parameters to be real except μ_3 , λ_5 , λ_6 and λ_7 ; thus, there are 14 real parameters.

The minimization conditions $\langle 0 | \Phi_1^T(x) | 0 \rangle = \frac{1}{\sqrt{2}}(0, v)$ and $\langle 0 | \Phi_2^T(x) | 0 \rangle = \frac{1}{\sqrt{2}}(0, 0)$ impose the relations

$$\mu_1 = -\lambda_1 v^2, \quad \mu_3 = -\frac{1}{2} \lambda_6 v^2. \quad (5.32)$$

The potential can then be decomposed into a quadratic term plus cubic and quartic interactions

$$V = -\frac{1}{4} \lambda_1 v^4 + V_2 + V_3 + V_4. \quad (5.33)$$

The mass terms take the form

$$\begin{aligned}
V_2 = & M_{H^\pm}^2 H^+ H^- + \frac{1}{2} (S_1, S_2, S_3) \mathcal{M} \begin{pmatrix} S_1 \\ S_2 \\ S_3 \end{pmatrix} \\
= & M_{H^\pm}^2 H^+ H^- + \frac{1}{2} M_h^2 h^2 + \frac{1}{2} M_H^2 H^2 + \frac{1}{2} M_A^2 A^2, \quad (5.34)
\end{aligned}$$

with

$$M_{H^\pm}^2 = \mu_2 + \frac{1}{2} \lambda_3 v^2 \quad (5.35)$$

and

$$\mathcal{M} = \begin{pmatrix} 2\lambda_1 v^2 & v^2 \lambda_6^R & -v^2 \lambda_6^I \\ v^2 \lambda_6^R & M_{H^\pm}^2 + v^2 \left(\frac{\lambda_4}{2} + \lambda_5^R \right) & -v^2 \lambda_5^I \\ -v^2 \lambda_6^I & -v^2 \lambda_5^I & M_{H^\pm}^2 + v^2 \left(\frac{\lambda_4}{2} - \lambda_5^R \right) \end{pmatrix}, \quad (5.36)$$

where $\lambda_i^{\text{R}} \equiv \text{Re}(\lambda_i)$ and $\lambda_i^{\text{I}} \equiv \text{Im}(\lambda_i)$. The symmetric mass matrix \mathcal{M} is diagonalized by an orthogonal matrix \mathcal{R} , which defines the neutral mass eigenstates:

$$\mathcal{M} = \mathcal{R}^T \begin{pmatrix} M_h^2 & 0 & 0 \\ 0 & M_H^2 & 0 \\ 0 & 0 & M_A^2 \end{pmatrix} \mathcal{R}, \quad \begin{pmatrix} h \\ H \\ A \end{pmatrix} = \mathcal{R} \begin{pmatrix} S_1 \\ S_2 \\ S_3 \end{pmatrix}. \quad (5.37)$$

Since the trace remains invariant, the masses satisfy the relation

$$M_h^2 + M_H^2 + M_A^2 = 2 M_{H^\pm}^2 + v^2 (2 \lambda_1 + \lambda_4). \quad (5.38)$$

The minimization conditions allow us to trade the parameters μ_1 and μ_3 by v and λ_6 . The freedom to rephase the field Φ_2 implies, moreover, that only the relative phases among λ_5 , λ_6 and λ_7 are physical; but only two of them are independent. Therefore, we can fully characterize the potential with 11 parameters: v , μ_2 , $|\lambda_{1,\dots,7}|$, $\arg(\lambda_5 \lambda_6^*)$ and $\arg(\lambda_5 \lambda_7^*)$. Four parameters can be determined through the physical scalar masses.

In the CP conserving limit $\lambda_5^{\text{I}} = \lambda_6^{\text{I}} = \lambda_7^{\text{I}} = 0$ and S_3 does not mix with the other neutral fields. The scalar spectrum contains then a CP-odd field $A = S_3$ and two CP-even scalars h and H which mix through the rotation matrix (5.3). In this case, the scalar masses are given by

$$\begin{aligned} \bar{M}_h^2 &= \frac{1}{2} (\Sigma - \Delta), & \bar{M}_H^2 &= \frac{1}{2} (\Sigma + \Delta), \\ \bar{M}_A^2 &= M_{H^\pm}^2 + v^2 \left(\frac{\lambda_4}{2} - \lambda_5^{\text{R}} \right), \end{aligned} \quad (5.39)$$

where

$$\Sigma = M_{H^\pm}^2 + v^2 \left(2 \lambda_1 + \frac{\lambda_4}{2} + \lambda_5^{\text{R}} \right), \quad (5.40)$$

$$\Delta = \sqrt{\left[M_{H^\pm}^2 + v^2 \left(-2 \lambda_1 + \frac{\lambda_4}{2} + \lambda_5^{\text{R}} \right) \right]^2 + 4v^4 (\lambda_6^{\text{R}})^2}, \quad (5.41)$$

and the mixing angle is determined through

$$\tan \tilde{\alpha} = \frac{\bar{M}_h^2 - 2 \lambda_1 v^2}{v^2 \lambda_6^{\text{R}}}. \quad (5.42)$$

We use the notation $\bar{M}_{\varphi_i^0}$ to emphasize that these are the neutral scalar masses in the CP-conserving limit. The cubic and quartic Higgs couplings involving the

charged and the neutral physical scalars (without Goldstone boson couplings) take the form,

$$\begin{aligned}
V_3 = & v H^+ H^- \left(\lambda_3 S_1 + \lambda_7^R S_2 - \lambda_7^I S_3 \right) + \frac{1}{2} v \left(2\lambda_5^R + \lambda_3 + \lambda_4 \right) S_1 S_2^2 \\
& + \lambda_1 v S_1^3 + \frac{1}{2} v \lambda_7^R S_2^3 + \frac{3}{2} v \lambda_6^R S_1^2 S_2 - \frac{1}{2} v \lambda_7^I S_3^3 - \frac{1}{2} v \lambda_7^I S_2^2 S_3 \\
& - \frac{1}{2} v \left(2\lambda_5^R - \lambda_3 - \lambda_4 \right) S_1 S_3^2 + \frac{1}{2} v \lambda_7^R S_2 S_3^2 - 2 v \lambda_5^I S_1 S_2 S_3 \\
& - \frac{3}{2} v \lambda_6^I S_1^2 S_3, \tag{5.43}
\end{aligned}$$

$$\begin{aligned}
V_4 = & H^+ H^- \left(\lambda_2 H^+ H^- + \frac{\lambda_3}{2} S_1^2 + \lambda_2 S_3^2 + \lambda_2 S_2^2 - \lambda_7^I S_1 S_3 + \lambda_7^R S_1 S_2 \right) \\
& + \frac{1}{4} \left(\lambda_3 + \lambda_4 + 2\lambda_5^R \right) (S_1 S_2)^2 + \frac{1}{4} \left(\lambda_3 + \lambda_4 - 2\lambda_5^R \right) (S_1 S_3)^2 \\
& - \frac{1}{2} \lambda_6^I S_1^3 S_3 - \lambda_5^I S_1^2 S_2 S_3 - \frac{\lambda_7^I}{2} S_1 S_2^2 S_3 - \frac{\lambda_7^I}{2} S_1 S_3^3 \\
& + \frac{\lambda_1}{4} S_1^4 + \frac{\lambda_2}{4} S_2^4 + \frac{\lambda_2}{4} S_3^4 + \frac{\lambda_2}{2} (S_2 S_3)^2 \\
& + \frac{\lambda_6^R}{2} S_1^3 S_2 + \frac{\lambda_7^R}{2} S_1 S_2^3 + \frac{\lambda_7^R}{2} S_1 S_2 S_3^2. \tag{5.44}
\end{aligned}$$

In the CP-conserving limit all vertices involving an odd number of S_3 fields vanish. A basis-independent discussion of the 2HDM scalar sector can be found in Ref. [91].

5.A.1 Neutral scalar mass matrix to lowest order in CP violation

Assuming that λ_5^I and λ_6^I are small, we can diagonalize the mass matrix (5.36) perturbatively as an expansion in powers of these CP-violating parameters. The leading corrections to the neutral scalar masses are quadratic in $\lambda_{5,6}^I$:

$$M_{\varphi_i^0}^2 = \bar{M}_{\varphi_i^0}^2 + \alpha_1^{\varphi_i^0} (\lambda_5^I)^2 + \alpha_2^{\varphi_i^0} (\lambda_6^I)^2 + \alpha_3^{\varphi_i^0} (\lambda_5^I \lambda_6^I), \tag{5.45}$$

where $\bar{M}_{\varphi_i^0}$ denote the corresponding masses in the CP-conserving limit given in (5.39) and

$$\begin{aligned}\alpha_1^{\varphi_i^0} &= \frac{v^4 \left(\bar{M}_{\varphi_i^0}^2 - 2\lambda_1 v^2 \right)}{\prod_{j \neq i} \left(\bar{M}_{\varphi_j^0}^2 - \bar{M}_{\varphi_i^0}^2 \right)}, \\ \alpha_2^{\varphi_i^0} &= \frac{v^4 \left(2\lambda_1 v^2 + \bar{M}_{\varphi_i^0}^2 - \bar{M}_H^2 - \bar{M}_h^2 \right)}{\prod_{j \neq i} \left(\bar{M}_{\varphi_j^0}^2 - \bar{M}_{\varphi_i^0}^2 \right)}, \\ \alpha_3^{\varphi_i^0} &= \frac{2v^6 \lambda_6^R}{\prod_{j \neq i} \left(\bar{M}_{\varphi_j^0}^2 - \bar{M}_{\varphi_i^0}^2 \right)}.\end{aligned}\tag{5.46}$$

The physical states $\varphi_i^0 = \{h, H, A\}$ receive corrections at first order in $\lambda_{5,6}^I$, which are given by

$$\begin{pmatrix} h \\ H \\ A \end{pmatrix} = \begin{pmatrix} \cos \tilde{\alpha} & \sin \tilde{\alpha} & \epsilon_{13} \\ -\sin \tilde{\alpha} & \cos \tilde{\alpha} & \epsilon_{23} \\ \epsilon_{31} & \epsilon_{32} & 1 \end{pmatrix} \begin{pmatrix} S_1 \\ S_2 \\ S_3 \end{pmatrix},\tag{5.47}$$

where

$$\begin{aligned}\epsilon_{13} &= \frac{v^2}{\left(\bar{M}_A^2 - \bar{M}_h^2 \right)} \left(\sin \tilde{\alpha} \lambda_5^I + \cos \tilde{\alpha} \lambda_6^I \right), \\ \epsilon_{23} &= \frac{v^2}{\left(\bar{M}_A^2 - \bar{M}_H^2 \right)} \left(\cos \tilde{\alpha} \lambda_5^I - \sin \tilde{\alpha} \lambda_6^I \right), \\ \epsilon_{31} &= -\frac{1}{2v^2} \left(\alpha_3^A \lambda_5^I + 2\alpha_2^A \lambda_6^I \right), \\ \epsilon_{32} &= -\frac{1}{2v^2} \left(2\alpha_1^A \lambda_5^I + \alpha_3^A \lambda_6^I \right).\end{aligned}\tag{5.48}$$

Note that for the case of a scalar potential with a softly-broken \mathcal{Z}_2 symmetry in the Higgs basis we have $\lambda_6 = \lambda_7 = 0$ and, therefore, $\epsilon_{31} = 0$.

5.B Scalar Couplings to the Gauge Bosons

The scalar doublets couple to the gauge bosons through the covariant derivative and gauge-fixing terms:

$$\mathcal{L}_K + \sum_{i=1}^2 (D_\mu \Phi_a)^\dagger D^\mu \Phi_a + \mathcal{L}_{\text{GF}} = \mathcal{L}_{V^2} + \mathcal{L}_{\phi^2} + \mathcal{L}_{\phi V} + \mathcal{L}_{\phi^2 V} + \mathcal{L}_{\phi V^2} + \mathcal{L}_{\phi^2 V^2}, \quad (5.49)$$

where \mathcal{L}_K is the usual gauge-boson kinetic term and the covariant derivative is given by⁶

$$D_\mu = \partial_\mu + ieQA_\mu + i\frac{g}{\cos\theta_W} Z_\mu(T_3 - Q\sin^2\theta_W) + ig[T_+W_\mu^\dagger + T_-W_\mu]. \quad (5.50)$$

It is convenient to adopt the following R_ξ gauge-fixing term ($\xi = 1$),

$$\begin{aligned} \mathcal{L}_{\text{GF}} = & -\frac{1}{2} (\partial_\mu A^\mu)^2 - (\partial^\mu W_\mu^\dagger + iM_W G^+) (\partial_\nu W^\nu - iM_W G^-) \\ & - \frac{1}{2} (\partial_\mu Z^\mu + M_Z G^0)^2, \end{aligned} \quad (5.51)$$

which cancels exactly the quadratic mixing terms between the gauge and Goldstone bosons generated by the covariant derivatives, so that $\mathcal{L}_{\phi V} = 0$, and provides the Goldstone bosons with the masses $M_{G^\pm} = M_W = gv/2$ and $M_{G^0} = M_Z = M_W/\cos\theta_W$. Then,

$$\begin{aligned} \mathcal{L}_{V^2} = & -\frac{1}{2} (\partial_\mu A^\mu)^2 - \frac{1}{2} (\partial_\mu Z^\mu)^2 + \frac{1}{2} M_Z^2 Z_\mu Z^\mu \\ & - (\partial^\mu W_\mu^\dagger) (\partial_\nu W^\nu) + M_W^2 W_\mu^\dagger W^\mu, \end{aligned} \quad (5.52)$$

while

$$\begin{aligned} \mathcal{L}_{\phi^2} = & \frac{1}{2} [\partial_\mu h \partial^\mu h + \partial_\mu H \partial^\mu H + \partial_\mu A \partial^\mu A] + \partial_\mu H^+ \partial^\mu H^- \\ & + \frac{1}{2} \partial_\mu G^0 \partial^\mu G^0 - \frac{1}{2} M_Z^2 (G^0)^2 \\ & + \partial_\mu G^+ \partial^\mu G^- - M_W^2 G^+ G^-. \end{aligned} \quad (5.53)$$

⁶The weak mixing angle θ_W is defined through the relation $g \sin\theta_W = g' \cos\theta_W = e$. The operators $T_\pm = \frac{1}{\sqrt{2}}(T_1 \pm T_2)$ and T_3 can be expressed in terms of the Pauli matrices by $T_i = \frac{\sigma_i}{2}$.

The interaction terms between the scalar and gauge bosons are given by:

$$\begin{aligned}
\mathcal{L}_{\phi^2 V} &= ie \left[A^\mu + \cot(2\theta_W) Z^\mu \right] \left[(H^+ \overleftrightarrow{\partial}_\mu H^-) + (G^+ \overleftrightarrow{\partial}_\mu G^-) \right] \\
&\quad + \frac{e}{\sin(2\theta_W)} Z^\mu \left[(G^0 \overleftrightarrow{\partial}_\mu S_1) + (S_3 \overleftrightarrow{\partial}_\mu S_2) \right] \\
&\quad + \frac{g}{2} W^{\mu\dagger} \left[(H^- \overleftrightarrow{\partial}_\mu S_3) - i (H^- \overleftrightarrow{\partial}_\mu S_2) \right. \\
&\quad\quad\quad \left. + (G^- \overleftrightarrow{\partial}_\mu G^0) - i (G^- \overleftrightarrow{\partial}_\mu S_1) \right] \\
&\quad + \frac{g}{2} W^\mu \left[(H^+ \overleftrightarrow{\partial}_\mu S_3) + i (H^+ \overleftrightarrow{\partial}_\mu S_2) \right. \\
&\quad\quad\quad \left. + (G^+ \overleftrightarrow{\partial}_\mu G^0) + i (G^+ \overleftrightarrow{\partial}_\mu S_1) \right], \quad (5.54)
\end{aligned}$$

$$\begin{aligned}
\mathcal{L}_{\phi^2 V^2} &= \frac{2}{v} S_1 \left[\frac{1}{2} M_Z^2 Z_\mu Z^\mu + M_W^2 W_\mu^\dagger W^\mu \right] \\
&\quad + \left(e M_W A^\mu - g M_Z \sin^2 \theta_W Z^\mu \right) \left(G^+ W_\mu + G^- W_\mu^\dagger \right), \quad (5.55)
\end{aligned}$$

$$\begin{aligned}
\mathcal{L}_{\phi^2 V^2} &= \frac{1}{v^2} \left[\frac{1}{2} M_Z^2 Z_\mu Z^\mu + M_W^2 W_\mu^\dagger W^\mu \right] \left[H^2 + h^2 + A^2 + (G^0)^2 \right] \\
&\quad + \left\{ e^2 [A^\mu + \cot(2\theta_W) Z^\mu]^2 + \frac{g^2}{2} W_\mu^\dagger W^\mu \right\} (G^+ G^- + H^+ H^-) \\
&\quad + \frac{eg}{2} (A^\mu - \tan \theta_W Z^\mu) \left[S_1 (G^+ W_\mu + G^- W_\mu^\dagger) \right. \\
&\quad\quad\quad + S_2 (H^+ W_\mu + H^- W_\mu^\dagger) + i S_3 (H^- W_\mu^\dagger - H^+ W_\mu) \\
&\quad\quad\quad \left. + i G^0 (G^- W_\mu^\dagger - G^+ W_\mu) \right], \quad (5.56)
\end{aligned}$$

with $S_i = \mathcal{R}_{ji} \varphi_j^0$ ($\varphi_j^0 = \{h, H, A\}$) and the usual notation $A \overleftrightarrow{\partial}_\mu B \equiv A(\partial_\mu B) - (\partial_\mu A)B$.

Table 5.2: *Higgs signal strengths in each of the channels considered in this work. Averages obtained from ATLAS and CMS data at $7 \oplus 8$ TeV together with CDF and DØ data at $\sqrt{s} = 1.96$ TeV. (*) We do not consider non-inclusive measurements in the $\tau\tau$ channel. Due to the large current errors associated with these measurements, our conclusions would not be modified at this level.*

Channel	$\hat{\mu}_k$	Comment
bbV	1.1 ± 0.44	ATLAS, CMS, CDF and DØ [1, 2, 11, 12] (our average)
$WWjj$	-0.2 ± 1.56	ATLAS and CMS [1, 2, 14] (our average)
WW	0.76 ± 0.21	ATLAS, CMS, CDF and DØ [1, 2, 10, 11, 13] (our average)
ZZ	0.96 ± 0.26	ATLAS and CMS [1, 2] (our average)
$\tau\tau$ (incl.) (*)	0.89 ± 0.86	ATLAS and CMS [1, 2] (our average)
$\gamma\gamma$	1.66 ± 0.32	ATLAS and CMS [1, 2] (our average)
$\gamma\gamma jj$	2.18 ± 0.84	ATLAS and CMS [1, 2] (our average)

5.C Statistical treatment and data

To obtain the preferred values for the parameters of the A2HDM we build a global χ^2 function

$$\chi^2 = \sum_k \frac{(\mu_k - \hat{\mu}_k)^2}{\sigma_k^2}, \quad (5.57)$$

where σ_i is the experimental error extracted from the data at 1σ . Errors on the reported Higgs signal strengths $\hat{\mu}_k$ are symmetrized using

$$\delta\hat{\mu}_k = \sqrt{\frac{(\delta\hat{\mu}_+)^2 + (\delta\hat{\mu}_-)^2}{2}}, \quad (5.58)$$

where $\delta\hat{\mu}_\pm$ are the one-sided errors given by the experimental collaborations. We use the latest data available after the ‘‘Hadron Collider Physics Symposium 2012 (HCP2012)’’, including the latest update from ATLAS of the high-resolution channels $\gamma\gamma$, $ZZ^{(*)}$ [1]. For the diphoton channels we use the data given by ATLAS and CMS at 7 and 8 TeV, provided in Refs. [1, 2, 13, 14]. For the rest of the channels we use the averages listed in Table 5.2, which include the $7 \oplus 8$ TeV data reported by ATLAS and CMS together with CDF and DØ data [10–12] at $\sqrt{s} = 1.96$ TeV.

For a general channel with inclusive production we have (neglecting the subdominant production channels)

$$\mu_k^{\varphi_i^0} = \frac{\sigma_{gg}}{\sigma_{gg}^{\text{SM}}} \cdot \frac{\text{Br}(\varphi_i^0 \rightarrow k)}{\text{Br}(\varphi_i^0 \rightarrow k)_{\text{SM}}}. \quad (5.59)$$

For the Higgs searches in the $\gamma\gamma$ channel, the ATLAS and CMS collaborations have established different categories. To take this into account, we write the Higgs signal strength in a given $\gamma\gamma$ channel as

$$\mu_{\gamma\gamma}^{\varphi_i^0} = \frac{\epsilon_{ggF} \sigma_{ggF} + \epsilon_{\text{VBF}} \sigma_{\text{VBF}} + \epsilon_{\text{VH}} \sigma_{\text{VH}}}{\epsilon_{ggF} \sigma_{ggF}^{\text{SM}} + \epsilon_{\text{VBF}} \sigma_{\text{VBF}}^{\text{SM}} + \epsilon_{\text{VH}} \sigma_{\text{VH}}^{\text{SM}}} \cdot \frac{\text{Br}(\varphi_i^0 \rightarrow \gamma\gamma)}{\text{Br}(\varphi_i^0 \rightarrow \gamma\gamma)_{\text{SM}}}, \quad (5.60)$$

where the coefficients $\epsilon_{(ggF, \text{VBF}, \text{VH})}$ accounting for the relative weight of each production channel have been provided by ATLAS and CMS [5, 6]. The top-quark-fusion contribution could be added in a similar way. In Eq. (5.60), the SM production cross sections and decay widths are taken from the web page of the LHC Higgs Cross Section Working Group [92]. For the gluon-fusion production mechanism we have

$$\sigma(gg \rightarrow \varphi_i^0) \equiv \sigma_{ggF} = C_{gg}^{\varphi_i^0} \sigma_{ggF}^{\text{SM}}, \quad (5.61)$$

where the scaling of the gluon-fusion cross section $C_{gg}^{\varphi_i^0}$ was defined in section 5.3. Vector-boson fusion scales with the coefficient \mathcal{R}_{i1} as

$$\sigma(qq' \rightarrow qq' \varphi_i^0) \equiv \sigma_{\text{VBF}} = (\mathcal{R}_{i1})^2 \sigma_{\text{VBF}}^{\text{SM}}, \quad (5.62)$$

and similarly for the associated production with a vector boson

$$\sigma(q\bar{q} \rightarrow V \varphi_i^0) \equiv \sigma_{\text{VH}} = (\mathcal{R}_{i1})^2 \sigma_{\text{VH}}^{\text{SM}}. \quad (5.63)$$

5.D Perturbativity Constraints

The charged Higgs boson contribution to $\varphi_i^0 \rightarrow \gamma\gamma$ depends crucially on the value of the neutral scalar coupling to a pair of charged Higgs bosons. To assure the validity of perturbation theory, upper bounds on the quartic Higgs self-couplings are usually imposed requiring these to be smaller than 8π (see [31, 32] and references therein). The cubic Higgs self-couplings are also bounded indirectly in this way. In this work we consider an alternative perturbativity bound on

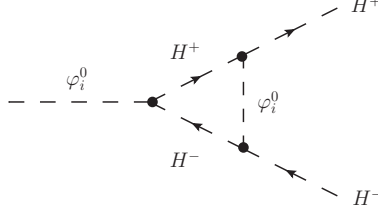


Figure 5.13: *Diagram contributing to the one-loop $\varphi_i^0 H^+ H^-$ vertex correction.*

the relevant Higgs cubic coupling which is more restrictive for light charged Higgs masses. Consider the $\varphi_i^0 H^+ H^-$ one-loop vertex correction given by Fig. 5.13. The contribution of this diagram is finite and can give us an idea about the allowed magnitude of the cubic coupling in order not to spoil the perturbative convergence. We obtain:

$$\begin{aligned}
 (\lambda_{\varphi_i^0 H^+ H^-})_{\text{eff}} &= \lambda_{\varphi_i^0 H^+ H^-} \left[1 + \frac{v^2 \lambda_{\varphi_i^0 H^+ H^-}^2}{16\pi^2 M_{H^\pm}^2} \mathcal{Z} \left(\frac{M_{\varphi_i^0}^2}{M_{H^\pm}^2} \right) \right] \\
 &\equiv \lambda_{\varphi_i^0 H^+ H^-} (1 + \Delta), \quad (5.64)
 \end{aligned}$$

where

$$\mathcal{Z}(X) = \int_0^1 dy \int_0^{1-y} dz \left[(y+z)^2 + X(1-y-z-yz) \right]^{-1}. \quad (5.65)$$

Allowing the correction to be at most 50% ($\Delta \leq 0.5$) constraints the allowed parameter space in the $(\lambda_{\varphi_i^0 H^+ H^-}, M_{H^\pm})$ plane to be within the blue (hashed) region indicated in Fig. 5.6.

5.E Oblique Parameters

Possible deviations from the SM in the gauge-boson self-energies are usually characterized through the oblique parameters S , T and U [93]. Taking as a reference SM Higgs mass $M_{h,\text{ref}} = 126$ GeV, the most recent global fit to electroweak precision observables quotes the values [76, 77]:

$$S = 0.03 \pm 0.10, \quad T = 0.05 \pm 0.12, \quad U = 0.03 \pm 0.10. \quad (5.66)$$

The expressions for the oblique parameters in the CP conserving A2HDM are adapted from Ref. [94]:

$$\begin{aligned}
S = \frac{1}{\pi M_Z^2} & \left\{ \cos^2 \tilde{\alpha} \left[\mathcal{B}_{22}(M_Z^2; M_Z^2, M_h^2) - M_Z^2 \mathcal{B}_0(M_Z^2; M_Z^2, M_h^2) \right. \right. \\
& \left. \left. + \mathcal{B}_{22}(M_Z^2; M_H^2, M_A^2) \right] \right. \\
& + \sin^2 \tilde{\alpha} \left[\mathcal{B}_{22}(M_Z^2; M_Z^2, M_H^2) - M_Z^2 \mathcal{B}_0(M_Z^2; M_Z^2, M_H^2) \right. \\
& \left. \left. + \mathcal{B}_{22}(M_Z^2; M_h^2, M_A^2) \right] \right. \\
& - \mathcal{B}_{22}(M_Z^2; M_{H^\pm}^2, M_{H^\pm}^2) - \mathcal{B}_{22}(M_Z^2; M_Z^2, M_{h,\text{ref}}^2) \\
& \left. \left. + M_Z^2 \mathcal{B}_0(M_Z^2; M_Z^2, M_{h,\text{ref}}^2) \right\}, \quad (5.67)
\end{aligned}$$

$$\begin{aligned}
T = \frac{1}{16\pi M_W^2 s_W^2} & \left\{ \cos^2 \tilde{\alpha} \left[\mathcal{F}(M_{H^\pm}^2, M_H^2) - \mathcal{F}(M_H^2, M_A^2) + 3\mathcal{F}(M_Z^2, M_h^2) \right. \right. \\
& \left. \left. - 3\mathcal{F}(M_W^2, M_h^2) \right] \right. \\
& + \sin^2 \tilde{\alpha} \left[\mathcal{F}(M_{H^\pm}^2, M_h^2) - \mathcal{F}(M_h^2, M_A^2) + 3\mathcal{F}(M_Z^2, M_H^2) \right. \\
& \left. \left. - 3\mathcal{F}(M_W^2, M_H^2) \right] \right. \\
& + \mathcal{F}(M_{H^\pm}^2, M_A^2) - 3\mathcal{F}(M_Z^2, M_{h,\text{ref}}^2) \\
& \left. \left. + 3\mathcal{F}(M_W^2, M_{h,\text{ref}}^2) \right\}, \quad (5.68)
\end{aligned}$$

$$\begin{aligned}
U = & \mathcal{H}(M_W^2) - \mathcal{H}(M_Z^2) + \frac{1}{\pi M_W^2} \left\{ \sin^2 \tilde{\alpha} \mathcal{B}_{22}(M_W^2; M_{H^\pm}^2, M_h^2) \right. \\
& + \cos^2 \tilde{\alpha} \mathcal{B}_{22}(M_W^2; M_{H^\pm}^2, M_H^2) + \mathcal{B}_{22}(M_W^2; M_{H^\pm}^2, M_A^2) \\
& \left. - 2 \mathcal{B}_{22}(M_W^2; M_{H^\pm}^2, M_{H^\pm}^2) \right\} \\
& - \frac{1}{\pi M_Z^2} \left\{ \sin^2 \tilde{\alpha} \mathcal{B}_{22}(M_Z^2; M_h^2, M_A^2) \right. \\
& \left. + \cos^2 \tilde{\alpha} \mathcal{B}_{22}(M_Z^2; M_H^2, M_A^2) - \mathcal{B}_{22}(M_Z^2; M_{H^\pm}^2, M_{H^\pm}^2) \right\}, \quad (5.69)
\end{aligned}$$

where

$$\begin{aligned}
\mathcal{H}(M_V^2) \equiv & \frac{1}{\pi M_V^2} \left\{ \cos^2 \tilde{\alpha} \left[\mathcal{B}_{22}(M_V^2; M_V^2, M_h^2) - M_V^2 \mathcal{B}_0(M_V^2; M_V^2, M_h^2) \right] \right. \\
& + \sin^2 \tilde{\alpha} \left[\mathcal{B}_{22}(M_V^2; M_V^2, M_H^2) - M_V^2 \mathcal{B}_0(M_V^2; M_V^2, M_H^2) \right] \\
& \left. - \mathcal{B}_{22}(M_V^2; M_V^2, M_{h,\text{ref}}^2) + M_V^2 \mathcal{B}_0(M_V^2; M_V^2, M_{h,\text{ref}}^2) \right\}. \quad (5.70)
\end{aligned}$$

The loop functions are given by

$$\begin{aligned}
\mathcal{B}_{22}(q^2; m_1^2, m_2^2) = & \frac{1}{4} (\Delta + 1) [m_1^2 + m_2^2 - \frac{1}{3} q^2] \\
& - \frac{1}{2} \int_0^1 dx X \log(X - i\epsilon), \quad (5.71)
\end{aligned}$$

$$\mathcal{B}_0(q^2; m_1^2, m_2^2) = \Delta - \int_0^1 dx \log(X - i\epsilon), \quad (5.72)$$

$$\mathcal{F}(m_1^2, m_2^2) = \frac{1}{2} (m_1^2 + m_2^2) - \frac{m_1^2 m_2^2}{m_1^2 - m_2^2} \log\left(\frac{m_1^2}{m_2^2}\right), \quad (5.73)$$

with

$$X \equiv m_1^2 x + m_2^2 (1 - x) - q^2 x(1 - x), \quad \Delta \equiv \frac{2}{4 - d} + \ln 4\pi - \gamma_E, \quad (5.74)$$

in d space-time dimensions, where γ_E is the Euler-Mascheroni constant, and where we have defined:

$$\mathcal{B}_{22}(q^2; m_1^2, m_2^2) \equiv B_{22}(q^2; m_1^2, m_2^2) - B_{22}(0; m_1^2, m_2^2), \quad (5.75)$$

$$\mathcal{B}_0(q^2; m_1^2, m_2^2) \equiv B_0(q^2; m_1^2, m_2^2) - B_0(0; m_1^2, m_2^2). \quad (5.76)$$

BIBLIOGRAPHY

- [1] G. Aad *et al.* [ATLAS Collaboration], Phys. Lett. B **716** (2012) 1 [arXiv:1207.7214 [hep-ex]]; ATLAS-CONF-2012-170 (December 13, 2012).
- [2] S. Chatrchyan *et al.* [CMS Collaboration], Phys. Lett. B **716** (2012) 30 [arXiv:1207.7235 [hep-ex]]; CMS-PAS-HIG-12-045 (November 16, 2012).
- [3] S. Chatrchyan *et al.* [CMS Collaboration], Phys. Rev. Lett. **108** (2012) 111804 [arXiv:1202.1997 [hep-ex]]; Phys. Rev. Lett. **110** (2013) 081803 [arXiv:1212.6639 [hep-ex]].
- [4] G. Aad *et al.* [ATLAS Collaboration], Phys. Lett. B **710** (2012) 383 [arXiv:1202.1415 [hep-ex]]; ATLAS-CONF-2012-169 (December 13, 2012).
- [5] G. Aad *et al.* [ATLAS Collaboration], Phys. Rev. Lett. **108** (2012) 111803 [arXiv:1202.1414 [hep-ex]]; ATLAS-CONF-2012-168 (December 13, 2012).
- [6] S. Chatrchyan *et al.* [CMS Collaboration], Phys. Lett. B **710** (2012) 403 [arXiv:1202.1487 [hep-ex]]; CMS-PAS-HIG-12-015 (July 8, 2012).
- [7] T. Aaltonen *et al.* [CDF and D0 Collaborations], Phys. Rev. Lett. **109** (2012) 071804 [arXiv:1207.6436 [hep-ex]].
- [8] R. Barate *et al.* [LEP Working Group for Higgs boson searches and ALEPH and DELPHI and L3 and OPAL Collaborations], Phys. Lett. B **565** (2003) 61 [hep-ex/0306033].
- [9] T. Aaltonen *et al.* [CDF and D0 Collaboration], Phys. Rev. Lett. **104** (2010) 061802 [arXiv:1001.4162 [hep-ex]]; V. M. Abazov *et al.* [D0 Collaboration], arXiv:1301.6122 [hep-ex].
- [10] Tevatron New Physics Higgs Working Group and CDF and D0 Collaborations, arXiv:1207.0449 [hep-ex]. V. M. Abazov *et al.* [D0 Collaboration], arXiv:1301.5358 [hep-ex].

-
- [11] T. Aaltonen *et al.* [CDF Collaboration], Phys. Rev. Lett. **109** (2012) 111802 [arXiv:1207.1707 [hep-ex]]; arXiv:1301.4440 [hep-ex]; arXiv:1301.6668 [hep-ex].
 - [12] V. M. Abazov *et al.* [D0 Collaboration], Phys. Rev. Lett. **109** (2012) 121802 [arXiv:1207.6631 [hep-ex]]. Yuji Enari talk at the Hadron Collider Physics Symposium, Kyoto (November, 2012).
 - [13] G. Aad *et al.* [ATLAS Collaboration], Phys. Rev. D **86** (2012) 032003 [arXiv:1207.0319 [hep-ex]].
 - [14] S. Chatrchyan *et al.* [CMS Collaboration], Phys. Lett. B **710** (2012) 26 [arXiv:1202.1488 [hep-ex]].
 - [15] J. R. Espinosa, C. Grojean, M. Muhlleitner and M. Trott, JHEP **1212** (2012) 045 [arXiv:1207.1717 [hep-ph]]; JHEP **1205** (2012) 097 [arXiv:1202.3697 [hep-ph]]; JHEP **1209** (2012) 126 [arXiv:1205.6790 [hep-ph]].
 - [16] M. Klute, R. Lafaye, T. Plehn, M. Rauch and D. Zerwas, Phys. Rev. Lett. **109** (2012) 101801 [arXiv:1205.2699 [hep-ph]].
 - [17] D. Carmi, A. Falkowski, E. Kuflik and T. Volansky, JHEP **1207** (2012) 136 [arXiv:1202.3144 [hep-ph]].
 - [18] A. Azatov, R. Contino and J. Galloway, JHEP **1204** (2012) 127 [arXiv:1202.3415 [hep-ph]].
 - [19] A. Azatov *et. al.*, JHEP **1206** (2012) 134 [arXiv:1204.4817 [hep-ph]].
 - [20] P. P. Giardino, K. Kannike, M. Raidal and A. Strumia, Phys. Lett. B **718** (2012) 469 [arXiv:1207.1347 [hep-ph]].
 - [21] T. Corbett, O. J. P. Eboli, J. González-Fraile and M. C. González-García, Phys. Rev. D **86** (2012) 075013 [arXiv:1207.1344 [hep-ph]]; Phys. Rev. D **87** (2013) 015022 [arXiv:1211.4580 [hep-ph]].
 - [22] E. Masso and V. Sanz, Phys. Rev. D **87** (2013) 033001 [arXiv:1211.1320 [hep-ph]].
 - [23] J. Ellis and T. You, JHEP **1209** (2012) 123 [arXiv:1207.1693 [hep-ph]].
 - [24] K. Cheung, J. S. Lee and P. -Y. Tseng, arXiv:1302.3794 [hep-ph].

-
- [25] A. Pich, Nucl. Phys. Proc. Suppl. **209** (2010) 182 [arXiv:1010.5217 [hep-ph]].
- [26] A. Pich and P. Tuzón, Phys. Rev. D **80** (2009) 091702 [arXiv:0908.1554 [hep-ph]].
- [27] M. Jung, A. Pich and P. Tuzón, JHEP **1011** (2010) 003 [arXiv:1006.0470 [hep-ph]].
- [28] M. Jung, A. Pich and P. Tuzón, Phys. Rev. D **83** (2011) 074011 [arXiv:1011.5154 [hep-ph]].
- [29] M. Jung, X. -Q. Li and A. Pich, JHEP **1210** (2012) 063 [arXiv:1208.1251 [hep-ph]].
- [30] A. Celis, M. Jung, X. -Q. Li and A. Pich, JHEP **1301** (2013) 054 [arXiv:1210.8443 [hep-ph]].
- [31] G. C. Branco *et. al.*, Phys. Rept. **516** (2012) 1 [arXiv:1106.0034 [hep-ph]].
- [32] J. F. Gunion, H. E. Haber, G. L. Kane and S. Dawson, Front. Phys. **80** (2000) 1.
- [33] N. Craig and S. Thomas, JHEP **1211** (2012) 083 [arXiv:1207.4835 [hep-ph]].
- [34] P. M. Ferreira, R. Santos, M. Sher and J. P. Silva, Phys. Rev. D **85** (2012) 077703 [arXiv:1112.3277 [hep-ph]].
- [35] P. M. Ferreira, R. Santos, M. Sher and J. P. Silva, Phys. Rev. D **85** (2012) 035020 [arXiv:1201.0019 [hep-ph]].
- [36] A. Barroso, P. M. Ferreira, R. Santos and J. P. Silva, Phys. Rev. D **86** (2012) 015022 [arXiv:1205.4247 [hep-ph]].
- [37] G. Burdman, C. E. F. Haluch and R. D. Matheus, Phys. Rev. D **85** (2012) 095016 [arXiv:1112.3961 [hep-ph]].
- [38] A. Arhrib, C. -W. Chiang, D. K. Ghosh and R. Santos, Phys. Rev. D **85** (2012) 115003 [arXiv:1112.5527 [hep-ph]].
- [39] A. Arhrib, R. Benbrik and N. Gaur, Phys. Rev. D **85** (2012) 095021 [arXiv:1201.2644 [hep-ph]].

-
- [40] E. Gabrielli, B. Mele and M. Raidal, *Phys. Lett. B* **716** (2012) 322 [arXiv:1202.1796 [hep-ph]].
- [41] K. Blum and R. T. D’Agnolo, *Phys. Lett. B* **714** (2012) 66 [arXiv:1202.2364 [hep-ph]].
- [42] G. Belanger, B. Dumont, U. Ellwanger, J. F. Gunion and S. Kraml, *JHEP* **1302** (2013) 053 [arXiv:1212.5244 [hep-ph]].
- [43] C. -Y. Chen and S. Dawson, *Phys. Rev. D* **87** (2013) 055016 [arXiv:1301.0309 [hep-ph]].
- [44] S. L. Glashow and S. Weinberg, *Phys. Rev. D* **15** (1977) 1958.
- [45] H. E. Haber, G. L. Kane and T. Sterling, *Nucl. Phys. B* **161** (1979) 493.
- [46] L. J. Hall and M. B. Wise, *Nucl. Phys. B* **187** (1981) 397.
- [47] J. F. Donoghue and L. F. Li, *Phys. Rev. D* **19** (1979) 945.
- [48] V. D. Barger, J. L. Hewett and R. J. N. Phillips, *Phys. Rev. D* **41** (1990) 3421.
- [49] Y. Grossman, *Nucl. Phys. B* **426** (1994) 355 [hep-ph/9401311].
- [50] A. G. Akeroyd and W. J. Stirling, *Nucl. Phys. B* **447** (1995) 3. A. G. Akeroyd, *Phys. Lett. B* **377** (1996) 95 [hep-ph/9603445]; *J. Phys. G* **24** (1998) 1983 [hep-ph/9803324].
- [51] M. Aoki, S. Kanemura, K. Tsumura and K. Yagyu, *Phys. Rev. D* **80** (2009) 015017 [arXiv:0902.4665 [hep-ph]].
- [52] N. G. Deshpande and E. Ma, *Phys. Rev. D* **18** (1978) 2574. E. Ma, *Mod. Phys. Lett. A* **23** (2008) 647 [arXiv:0802.2917 [hep-ph]]; *Phys. Rev. D* **73** (2006) 077301 [hep-ph/0601225].
- [53] W. Altmannshofer, S. Gori and G. D. Kribs, *Phys. Rev. D* **86** (2012) 115009 [arXiv:1210.2465 [hep-ph]].
- [54] Y. Bai, V. Barger, L. L. Everett and G. Shaughnessy, arXiv:1210.4922 [hep-ph].
- [55] E. Cervero and J. -M. Gerard, *Phys. Lett. B* **712** (2012) 255 [arXiv:1202.1973 [hep-ph]].

-
- [56] G. C. Branco, W. Grimus and L. Lavoura, *Phys. Lett. B* **380** (1996) 119 [hep-ph/9601383].
- [57] F. J. Botella, G. C. Branco and M. N. Rebelo, *Phys. Lett. B* **687** (2010) 194 [arXiv:0911.1753 [hep-ph]].
- [58] F. J. Botella, G. C. Branco, M. Nebot and M. N. Rebelo, *JHEP* **1110** (2011) 037 [arXiv:1102.0520 [hep-ph]].
- [59] N. Cabibbo, *Phys. Rev. Lett.* **10** (1963) 531; M. Kobayashi, T. Maskawa, *Prog. Theor. Phys.* **49** (1973) 652.
- [60] P. M. Ferreira, L. Lavoura and J. P. Silva, *Phys. Lett. B* **688** (2010) 341 [arXiv:1001.2561 [hep-ph]].
- [61] C. B. Braeuninger, A. Ibarra and C. Simonetto, *Phys. Lett. B* **692** (2010) 189 [arXiv:1005.5706 [hep-ph]].
- [62] H. Serodio, *Phys. Lett. B* **700** (2011) 133 [arXiv:1104.2545 [hep-ph]].
- [63] I. de Medeiros Varzielas, *Phys. Lett. B* **701** (2011) 597 [arXiv:1104.2601 [hep-ph]].
- [64] G. Cree and H. E. Logan, *Phys. Rev. D* **84** (2011) 055021 [arXiv:1106.4039 [hep-ph]].
- [65] M. Farina, C. Grojean and E. Salvioni, *JHEP* **1207** (2012) 012 [arXiv:1205.0011 [hep-ph]].
- [66] M. Farina, C. Grojean, F. Maltoni, E. Salvioni and A. Thamm, arXiv:1211.3736 [hep-ph].
- [67] S. Biswas, E. Gabrielli and B. Mele, *JHEP* **1301** (2013) 088 [arXiv:1211.0499 [hep-ph]].
- [68] CMS Collaboration, CMS-PAS-HIG-12-025 (July 8, 2012).
- [69] ATLAS Collaboration, ATLAS-CONF-2012-135 (September 28, 2012).
- [70] LEP Higgs Working Group for Higgs boson searches and ALEPH and DELPHI and L3 and OPAL Collaborations, hep-ex/0107031; arXiv:1301.6065 [hep-ex].

- [71] A. Abulencia *et al.* [CDF Collaboration], Phys. Rev. Lett. **96** (2006) 042003 [hep-ex/0510065]. V. M. Abazov *et al.* [D0 Collaboration], Phys. Lett. B **682** (2009) 278 [arXiv:0908.1811 [hep-ex]].
- [72] G. Aad *et al.* [ATLAS Collaboration], JHEP **1206** (2012) 039 [arXiv:1204.2760 [hep-ex]]. S. Chatrchyan *et al.* [CMS Collaboration], JHEP **1207** (2012) 143 [arXiv:1205.5736 [hep-ex]].
- [73] M. Gustafsson, S. Rydbeck, L. Lopez-Honorez and E. Lundstrom, Phys. Rev. D **86** (2012) 075019 [arXiv:1206.6316 [hep-ph]]; B. Swiezewska and M. Krawczyk, arXiv:1212.4100 [hep-ph].
- [74] L. Wang and X. -F. Han, JHEP **1205** (2012) 088 [arXiv:1203.4477 [hep-ph]].
- [75] G. Abbiendi *et al.* [OPAL Collaboration], Eur. Phys. J. C **27** (2003) 311 [hep-ex/0206022].
- [76] M. Baak *et al.*, Eur. Phys. J. C **72** (2012) 2205 [arXiv:1209.2716 [hep-ph]]; <http://gfitter.desy.de/>.
- [77] LEP Electroweak Working Group, <http://lepewwg.web.cern.ch/LEPEWWG/>.
- [78] ATLAS Collaboration, ATLAS-CONF-2012-079 (June 28, 2012).
- [79] J. F. Gunion, Y. Jiang and S. Kraml, Phys. Rev. D **86** (2012) 071702 [arXiv:1207.1545 [hep-ph]].
- [80] A. Drozd, B. Grzadkowski, J. F. Gunion and Y. Jiang, arXiv:1211.3580 [hep-ph].
- [81] S. Chang, S. K. Kang, J. -P. Lee, K. Y. Lee, S. C. Park and J. Song, arXiv:1210.3439 [hep-ph].
- [82] P. M. Ferreira, H. E. Haber, R. Santos and J. P. Silva, Phys. Rev. D **87** (2013) 055009 [arXiv:1211.3131 [hep-ph]].
- [83] J. F. Gunion, Y. Jiang and S. Kraml, Phys. Rev. Lett. **110** (2013) 051801 [arXiv:1208.1817 [hep-ph]].
- [84] Y. Grossman, Z. 'e. Surujon and J. Zupan, JHEP **1303** (2013) 176 [arXiv:1301.0328 [hep-ph]].
- [85] E. Accomando *et al.*, hep-ph/0608079.

-
- [86] A. Pilaftsis, Nucl. Phys. B **504** (1997) 61 [hep-ph/9702393].
- [87] J. R. Ellis, J. S. Lee and A. Pilaftsis, Phys. Rev. D **70** (2004) 075010 [hep-ph/0404167].
- [88] S. Y. Choi, J. Kalinowski, Y. Liao and P. M. Zerwas, Eur. Phys. J. C **40** (2005) 555 [hep-ph/0407347].
- [89] ATLAS Collaboration, ATLAS-CONF-2013-034 (March 14, 2013).
- [90] CMS Collaboration, CMS-PAS-HIG-13-005 (April 18, 2013).
- [91] H. E. Haber and D. O'Neil, Phys. Rev. D **74** (2006) 015018 [hep-ph/0602242].
- [92] S. Dittmaier *et al.* [LHC Higgs Cross Section Working Group Collaboration], arXiv:1101.0593 [hep-ph].
- [93] M. E. Peskin and T. Takeuchi, Phys. Rev. D **46** (1992) 381; Phys. Rev. Lett. **65** (1990) 964.
- [94] H. E. Haber and D. O'Neil, Phys. Rev. D **83** (2011) 055017 [arXiv:1011.6188 [hep-ph]].

6. TOWARDS A GENERAL ANALYSIS OF LHC DATA WITHIN TWO-HIGGS DOUBLET MODELS

Alejandro Celis, Victor Ilisie and Antonio Pich

IFIC, Universitat de València – CSIC, Apt. Correus 22085, E-46071 València, Spain

Journal of High Energy Physics: JHEP 12(2013)095, arXiv: 1310.7941

Abstract: The data accumulated so far confirm the Higgs-like nature of the new boson discovered at the LHC. The Standard Model Higgs hypothesis is compatible with the collider results and no significant deviations from the Standard Model have been observed neither in the flavour sector nor in electroweak precision observables. We update the LHC and Tevatron constraints on CP-conserving two-Higgs-doublet models without tree-level flavour-changing neutral currents. While the relative sign between the top Yukawa and the gauge coupling of the 126 GeV Higgs is found to be the same as in the SM, at 90% CL, there is a sign degeneracy in the determination of its bottom and tau Yukawa couplings. This results in several disjoint allowed regions in the parameter space. We show how generic sum rules governing the scalar couplings determine the properties of the additional Higgs bosons in the different allowed regions. The role of electroweak precision observables, low-energy flavour constraints and LHC searches for additional scalars to further restrict the available parameter space is also discussed.

6.1 Introduction

Experimental data from the ATLAS [1, 2], CMS [3, 4], $D\bar{O}$ and CDF [5] collaborations confirm that the new boson discovered at the LHC is related to the mechanism of electroweak symmetry breaking. The masses of the new boson measured by ATLAS ($125.5 \pm 0.2^{+0.5}_{-0.6}$ GeV) and CMS ($125.7 \pm 0.3 \pm 0.3$ GeV) are in good agreement, giving the average value $M_h = 125.64 \pm 0.35$ GeV, and its spin/parity is compatible with the Standard Model (SM) Higgs boson hypothesis, $J^P = 0^+$ [6–8]. Global analyses of current data find to a good accuracy that the new $h(126)$ boson couples to the vector bosons (W^\pm, Z) with the required strength to restore perturbative unitarity in vector boson scattering amplitudes. The $h(126)$ couplings to fermions of the third generation are also found to be compatible with the SM Higgs scenario [9, 10].

A complex scalar field transforming as a doublet under $SU(2)_L$ seems at present the most elegant and simple explanation for elementary particle masses. None of the fundamental principles of the SM, however, forbids the possibility that a richer scalar sector is responsible for the electroweak symmetry breaking. Unlike the addition of new fermion generations or new gauge bosons, an enlarged scalar sector remains in general much more elusive to experimental constraints. Two-Higgs-doublet models (2HDMs) provide a minimal extension of the SM scalar sector that naturally accommodates the electroweak precision tests, giving rise at the same time to many interesting phenomenological effects [11]. The scalar spectrum of a two-Higgs-doublet model consists of three neutral and one charged Higgs bosons. The direct search for additional scalar states at the LHC or indirectly via precision flavour experiments will therefore continue being an important task in the following years.

Many analyses of LHC and Tevatron data have been performed recently within the framework of CP-conserving 2HDMs with natural flavour conservation (NFC) [12–27]. These works have focused on different versions of the 2HDM in which a discrete \mathcal{Z}_2 symmetry is imposed in the Lagrangian to eliminate tree-level flavour-changing neutral currents (FCNCs). A more general alternative is to assume the alignment in flavour space of the Yukawa matrices for each type of right-handed fermion [28]. The so-called aligned two-Higgs-doublet model (A2HDM) contains as particular cases the different versions of the 2HDM with NFC, while at the same time introduces new sources of CP violation beyond the CKM phase. First studies of the $h(126)$ boson data within the A2HDM, in the CP-conserving limit, were performed in Refs. [29–32] and more recently in

Refs. [33–35]. The implications of new sources of CP violation within this model for the $h(126)$ phenomenology were also analyzed in Ref. [32].

In this work we extend the analysis of Ref. [32] and update the bounds that current LHC and Tevatron data impose on the CP-conserving A2HDM, taking into account the latest results released by the experimental collaborations after the first LHC shutdown. We also discuss the role of electroweak precision observables and flavour constraints to further restrict the parameter space. The allowed regions are classified according to the sign of the bottom and tau Yukawa couplings of the $h(126)$ boson, relative to its coupling to vector bosons. Due to generic sum rules governing the scalar couplings [32, 36–38], the properties of the additional scalar fields of the model are very different in each of these allowed regions. We consider also current limits from the search of additional scalars at the LHC and its impact on our knowledge of the $h(126)$ properties. The possibility of a fermiophobic charged Higgs [32] is also analyzed in light of the latest LHC data. A study of CP-violating effects in the 2HDM along the lines of Ref. [32] will be deferred to a future work.

This paper is organized as follows. The present bounds from LHC and Tevatron data are analyzed in section 6.2, discussing also the role of the loop-induced processes $Z \rightarrow \bar{b}b$ and $\bar{B} \rightarrow X_s \gamma$ to further constrain the available parameter space. In section 6.3 we consider the search for additional Higgs bosons at the LHC. The particular case of a fermiophobic charged Higgs is analyzed in section 6.4. A comparison of our findings with those of related works is done in section 6.5 and a summary of our results is finally given in section 6.6.

6.2 A2HDM fit in the CP-conserving limit

Let us consider the scalar sector of the CP-conserving 2HDM. In the so-called Higgs basis where only one of the doublets acquires a vacuum expectation value, the two doublets are parametrized as [32]

$$\Phi_1 = \begin{bmatrix} G^+ \\ \frac{1}{\sqrt{2}}(v + S_1 + iG^0) \end{bmatrix}, \quad \Phi_2 = \begin{bmatrix} H^+ \\ \frac{1}{\sqrt{2}}(S_2 + iS_3) \end{bmatrix}. \quad (6.1)$$

Thus, Φ_1 plays the role of the SM scalar doublet with $v = (\sqrt{2}G_F)^{-1/2} \simeq 246$ GeV. The physical scalar spectrum consists of five degrees of freedom: two charged fields $H^\pm(x)$ and three neutral scalars $\varphi_i^0(x) = \{h(x), H(x), A(x)\}$. The later are related with the S_i fields through an orthogonal transformation $\varphi_i^0(x) = \mathcal{R}_{ij}S_j(x)$, which is determined by the scalar potential [32]. In the most

general case, the CP-odd component S_3 mixes with the CP-even fields $S_{1,2}$ and the resulting mass eigenstates do not have definite CP quantum numbers. For a CP-conserving potential this admixture disappears, giving $A(x) = S_3(x)$ and¹

$$\begin{pmatrix} h \\ H \end{pmatrix} = \begin{bmatrix} \cos \tilde{\alpha} & \sin \tilde{\alpha} \\ -\sin \tilde{\alpha} & \cos \tilde{\alpha} \end{bmatrix} \begin{pmatrix} S_1 \\ S_2 \end{pmatrix}. \quad (6.2)$$

Performing a phase redefinition of the neutral CP-even fields, it is possible to fix the sign of $\sin \tilde{\alpha}$. In this work we adopt the conventions $M_h \leq M_H$ and $0 \leq \tilde{\alpha} \leq \pi$, so that $\sin \tilde{\alpha}$ is always positive. To avoid FCNCs, we assume the alignment in flavour space of the Yukawa matrices. In terms of the fermion mass-eigenstate fields, the Yukawa interactions of the A2HDM read [28]

$$\begin{aligned} \mathcal{L}_Y &= -\frac{\sqrt{2}}{v} H^+ \{ \bar{u} [\zeta_d V M_d \mathcal{P}_R - \zeta_u M_u V \mathcal{P}_L] d + \zeta_l \bar{\nu} M_l \mathcal{P}_R l \} \\ &\quad - \frac{1}{v} \sum_{\varphi_i^0, f} y_f^{\varphi_i^0} \varphi_i^0 [\bar{f} M_f \mathcal{P}_R f] + \text{h.c.}, \end{aligned} \quad (6.3)$$

where $\mathcal{P}_{R,L} \equiv \frac{1 \pm \gamma_5}{2}$ are the right-handed and left-handed chirality projectors, M_f the diagonal fermion mass matrices and ζ_f ($f = u, d, l$) the family-universal alignment parameters. The only source of flavour-changing phenomena is the CKM matrix V . The well-known versions of the 2HDM with NFC are recovered as particular limits of this parametrization, given in Table 6.1.

In the present analysis we neglect possible CP-violating effects; *i.e.*, we consider a CP-conserving scalar potential and real alignment parameters ζ_f . The couplings of the neutral scalar fields are then given, in units of the SM Higgs couplings, by

$$\begin{aligned} y_f^h &= \cos \tilde{\alpha} + \zeta_f \sin \tilde{\alpha}, & y_{d,l}^A &= i \zeta_{d,l}, \\ y_f^H &= -\sin \tilde{\alpha} + \zeta_f \cos \tilde{\alpha}, & y_u^A &= -i \zeta_u, \end{aligned} \quad (6.4)$$

¹In a generic scalar basis $\phi_a(x)$ ($a = 1, 2$) in which both doublets acquire vacuum expectation values: $\langle 0 | \phi_a^T(x) | 0 \rangle = \frac{1}{\sqrt{2}} (0, v_a e^{i\theta_a})$, we have $\tilde{\alpha} = \alpha - \beta$ in the usually adopted notation. The angle α determines h and H in terms of the CP-even fields and $\tan \beta = v_2/v_1$ is the ratio of vacuum expectation values. Given that the choice of basis is arbitrary, the parameters α and β are in general unphysical. These angles are meaningful only in particular models in which a specific basis is singled out (through a symmetry for example) [39].

Table 6.1: *CP-conserving 2HDMs based on discrete Z_2 symmetries.*

Model	ς_d	ς_u	ς_l
Type I	$\cot \beta$	$\cot \beta$	$\cot \beta$
Type II	$-\tan \beta$	$\cot \beta$	$-\tan \beta$
Type X (lepton-specific)	$\cot \beta$	$\cot \beta$	$-\tan \beta$
Type Y (flipped)	$-\tan \beta$	$\cot \beta$	$\cot \beta$
Inert	0	0	0

for the fermionic couplings and ($\kappa_V^{\varphi_i^0} \equiv g_{\varphi_i^0 V V} / g_{h V V}^{\text{SM}}$, $V = W, Z$)

$$\kappa_V^h = \cos \tilde{\alpha}, \quad \kappa_V^H = -\sin \tilde{\alpha}, \quad \kappa_V^A = 0, \quad (6.5)$$

for the gauge couplings. The CP symmetry implies a vanishing gauge coupling of the CP-odd scalar. In the limit $\tilde{\alpha} \rightarrow 0$, the h couplings are identical to those of the SM Higgs field and the heavy CP-even scalar H decouples from the gauge bosons.²

6.2.1 Implications of LHC and Tevatron data for the $h(126)$ boson

We assume that the $h(126)$ boson corresponds to the lightest CP-even scalar h of the CP-conserving A2HDM. Current experimental data require its gauge coupling to have a magnitude close to the SM one; *i.e.*, $|\cos \tilde{\alpha}| \sim 1$ [32]. A global fit of the parameters $(\cos \tilde{\alpha}, \varsigma_u, \varsigma_d, \varsigma_l)$ to the latest LHC and Tevatron data gives ($\chi_{\text{min}}^2/\text{dof} \simeq 0.73$)

$$|\cos \tilde{\alpha}| > 0.90 \quad (0.80), \quad (6.6)$$

or equivalently $\sin \tilde{\alpha} < 0.44$ (0.60), at 68% CL (90% CL). The resulting constraints on the Yukawa couplings of h are shown in Figure 6.1. The charged Higgs contribution to the $h \rightarrow \gamma\gamma$ amplitude has been assumed to be negligible in this fit. The global fit determines the relative sign between y_u^h and $g_{h V V}$ to be the same as in the SM. The flipped sign solution for the top Yukawa coupling, which was preferred before Moriond 2013 due to the observed excess in the $\gamma\gamma$ channel [32], is ruled out by current data at 90% CL.

² The scalar mixing is often parametrized in terms of $\alpha' = \tilde{\alpha} + \frac{\pi}{2}$, so that $\kappa_V^h = \sin \alpha'$ and the SM limit corresponds to $\alpha' = \pi/2$ [11]. We prefer to describe small deviations from the SM limit with $\tilde{\alpha} \simeq 0$.

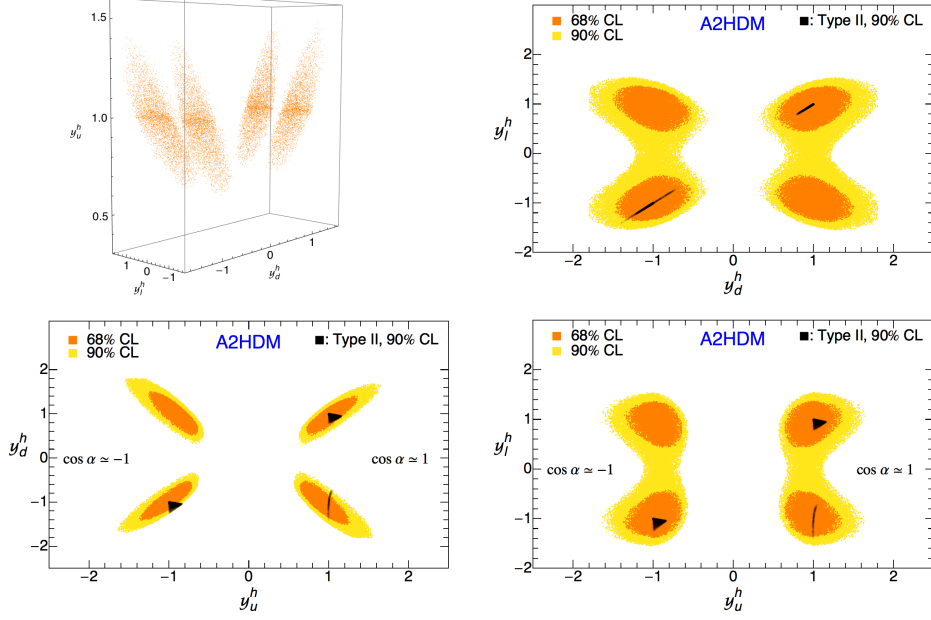


Figure 6.1: Allowed regions in the planes $y_d^h - y_l^h$ (top-right), $y_u^h - y_d^h$ (bottom-left) and $y_u^h - y_l^h$ (bottom-right) at 68% (orange, dark) and 90% (yellow, light) CL from a global fit of LHC and Tevatron data, within the CP-conserving A2HDM. The particular case of the discrete Z_2 model of type II is also indicated at 90% CL (black). Top-left panel: Allowed region in the space (y_u^h, y_d^h, y_l^h) with $\cos \tilde{\alpha} > 0$ at 68% CL (orange).

The partial decay widths of the Higgs decaying into a pair of fermions are not sensitive to the sign of the Yukawa couplings, $\Gamma(h \rightarrow \bar{f}f) \propto |y_f^h|^2$. The loop-induced processes $h \rightarrow \gamma\gamma$ and $gg \rightarrow h$, on the other hand, are sensitive in principle to the $y_{f=u,d,l}^h$ signs. The decay widths, normalized to the SM prediction, can be written in terms of the modified Higgs couplings as,

$$\frac{\Gamma(h \rightarrow \gamma\gamma)}{\Gamma(h \rightarrow \gamma\gamma)_{\text{SM}}} \simeq \left(0.28 y_u^h - 0.004 y_d^h - 0.0035 y_l^h - 1.27 \kappa_V^h\right)^2 + \left(0.006 y_d^h + 0.003 y_l^h\right)^2, \quad (6.7)$$

where we have neglected a possible charged Higgs contribution to $h \rightarrow 2\gamma$, and

$$\frac{\Gamma(h \rightarrow gg)}{\Gamma(h \rightarrow gg)_{\text{SM}}} \simeq \left(1.06 y_u^h - 0.06 y_d^h\right)^2 + \left(0.09 y_d^h\right)^2. \quad (6.8)$$

The last terms in (6.7) and (6.8) are the absorptive contributions from $\tau^+\tau^-$ and $b\bar{b}$ loops. Neglecting the charged Higgs contribution to $h \rightarrow \gamma\gamma$ is well justified if the charged Higgs is very heavy and/or if the cubic Higgs self-coupling hH^+H^- is very small. Due to their small masses, the tau and bottom contributions are very suppressed and, therefore, flipping the sign of $y_{d,l}^h$ has only a very small effect on the relevant partial widths.

The top-left panel in Figure 6.1 shows the 68% CL allowed regions in the space (y_u^h, y_d^h, y_l^h) with $\cos \tilde{\alpha} > 0$. Four disjoint possibilities can be observed, which can be characterized by the relative signs of $y_{d,l}^h$ to that of κ_V^h ; four additional, equivalent, solutions are found flipping simultaneously the signs of y_f^h and $\cos \tilde{\alpha}$. We restrict in the rest of this work to the solutions with $\cos \tilde{\alpha} > 0$. The other panels show the projections in the planes $y_d^h - y_l^h$ (top-right), $y_u^h - y_d^h$ (bottom-left) and $y_u^h - y_l^h$ (bottom-right), at 68% (orange, dark) and 90% (yellow, light) CL. The sign degeneracy in the determination of the bottom and tau Yukawa couplings from current data is clearly observed. At 90% CL, the leptonic Yukawa coupling y_l^h is found to be compatible with zero and therefore only two disjoint islands remain ($y_d^h < 0$ and $y_d^h > 0$).

Figure 6.1 shows also (small black areas, $\chi_{\min}^2/\text{dof} \simeq 0.65$) the constraints in the particular case of the type II model ($\varsigma_{d,l} = -1/\varsigma_u = -\tan \beta$), usually assumed in the literature and realized in minimal supersymmetric scenarios. The allowed regions get considerably reduced in this case. This illustrates that there is a much wider range of open phenomenological possibilities waiting to be explored. The only allowed regions in the type II model are those with identical y_d^h and y_l^h couplings, making a straight line with slope +1 in the $y_d^h - y_l^h$ plane. The $y_{d,l}^h < 0$ region with $\cos \tilde{\alpha} > 0$ requires a relatively large value of $\tan \beta$ to flip the sign of $y_{d,l}^h$. Similar arguments can be made for the other types of 2HDMs with NFC. For instance, in the type I model ($\varsigma_{u,d,l} = \cot \beta$) the allowed regions are straight lines with slope +1 in the three $y_f^h - y_{f'}^h$ planes.

In the following we will keep the discussion within the more general framework provided by the A2HDM. In case any of the versions of the 2HDM with NFC turns out to be (approximately) realized in Nature, an analysis of experimental data within the A2HDM would reveal it.

Figures 6.2, 6.3 and 6.4 show the allowed values for the alignment parameters ς_f , at 68% (orange, dark) and 90% (yellow, light) CL, as function of $\sin \tilde{\alpha}$. Since y_u^h has the same positive sign as $\cos \tilde{\alpha}$ and a similar magnitude, the product $|\varsigma_u| \sin \tilde{\alpha}$ cannot be large. Therefore, $|\varsigma_u|$ gets tightly bounded at large values of $\sin \tilde{\alpha}$ as indicated in Figure 6.2. On the other hand, as $\sin \tilde{\alpha}$ approaches zero, all information on ς_u is lost since in this limit the h couplings are SM-like. The

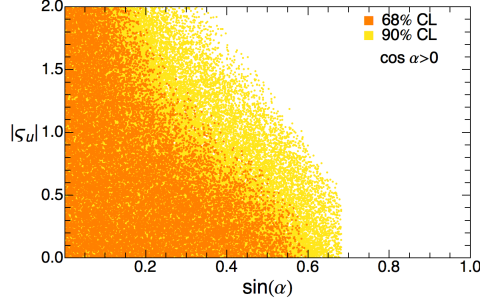


Figure 6.2: Allowed values for ς_u , at 68% CL (orange) and 90% CL (yellow) CL, when $\cos \tilde{\alpha} > 0$.

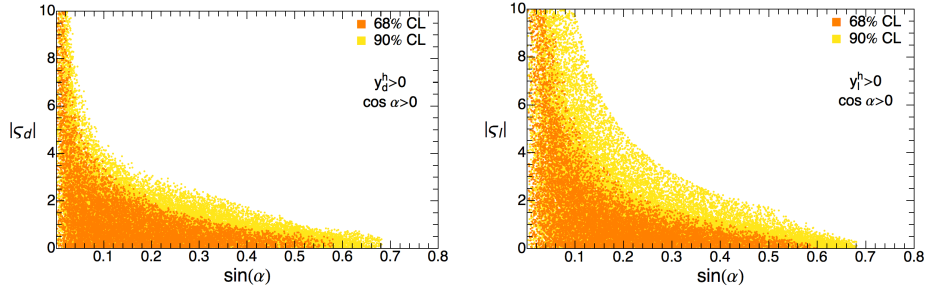


Figure 6.3: Allowed values for $\varsigma_{d,l}$ at 68% CL (orange, dark) and 90% CL (yellow, light) in the regions where $y_d^h > 0$ (left) or $y_l^h > 0$ (right), keeping only solutions with $\cos \tilde{\alpha} > 0$.

same behaviour is observed in Figure 6.3, which shows the allowed values for the alignment parameters ς_d (left panel) and ς_l (right panel), in the regions with $y_d^h > 0$ or $y_l^h > 0$, respectively. Important bounds on the magnitudes of ς_d and ς_l are obtained, again, as long as $\sin \tilde{\alpha} \neq 0$.

A quite different result is obtained in those regions where the Yukawa couplings are negative (again, with $\cos \tilde{\alpha} > 0$). Figure 6.4 shows the allowed values for the alignment parameters $\varsigma_{d,l}$ when $y_d^h < 0$ (left panel) or $y_l^h < 0$ (right panel). A relatively large and negative value for $\varsigma_{d,l}$ is needed to flip the sign in $y_{d,l}^h$, given that $\cos \tilde{\alpha} \simeq 1$. Within the 90% CL allowed region, $y_d^h < 0$ requires $\varsigma_d \lesssim -2.3$, while $y_l^h < 0$ implies $\varsigma_l \lesssim -2.7$. When $\sin \tilde{\alpha} \lesssim 0.1$, the corresponding values for $|\varsigma_{d,l}|$ become very large: $\varsigma_{d,l} \lesssim -24$.

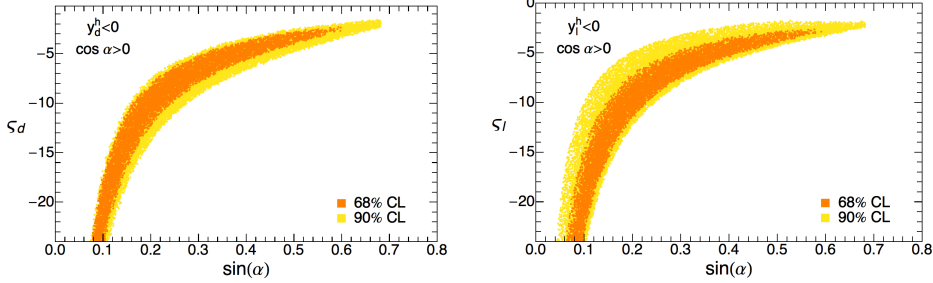


Figure 6.4: Allowed values for the alignment parameters $s_{d,l}$, at 68% CL (orange) and 90% CL (yellow), in the regions where $y_d^h < 0$ (left) or $y_l^h < 0$ (right), keeping only solutions with $\cos \tilde{\alpha} > 0$.

6.2.2 SM-like gauge coupling, $\kappa_V^h \sim 1$, without decoupling

If it is the case that Nature possesses an elementary scalar sector composed of two-Higgs doublets, the fact that no large deviations of the $h(126)$ boson properties from the SM have been observed could be pointing towards a decoupling scenario. In the decoupling limit one of the Higgs doublets can be integrated out, leaving an effective low-energy theory with a SM-like Higgs doublet. The lightest CP-even Higgs appears with a mass around the electroweak scale and SM-like couplings, while the other scalars are much heavier and degenerate, up to corrections of $\mathcal{O}(v^2)$, $M_H^2 \simeq M_A^2 \simeq M_{H^\pm}^2 \gg v^2$. The decoupling limit implies that $|\kappa_V^h| \rightarrow 1$, the opposite however is not true. In the limit $|\kappa_V^h| \rightarrow 1$, the masses of the additional scalars, H , A and H^\pm , can still be of the order of the electroweak scale [40].³

The decoupling regime is very elusive to experimental tests, leaving a low-energy theory with a light SM-like Higgs, while putting the additional scalars beyond the reach of direct searches at colliders. Flavour physics constraints are naturally evaded in this case also due to the heaviness of the additional scalars. Distinguishing signatures of a 2HDM near the decoupling limit would require high-precision measurements of the $h(126)$ boson properties, for example at a future Higgs factory [40]. In this work, we are interested in the more testable case in which the scalar sector is not in the decoupling regime and all the additional

³ In the Higgs basis [32], the decoupling limit occurs for $\mu_2 \gg v^2$, where μ_2 is the coefficient of the quadratic $\Phi_2^\dagger \Phi_2$ term in the scalar potential, while keeping perturbative quartic scalar couplings $|\lambda_i/4\pi| \lesssim 1$. The limit $|\kappa_V^h| \rightarrow 1$ without decoupling arises when $\mu_3, \lambda_6 \rightarrow 0$; *i.e.*, for vanishing $\Phi_1^\dagger \Phi_2$ and $\Phi_1^\dagger \Phi_1 \Phi_1^\dagger \Phi_2$ terms. For a recent discussion see also Refs. [34, 41, 42].

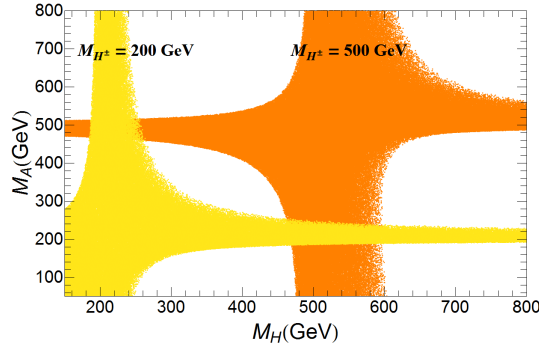


Figure 6.5: Constraints (68% CL) on the masses of the H and A bosons from the oblique parameters while varying $\cos\tilde{\alpha} \in [0.9, 1]$. The charged Higgs mass is fixed at $M_{H^\pm} = 200$ GeV (yellow, light) and 500 GeV (orange, dark).

scalars lie around the electroweak scale. We will assume in particular that the charged Higgs lies in the mass range $M_{H^\pm} \in [80, 500]$ GeV.

Deviations from the SM in the gauge-boson self-energies constrain the mass splittings between the additional physical scalars of the 2HDM. The induced corrections to the oblique parameters have been calculated in Ref. [43] and summarized for the conventions adopted here in Ref. [32]. To satisfy the precision electroweak constraints, the mass differences $|M_{H^\pm} - M_H|$ and $|M_{H^\pm} - M_A|$ cannot be both large ($\gg v$) at the same time. If there is a light charged Higgs below the TeV scale, an additional neutral boson should be around and vice versa. Figure 6.5 shows the 1σ oblique constraints on the $M_H - M_A$ plane, taking $M_{H^\pm} = 200$ GeV (yellow, light) and 500 GeV (orange, dark), while varying $\cos\tilde{\alpha} \in [0.9, 1]$. The bounds on the mass splittings from the oblique parameters, together with the perturbativity and perturbative unitarity bounds on the quartic-Higgs couplings [44], imply that both H and A should have masses below the TeV if $M_{H^\pm} < 500$ GeV. This is the scenario we will be interested in the following, where a rich interplay between precision flavour physics and direct Higgs searches at the LHC can be explored.

Interesting constraints are obtained in this case from flavour physics, specially from loop-induced processes with virtual charged Higgs and top quark contributions. The measured $\bar{B}^0 - B^0$ mixing and the $Z \rightarrow b\bar{b}$ decay width require for example that $|\zeta_u| \lesssim 1.5$, for a charged Higgs below 500 GeV [45]. A more subtle condition can be derived from the radiative decay $\bar{B} \rightarrow X_s \gamma$. The relevant Wilson coefficients for this process take the form $C_i^{\text{eff}} = C_{i,SM} + |\zeta_u|^2 C_{i,uu} - (\zeta_u^* \zeta_d) C_{i,ud}$, where $C_{i,uu}$ and $C_{i,ud}$ contain the dominant virtual top contributions. Thus, their

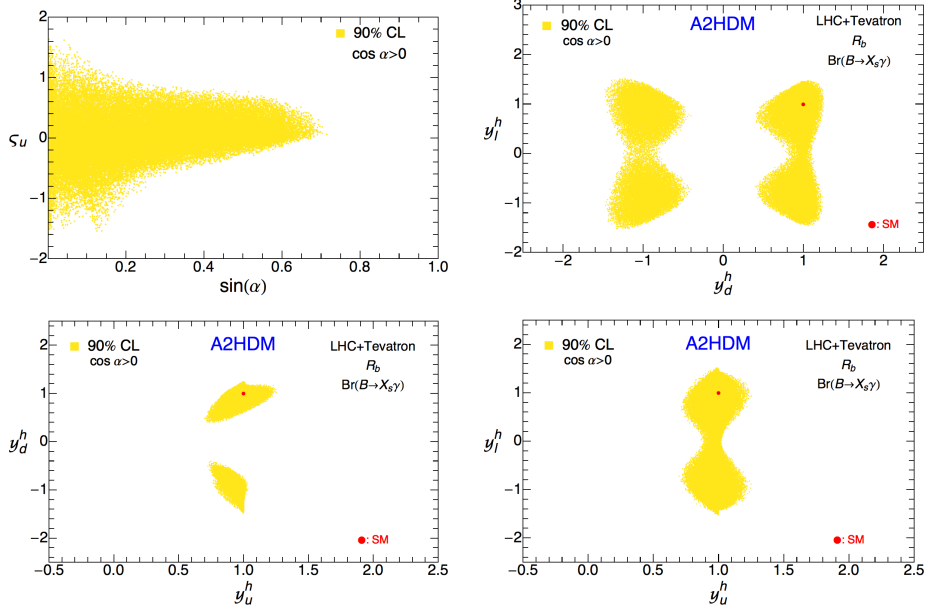


Figure 6.6: Allowed 90% CL regions in the planes $\sin \tilde{\alpha} - s_u$ (top-left), $y_d^h - y_l^h$ (top-right), $y_u^h - y_d^h$ (bottom-left), and $y_u^h - y_l^h$ (bottom-right), from a global fit of LHC and Tevatron data together with R_b and $\text{Br}(\bar{B} \rightarrow X_s \gamma)$, within the CP-conserving A2HDM. The mass of the charged Higgs is varied within $M_{H^\pm} \in [80, 500]$ GeV and $\cos \tilde{\alpha} > 0$.

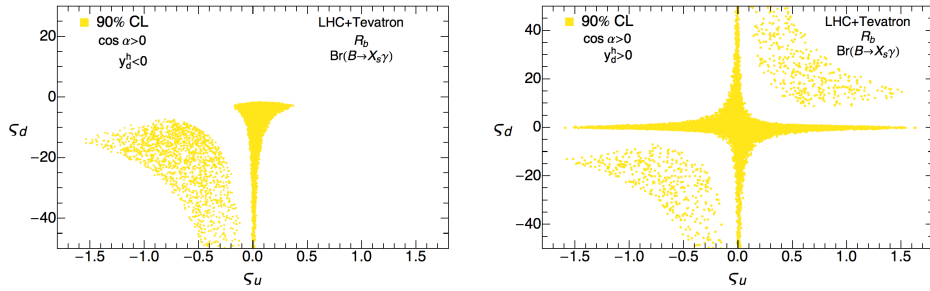


Figure 6.7: Allowed 90% CL region in the plane $s_u - s_d$, from LHC and Tevatron data together with R_b and $\text{Br}(\bar{B} \rightarrow X_s \gamma)$, for $y_d^h < 0$ (left) or $y_d^h > 0$ (right), with $M_{H^\pm} \in [80, 500]$ GeV and $\cos \tilde{\alpha} > 0$.

combined effect can be very different for different values of the ratio s_d/s_u [45–47]. For real values of the alignment parameters, this provides a very strong bound. For instance, in the type II model, where the two terms interfere constructively,

the $\bar{B} \rightarrow X_s \gamma$ rate excludes a charged Higgs mass below 380 GeV [48] at 95% CL for any value of $\tan \beta$. In the more general A2HDM framework, a much lighter charged Higgs is still allowed, but in a very restricted region of the parameter space $\varsigma_u - \varsigma_d$ [45–47].

Semileptonic and leptonic meson decays ($B \rightarrow \tau \nu_\tau$, $D_{(s)} \rightarrow \tau \nu_\tau (\mu \nu_\mu)$, $B \rightarrow D^{(*)} \tau \nu_\tau$), have been analyzed in detail within the A2HDM in Refs. [45, 49]. These processes put bounds on the combinations $\varsigma_u \varsigma_l / M_{H^\pm}^2$ and on $\varsigma_d \varsigma_l / M_{H^\pm}^2$, but the (tree-level) charged Higgs contribution decouples very fast. Given that we allow the possibility of a relatively heavy charged Higgs, $M_{H^\pm} < 500$ GeV, semileptonic and leptonic decays will not provide complementary information in our analysis. If one were to focus the discussion to a very light charged Higgs boson, these processes would certainly need to be taken into account.⁴

In Figure 6.6 we show the effect of including $\bar{B} \rightarrow X_s \gamma$ and $R_b = \Gamma(Z \rightarrow \bar{b}b) / \Gamma(Z \rightarrow \text{hadrons})$ in the fit of $(\cos \tilde{\alpha}, \varsigma_u, \varsigma_d, \varsigma_l)$ while varying $M_{H^\pm} \in [80, 500]$ GeV and, as usual, keeping only solutions with $\cos \tilde{\alpha} > 0$. The down-quark and leptonic alignment parameters are varied within $|\varsigma_{d,l}| \leq 50$ to maintain perturbative scalar interactions for bottom quarks and tau leptons. The charged Higgs contribution to the 2γ channel is also neglected in this fit; therefore, M_{H^\pm} only enters in the fit through the flavour observables considered. Strictly, the analysis is then only valid in those regions of the parameter space in which the charged Higgs is reasonably heavy and/or the cubic Higgs self-coupling hH^+H^- is very small. The results, however, would not change significantly if the H^\pm contribution to $h \rightarrow 2\gamma$ were included in the fit, since it would be compatible with zero, see section 6.4. In the $y_u^h - y_d^h$ plane, it can be observed that a significant part of the previously allowed region is excluded by flavour observables when compared to Figure 6.1. This is due to the effect of $\text{Br}(\bar{B} \rightarrow X_s \gamma)$ which induces severe constraints in the plane $\varsigma_u - \varsigma_d$, as shown in Figure 6.7.

For the case $y_d^h > 0$, collider data do not put any bound on $\varsigma_{u,d}$ in the limit $\sin \tilde{\alpha} \rightarrow 0$; the only constraint that appears in Figure 6.7 (right-panel) is therefore coming from $Z \rightarrow \bar{b}b$ and $\bar{B} \rightarrow X_s \gamma$. For $y_d^h < 0$, LHC and Tevatron data determine that $\varsigma_d \lesssim -2$ in order to flip the Yukawa sign, thus excluding a large region that would otherwise be allowed by flavour observables alone. Compared with Figure 6.2, the value of $|\varsigma_u|$ is slightly more constrained by R_b ; when $M_{H^\pm} < 500$ GeV, one finds $|\varsigma_u| \lesssim 1.5$ for $\sin \tilde{\alpha} \simeq 0$ while a stronger limit is obtained for

⁴The current excess observed by the BaBar collaboration in exclusive $b \rightarrow c \tau \nu$ transitions can only be accommodated within the framework of 2HDMs if one allows for a departure of the Yukawa alignment hypothesis [49, 50]. More theoretical studies on the relevant hadronic matrix elements as well as an update of these modes from the Belle collaboration using the full dataset, are needed to further assess the significance of this excess.

larger values of $\sin \tilde{\alpha}$ due to LHC and Tevatron data. The corresponding allowed regions shown in Figures 6.3 and 6.4 remain almost identical after adding the flavour observables and, therefore, are not shown here.

6.3 Searches for additional Higgs bosons

The search for additional Higgs bosons is one of the most important tasks for the next LHC run. The current information on the $h(126)$ properties puts relevant constraints on the couplings of the other scalars. In particular, Eqs. (6.4) and (6.5) imply the sum rules

$$|\kappa_V^H|^2 = 1 - |\kappa_V^h|^2, \quad (6.9)$$

$$|y_f^H|^2 - |y_f^A|^2 = 1 - |y_f^h|^2, \quad (6.10)$$

$$\kappa_V^H y_f^H = 1 - \kappa_V^h y_f^h. \quad (6.11)$$

The first one is just the trivial trigonometric relation between $\sin \tilde{\alpha}$ and $\cos \tilde{\alpha}$, which implies that the gauge coupling g_{HVV} goes to zero when g_{hVV} approaches the SM value. The lower bound on $|\cos \tilde{\alpha}|$ in Eq. (6.6) gives a direct limit on the coupling of the heavy CP-even scalar H to two gauge bosons, with important implications for searches in the $H \rightarrow VV$ channels. The relation (6.10) constrains the difference of the magnitudes of the H and A Yukawa couplings. When the mixing angle $\tilde{\alpha}$ becomes zero, $y_f^h = 1$ and $|y_f^H| = |y_f^A| = \zeta_f$. Relation (6.11) shows that whenever h has a flipped sign Yukawa ($\kappa_V^h \sim 1, y_f^h \sim -1$), the corresponding Yukawa coupling of H must be very large $y_f^H \kappa_V^H \sim 2$. This sum rule plays a crucial role in the restoration of perturbative unitarity in $W_L^+ W_L^- \rightarrow f \bar{f}$ scattering and is behind the particular shape of the allowed regions in Figure 6.4. The allowed values for κ_V^h and y_f^h , obtained in section 6.2.2 from $h(126)$ collider data and flavour constraints, imply, due to the sum rules, the following 90% CL bounds:

$$\begin{aligned} |y_u^H|^2 - |y_u^A|^2 &\in [-0.6, 0.5], & \kappa_V^H y_u^H &\in [-0.17, 0.5], \\ |y_d^H|^2 - |y_d^A|^2 &\in [-1.2, 0.9], & \kappa_V^H y_d^H &\in [-0.3, 0.7] \cup [1.3, 2.5], \\ |y_t^H|^2 - |y_t^A|^2 &\in [-1.3, 1.0], & \kappa_V^H y_t^H &\in [-0.5, 2.5]. \end{aligned} \quad (6.12)$$

A generic $h(126)$ boson with modified couplings to fermions and gauge bosons would violate perturbative unitarity at high energies, in certain physical processes. Partial-wave unitarity bounds would be violated for example in $W_L^+ W_L^- \rightarrow$

$f\bar{f}$ inelastic scattering at a scale $\sqrt{s} \simeq \Lambda = 16\pi v^2/(m_f |1 - y_f^h \kappa_V^h|)$ [51]. For flipped-sign Yukawa couplings, $\kappa_V^h \simeq 1$ and $y_f^h \simeq -1$, we obtain an approximate value of $\Lambda \sim 9$ TeV for the top quark, while $\Lambda \sim 400$ TeV is obtained for the bottom quark and tau lepton due to the fact that they have smaller masses. A modified hVV coupling would also lead to a violation of perturbative unitarity in $W_L^- W_L^+ \rightarrow W_L^- W_L^+$ elastic scattering; for $\kappa_V^h = 0.89$ (0.95) this occurs at a scale $\sqrt{s} = 2.7$ (3.8) TeV respectively [52]. The scalar couplings in the 2HDM satisfy generic sum rules which ensure that perturbative unitarity is restored, provided the additional scalar states are light enough. In the processes considered previously, $W_L^+ W_L^- \rightarrow f\bar{f}$ and $W_L^- W_L^+ \rightarrow W_L^- W_L^+$, the heavier CP-even Higgs enters with the required couplings to cancel the bad high-energy behavior of the amplitudes. It must be noted that a given physical state needed to restore perturbative unitarity can appear well below the scale at which the partial-wave unitarity bounds are violated. This is well known in the SM where the Higgs mass is only weakly bounded by perturbative unitarity: $M_h \lesssim 1$ TeV [53].

The possibility of flipped-sign bottom and/or tau Yukawa couplings has important implications for the properties of the additional Higgs bosons but only subtle effects in the $h(126)$ phenomenology. Relatively large values for the alignment parameters $\varsigma_{d,l}$ are needed to flip the sign of $y_{d,l}^h$ given that $|\kappa_V^h| \simeq 1$, implying that the additional Higgs bosons H^\pm, H and A should possess very large couplings to bottom and/or tau leptons.

The couplings of the missing Higgs bosons H^\pm, H and A , and therefore their phenomenology, are very different in each of the allowed regions shown in Figure 6.1. It thus seems appropriate to discuss the search strategy for additional scalar states and the experimental constraints in each allowed island separately. An obvious question to address is how future Higgs searches at the LHC, combined with low-energy precision experiments at the intensity frontier, can be used to exclude some of the allowed islands and/or determine the right solution chosen by Nature.

The SM-like region with $y_f^h > 0$ ($f = u, d, l$) includes the trivial solution $\varsigma_f = 0$. Moreover, the Yukawa couplings y_f^H are also compatible with zero. Therefore, one has to face the possibility of a SM-like scalar h plus a fermiophobic scalar doublet including the H, A and H^\pm fields. This is a very difficult experimental scenario where the missing scalars decouple from the fermionic sector and also the coupling $g_{HVV} = 0$. In this case, the production of the additional scalars can occur for example through the $ZHA, ZH^\pm H^\mp, W^\pm H^\mp H$ and $W^\pm H^\mp A$ couplings or through the scalar potential. In the limit $\sin \tilde{\alpha} = 0$, the $h(126)$ data does not provide any constraints on the alignment parameters ς_f (see Figures 6.2

and 6.3). This opens a more interesting possibility with $|y_f^H| = |y_f^A| = \varsigma_f$; the H and A bosons could then be produced through the gluon-fusion mechanism or in associated production with a heavy-quark pair. Moreover, since ς_d and ς_l are only weakly constrained by flavour observables, the couplings to bottom quarks and tau leptons could be very sizeable, generating interesting phenomenological signals. For a very large $|\varsigma_d|$ for example, b-quark associated Higgs production $b\bar{b} \rightarrow \Phi$ or $gb \rightarrow \Phi b$ can become the dominant production mechanism of the heavy scalars H and A at the LHC. Similarly, charged Higgs production in association with top and bottom quarks, $gg \rightarrow t\bar{b}H^-$ or $q\bar{q} \rightarrow t\bar{b}H^-$, can be considerably enhanced in this case. If on the other hand $|\varsigma_l|$ is very large, heavy neutral scalars would probably decay dominantly into leptons, opening the interesting possibility of discovery in the very clean $\Phi \rightarrow \mu^+\mu^-$ channel. The charged Higgs also, would be expected to decay dominantly into a $\tau\nu_\tau$ pair in this case.

The situation is rather different in the other three regions with flipped-sign Yukawas: (a) $y_d^h < 0$ and $y_l^h > 0$, (b) $y_d^h > 0$ and $y_l^h < 0$, and (c) $y_{d,l}^h < 0$. As shown in Figure 6.4, the alignment parameters are tightly constrained in these regions and the missing Higgs bosons could have a relatively large coupling to the bottom and/or tau fermions. In all four allowed regions the alignment parameter ς_u is compatible with zero, therefore there exists the possibility that all production mechanisms of the remaining scalars involving the coupling with top-quarks could be greatly suppressed.

6.3.1 Charged Higgs searches

There are already important exclusion limits coming from charged Higgs searches at colliders, but most of them depend on the assumed Yukawa structure or some hypothesis about the scalar spectrum. In some cases, however, it is possible to set more general limits. For instance, a very light charged Higgs would modify the Z boson decay width if the channel $Z \rightarrow H^+H^-$ is open. Since the coupling ZH^+H^- is completely fixed by the gauge symmetry and does not depend on any free parameter of the model, the constraint $\Gamma_Z^{\text{non-SM}} < 2.9$ MeV (95% CL) on non-SM decays of the Z boson implies $M_{H^\pm} \gtrsim 39.6$ GeV (95% CL) [54]. A much stronger lower bound on the H^\pm mass, $M_{H^\pm} \gtrsim 80$ GeV (95% CL) [54], was set at LEP, assuming that the charged Higgs only decays into $\tau\nu$ or cs final states. A softer limit would be obtained on the other hand if the $H^+ \rightarrow W^+A$ decay is kinematically allowed. Assuming that $M_A > 12$ GeV and a type-I Yukawa structure, the limit $M_{H^\pm} \gtrsim 72.5$ GeV was obtained in $H^+ \rightarrow W^+A \rightarrow W^+b\bar{b}$ searches [54].

In this section, we consider the LHC searches for a light charged Higgs produced via $t \rightarrow H^+ b$, in the decay channels $H^+ \rightarrow \tau^+ \nu_\tau$ [55,56] and $H^+ \rightarrow c \bar{s}$ [57], which are kinematically limited to $M_{H^\pm} < m_t - m_b$. We focus on the constraints that can be extracted on the A2HDM from direct charged Higgs searches and flavour observables; the only parameters entering in this analysis are therefore $(M_{H^\pm}, \varsigma_u, \varsigma_d, \varsigma_l)$. A full scan of the A2HDM parameter space, taking into account electroweak precision data, perturbativity and perturbative unitarity bounds, would give as a result that the neutral scalars H and A cannot be arbitrarily heavy and strong correlations in the $M_H - M_A$ plane will appear as those shown in Figure 6.5. We refer the reader to appendix 6.A for relevant formulae used here. To a good approximation, the branching ratio for $t \rightarrow H^+ b$ is given by

$$\text{Br}(t \rightarrow H^+ b) \simeq \frac{\Gamma(t \rightarrow H^+ b)}{\Gamma(t \rightarrow W^+ b) + \Gamma(t \rightarrow H^+ b)}, \quad (6.13)$$

where we have neglected CKM-suppressed channels in the total top width. We do not consider the possibility of a very light CP-odd Higgs boson which could open decay channels like $H^+ \rightarrow W^+ A$; therefore, the charged Higgs decays only into fermions. Searches into the final state $\tau^+ \nu_\tau$ put bounds on the combination $\text{Br}(t \rightarrow H^+ b) \times \text{Br}(H^+ \rightarrow \tau^+ \nu)$, while current searches for quark decay modes are usually interpreted as limits on $\text{Br}(t \rightarrow H^+ b) \times \text{Br}(H^+ \rightarrow c \bar{s})$. This is due to the expected dominant decay modes of the charged Higgs in the MSSM scenario or in the type-II 2HDM. In general, these searches really put bounds on $\text{Br}(t \rightarrow H^+ b) \times [\text{Br}(H^+ \rightarrow c \bar{s}) + \text{Br}(H^+ \rightarrow c \bar{b})]$. Other final states involving light quarks are neglected as they bring much smaller contributions.

For the next discussion it is useful to write down the following approximate formulae

$$\begin{aligned} \frac{\Gamma(H^+ \rightarrow c \bar{b})}{\Gamma(H^+ \rightarrow c \bar{s})} &\simeq \frac{|V_{cb}|^2 (|\varsigma_d|^2 m_b^2 + |\varsigma_u|^2 m_c^2)}{|V_{cs}|^2 (|\varsigma_d|^2 m_s^2 + |\varsigma_u|^2 m_c^2)}, \\ \frac{\Gamma(H^+ \rightarrow c \bar{b})}{\Gamma(H^+ \rightarrow \tau^+ \nu_\tau)} &\simeq \frac{N_C |V_{cb}|^2 (|\varsigma_d|^2 m_b^2 + |\varsigma_u|^2 m_c^2)}{m_\tau^2 |\varsigma_l|^2}. \end{aligned} \quad (6.14)$$

We can observe that the decay channel $H^+ \rightarrow c \bar{b}$ can be important, compared with $H^+ \rightarrow c \bar{s}$, in certain regions of the A2HDM parameter space in which the strong CKM suppression ($|V_{cb}| \ll |V_{cs}|$) is compensated by a hierarchy of the alignment parameters [58]. Indeed, for $|\varsigma_d| \gg |\varsigma_u|, |\varsigma_l|$ the decay channel $H^+ \rightarrow c \bar{b}$ becomes significant compared with $H^+ \rightarrow c \bar{s}, \tau^+ \nu_\tau$, as shown in Eq. (6.14). This does not occur in the 2HDMs of types I, II and X, due to correlations between

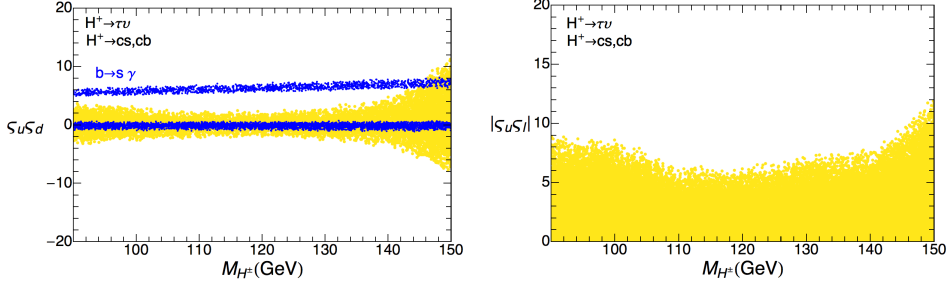


Figure 6.8: *Left-panel:* Allowed values for $\varsigma_u \varsigma_d$ as a function of the charged Higgs mass (yellow-light) obtained from the experimental 95% CL upper bounds on $\text{Br}(t \rightarrow H^+ b) \times [\text{Br}(H^+ \rightarrow c\bar{s}) + \text{Br}(H^+ \rightarrow c\bar{b})]$ and $\text{Br}(t \rightarrow H^+ b) \times \text{Br}(H^+ \rightarrow \tau^+ \nu)$. Allowed values for $\varsigma_u \varsigma_d$ from $\text{Br}(\bar{B} \rightarrow X_s \gamma)$ are shown in blue-dark. *Right-panel:* Similar constraints on the combination $|\varsigma_u \varsigma_l|$ from direct charged Higgs searches. The alignment parameters have been varied in the range $|\varsigma_u| \leq 1$ and $|\varsigma_{d,l}| \leq 50$.

the parameters $\varsigma_{f=u,d,l}$, see Table 6.1. In the type-Y 2HDM, on the other hand, the limit $|\varsigma_d| \gg |\varsigma_u|, |\varsigma_l|$ is achieved for large $\tan \beta$; in this case, however, the $\text{Br}(\bar{B} \rightarrow X_s \gamma)$ constraints forbid a light charged Higgs because $\varsigma_u = -1/\varsigma_d$ [58]. It has been shown in Ref. [58] that a dedicated search for $H^\pm \rightarrow c\bar{b}$ decays, implementing a b tag on one of the jets coming from H^\pm , could provide important constraints on the parameter space region with $|\varsigma_d| \gg |\varsigma_u|, |\varsigma_l|$ where this channel becomes important.

In Figure 6.8 we show the bounds on the A2HDM parameter space from direct searches of a light charged Higgs at the LHC. Note that the present upper bounds on $\text{Br}(t \rightarrow H^+ b) \times [\text{Br}(H^+ \rightarrow c\bar{s}) + \text{Br}(H^+ \rightarrow c\bar{b})]$ and $\text{Br}(t \rightarrow H^+ b) \times \text{Br}(H^+ \rightarrow \tau^+ \nu)$ set an upper limit on $|\varsigma_u \varsigma_l|/M_{H^\pm}^2$ of $\mathcal{O}(\lesssim 10^{-3}) \text{ GeV}^{-2}$. Leptonic B , D and D_s meson decays put weaker constraints on this combination, $\varsigma_u \varsigma_l/M_{H^\pm}^2 \in [-0.006, 0.037] \cup [0.511, 0.535] \text{ GeV}^{-2}$ at 95% CL [45]. Moreover an upper bound on the combination $|\varsigma_u \varsigma_d|$ is obtained from direct charged Higgs searches. Semileptonic and leptonic meson decays, on the other hand, only constrain the combinations $\varsigma_u \varsigma_l$ and $\varsigma_d \varsigma_l$ [45]. For both decay rates: $\Gamma(t \rightarrow H^+ b)$ and $\Gamma(H^+ \rightarrow u_i \bar{d}_j, \tau^+ \nu)$, see Eqs. (6.17) and (6.18), terms proportional to $\varsigma_u \varsigma_d$ or $\varsigma_u \varsigma_l$ are negligible. Thus, no information on the relative sign between ς_u and $\varsigma_{d,l}$ is obtained.

Allowed values at 90% CL from the loop-induced process $\bar{B} \rightarrow X_s \gamma$ [46, 47] on the $(M_{H^\pm}, \varsigma_u \varsigma_d)$ plane are also shown in Figure 6.8. They are given by the two narrow (blue, dark) horizontal strips. We observe that, with the exception

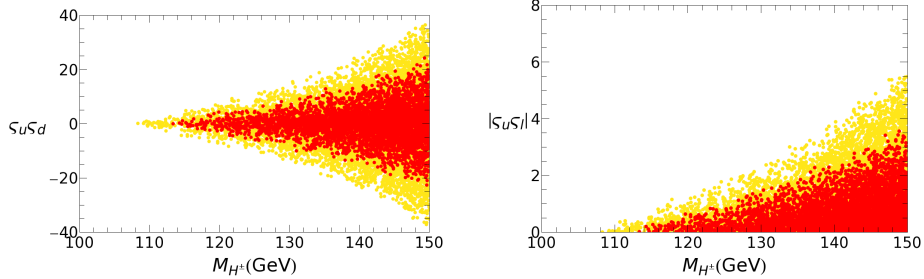


Figure 6.9: Region in the $M_{H^\pm} - \varsigma_u \varsigma_d$ (left) and $M_{H^\pm} - |\varsigma_u \varsigma_l|$ (right) planes which satisfy the condition $\text{Br}(H^+ \rightarrow W^+ b\bar{b}) > 10\%$ (yellow, light) and $\text{Br}(H^+ \rightarrow W^+ b\bar{b}) > 20\%$ (red, dark). The alignment parameters have been varied in the range $|\varsigma_u| \leq 1$ and $|\varsigma_{d,l}| \leq 50$.

of the small region for which $M_{H^\pm} \sim [140, 150]$ GeV, the upper strip is already excluded by direct H^\pm searches. $\bar{B} \rightarrow X_s \gamma$ impose no additional constraints on the combination $(M_{H^\pm}, |\varsigma_u \varsigma_l|)$. For all given points in Figure 6.8 we find that $|\varsigma_u| \leq 0.5$, which is fully compatible with the flavour constraints given by R_b and neutral meson mixing [45].

In the A2HDM, the three-body decay $H^+ \rightarrow t^* \bar{b} \rightarrow W^+ b\bar{b}$ can also play an important role for a light charged Higgs when $M_{H^\pm} > M_W + 2m_b$, see appendix 6.A. This decay is normally very suppressed for a large region of the parameter space. It has been previously analyzed in Refs. [59–63] and it was found that it can bring a sizeable contribution to the total charged Higgs decay rate in the \mathcal{Z}_2 models or in the MSSM when $M_{H^\pm} > 135\text{--}145$ GeV, depending on the model and on the chosen value of $\tan \beta$. In the A2HDM it can bring sizeable contributions to the branching fraction, of the order of 10–20%, already when $M_{H^\pm} \gtrsim 110$ GeV. Figure 6.9 shows the regions satisfying the condition $\text{Br}(H^+ \rightarrow W^+ b\bar{b}) > 10\%$ (20%), in the planes $M_{H^\pm} - \varsigma_u \varsigma_d$ and $M_{H^\pm} - |\varsigma_u \varsigma_l|$. There are wide regions that can bring potentially large contributions to the decay rate, and that partially overlap with the allowed regions shown in Figure 6.8. If we reanalyze the previous experimental constraints from the direct charged Higgs searches by adding this channel to the total decay rate, the allowed regions stay roughly the same, however, the allowed points concentrate in the region $|\varsigma_u \varsigma_d| \lesssim 1.5$. Thus, we conclude that experimental direct searches for a charged Higgs should be enlarged by also including this channel.

It is also worth noticing that for a fermiophobic charged Higgs, for which $\varsigma_{f=u,d,l} = 0$ and hence, H^\pm does not couple to fermions at tree-level, all experimental constraints are trivially satisfied. Other production mechanisms and

decay channels would have to be considered in this case to experimentally probe such scenario.

6.3.2 Neutral Higgs searches

The ATLAS and CMS collaborations have searched for additional neutral Higgs bosons up to masses of 1 TeV in the $\varphi \rightarrow ZZ$ and $\varphi \rightarrow WW$ channels [64, 65]. These searches are sensitive in principle to the heavy CP-even Higgs H , given that the CP-odd Higgs does not couple at tree-level with vector bosons. Having observed no signal, they have set upper bounds on the relevant cross section $\sigma(pp \rightarrow \varphi \rightarrow VV)$, using $\sim 5 \text{ fb}^{-1}$ and $\sim 20 \text{ fb}^{-1}$ of collected data at $\sqrt{s} = 7 \text{ TeV}$ and $\sqrt{s} = 8 \text{ TeV}$ respectively. Searches for neutral bosons in the leptonic final state $\tau^+\tau^-$ with masses up to 500 GeV have been performed by the ATLAS collaboration, using $\sim 5 \text{ fb}^{-1}$ of collected data at $\sqrt{s} = 7 \text{ TeV}$ [66]. Bounds in the $\tau^+\tau^-$ channel have also been presented recently by the CMS collaboration, using the full 2011+2012 dataset, for Higgs masses up to 1 TeV [67]. These searches are sensitive to both CP-even and CP-odd Higgs bosons. Since the CP-odd Higgs does not couple at tree-level with vector bosons, its decay branching ratios into fermions are expected to be large. We assume in this section that the heavy scalars H and A cannot decay in non-SM decay channels like $H/A \rightarrow hh$; the bounds obtained here would be weaker if these decay channels were relevant. This assumption is well justified only in certain regions of the parameter space, namely, when $M_H < 2M_h$ or if the relevant cubic Higgs self-couplings are very small.

At present, searches for heavy scalars in the $H \rightarrow ZZ$ channel are the most sensitive, reaching $\sigma(pp \rightarrow H \rightarrow ZZ)/\sigma(pp \rightarrow H \rightarrow ZZ)_{\text{SM}} \sim 10^{-1}$ for $M_H \lesssim 600 \text{ GeV}$. Generic constraints on the properties of the missing 2HDM scalars can also be obtained from $h(126)$ collider data and flavour observables due to the sum rules governing the scalar couplings. Bounds on the combination $\kappa_V^H y_u^H$, as determined in Eq. (6.12), are shown in Figure 6.10 (yellow-light). Current experimental limits on $\sigma(pp \rightarrow H \rightarrow ZZ)$ are also included in Figure 6.10, reducing the allowed parameter space to the purple-dark area. It can be observed that for heavier Higgs masses the bounds become weaker as expected.

To assess the impact of direct searches for additional scalars to further restrict the available parameter space of the 2HDM, we take the heavy CP-even and CP-odd Higgses to lie in the mass ranges: $M_H \in [200, 600] \text{ GeV}$ and $M_A \in [150, 600] \text{ GeV}$. Of course, a similar analysis could be performed in any other mass ranges for H and A , or by also including constraints from collider searches of a charged Higgs. Here, we have varied the masses of the CP-even and CP-odd

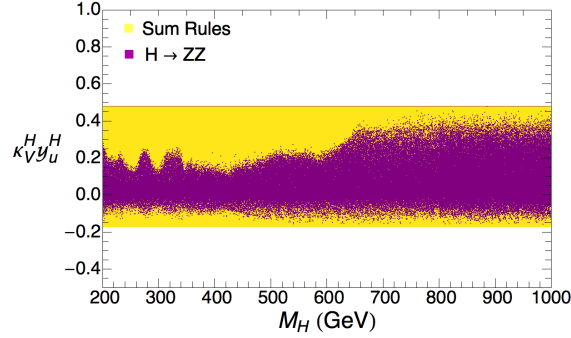


Figure 6.10: Allowed values (90% CL) for the combination $\kappa_V^H y_u^H$ due to generic sum rules, taking into account $h(126)$ collider data and flavour constraints (yellow-light). Experimental limits on $\sigma(pp \rightarrow H \rightarrow ZZ)$ are also included, shrinking the allowed region to the purple-dark area.

scalars independently. Electroweak precision data gives rise to correlations in the $M_H - M_A$ plane depending on the value of the charged Higgs mass, as shown in Figure 6.5. At this point however, this does not have any impact on the allowed regions found in Figures 6.10 and 6.11.

In Figure 6.11 we show the allowed regions (yellow-light) obtained in section 6.2.2, considering the $h(126)$ collider data together with the flavour observables R_b and $\text{Br}(\bar{B} \rightarrow X_s \gamma)$. The allowed regions get reduced when taking into account the limits from direct searches of additional scalars at the LHC (purple-dark). The most important effects are a lower bound on y_u^h and a smaller allowed area in the $\varsigma_u - \sin \tilde{\alpha}$ plane, which are mainly due to the present experimental upper limits on $\sigma(pp \rightarrow H \rightarrow ZZ)$; current searches in the $\tau^+ \tau^-$ and $W^+ W^-$ channels put weaker constraints. The production cross section via gluon fusion scales as $\sigma(gg \rightarrow H) \hat{E} \propto |y_u^H|^2 = |\sin \tilde{\alpha} - \varsigma_u \cos \tilde{\alpha}|^2$ (neglecting the contributions from other quarks which are in general subdominant). When $\sin \tilde{\alpha}$ is far from zero, the decay channels $H \rightarrow VV$ ($V = ZZ, W^+ W^-$) are the dominating ones, given that the fermionic couplings are not very large as the LHC and Tevatron data seem to suggest. The production cross section $\sigma(gg \rightarrow H)$ will then grow for negative values of ς_u , giving rise to a significant total cross section that becomes excluded by the present upper limits on $\sigma(pp \rightarrow H \rightarrow ZZ)$.

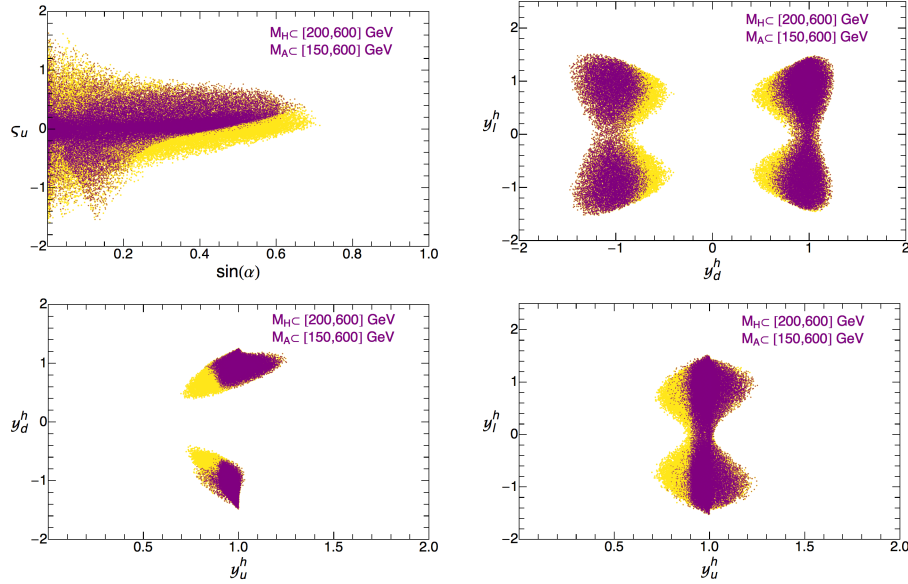


Figure 6.11: Allowed regions in the planes $\sin \tilde{\alpha} - \zeta_u$ (top-left), $y_d^h - y_l^h$ (top-right), $y_u^h - y_d^h$ (bottom-left), and $y_u^h - y_l^h$ (bottom-right) at 90% CL, from a global fit of $h(126)$ collider data together with R_b and $\text{Br}(\bar{B} \rightarrow X_s \gamma)$, within the CP-conserving $A2HDM$, are shown in yellow-light. Constraints from neutral Higgs searches at the LHC have also been included taking $M_H \in [200, 600]$ GeV and $M_A \in [150, 600]$ GeV, shrinking the allowed region to the purple-dark area, see text for details.

6.4 The fermiophobic charged Higgs scenario

In the limit $\zeta_{f=u,d,l} = 0$ the charged Higgs does not couple to fermions at tree level. A very light fermiophobic charged Higgs, even below 80 GeV, is perfectly allowed by data. All bounds coming from flavour physics or direct charged Higgs searches that involve the H^\pm couplings to fermions are naturally evaded in this case. It is also known that when $|\kappa_V^h| = |\cos \tilde{\alpha}| \simeq 1$ (which is presently favoured by LHC and Tevatron data), the process $h \rightarrow 2\gamma$ provides a unique place where non-decoupling effects can be manifest if $M_{H^\pm} \sim \mathcal{O}(v)$ [40]. This motivates a dedicated analysis of this scenario in light of the latest collider data. Here we assume that the lightest CP-even state h is the 126 GeV boson and that CP is a good symmetry of the scalar sector, as in the previous section. The scaling of the neutral Higgs couplings to vector bosons and fermions becomes equal in this limit, $y_f^h = \kappa_V^h$, which makes this scenario very predictive in the neutral scalar

sector. The $h \rightarrow 2\gamma$ decay width is approximately given in this case by

$$\frac{\Gamma(h \rightarrow \gamma\gamma)}{\Gamma(h \rightarrow \gamma\gamma)_{\text{SM}}} \simeq \left(\kappa_V^h - 0.15 C_{H^\pm}^h \right)^2, \quad (6.15)$$

where $C_{H^\pm}^h$ encodes the charged Higgs contribution to the $h \rightarrow 2\gamma$ decay width. More specifically, $C_{H^\pm}^h = v^2/(2M_{H^\pm}^2) \lambda_{hH^+H^-} \mathcal{A}(x_{H^\pm})$ with $x_{H^\pm} = 4M_{H^\pm}^2/M_h^2$, the cubic Higgs coupling is defined through $\mathcal{L}_{hH^+H^-} = -v \lambda_{hH^+H^-} hH^+H^-$ and the loop function $\mathcal{A}(x)$ is given by

$$\mathcal{A}(x) = -x - \frac{x^2}{4} f(x), \quad f(x) = -4 \arcsin^2(1/\sqrt{x}). \quad (6.16)$$

Here we have assumed that $M_{H^\pm} > M_h/2 \simeq 63$ GeV so that $C_{H^\pm}^h$ does not contain an imaginary absorptive part. The cubic Higgs self coupling $\lambda_{hH^+H^-}$ can be expressed as a linear combination of quartic couplings of the scalar potential in the Higgs basis, see for example Ref. [32]. To reduce the number of parameters to a minimal set, we perform a fit to $(\cos \tilde{\alpha}, C_{H^\pm}^h)$, treating $C_{H^\pm}^h$ as a free real variable. A full scan of the scalar parameter space, taking into account electroweak precision data, vacuum stability of the potential, perturbativity and perturbative unitarity bounds, would of course give rise to non-trivial correlations between the relevant Higgs self couplings and the scalar masses.

The best fit to the data is obtained for $(\cos \tilde{\alpha}, C_{H^\pm}^h) = (0.99, -0.58)$ with $\chi_{\text{min}}^2/\text{dof} \simeq 0.65$. In Figure 6.12 (left) we show the allowed regions at 68% (orange), 90% (yellow) and 99% (gray) CL in the variables $(\sin \tilde{\alpha}, C_{H^\pm}^h)$. In the right panel of Figure 6.12, the resulting constraint on $C_{H^\pm}^h$ at 68% CL is shown in terms of the cubic Higgs coupling $\lambda_{hH^+H^-}$ and the charged Higgs mass M_{H^\pm} . The perturbativity limits on the cubic Higgs coupling hH^+H^- , discussed in Ref. [32], are also indicated (light-blue). The allowed region in the plane $(\lambda_{hH^+H^-}, M_{H^\pm})$ is slightly tilted towards negative $\lambda_{hH^+H^-}$ values, since the best fit point prefers a small negative charged Higgs contribution to the $h \rightarrow 2\gamma$ decay amplitude.

At 90% CL, we find for the Higgs signal strengths:⁵ $\mu_{bb}^h = \mu_{\tau\tau}^h = \mu_{\bar{W}W, ZZ}^h = \cos^2 \tilde{\alpha} \in [0.74, 1]$ and $\mu_{\gamma\gamma}^h = 1.13 \pm 0.48$. These relations between the Higgs signal strengths hold in any of the relevant Higgs production mechanisms [32].

Heavy Higgs boson searches in the channels W^+W^- and ZZ are sensitive to the gauge coupling κ_V^H and to cubic scalar couplings relevant to describe possible non-SM decay channels like $H \rightarrow hh$. In the following we assume that the later

⁵Higgs signal strengths refer to Higgs cross sections normalized by the SM prediction, $\mu_X^\varphi = \sigma(pp \rightarrow \varphi \rightarrow X)/\sigma(pp \rightarrow \varphi \rightarrow X)_{\text{SM}}$.

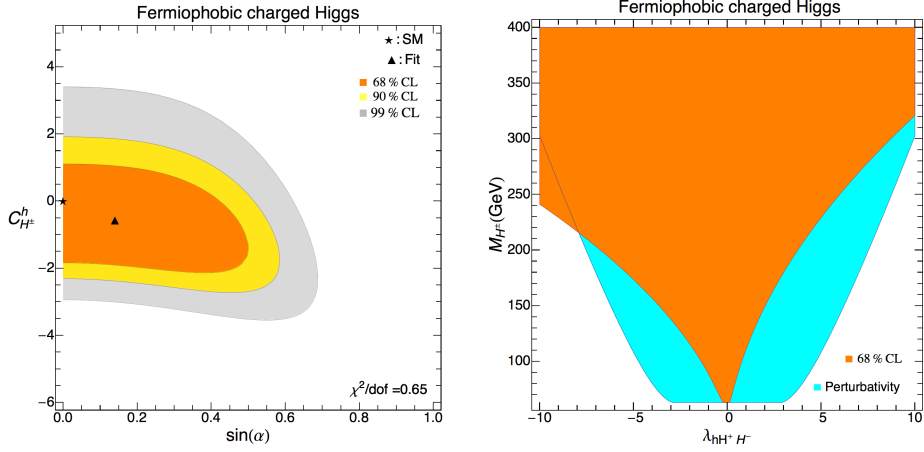


Figure 6.12: Allowed regions at 68% (orange), 90% (yellow) and 99% CL (grey) for a fermiophobic charged Higgs in the plane $\sin \tilde{\alpha} - C_{H^\pm}^h$ (left). The right plot shows the corresponding 68% CL (orange) region in the parameters $\lambda_{hH^+H^-}$ and M_{H^\pm} . The region where perturbation theory remains valid is indicated in light-blue.

can be neglected, this implies that the analysis presented here is only valid in certain regions of the parameter space. We find then that $\mu_{WW,ZZ}^H = \sin^2 \tilde{\alpha} \leq 0.26$ at 90% CL. Considering the current experimental limits on $\mu_{WW,ZZ}^H$ [64, 65], one can rule out a heavy CP-even Higgs in the mass range $M_H \in [130, 630]$ GeV when $\sin^2 \tilde{\alpha} = 0.26$; this bound disappears of course when $\sin \tilde{\alpha} \rightarrow 0$, since H decouples from the vector bosons and the fermions. Associated charged Higgs production with a W^\pm boson via neutral Higgs decays, $\varphi_j^0 \rightarrow H^\pm W^\mp$, with the charged Higgs decaying later to lighter neutral Higgs bosons, is a possible channel to probe the fermiophobic charged Higgs scenario. Sum rules among the couplings $g_{\varphi_j^0 H^\pm W^\mp}$ imply that $|g_{hH^\pm W^\mp}/g_{HH^\pm W^\mp}| = |\sin \tilde{\alpha}/\cos \tilde{\alpha}| < 0.6$ at 90% CL, while $g_{AH^\pm W^\mp}$ is completely fixed by the gauge symmetry [32]. Since the charged Higgs does not decay into fermions at tree level, branching fractions for $H^\pm \rightarrow \varphi_j^0 W^\pm$ decays can be particularly large.

An even more restricted scenario in which the charged Higgs decouples from the fermions is given by the Inert 2HDM. In this case a \mathcal{Z}_2 symmetry is imposed in the Higgs basis so that all SM fields and Φ_1 are even under this symmetry while $\Phi_2 \rightarrow -\Phi_2$. Therefore, there is no mixing between the CP-even neutral Higgs bosons h and H . Assuming that the $h(126)$ boson corresponds to the lightest CP-even Higgs, we then have that $y_f^h = 1$ and $\cos \tilde{\alpha} = 1$. If furthermore one assumes that there are no open decay channels other than the SM ones, only the

diphoton channel can show a deviation from the SM due to the charged Higgs contribution. From a global fit of this scenario to LHC and Tevatron data we obtain $C_{H^\pm}^h \in [-1.9, 1.2]$ at 90% CL ($\chi_{\min}^2/\text{dof} \simeq 0.6$). This can be compared with the situation before Moriond 2013 in which $C_{H^\pm}^h \in [-2.4, -0.1]$ at 90% CL, driven by the excess in the diphoton signal observed at the moment [32]. Detailed studies of the Inert 2HDM, discussing the possibility to account for the Dark Matter in the Universe, can be found in Refs. [20–22] and references therein.

6.5 Comparison with other works

Following the discovery of the $h(126)$ boson, a large number of works have appeared, analyzing the implications of collider data within the framework of 2HDMs. The majority of these analyses have been performed assuming NFC [12–27], thus restricting considerably the Yukawa structure of the model and the phenomenological possibilities. The ATLAS and CMS collaborations were initially observing a significant excess in the diphoton channel. The most natural explanation for such excess was a large charged Higgs contribution to the $h \rightarrow \gamma\gamma$ decay amplitude, other alternatives being usually in conflict with flavour constraints or perturbativity bounds, see Ref. [32] and references therein. The situation has changed drastically after Moriond 2013, given that the CMS collaboration now reports a diphoton signal that is no longer enhanced. The main message that can be extracted from recent analyses is that current collider data can be accommodated very well in the SM; the addition of a second Higgs doublet does not improve in a significant way the agreement with the data. Important constraints start to appear for 2HDMs with NFC, restricting them to lie closer to the SM-limit.

Considerable work has also been done recently to analyze the future prospects at the LHC, as well as in possible future machines, to detect additional Higgs bosons within 2HDMs. Compared with the vast literature on the subject before the $h(126)$ discovery, information about the $h(126)$ boson properties is now being included in these analyses. Phenomenological studies within 2HDMs with NFC, relevant for the search of additional scalars, have been done in Refs. [13–16, 19, 24, 25, 41, 68–70]. Promising production mechanisms and decay channels have been pointed out in these works. In particular, if the $h(126)$ couplings are found to be very close to those of the SM, searches for heavy neutral Higgs bosons in the channels $\gamma\gamma$ or $\tau^+\tau^-$ become particularly relevant [16]. It could also be possible that heavy Higgs bosons decay mostly into the lightest state h , assumed to be the $h(126)$ boson. In this case, h production via heavy Higgs decays could be

the way to detect these heavy states [70]. Some possibilities for this scenario are $H \rightarrow hh$, $A \rightarrow Zh$, and $H^\pm \rightarrow W^\pm h$. In any case, the non-observation of additional Higgs bosons will provide complementary information, together with direct measurements of the $h(126)$ boson properties, to restrict the parameter space of 2HDMs.

The experimental collaborations have also shown interest to search for signatures of extended Higgs sectors at the LHC, beyond the usually tested minimal supersymmetric scenarios. The ATLAS collaboration, for example, has released a search for a heavy CP-even Higgs boson in the $H \rightarrow WW \rightarrow e\nu\mu\nu$ channel within the types I and II 2HDMs, in the mass range [135, 300] GeV, using 13 fb^{-1} of data at $\sqrt{s} = 8 \text{ TeV}$ center of mass energy [71]. The CMS collaboration, on the other hand, has analyzed the future prospects in the search for heavy neutral Higgs bosons at the LHC. The analysis was performed in the channels $H \rightarrow ZZ \rightarrow 4\ell$ ($\ell = e, \mu$) and $A \rightarrow Zh \rightarrow \ell\ell bb$, assuming an integrated luminosity of 3000 fb^{-1} at $\sqrt{s} = 14 \text{ TeV}$ center of mass energy [72]. On the experimental side, the main challenge seems to account for the large number of free parameters present in the 2HDM, even in the more restricted versions with NFC. On the theoretical side there is still a lot of work to be done to be able to start a precision study of these more general extended Higgs sectors. Theoretical predictions for cross-sections and branching ratios, taking into account relevant electroweak and QCD corrections, as well as its implementation in standard tools will be of utmost importance as experimental data becomes more precise, see for example Refs. [73–76] for some relevant works in this direction.

In this work, we have focused on the possibility of performing a more general analysis of collider data within the framework of 2HDMs, without resorting to any symmetry in the Yukawa sector as is done in the different scenarios with NFC. The A2HDM provides a rich Yukawa structure that includes all the different 2HDMs with a \mathcal{Z}_2 symmetry as particular limits while, at the same time, suppresses flavour changing transitions in low-energy systems to acceptable levels [28, 45–47]. First studies of the $h(126)$ boson data within the A2HDM, in the CP-conserving limit, were performed in Refs. [29–32] and more recently in Refs. [33, 34]. The role of new sources of CP-violation beyond the CKM-phase present in the A2HDM were also discussed in Ref. [32]; we will consider this possibility in more detail in a future work. The main problem one has to face in this approach is the larger number of free parameters, compared with the NFC models. On the other hand, one is able to perform in this way non-biased analyses of the scalar sector of the 2HDM, without imposing symmetries which at first hand might seem ad-hoc. We have shown for example how generic sum-rules governing the scalar

couplings provide a direct connection between the $h(126)$ properties and those of the missing scalars, see Eq. (6.12).

A comprehensive analysis of current $h(126)$ data within extended Higgs sectors has been recently performed in Ref. [34], including comparisons between the A2HDM and different \mathcal{Z}_2 2HDMs. Also of relevance in this work, is a discussion of the effect of quantum corrections in relation to high-precision studies of the Higgs sector. In Ref. [33], emphasis was given on an estimation of the future sensitivity that can be achieved at a high-luminosity LHC, a linear electron-positron collider and a muon collider, making the relevant comparisons between the A2HDM and the different NFC scenarios. A discussion of possible phenomenological strategies to test the 2HDM has been done recently in the Higgs basis [41], following the basis independent methods developed in Ref. [39].

Information about the $h(126)$ boson properties is crucial for making simplifying assumptions and reducing the number of relevant variables, in order to perform a viable scan of the 2HDM parameter space at the LHC or at future colliders. In this work, we have analyzed the current data, keeping only a minimal set of parameters that are of relevance while capturing the rich phenomenology provided by the Yukawa structure of the A2HDM.

6.6 Summary

We have studied the implications of LHC and Tevatron data, after the first LHC shutdown, for CP-conserving 2HDMs, assuming that the $h(126)$ boson corresponds to the lightest CP-even state of the scalar spectrum. The phenomenological analysis has been done within the general framework of the A2HDM, which contains as particular limits all different 2HDMs based on \mathcal{Z}_2 symmetries. Interesting bounds on the properties of the additional Higgs bosons of the model can be extracted, due to the existence of sum rules relating the different scalar couplings.

The $h(126)$ coupling to vector bosons is found to be very close to the SM limit, implying an upper bound on the heavy CP-even Higgs coupling to vector bosons: $|\kappa_V^H| < 0.6$ at 90% CL. Other bounds on the couplings of the missing neutral scalars have been summarized in Eq. (6.12). The flipped-sign solution for the top-quark Yukawa coupling, which was preferred by the fit before Moriond 2013 in order to explain the excess in the 2γ channel [32], is now found to be excluded at 90% CL. A sign degeneracy in the determination of the bottom and tau Yukawa couplings however remains.

We have discussed the role of flavour physics constraints, electroweak precision observables and LHC searches for additional scalars to further restrict the parameter space. Some results of our analysis can be pointed out. Loop-induced processes ($Z \rightarrow \bar{b}b$ and $\bar{B} \rightarrow X_s \gamma$) set important constraints on the quark Yukawa couplings, y_u^h and y_d^h , for charged Higgs masses below 500 GeV. Also, heavy Higgs searches in the ZZ channel put significant limits on the up-type quark Yukawa coupling y_u^h . Regarding direct charged Higgs searches at colliders, decays of the charged Higgs into a $c\bar{b}$ pair and three-body decays $H^+ \rightarrow t^* \bar{b} \rightarrow W^+ b \bar{b}$, can have sizable decay rates in some regions of the allowed parameter space. Future searches for a light charged Higgs at the LHC in hadronic final states should take these possibilities into account, perhaps through the implementation of b-tagging techniques as suggested in Ref. [58].

The fermiophobic charged-Higgs scenario has been discussed in light of current experimental data. Though this is a particular limit of the A2HDM, it deserved a separate analysis for different reasons. A very light fermiophobic charged Higgs boson can give unusually large contributions to the $h \rightarrow \gamma\gamma$ amplitude. Another reason is that in this case many simple relations arise between the properties of the neutral Higgs bosons, making this scenario particularly predictive when analyzing the searches for additional Higgs bosons at the LHC. We find that current data still allow for very light charged scalars and sizable contributions from a charged Higgs to the $h \rightarrow 2\gamma$ amplitude.

6.A Useful formulae for a light charged Higgs

A light charged Higgs with $M_{H^\pm} < m_t + m_b$ can be produced at the LHC via top-quark decays. The relevant partial decay widths are given by

$$\Gamma(t \rightarrow W^+ b) = \frac{g^2 |V_{tb}|^2}{64 \pi m_t^3} \lambda^{1/2}(m_t^2, m_b^2, M_W^2) \times \left(m_t^2 + m_b^2 + \frac{(m_t^2 - m_b^2)^2}{M_W^2} - 2M_W^2 \right),$$

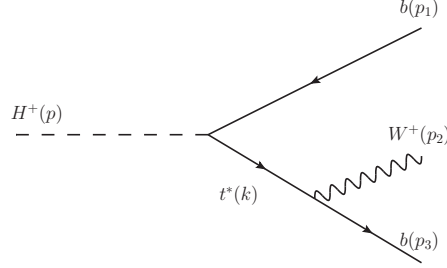


Figure 6.13: *Feynman diagram for the three-body charged Higgs decay $H^+ \rightarrow t^* \bar{b} \rightarrow W^+ b \bar{b}$.*

$$\begin{aligned} \Gamma(t \rightarrow H^+ b) &= \frac{|V_{tb}|^2}{16\pi m_t^3 v^2} \lambda^{1/2}(m_t^2, m_b^2, M_{H^\pm}^2) \\ &\quad \times \left[(m_t^2 + m_b^2 - M_{H^\pm}^2)(m_b^2 |\varsigma_d|^2 + m_t^2 |\varsigma_u|^2) \right. \\ &\quad \left. - 4m_b^2 m_t^2 \operatorname{Re}(\varsigma_d \varsigma_u^*) \right], \end{aligned} \quad (6.17)$$

with $\lambda(x, y, z) = x^2 + y^2 + z^2 - 2(xy + xz + yz)$ and $g = 2M_W/v$. QCD vertex corrections to $t \rightarrow H^\pm b$ and $t \rightarrow W^\pm b$ cancel to a large extent in $\operatorname{Br}(t \rightarrow H^\pm b)$ [77]. The charged Higgs decays into quarks and leptons are described in the A2HDM by the following expressions:

$$\begin{aligned} \Gamma(H^+ \rightarrow l^+ \nu_l) &= \frac{m_l^2}{8\pi v^2} \left(1 - \frac{m_l^2}{M_{H^\pm}^2} \right)^2 M_{H^\pm} |\varsigma_l|^2, \\ \Gamma(H^+ \rightarrow u_i \bar{d}_j) &= \frac{N_C |V_{ij}|^2}{8\pi v^2 M_{H^\pm}^3} \lambda^{1/2}(M_{H^\pm}^2, m_{u_i}^2, m_{d_j}^2) \left(1 + \frac{17}{3} \frac{\alpha_s(M_{H^\pm})}{\pi} \right) \\ &\quad \times \left[(M_{H^\pm}^2 - m_{u_i}^2 - m_{d_j}^2)(|\varsigma_d|^2 m_{d_j}^2 + |\varsigma_u|^2 m_{u_i}^2) \right. \\ &\quad \left. + 4m_{u_i}^2 m_{d_j}^2 \operatorname{Re}(\varsigma_d \varsigma_u^*) \right], \end{aligned} \quad (6.18)$$

where N_C is the number of colours. Running $\overline{\text{MS}}$ quark masses entering in these expressions are evaluated at the scale M_{H^\pm} , and the leading QCD vertex correction to $H^+ \rightarrow u \bar{d}$ has been taken into account [78].

When the charged Higgs mass satisfies $M_{H^\pm} > M_W + 2m_b$, three-body decays of the charged Higgs mediated by a virtual top quark can be relevant, see

Figure 6.13. The decay width for $H^+ \rightarrow t^* \bar{b} \rightarrow W^+ b \bar{b}$ is given in the A2HDM by

$$\Gamma(H^\pm \rightarrow t^* \bar{b} \rightarrow W^+ b \bar{b}) = \frac{N_C g^2 |V_{tb}|^4}{128\pi^3 M_{H^\pm}^3 M_W^2 v^2} \times \int ds_{23} \int ds_{13} \frac{G(s_{23}, s_{13})}{[s_{23} - m_t^2]^2}, \quad (6.19)$$

where

$$\begin{aligned} G(s_{23}, s_{13}) = & \left[M_W^2 (p_1 p_3) + 2 (p_2 p_3) (p_1 p_2) \right] \left[|\varsigma_u|^2 m_t^4 - |\varsigma_d|^2 m_b^2 k^2 \right] \\ & + \left[M_W^2 m_b^2 (p_3 k) + 2 m_b^2 (p_2 p_3) (p_2 k) \right] \\ & \times \left[2 |\varsigma_d|^2 (p_1 k) + 2 m_t^2 \operatorname{Re}(\varsigma_u \varsigma_d^*) \right], \end{aligned} \quad (6.20)$$

with:

$$\begin{aligned} k = p_2 + p_3, \quad k^2 = s_{23}, \quad (p_1 p_3) &= \frac{1}{2} (s_{13} - 2m_b^2), \\ (p_2 p_3) = \frac{1}{2} (s_{23} - M_W^2 - m_b^2), \quad (p_1 p_2) &= \frac{1}{2} (M_{H^\pm}^2 + m_b^2 - s_{23} - s_{13}). \end{aligned} \quad (6.21)$$

The integration limits are:

$$\begin{aligned} s_{23}^{\min} &= \frac{1}{4s_{13}} \left\{ (M_{H^\pm}^2 - M_W^2)^2 - \left[\lambda^{1/2}(M_{H^\pm}^2, s_{13}, M_W^2) \right. \right. \\ & \quad \left. \left. + \lambda^{1/2}(s_{13}, m_b^2, m_b^2) \right]^2 \right\}, \\ s_{23}^{\max} &= \frac{1}{4s_{13}} \left\{ (M_{H^\pm}^2 - M_W^2)^2 - \left[\lambda^{1/2}(M_{H^\pm}^2, s_{13}, M_W^2) \right. \right. \\ & \quad \left. \left. - \lambda^{1/2}(s_{13}, m_b^2, m_b^2) \right]^2 \right\}, \end{aligned} \quad (6.22)$$

with

$$4m_b^2 \leq s_{13} \leq (M_{H^\pm} - M_W)^2. \quad (6.23)$$

6.B Statistical treatment and experimental data

The experimental $h(126)$ data used in the fit can be found in Tables 6.2 and 6.3; experimental uncertainties are assumed to be Gaussian. To obtain the pre-

Table 6.2: *Experimental data from the ATLAS and CMS collaborations at $\sqrt{s} = 7 + 8$ TeV.*

Channel	$\hat{\mu}$ (ATLAS)	Comment	$\hat{\mu}$ (CMS)	Comment
$bb(\text{VH})$	0.25 ± 0.65	Ref. [2]	1.0 ± 0.5	Ref. [4]
$\tau\tau(\text{ggF})$	2.19 ± 2.2	$\rho = -0.50$	0.68 ± 1.05	$\rho = -0.5$
$\tau\tau(\text{VBF} + \text{VH})$	-0.31 ± 1.25	Ref. [2]	1.57 ± 1.13	Ref. [4]
$WW(\text{ggF})$	0.79 ± 0.52	$\rho = -0.2$	0.76 ± 0.35	$\rho = -0.3$
$WW(\text{VBF} + \text{VH})$	1.6 ± 1.25	Ref. [2]	0.24 ± 1.14	Ref. [4]
$ZZ(\text{incl.})$	1.5 ± 0.4	Ref. [2]	0.92 ± 0.28	Ref. [4]
$\gamma\gamma(\text{ggF})$	1.6 ± 0.6	$\rho = -0.3$	0.47 ± 0.49	$\rho = -0.6$
$\gamma\gamma(\text{VBF} + \text{VH})$	1.76 ± 1.28	Ref. [2]	1.6 ± 1.14	Ref. [4]

Table 6.3: *Experimental data from CDF and DØ at $\sqrt{s} = 1.96$ TeV.*

Channel	$\hat{\mu}$	Comment
$bb(\text{VH})$	1.59 ± 0.71	Ref. [5]
$\tau\tau(\text{incl.})$	1.7 ± 2.0	Ref. [5]
$WW(\text{incl.})$	0.94 ± 0.84	Ref. [5]
$\gamma\gamma(\text{incl.})$	5.97 ± 3.25	Ref. [5]

ferred values for the parameters of the A2HDM we build a global χ^2 function. For some channels the correlation coefficient ρ between different production modes can be estimated from the 68% CL contours provided by the experimental collaborations, assuming that the $\Delta\chi^2 = \chi^2 - \chi_{\min}^2$ is well described by a bivariate normal distribution. This information is taken into account in the fit. The 68% and 90% one-dimensional confidence level (CL) intervals are given by $\Delta\chi^2 = 1$ and 2.71, respectively. Two-dimensional 68% and 90% CL intervals are given by $\Delta\chi^2 = 2.30$ and 4.31, respectively.

Regarding the flavour observables considered in this work, we use the latest $\bar{B} \rightarrow X_s \gamma$ experimental measurement, $\text{Br}(\bar{B} \rightarrow X_s \gamma)_{E_0 > 1.6 \text{ GeV}} = (3.41 \pm 0.22) \times 10^{-4}$ [79]. The theoretical prediction of this quantity is obtained following Ref. [80]. The calculation of R_b within 2HDMs was detailed in Ref. [81]; the experimental value is $R_b = \Gamma(Z \rightarrow \bar{b}b)/\Gamma(Z \rightarrow \text{hadrons}) = 0.21629 \pm 0.00066$ [82].

Acknowledgements

We thank Xin-Qiang Li and Martin Jung for fruitful collaborations related to the flavour constraints on the A2HDM. We also acknowledge useful discussions with Luca Fiorini and Emilie Passemar regarding the experimental data. This work has been supported in part by the Spanish Government and ERDF funds from the EU Commission [Grants FPA2011-23778 and CSD2007-00042 (Consolider Project CPAN)] and by Generalitat Valenciana under Grant No. PROMETEOII/2013/007. The work of A.C. is supported by the Spanish Ministry MECD through the FPU grant AP2010-0308. The work of V.I. is supported by the Spanish Ministry MEC through the FPI grant BES-2012-054676.

BIBLIOGRAPHY

- [1] ATLAS Collaboration, Phys. Lett. B **716** (2012) 1 [arXiv:1207.7214 [hep-ex]].
- [2] ATLAS Collaboration, Phys. Lett. B **726** (2013) 88 [arXiv:1307.1427 [hep-ex]]; ATLAS-CONF-2013-079 (July 19, 2013); ATLAS-CONF-2013-034 (March 13, 2013); David López Mateos talk at EPS 2013 for the ATLAS collaboration.
- [3] CMS Collaboration, Phys. Lett. B **716** (2012) 30 [arXiv:1207.7235 [hep-ex]].
- [4] CMS Collaboration, JHEP **06** (2013) 081 [arXiv:1303.4571 [hep-ex]]; CMS-PAS-HIG-13-005 (April 17, 2013).
- [5] CDF and D0 Collaborations, Phys. Rev. Lett. **109** (2012) 071804 [arXiv:1207.6436 [hep-ex]]; Phys. Rev. D **88** (2013) 052014 [arXiv:1303.6346 [hep-ex]].
- [6] ATLAS Collaboration, Phys. Lett. B **726** (2013) 120 [arXiv:1307.1432 [hep-ex]].
- [7] CMS Collaboration, Phys. Rev. Lett. **110** (2013) 081803 [arXiv:1212.6639 [hep-ex]].
- [8] D0 Collaboration, D0 Note 6387-CONF (July 22, 2013).
- [9] K. Cheung, J. S. Lee and P. -Y. Tseng, JHEP **1305** (2013) 134 [arXiv:1302.3794 [hep-ph]]; J. Ellis and T. You, JHEP **1306** (2013) 103 [arXiv:1303.3879 [hep-ph]]; A. Falkowski, F. Riva and A. Urbano, JHEP **1311** (2013) 111 [arXiv:1303.1812 [hep-ph]]; P. P. Giardino, K. Kannike, I. Masina, M. Raidal and A. Strumia, arXiv:1303.3570 [hep-ph].
- [10] A. Pich, arXiv:1307.7700.

-
- [11] J. F. Gunion, H. E. Haber, G. L. Kane and S. Dawson, *Front. Phys.* **80** (2000) 1; G. C. Branco, P. M. Ferreira, L. Lavoura, M. N. Rebelo, M. Sher and J. P. Silva, *Phys. Rept.* **516** (2012) 1 [arXiv:1106.0034 [hep-ph]].
 - [12] A. Barroso, P. M. Ferreira, R. Santos, M. Sher and J. P. Silva, arXiv:1304.5225 [hep-ph].
 - [13] B. Grinstein and P. Uttayarat, *JHEP* **1306** (2013) 094 [arXiv:1304.0028 [hep-ph]].
 - [14] O. Eberhardt, U. Nierste and M. Wiebusch, *JHEP* **1307** (2013) 118 [arXiv:1305.1649 [hep-ph]].
 - [15] C. -Y. Chen, S. Dawson and M. Sher, *Phys. Rev. D* **88** (2013) 015018 [arXiv:1305.1624 [hep-ph]].
 - [16] N. Craig, J. Galloway and S. Thomas, arXiv:1305.2424 [hep-ph].
 - [17] B. Coleppa, F. Kling and S. Su, arXiv:1305.0002 [hep-ph].
 - [18] J. Shu and Y. Zhang, *Phys. Rev. Lett.* **111** (2013) 091801 [arXiv:1304.0773 [hep-ph]].
 - [19] C. -W. Chiang and K. Yagyu, *JHEP* **1307** (2013) 160 [arXiv:1303.0168 [hep-ph]].
 - [20] M. Krawczyk, D. Sokolowska, P. Swaczyna and B. Swiezewska, *JHEP* **1309** (2013) 055 [arXiv:1305.6266 [hep-ph]].
 - [21] A. Goudelis, B. Herrmann and O. Stål, *JHEP* **1309** (2013) 106 [arXiv:1303.3010 [hep-ph]].
 - [22] A. Arhrib, Y. -L. S. Tsai, Q. Yuan and T. -C. Yuan, arXiv:1310.0358 [hep-ph].
 - [23] G. Belanger, B. Dumont, U. Ellwanger, J. F. Gunion and S. Kraml, *Phys. Rev. D* **88** (2013) 075008 [arXiv:1306.2941 [hep-ph]].
 - [24] R. Enberg, J. Rathsman and G. Wouda, *JHEP* **1308** (2013) 079 [arXiv:1304.1714 [hep-ph]].
 - [25] R. Enberg, J. Rathsman and G. Wouda, arXiv:1311.4367 [hep-ph].

-
- [26] S. Chang, S. K. Kang, J. -P. Lee, K. Y. Lee, S. C. Park and J. Song, arXiv:1310.3374 [hep-ph].
- [27] K. Cheung, J. S. Lee and P. -Y. Tseng, arXiv:1310.3937 [hep-ph].
- [28] A. Pich and P. Tuzón, Phys. Rev. D **80** (2009) 091702 [arXiv:0908.1554 [hep-ph]].
- [29] E. Cervero and J. -M. Gerard, Phys. Lett. B **712** (2012) 255 [arXiv:1202.1973 [hep-ph]].
- [30] W. Altmannshofer, S. Gori and G. D. Kribs, Phys. Rev. D **86** (2012) 115009 [arXiv:1210.2465 [hep-ph]].
- [31] Y. Bai, V. Barger, L. L. Everett and G. Shaughnessy, Phys. Rev. D **87** (2013) 115013 [arXiv:1210.4922 [hep-ph]].
- [32] A. Celis, V. Ilisie and A. Pich, JHEP **1307** (2013) 053 [arXiv:1302.4022 [hep-ph]].
- [33] V. Barger, L. L. Everett, H. E. Logan and G. Shaughnessy, arXiv:1308.0052 [hep-ph].
- [34] D. Lopez-Val, T. Plehn and M. Rauch, JHEP **1310** (2013) 134 [arXiv:1308.1979 [hep-ph]].
- [35] V. Ilisie, arXiv:1310.0931 [hep-ph].
- [36] J. F. Gunion, H. E. Haber and J. Wudka, Phys. Rev. D **43** (1991) 904.
- [37] B. Grzadkowski, J. F. Gunion and J. Kalinowski, Phys. Lett. B **480** (2000) 287 [hep-ph/0001093].
- [38] I. F. Ginzburg and M. Krawczyk, Phys. Rev. D **72** (2005) 115013 [hep-ph/0408011].
- [39] S. Davidson and H. E. Haber, Phys. Rev. D **72**, 035004 (2005) [Erratum-ibid. D **72**, 099902 (2005)] [hep-ph/0504050]; H. E. Haber and D. O'Neil, Phys. Rev. D **74** (2006) 015018 [hep-ph/0602242].
- [40] J. F. Gunion and H. E. Haber, Phys. Rev. D **67** (2003) 075019 [hep-ph/0207010].

-
- [41] D. M. Asner, T. Barklow, C. Calancha, K. Fujii, N. Graf, H. E. Haber, A. Ishikawa and S. Kanemura *et al.*, arXiv:1310.0763 [hep-ph].
- [42] M. Carena, I. Low, N. R. Shah and C. E. M. Wagner, arXiv:1310.2248 [hep-ph].
- [43] H. -J. He, N. Polonsky and S. -f. Su, Phys. Rev. D **64** (2001) 053004 [hep-ph/0102144]; W. Grimus, L. Lavoura, O. M. Ogreid and P. Osland, Nucl. Phys. B **801** (2008) 81 [arXiv:0802.4353 [hep-ph]]; H. E. Haber and D. O’Neil, Phys. Rev. D **83** (2011) 055017 [arXiv:1011.6188 [hep-ph]].
- [44] J. Maalampi, J. Sirkka and I. Vilja, Phys. Lett. B **265** (1991) 371; S. Kanemura, T. Kubota and E. Takasugi, Phys. Lett. B **313** (1993) 155 [hep-ph/9303263]; A. G. Akeroyd, A. Arhrib and E. -M. Naimi, Phys. Lett. B **490** (2000) 119 [hep-ph/0006035]; I. F. Ginzburg and I. P. Ivanov, Phys. Rev. D **72** (2005) 115010 [hep-ph/0508020]; P. Osland, P. N. Pandita and L. Selbuz, Phys. Rev. D **78** (2008) 015003 [arXiv:0802.0060 [hep-ph]].
- [45] M. Jung, A. Pich and P. Tuzón, JHEP **1011** (2010) 003 [arXiv:1006.0470 [hep-ph]].
- [46] M. Jung, A. Pich and P. Tuzón, Phys. Rev. D **83** (2011) 074011 [arXiv:1011.5154 [hep-ph]].
- [47] M. Jung, X. -Q. Li and A. Pich, JHEP **1210** (2012) 063 [arXiv:1208.1251 [hep-ph]].
- [48] T. Hermann, M. Misiak and M. Steinhauser, JHEP **1211** (2012) 036 [arXiv:1208.2788 [hep-ph]].
- [49] A. Celis, M. Jung, X. -Q. Li and A. Pich, JHEP **1301** (2013) 054 [arXiv:1210.8443 [hep-ph]].
- [50] J. P. Lees *et al.* [BaBar Collaboration], Phys. Rev. Lett. **109** (2012) 101802 [arXiv:1205.5442 [hep-ex]].
- [51] M. Farina, C. Grojean, F. Maltoni, E. Salvioni and A. Thamm, JHEP **1305** (2013) 022 [arXiv:1211.3736 [hep-ph]].
- [52] K. Cheung, C. -W. Chiang and T. -C. Yuan, Phys. Rev. D **78** (2008) 051701 [arXiv:0803.2661 [hep-ph]].
- [53] B. W. Lee, C. Quigg and H. B. Thacker, Phys. Rev. D **16** (1977) 1519.

-
- [54] ALEPH, DELPHI, L3 and OPAL Collaborations, *Eur. Phys. J. C* **73** (2013) 2463 [arXiv:1301.6065 [hep-ex]].
- [55] ATLAS Collaboration, *JHEP* **1206** (2012) 039 [arXiv:1204.2760 [hep-ex]]; ATLAS-CONF-2013-090 (August 25, 2013).
- [56] CMS Collaboration, *JHEP* **1207** (2012) 143 [arXiv:1205.5736 [hep-ex]].
- [57] ATLAS Collaboration, *Eur. Phys. J. C* **73** (2013) 2465 [arXiv:1302.3694 [hep-ex]].
- [58] A. G. Akeroyd, S. Moretti and J. Hernández-Sánchez, *Phys. Rev. D* **85** (2012) 115002 [arXiv:1203.5769 [hep-ph]].
- [59] A. Djouadi, J. Kalinowski and P. M. Zerwas, *Z. Phys. C* **70** (1996) 435 [hep-ph/9511342].
- [60] E. Ma, D. P. Roy and J. Wudka, *Phys. Rev. Lett.* **80** (1998) 1162 [hep-ph/9710447].
- [61] F. Borzumati and A. Djouadi, *Phys. Lett. B* **549** (2002) 170 [hep-ph/9806301].
- [62] S. Moretti and W. J. Stirling, *Phys. Lett. B* **347** (1995) 291 [Erratum-ibid. *B* **366** (1996) 451] [hep-ph/9412209, hep-ph/9511351].
- [63] X. -J. Bi, Y. -B. Dai and X. -Y. Qi, *Phys. Rev. D* **61** (2000) 015002 [hep-ph/9907326].
- [64] ATLAS Collaboration, ATLAS-CONF-2013-013; ATLAS-CONF-2013-067.
- [65] CMS Collaboration, *Eur. Phys. J. C* **73** (2013) 2469 [arXiv:1304.0213 [hep-ex]]; CMS-HIG-12-024 (July 24, 2013).
- [66] ATLAS Collaboration, *JHEP* **1302** (2013) 095 [arXiv:1211.6956 [hep-ex]].
- [67] CMS Collaboration, CMS-PAS-HIG-13-021 (November 1, 2013).
- [68] C. -Y. Chen, arXiv:1308.3487 [hep-ph].
- [69] E. Brownson, N. Craig, U. Heintz, G. Kukartsev, M. Narain, N. Parashar and J. Stupak, arXiv:1308.6334 [hep-ex].
- [70] A. Arhrib, P. M. Ferreira and R. Santos, arXiv:1311.1520 [hep-ph].

-
- [71] ATLAS Collaboration, ATLAS-CONF-2013-027 (March 10, 2013).
- [72] CMS Collaboration, CMS-PAS-FTR-13-024 (October 9, 2013).
- [73] D. Eriksson, J. Rathsman and O. Stål, *Comput. Phys. Commun.* **181** (2010) 189 [arXiv:0902.0851 [hep-ph]].
- [74] R. V. Harlander, S. Liebler and H. Mantler, *Computer Physics Communications* **184** (2013) 1605 [arXiv:1212.3249 [hep-ph]].
- [75] R. V. Harlander, S. Liebler and T. Zirke, arXiv:1307.8122 [hep-ph].
- [76] C. Englert, M. McCullough and M. Spannowsky, arXiv:1310.4828 [hep-ph].
- [77] C. S. Li and T. C. Yuan, *Phys. Rev. D* **42** (1990) 3088 [Erratum-ibid. *D* **47** (1993) 2156]; A. Czarnecki and S. Davidson, *Phys. Rev. D* **48** (1993) 4183 [hep-ph/9301237].
- [78] E. Braaten and J. P. Leveille, *Phys. Rev. D* **22** (1980) 715; M. Drees and K. -i. Hikasa, *Phys. Lett. B* **240** (1990) 455 [Erratum-ibid. *B* **262** (1991) 497].
- [79] BaBar Collaboration, *Phys. Rev. Lett.* **109** (2012) 191801 [arXiv:1207.2690 [hep-ex]]; *Phys. Rev. D* **86** (2012) 112008 [arXiv:1207.5772 [hep-ex]].
- [80] M. Misiak and M. Steinhauser, *Nucl. Phys. B* **764** (2007) 62 [hep-ph/0609241].
- [81] G. Degrossi and P. Slavich, *Phys. Rev. D* **81** (2010) 075001 [arXiv:1002.1071 [hep-ph]].
- [82] ALEPH, CDF, D0, DELPHI, L3, OPAL and SLD Collaborations, arXiv:0911.2604 [hep-ex].

7. LOW-MASS FERMIOPHOBIC CHARGED HIGGS PHENOMENOLOGY IN TWO-HIGGS-DOUBLET MODELS

Victor Ilisie and Antonio Pich

IFIC, Universitat de València – CSIC, Apt. Correus 22085, E-46071 València, Spain

Journal of High Energy Physics: JHEP 09(2014)089, arXiv: 1405.6639

Abstract: After the recent discovery of a Higgs-like boson, the possibility of an enlarged scalar sector arises as a natural question. Experimental searches for charged scalars have been already performed with negative results. We analyze the phenomenology associated with a fermiophobic charged Higgs (it does not couple to fermions at tree level), in two-Higgs-doublet models. All present experimental bounds are evaded trivially in this case, and one needs to consider other decay and production channels. We study the associated production of a charged Higgs with either a W or a neutral scalar boson, and the relevant decays for a light fermiophobic charged Higgs. The interesting features of this scenario should result encouraging for the LHC collaborations to perform searches for such a particle.

7.1 Introduction

The recent discovery of a boson with mass around 125 GeV by the ATLAS [1–4], CMS [5–7], DØ and CDF [8, 9] collaborations is the first direct hint of the electroweak symmetry-breaking mechanism. The experimental data confirm that it is a Higgs-like scalar with couplings compatible with the Standard Model (SM) predictions. However, this new particle could belong to an enlarged scalar sector.

In order to give mass to fermions and gauge bosons while preserving gauge invariance, the SM assumes the presence of one SU(2) electroweak scalar doublet with a non-zero vacuum expectation value. However, no fundamental principle or symmetry forbids the presence of additional scalar doublets. The simplest extension of the SM is the two-Higgs-doublet model (2HDM) [10, 11], which leads to a richer scalar sector and very interesting phenomenological implications [12–44]. Generic multi-Higgs doublet models give rise to unwanted flavour-changing neutral current (FCNC) interactions, which are found to be very suppressed experimentally. The FCNCs can be eliminated at tree level by requiring the alignment in flavour space of the Yukawa matrices [15]. The so-called aligned two-Higgs-doublet model (A2HDM) contains as particular cases the different versions of 2HDMs with discrete \mathcal{Z}_2 symmetries while at the same time introduces new sources of CP violation beyond the CKM phase.

The main feature of the 2HDM is the presence of three neutral and one charged Higgs bosons. Finding extra neutral or charged scalar bosons would be a clear signal of an extended scalar sector. The ATLAS [45, 46] and CMS collaborations [47] have performed direct searches for a charged Higgs particle. However, since no excess has been found over the SM background, this only allows us to further constrain the parameter space of the various types of 2HDMs; recent analyses within the A2HDM have been performed in [12–14]. In their searches, both collaborations assume that the charged Higgs is produced in a top-quark decay ($t \rightarrow H^+b$) and that it decays dominantly into fermions; *i.e.*, $H^+ \rightarrow q_u\bar{q}_d, l^+\nu_l$. However, all experimental bounds would be trivially evaded for a fermiophobic charged Higgs, *i.e.*, a charged scalar which does not couple to fermions at tree level. In order to probe such scenario, other production channels and decay rates would have to be considered. Although such analyses have not been yet performed by the LHC collaborations, they become more compelling as the experimental bounds on a non-fermiophobic charged Higgs are getting stronger, at least in the low mass region. The fermiophobic scenario is a simplified model that, if it turns out to be the one preferred by Nature, would allow us to measure (or at least estimate) for the first time the parameters of the scalar

potential. This is usually a rather difficult task in more generic 2HDM settings. It is also worth mentioning that a fermiophobic charged Higgs is present in the *inert* 2HDM [48, 49], where one of the neutral scalars is a nice candidate for dark matter [32–35, 37, 50–58]. The discovery of a fermiophobic H^\pm particle could be interpreted in this case as an indirect signal of the presence of dark matter.

In this work, we shall focus our analysis on the search of a light fermiophobic charged Higgs H^\pm , with mass in the range $M_{H^\pm} \in [M_W, M_W + M_Z]$ so that only a few relevant decay modes are kinematically open. We will study the two most important production channels for a fermiophobic H^\pm : associated production with either a W^\mp boson or a neutral scalar. Due to their similarity with the SM Higgs production channels, one expects them to be experimentally accessible at LHC energies. Next-to-leading order (NLO) QCD corrections will be included for both cross sections, and the bounds on the various parameters of the model from the current LHC data [12] will also be taken into account. The main features of the A2HDM are briefly presented in section 2. Section 3 discusses the calculation of the various decay rates and production modes. Finally, in section 4 we perform a phenomenological analysis, assuming different scenarios for the scalar spectrum, and conclude in section 5 with a summary of our results. Some technical details are given in four appendices.

7.2 The Aligned Two-Higgs-Doublet Model

The 2HDM extends the SM with a second scalar doublet of hypercharge $Y = \frac{1}{2}$. The neutral components of the two scalar doublets acquire vacuum expectation values that are in general complex, $\langle 0 | \phi_a^{(0)}(x) | 0 \rangle = \frac{1}{\sqrt{2}} v_a e^{i\theta_a}$ ($a = 1, 2$), although only the relative phase $\theta \equiv \theta_2 - \theta_1$ is observable. It is convenient to perform a global $SU(2)$ transformation in the scalar space (ϕ_1, ϕ_2) , characterized by the angle $\beta = \arctan(v_2/v_1)$, and work in the so-called Higgs basis (Φ_1, Φ_2) , where only one doublet acquires a vacuum expectation value:

$$\Phi_1 = \begin{bmatrix} G^+ \\ \frac{1}{\sqrt{2}}(v + S_1 + iG^0) \end{bmatrix}, \quad \Phi_2 = \begin{bmatrix} H^+ \\ \frac{1}{\sqrt{2}}(S_2 + iS_3) \end{bmatrix}, \quad (7.1)$$

where G^\pm and G^0 denote the Goldstone fields. Thus, Φ_1 plays the role of the SM scalar doublet with $v \equiv \sqrt{v_1^2 + v_2^2} \simeq (\sqrt{2} G_F)^{-1/2} = 246$ GeV.

The physical scalar spectrum contains five degrees of freedom: the two charged fields $H^\pm(x)$ and three neutral scalars $\varphi_i^0(x) = \{h(x), H(x), A(x)\}$, which are related with the S_i fields through an orthogonal transformation $\varphi_i^0(x) = \mathcal{R}_{ij} S_j(x)$.

The form of the \mathcal{R} matrix is fixed by the scalar potential [14], which determines the neutral scalar mass matrix and the corresponding mass eigenstates. A detailed discussion is given in appendix 7.A. In general, the CP-odd component S_3 mixes with the CP-even fields $S_{1,2}$ and the resulting mass eigenstates do not have a definite CP quantum number. If the scalar potential is CP symmetric this admixture disappears; in this particular case, $A(x) = S_3(x)$ and

$$\begin{pmatrix} h \\ H \end{pmatrix} = \begin{bmatrix} \cos \tilde{\alpha} & \sin \tilde{\alpha} \\ -\sin \tilde{\alpha} & \cos \tilde{\alpha} \end{bmatrix} \begin{pmatrix} S_1 \\ S_2 \end{pmatrix}. \quad (7.2)$$

Performing a phase redefinition of the neutral CP-even fields, we can fix the sign of $\sin \tilde{\alpha}$. In this work we adopt the conventions $M_h \leq M_H$ and $0 \leq \tilde{\alpha} \leq \pi$, so that $\sin \tilde{\alpha}$ is positive.

The most generic Yukawa Lagrangian with the SM fermionic content gives rise to FCNCs because the fermionic couplings of the two scalar doublets cannot be simultaneously diagonalized in flavour space. The non-diagonal neutral couplings can be eliminated by requiring the alignment in flavour space of the Yukawa matrices [15]; *i.e.*, the two Yukawa matrices coupling to a given type of right-handed fermions are assumed to be proportional to each other and can, therefore, be diagonalized simultaneously. The three proportionality parameters ς_f ($f = u, d, l$) are arbitrary complex numbers and introduce new sources of CP violation. In terms of the fermion mass-eigenstate fields, the Yukawa interactions of the A2HDM read [15]

$$\begin{aligned} \mathcal{L}_Y = & -\frac{\sqrt{2}}{v} H^+ \left\{ \bar{u} \left[\varsigma_d V M_d \mathcal{P}_R - \varsigma_u M_u^\dagger V \mathcal{P}_L \right] d + \varsigma_l \bar{\nu} M_l \mathcal{P}_R l \right\} \\ & - \frac{1}{v} \sum_{\varphi_i^0, f} y_f^{\varphi_i^0} \varphi_i^0 \left[\bar{f} M_f \mathcal{P}_R f \right] + \text{h.c.}, \end{aligned} \quad (7.3)$$

where $\mathcal{P}_{R,L} \equiv \frac{1 \pm \gamma_5}{2}$ are the right-handed and left-handed chirality projectors, M_f the diagonal fermion mass matrices and the couplings of the neutral scalar fields are given by:

$$y_{d,l}^{\varphi_i^0} = \mathcal{R}_{i1} + (\mathcal{R}_{i2} + i \mathcal{R}_{i3}) \varsigma_{d,l}, \quad y_u^{\varphi_i^0} = \mathcal{R}_{i1} + (\mathcal{R}_{i2} - i \mathcal{R}_{i3}) \varsigma_u^*. \quad (7.4)$$

As in the SM, all scalar-fermion couplings are proportional to the corresponding fermion masses, and the only source of flavour-changing interactions is the Cabibbo-Kobayashi-Maskawa (CKM) quark mixing matrix V [59, 60]. The usual

models with natural flavour conservation, based on discrete \mathcal{Z}_2 symmetries, are recovered for particular (real) values of the couplings ζ_f [15].

The full set of interactions among the gauge and scalar bosons is given in [14]. The coupling of a single neutral scalar with a pair of gauge bosons takes the form ($V = W, Z$)

$$g_{\varphi_i^0 VV} = \mathcal{R}_{i1} g_{hVV}^{\text{SM}}, \quad (7.5)$$

which implies $g_{hVV}^2 + g_{HVV}^2 + g_{AVV}^2 = (g_{hVV}^{\text{SM}})^2$. Thus, the strength of the SM Higgs interaction is shared by the three 2HDM neutral bosons. In the CP-conserving limit, the CP-odd field decouples while the strength of the h and H interactions is governed by the corresponding $\cos \tilde{\alpha}$ and $\sin \tilde{\alpha}$ factors.

In the following analysis we are also going to need the coupling of a neutral scalar with a pair of charged Higgses. We have parametrized the corresponding interaction as:

$$\mathcal{L}_{\varphi_i^0 H^+ H^-} = -v \sum_{\varphi_i^0} \lambda_{\varphi_i^0 H^+ H^-} \varphi_i^0 H^+ H^-. \quad (7.6)$$

Explicit expressions for the reduced cubic couplings $\lambda_{\varphi_i^0 H^+ H^-}$, in terms of the generic Higgs potential parameters, can be found in [14].

The phenomenological constraints on the A2HDM parameters have been studied in detail in Refs. [12–21]. For a light H^\pm , loop-induced processes dominated by top contributions (ε_K , $Z \rightarrow b\bar{b}$, $B^0 - \bar{B}^0$ mixing) impose a tight (95% CL) upper bound on the up-type alignment parameter: $|\zeta_u| < 0.77$ (1.7), for $M_{H^\pm} = 80$ (500) GeV. Owing to the much smaller fermion masses, the constraints on the down-type (and lepton) parameter are very weak; one imposes instead $|\zeta_d| \leq 50$ to guarantee a perturbative Yukawa coupling. In the popular type-II 2HDM ($\zeta_u = -1/\zeta_d = -1/\zeta_l = \cot \beta$), the decay $\bar{B} \rightarrow X_s \gamma$ excludes charged Higgs masses below 380 GeV [61] at 95% CL, because the SM and charged-Higgs contributions interfere constructively. This is no longer true in the more general A2HDM framework, where one only gets a combined correlated constraint on M_{H^\pm} , ζ_u and ζ_d , which allows much lighter values of the charged-scalar mass in a restricted region of the parameter space $\zeta_u - \zeta_d$ [16–18].

The symmetries of the A2HDM protect in a very efficient way the flavour-blind phases of the alignment parameters from undesirable phenomenological consequences. The experimental upper bounds on fermion electric dipole moments provide the strongest constraints on $\text{Im}(\zeta_f)$, but $\mathcal{O}(1)$ contributions remain allowed at present [20]. For simplicity, in section 7.4, we will restrict our analysis

to the CP-conserving limit and, therefore, will consider real alignment parameters. The LHC data require the gauge coupling of the 125 GeV boson to have a magnitude close to the SM one. Assuming that it corresponds to the lightest CP-even scalar h of the CP-conserving A2HDM, the measured Higgs signal strengths imply $|\cos \tilde{\alpha}| > 0.90$ (0.80) at 68% (90%) CL [12–14]. Direct searches for a heavier neutral scalar (H) provide upper bounds on $|\sin \tilde{\alpha}|$ as a function of M_H , which at present result in a weaker constraint on the mixing angle [12].

In the following we will explore the intriguing possibility that the charged scalar could be fermiophobic, *i.e.*, that its tree-level couplings to fermions vanish ($\varsigma_{u,d,l} = 0$). All current experimental bounds are then trivially avoided, in particular the flavour constraints [16]. The Yukawa couplings of the $h(125)$ boson scale in this case, with respect to the SM ones, with the same factor as the gauge couplings: $y_f^h = \mathcal{R}_{11} = \cos \tilde{\alpha}$. The global fit to the Higgs signal strengths results in the slightly improved bound $|\cos \tilde{\alpha}| > 0.86$ at 90% CL [12].

In the fermiophobic (and CP-conserving) limit, the CP-odd scalar A has also vanishing Yukawa couplings. Therefore, it only couples via multi-Higgs interactions with an even number of A bosons, or through its gauge couplings ($AW^\pm H^\mp$, AZh , AZH , A^2Z^2 , $A^2W^+W^-$, $AH^\pm W^\mp \gamma$, $AH^\pm W^\mp Z$). Thus, a light A boson might be very long-lived. While this could have cosmological implications, it is not in conflict with the relic-density constraints [32, 33, 50–58].

A more specific version of the fermiophobic scenario is provided by the *inert* 2HDM [48, 49], which assumes a discrete \mathcal{Z}_2 symmetry in the Higgs basis such that all SM fields and Φ_1 are even ($\Phi_1 \rightarrow \Phi_1$) under this symmetry while the second (inert) scalar doublet is odd ($\Phi_2 \rightarrow -\Phi_2$). In this restricted case, there is no mixing between the CP-even neutral scalars h and H ; *i.e.*, $\cos \tilde{\alpha} = 1$. The spectrum of the *inert* 2HDM is described in appendix 7.A.1.

7.3 Decay and Production modes

We are going to analyse the possibility of having a fermiophobic charged Higgs with a mass in the restricted interval $M_{H^\pm} \in [M_W, M_W + M_Z]$. In this region, the only relevant decay rates are $H^+ \rightarrow W^+ \gamma$ and $H^+ \rightarrow W^+ \varphi_i^0$. We are mainly interested in the one-loop suppressed decay $H^+ \rightarrow W^+ \gamma$, the only two-body kinematically allowed decay mode, but we need to account also for the tree-level decay into a W^+ boson and a neutral scalar, which cannot be both on-shell simultaneously for the whole considered kinematical region. Thus, we shall consider three-body decays like $H^+ \rightarrow W^+ f \bar{f}$ mediated by the neutral scalars φ_i^0 and $H^+ \rightarrow \varphi_i^0 f_u \bar{f}_d$ mediated by a virtual W^+ , where $f_u \bar{f}_d$ stands for

quark pairs $q_u \bar{q}_d$, or lepton-neutrino pairs $l^+ \nu_l$. The loop-induced decay $H^+ \rightarrow f_u \bar{f}_d$ has a strong Yukawa suppression m_f^2/v^2 and, therefore, it is irrelevant for this discussion. When surpassing the $M_W + M_Z$ threshold, the one-loop decay $H^+ \rightarrow W^+ Z$ would enter the game and we would also be close to the top-quark production threshold. The analysis of these two extra decay modes lays beyond the goal of this paper.

7.3.1 $H^+ \rightarrow W^+ \gamma$

The first process that we are going to analyse is $H^+(k+q) \rightarrow W^+(k) \gamma(q)$. Owing to the conservation of the electromagnetic current, the decay amplitude must adopt the form:

$$\begin{aligned} \mathcal{M} &= \Gamma^{\mu\nu} \varepsilon_\mu^*(q) \varepsilon_\nu^*(k), \\ \Gamma^{\mu\nu} &= (g^{\mu\nu} k \cdot q - k^\mu q^\nu) S + i \epsilon^{\mu\nu\alpha\beta} k_\alpha q_\beta \tilde{S}, \end{aligned} \quad (7.7)$$

where S and \tilde{S} are scalar form factors. To obtain this expression, we have considered the most general Lorentz structure for the effective $\Gamma^{\mu\nu}$ vertex, and have imposed the electromagnetic current conservation condition $q_\mu \Gamma^{\mu\nu} = 0$. All terms proportional to q^μ and k^ν have been also eliminated, as they cancel when contracted with the polarization vectors of the photon and the W boson. Note that, accidentally, the Ward-like identity $k_\nu \Gamma^{\mu\nu} = 0$ also holds for (7.7).

In the unitary gauge, the decay proceeds at one loop through the three sets of diagrams shown in Fig. 7.1: fermionic loops (set 1), scalar loops (set 2) and loops with both gauge and scalar bosons (set 3). Each set is transverse by itself, *i.e.*, of the form given in (7.7). We can then decompose the result into the three separate contributions: $S = S_{(1)} + S_{(2)} + S_{(3)}$ and $\tilde{S} = \tilde{S}_{(1)}$ (the only contribution to the structure $\epsilon^{\mu\nu\alpha\beta} k_\alpha q_\beta$ comes from the fermionic loops). One can further simplify the calculation of $S_{(j)}$ by only considering the terms of the transverse set j that contribute to the structure $k^\mu q^\nu$. In order to calculate these contributions, one only needs to compute diagrams 1.a and 1.b for the first set, 2.a for the second set and 3.a for the third one.

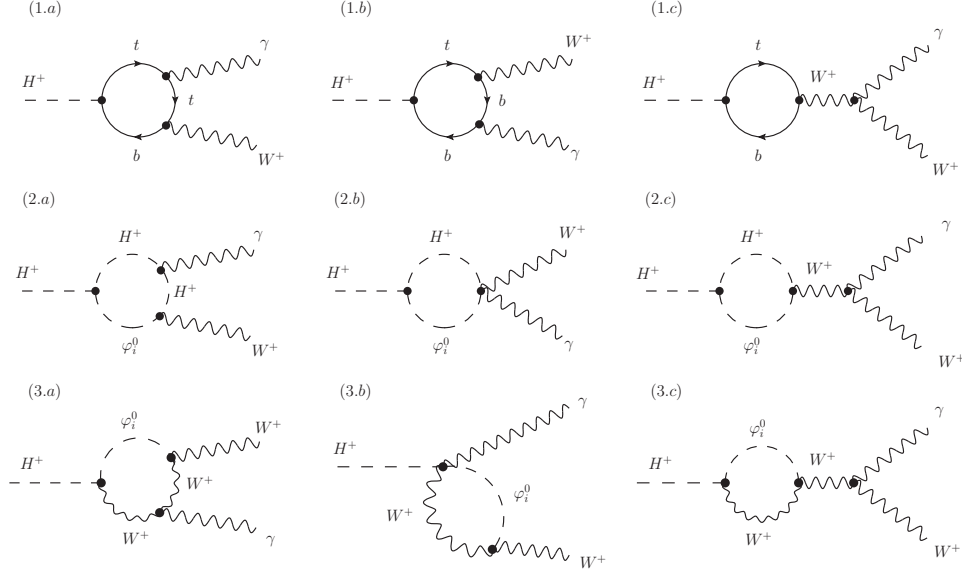


Figure 7.1: *One-loop diagrams contributing to $H^+ \rightarrow W^+\gamma$ in the unitary gauge.*

We obtain the following expressions for the form factors:

$$\begin{aligned}
 S_{(1)} &= \frac{\alpha N_C |V_{tb}|^2}{2\pi v s_W} \int_0^1 dx \int_0^1 dy [Q_t x + Q_b (1-x)] \\
 &\times \frac{-\varsigma_u m_t^2 x (2xy - 2y + 1) + \varsigma_d m_b^2 (1-x)(1-2xy)}{M_W^2 x(x-1) + m_b^2(1-x) + m_t^2 x + (M_W^2 - M_{H^\pm}^2) xy(1-x)}, \quad (7.8)
 \end{aligned}$$

$$\begin{aligned}
 S_{(2)} &= \frac{\alpha v}{2\pi s_W} \sum_i \lambda_{\varphi_i^0 H^+ H^-} (\mathcal{R}_{i2} - i\mathcal{R}_{i3}) \int_0^1 dx \int_0^1 dy \\
 &\times \frac{x^2 y (1-x)}{M_W^2 x(x-1) + M_{\varphi_i^0}^2 (1-x) + M_{H^\pm}^2 x + (M_W^2 - M_{H^\pm}^2) xy(1-x)}, \quad (7.9)
 \end{aligned}$$

$$\begin{aligned}
S_{(3)} &= \frac{\alpha}{2\pi v s_W} \sum_i \mathcal{R}_{i1} (\mathcal{R}_{i2} - i\mathcal{R}_{i3}) \int_0^1 dx \int_0^1 dy x^2 \\
&\times \frac{2M_W^2 + (M_{H^\pm}^2 + M_W^2 - M_{\varphi_i^0}^2) y (x-1)}{M_W^2 x^2 + M_{\varphi_i^0}^2 (1-x) + (M_W^2 - M_{H^\pm}^2) xy (1-x)}, \quad (7.10)
\end{aligned}$$

$$\begin{aligned}
\tilde{S} &= \frac{\alpha N_C |V_{tb}|^2}{2\pi v s_W} \int_0^1 dx \int_0^1 dy [Q_t x + Q_b (1-x)] \\
&\times \frac{\varsigma_u m_t^2 x + \varsigma_d m_b^2 (1-x)}{M_W^2 x (x-1) + m_b^2 (1-x) + m_t^2 x + (M_W^2 - M_{H^\pm}^2) xy (1-x)}, \quad (7.11)
\end{aligned}$$

with $s_W \equiv \sin \theta_W$. The calculation of $S_{(3)}$ has been also performed in the Feynman ($\xi = 1$) gauge, where additional diagrams with Goldstone bosons are present, verifying that these expressions are gauge independent. Our results are in agreement with the recent calculation of the $H^+ W^- \gamma$ effective vertex in Ref. [62]. This calculation was also done many years ago by several groups [63–66] using a somewhat different notation.

The $H^+ \rightarrow W^+ \gamma$ decay width is easily found to be:

$$\Gamma(H^+ \rightarrow W^+ \gamma) = \frac{M_{H^\pm}^3}{32\pi} \left(1 - \frac{M_W^2}{M_{H^\pm}^2}\right)^3 (|S|^2 + |\tilde{S}|^2). \quad (7.12)$$

This one-loop decay rate is in general much smaller than the tree-level decay rates of a charged Higgs into fermions. However, it becomes relevant if the charged Higgs is fermiophobic ($\varsigma_f \rightarrow 0$). In this case, the first set of diagrams (which has only been presented for completeness) does not contribute.

7.3.2 $H^+ \rightarrow W^+ \varphi_1^0$

The H^+ decay rate to on-shell W^+ and φ_i^0 bosons is given by

$$\Gamma(H^+ \rightarrow W^+ \varphi_i^0) = \frac{\alpha}{16 s_W^2 M_{H^\pm}^3 M_W^2} (\mathcal{R}_{i2}^2 + \mathcal{R}_{i3}^2) \lambda^{3/2}(M_{\varphi_i^0}^2, M_{H^\pm}^2, M_W^2), \quad (7.13)$$

with the usual definition of the lambda function $\lambda(x, y, z) \equiv x^2 + y^2 + z^2 - 2xy - 2xz - 2yz$.

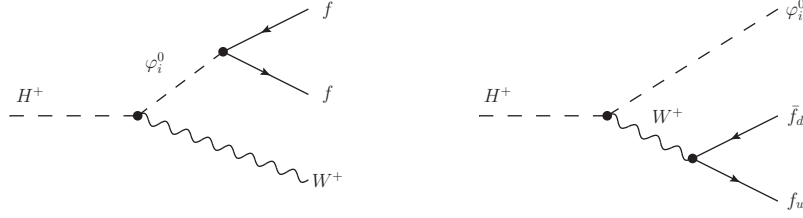


Figure 7.2: $H^+ \rightarrow W^+ f \bar{f}$ process mediated by the virtual neutral scalars φ_i^0 (left) and $H^+ \rightarrow \varphi_i^0 f_u \bar{f}_d$ mediated by a virtual W^+ (right).

The corresponding three-body decay rate to $W^+ f \bar{f}$, with off-shell neutral scalars (Fig. 7.2, left), takes the form:

$$\begin{aligned} \Gamma(H^+ \rightarrow W^+ f \bar{f}) &= \frac{\alpha^2 N_C^f m_f^2}{128 \pi s_W^4 M_{H^\pm}^3 M_W^4} \int_{4m_f^2}^{(M_{H^\pm} - M_W)^2} ds_{23} \\ &\times \lambda^{3/2}(M_{H^\pm}^2, M_W^2, s_{23}) \left(1 - \frac{4m_f^2}{s_{23}}\right)^{1/2} \\ &\times \sum_{i,j} (\mathcal{R}_{i2} - i\mathcal{R}_{i3})(\mathcal{R}_{j2} + i\mathcal{R}_{j3}) \mathcal{M}_{ij}, \quad (7.14) \end{aligned}$$

where N_C^f stands for the number of colours of the fermion f , 3 for quarks and 1 for leptons, s_{23} is the square of the fermion-antifermion invariant mass and

$$\mathcal{M}_{ij} \equiv \frac{(s_{23} - 2m_f^2) \operatorname{Re}(y_f^{\varphi_i^0} y_f^{\varphi_j^0*}) - 2m_f^2 \operatorname{Re}(y_f^{\varphi_i^0} y_f^{\varphi_j^0})}{(s_{23} - M_{\varphi_i^0}^2)(s_{23} - M_{\varphi_j^0}^2)}. \quad (7.15)$$

Obviously, the b -quark contribution will dominate because of the global factor m_f^2 . Therefore, we will neglect the other fermionic final states.

For the decay $H^+ \rightarrow \varphi_i^0 f_u \bar{f}_d$, with an of-shell W^+ (Fig. 7.2, right), we are going to consider all possible final states, quarks and leptons. We exclude the top quark, since this process is well below its production threshold. Neglecting the final fermion masses, the sum over all kinematically-allowed decay modes

amounts to a global factor

$$\Omega = \left(3 + N_C \sum_{u_i=u,c} \sum_{d_j=d,s,b} |V_{u_i d_j}|^2 \right) = 9, \quad (7.16)$$

where the unitarity of the CKM matrix has been used. The total decay width can be expressed as an integral over the fermion-antifermion invariant-mass squared:

$$\begin{aligned} \Gamma(H^+ \rightarrow \varphi_i^0 \sum_{f_u, f_d} f_u \bar{f}_d) &= \frac{\Omega}{9} \frac{3\alpha^2 (\mathcal{R}_{i2}^2 + \mathcal{R}_{i3}^2)}{64\pi s_W^4 M_{H^\pm}^3} \int_0^{(M_{H^\pm} - M_{\varphi_i^0})^2} ds_{23} \\ &\times \frac{\lambda^{3/2}(M_{H^\pm}^2, M_{\varphi_i^0}^2, s_{23})}{(s_{23} - M_W^2)^2}. \end{aligned} \quad (7.17)$$

7.3.3 Charged-Higgs Production

In order to see if the fermiophobic scenario can be experimentally probed, one needs an estimation of the production cross sections for different channels. Here we will consider two possibilities, the associated production with a neutral scalar and the associated production with a W boson (Fig. 7.3). The $q_u \bar{q}_d \rightarrow H^+ \varphi_i^0$ production process is by far the most interesting channel, as it requires the least number of new parameters. For initial-state massless quarks, the leading-order (LO) partonic cross section reads

$$\hat{\sigma}(q_u \bar{q}_d \rightarrow H^+ \varphi_i^0) = \frac{g^4 |V_{ud}|^2}{768 \pi N_c \hat{s}^2} \frac{(\mathcal{R}_{i2}^2 + \mathcal{R}_{i3}^2)}{(\hat{s} - M_W^2)^2} \lambda^{3/2}(\hat{s}, M_{H^\pm}^2, M_{\varphi_i^0}^2), \quad (7.18)$$

where \hat{s} is the partonic invariant-mass squared. The NLO QCD corrections are available and can be expressed in a very simple form, as shown in appendix 7.C.

The associated production with a W boson can proceed through either $q\bar{q}$ or gg fusion. The partonic LO cross section for the $q\bar{q}$ fusion process, is given by

$$\begin{aligned} \hat{\sigma}(q\bar{q} \rightarrow H^+ W^-) &= \frac{g^2}{128 \pi M_W^2 \hat{s}^2} \frac{m_q^2}{v^2} \frac{1}{N_c} \\ &\times \lambda^{3/2}(\hat{s}, M_{H^\pm}^2, M_W^2) \left(1 - \frac{4m_q^2}{\hat{s}} \right)^{-1/2} \\ &\times \sum_{i,j} (\mathcal{R}_{i2} + i\mathcal{R}_{i3})(\mathcal{R}_{j2} - i\mathcal{R}_{j3}) \mathcal{N}_{ij}, \end{aligned} \quad (7.19)$$

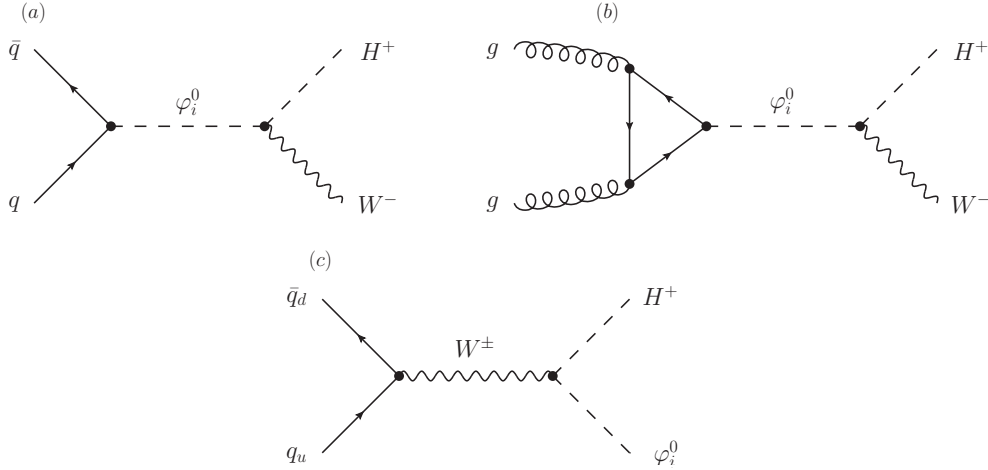


Figure 7.3: *LO contributions to the charged-Higgs associated production with a W boson (diagrams a, b) or a neutral scalar (diagram c), in the fermiophobic scenario.*

with the reduced amplitudes

$$\mathcal{N}_{ij} \equiv \frac{(\hat{s} - 2m_q^2) \operatorname{Re}(y_q^{\varphi_i^0} y_q^{\varphi_j^{0*}}) - 2m_q^2 \operatorname{Re}(y_q^{\varphi_i^0} y_q^{\varphi_j^0})}{(\hat{s} - M_{\varphi_i^0}^2 + iM_{\varphi_i^0} \Gamma_{\varphi_i^0})(\hat{s} - M_{\varphi_j^0}^2 - iM_{\varphi_j^0} \Gamma_{\varphi_j^0})}. \quad (7.20)$$

We have kept the dependence on the initial quark masses, since otherwise the $q\bar{q}$ Yukawa coupling vanishes. This implies a strong suppression of this production mechanism by a factor m_q^2/v^2 .

The gluon fusion mechanism dominates by far the previous one. The corresponding LO cross section at the partonic level takes the form

$$\hat{\sigma}(gg \rightarrow H^+ W^-) = \frac{\alpha_s^2 T_F^2}{4096 \pi^3 v^4} \lambda^{3/2}(\hat{s}, M_{H^\pm}^2, M_W^2) \times \sum_{i,j} (\mathcal{R}_{i2} + i\mathcal{R}_{i3})(\mathcal{R}_{j2} - i\mathcal{R}_{j3}) \mathcal{G}_{ij}, \quad (7.21)$$

where $T_F = 1/2$ is the $SU(3)$ colour group factor and the reduced amplitudes \mathcal{G}_{ij} are given by

$$\mathcal{G}_{ij} \equiv \sum_{qq'} \frac{\operatorname{Re}(y_q^{\varphi_i^0}) \operatorname{Re}(y_{q'}^{\varphi_j^0}) \mathcal{F}(x_q) \mathcal{F}(x_{q'})^* + \operatorname{Im}(y_q^{\varphi_i^0}) \operatorname{Im}(y_{q'}^{\varphi_j^0}) \mathcal{K}(x_q) \mathcal{K}(x_{q'})^*}{(\hat{s} - M_{\varphi_i^0}^2 + iM_{\varphi_i^0} \Gamma_{\varphi_i^0}) (\hat{s} - M_{\varphi_j^0}^2 - iM_{\varphi_j^0} \Gamma_{\varphi_j^0})}, \quad (7.22)$$

with $x_q \equiv 4m_q^2/\hat{s}$. The explicit expressions of the different loop functions are:

$$\mathcal{F}(x) = \frac{x}{2} [4 + (x-1)f(x)], \quad \mathcal{K}(x) = -\frac{x}{2} f(x), \quad (7.23)$$

with

$$f(x) = \begin{cases} -4 \arcsin^2(1/\sqrt{x}), & x \geq 1 \\ \left[\ln \left(\frac{1+\sqrt{1-x}}{1-\sqrt{1-x}} \right) - i\pi \right]^2, & x < 1 \end{cases}. \quad (7.24)$$

We have regulated the propagator poles with the term $iM_{\varphi_i^0} \Gamma_{\varphi_i^0}$, both in Eqs. (7.20) and (7.22), because in our analysis one of the neutral scalars will, most likely, reach the on-shell kinematical region. NLO QCD corrections to the gluon fusion channel are also available and will be taken into account; the details are given in appendix 7.D.

7.4 Phenomenology

In the following phenomenological analysis, besides the fermiophobic charged-Higgs assumption ($\varsigma_f \rightarrow 0$), we are also going to consider that the Higgs potential is CP-conserving. The consequence of this last hypothesis is that the CP-odd neutral Higgs A will also be fermiophobic, as we have mentioned before in section 7.2; moreover $\lambda_{AH^+H^-} = 0$. This means that the decay $H^+ \rightarrow W^+ A^* \rightarrow W^+ f \bar{f}$ does not occur and A does not contribute either to $H^+ \rightarrow W^+ \gamma$. The charged-Higgs production amplitudes mediated by a virtual A also vanish. The CP-odd scalar can contribute to H^\pm production in a direct way through the $q_u \bar{q}_d \rightarrow W^* \rightarrow H^\pm A$ production channel or, in an indirect way, by modifying the total decay rate $\Gamma_{\varphi_i^0}$, which regulates the pole in the CP-even scalar propagators ($\varphi_i^0 = h, H$), through decays like $\varphi_i^0 \rightarrow AA$ or $\varphi_i^0 \rightarrow AZ$. The decay $H \rightarrow Ah$ cannot occur at tree level because all cubic vertices of the scalar potential involving an odd number of A fields vanish in the CP-conserving limit. The total decay width $\Gamma_{\varphi_i^0}$ is the sum of all the decay rates explicitly presented in appendix 7.B.

In our particular case, the expressions for the Yukawa couplings simplify and become equal to the reduced scalar couplings to two gauge bosons. They are given by

$$y_f^h = \frac{g_{hVV}}{g_{hVV}^{\text{SM}}} = \mathcal{R}_{11} = \cos \tilde{\alpha}, \quad y_f^H = \frac{g_{HVV}}{g_{hVV}^{\text{SM}}} = \mathcal{R}_{21} = -\sin \tilde{\alpha}, \quad (7.25)$$

$$y_f^A = g_{AVV} = \mathcal{R}_{31} = 0. \quad (7.26)$$

Even within the restricted range of charged-Higgs masses we are interested in, $M_{H^\pm} \in [M_W, M_W + M_Z]$, the possible phenomenological signals depend on the choice of masses for the remaining scalars. In the following subsections, we will therefore consider different scenarios for the scalar spectrum. The first part of the analysis will be dedicated to the study of the various decay modes of the charged Higgs and the second part will focus on estimating the production cross sections.

7.4.1 Decay rates and branching ratios

One of the two CP-even scalars should correspond to the Higgs boson discovered at the LHC, but a broad range of masses is allowed for the other two neutral scalars. We will consider the following four scenarios, which cover the different possibilities:

1. $M_h = 125 \text{ GeV}$ and $M_{A,H} > M_W + M_Z$.
2. $M_h = 125 \text{ GeV}$ and $M_A < M_W + M_Z < M_H$.
3. $M_h = 125 \text{ GeV} < M_H < M_W + M_Z$ and three different options for A ($M_A < M_H$, $M_H < M_A < M_W + M_Z$ and $M_A > M_W + M_Z$).
4. $M_H = 125 \text{ GeV}$, $M_h = 90 \text{ GeV}$ and $M_A < M_W + M_Z$.

7.4.1.1 First Scenario

In the first scenario the mass of the lightest CP-even scalar is set to $M_h = 125 \text{ GeV}$. Therefore, the strong constraint on the scalar mixing angle, from the global fit to the light Higgs boson signal strengths using the LHC data, must be used: $|\cos \tilde{\alpha}| > 0.9$ at 68% CL [12–14]. The masses of the remaining neutral scalars are considered to be greater than $M_W + M_Z$ so that decays of a charged Higgs into an on-shell H or A are kinematically forbidden. In the limit $\cos \tilde{\alpha} \rightarrow 1$, the only surviving decay amplitude (not proportional to $\sin \tilde{\alpha}$) is the contribution of

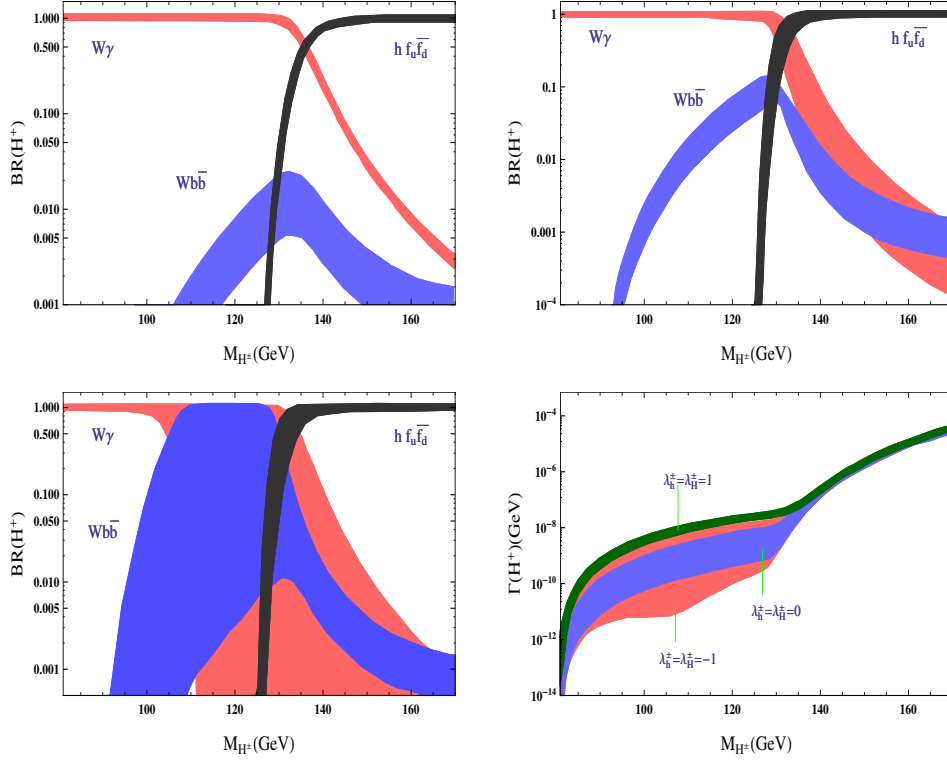


Figure 7.4: Charged-Higgs branching ratios as functions of $M_{H^\pm} \in [M_W, M_W + M_Z]$, for $\cos \tilde{\alpha} = 0.9$, $M_H \in [M_W + M_Z, 500 \text{ GeV}]$ and $\lambda_{hH^+H^-} = \lambda_{HH^+H^-} = 1$ (top-left), 0 (top-right) and -1 (bottom-left). The corresponding total decay widths are shown in the bottom-right panel ($\lambda_h^\pm \equiv \lambda_{hH^+H^-}$, $\lambda_H^\pm \equiv \lambda_{HH^+H^-}$).

H to the amplitude $S_{(2)}$. Thus, in this limit the branching ratio of $H^+ \rightarrow W^+\gamma$ is 100%; all the other decay channels vanish.

If we set $\cos \tilde{\alpha} = 0.9$, $\lambda_{hH^+H^-} = \lambda_{HH^+H^-} = 1$, vary the charged Higgs mass in the region $M_{H^\pm} \in [M_W, M_W + M_Z]$ and M_H from $M_W + M_Z$ up to 500 GeV, we obtain the branching ratios (top-left) and total decay width (bottom-right) shown in Fig. 7.4. The width of the branching ratio bands reflects the variation of the input parameters in the mentioned ranges. The same consideration is valid for the following scenarios. The decay channel $H^+ \rightarrow W^+\gamma$ dominates for $M_{H^\pm} \lesssim M_h$. When the charged Higgs is kinematically allowed to decay into an on-shell h , then $H^+ \rightarrow h f_u \bar{f}_d$ rapidly becomes the dominant channel as M_{H^\pm} grows. The remaining $H^+ \rightarrow W^+ b \bar{b}$ branching ratio stays at a few percent level or less for

the whole allowed region. The total decay width approximately grows from 10^{-14} up to 10^{-8} GeV, in the region dominated by the radiative $H^+ \rightarrow W^+\gamma$ decay, and sizeably increases up to 10^{-5} GeV, once the $hf_u\bar{f}_d$ production threshold is reached. The tree-level decay rates are significantly larger than the loop-induced one. Flipping the sign of $\cos\tilde{\alpha}$ leads to an equivalent solution with a sign flip of the coupling $\lambda_{hH^+H^-}$. This is also valid for the next scenarios.

If, instead, we consider all the previous settings but taking this time $\lambda_{hH^+H^-} = \lambda_{HH^+H^-} = 0$, then the only amplitude that contributes to the $H^+ \rightarrow W^+\gamma$ decay channel is $S_{(3)}$, which is suppressed by a factor $\sin\tilde{\alpha}$. As shown in Fig. 7.4 (top-right), this channel remains the dominant one up to $M_{H^\pm} \gtrsim M_h$, but with a sizeably smaller decay width (bottom-right). The $H^+ \rightarrow W^+b\bar{b}$ branching ratio is also more sizeable, raising up to the 10% level.

Let us now consider $\lambda_{hH^+H^-} = \lambda_{HH^+H^-} = -1$ and everything else as previously. In this particular case the amplitudes $S_{(2)}$ and $S_{(3)}$ interfere destructively and, as a consequence, the decay $H^+ \rightarrow W^+b\bar{b}$ competes with $H^+ \rightarrow W^+\gamma$. Thus, the $Wb\bar{b}$ decay channel can dominate in some cases. However, as soon as the charged Higgs reaches $M_{H^\pm} \gtrsim M_h$, the dominant decay mode is again $H^+ \rightarrow hf_u\bar{f}_d$, as in the previous cases (Fig. 7.4, bottom-left).

7.4.1.2 Second Scenario

In the second scenario the mass of lightest CP-even scalar is set to $M_h = 125$ GeV and $M_H > M_W + M_Z$, as in the first one, but this time we assume the CP-odd Higgs boson A to have its mass below the WZ threshold ($M_A < M_W + M_Z$). The decay of the charged Higgs into an on-shell A is then kinematically allowed, but into an on-shell H is forbidden. The same constraint as before is considered for the scalar mixing angle. Taking the limit $\cos\tilde{\alpha} \rightarrow 1$, this time there are two surviving decay amplitudes, $H^+ \rightarrow W^+\gamma$ and $H^+ \rightarrow Af_u\bar{f}_d$.

Let us consider $\cos\tilde{\alpha} = 0.9$, $\lambda_{hH^+H^-} = \lambda_{HH^+H^-} = 1$ and $M_A = 90, 130$ and 150 GeV. For each value we shall vary M_H from $M_W + M_Z$ up to its allowed upper bound from the oblique parameters (at 68% CL) [12–14], with a maximum limit of 500 GeV. We obtain then the branching ratios and total decay widths in Fig. 7.5. We observe that for $M_A = 90$ GeV (top-left), when kinematically allowed, the decay to an on-shell A boson rapidly becomes the dominant one as M_{H^\pm} increases. For this configuration the $Wb\bar{b}$ channel is insignificant. When $M_A = 130$ GeV (top-right), which is close to M_h , the decays into an on-shell h or A boson compete. However, the decay to $Af_u\bar{f}_d$ still dominates even if the masses are similar because of the relative suppression factor $\sin^2\tilde{\alpha}$ of the $hf_u\bar{f}_d$ width. As M_A becomes heavier, $M_A = 150$ GeV (bottom-left), the decay rate into an

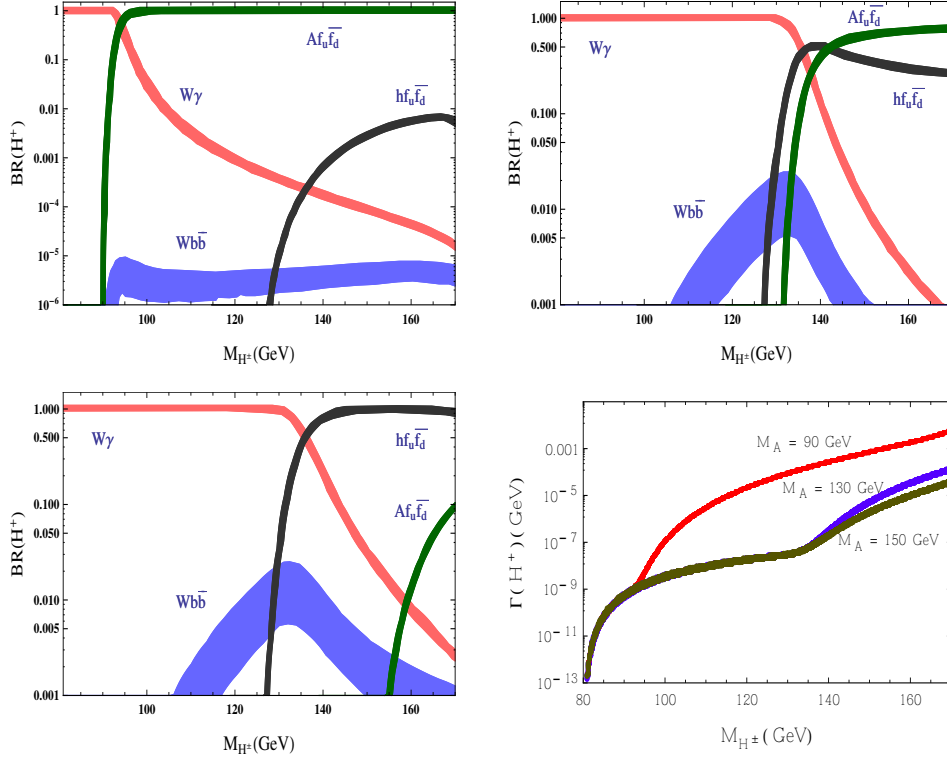


Figure 7.5: Charged-Higgs branching ratios as functions of M_{H^\pm} , for $\lambda_{hH^+H^-} = \lambda_{HH^+H^-} = 1$, $\cos \tilde{\alpha} = 0.9$ and $M_A = 90$ (top-left), 130 (top-right) and 150 (bottom-left) GeV. M_H is varied from $M_W + M_Z$ up to its permitted value by the oblique parameters. The bottom-right panel shows the corresponding total decay widths.

on-shell A boson does not grow as rapidly as in the previous cases; thus, $hf_u\bar{f}_d$ dominates over $Af_u\bar{f}_d$ in the considered region. For the last two configurations, that is $M_A = 130$ and 150 GeV, the $H^+ \rightarrow W^+b\bar{b}$ decay channel can also bring sizeable contributions.

The total decay width in this scenario can reach as high as 10^{-3} GeV, see Fig. 7.5 (bottom-right). This is approximately two orders of magnitude larger than in the previous case and it is due to the tree-level decays, as we mentioned earlier. The maximum values are reached for the smallest mass of the CP-odd scalar ($M_A = 90$ GeV).

It is worth mentioning that, just as in the previous scenario, the $Wb\bar{b}$ branching ratio can be sizeably increased by decreasing the $W\gamma$ decay width through a sign flip of the $\lambda_{\varphi_i^0 H^+ H^-}$ couplings, creating destructive interference among the various loop contributions. The same consideration is also valid for the next scenario.

7.4.1.3 Third Scenario

In this scenario the mass of the lightest CP-even scalar is also set to $M_h = 125$ GeV, while the heavy CP-even Higgs boson H has its mass in the range $M_h < M_H < M_W + M_Z$. For the mass of the remaining CP-odd scalar we consider three different possibilities: a) $M_A > M_W + M_Z$, so that the decay into an on-shell A is forbidden; b) $M_H < M_A < M_W + M_Z$, and c) $M_A < M_H < M_W + M_Z$. In the last two situations the H^\pm boson could decay into any of the three neutral scalars. Again, we use the LHC constraint $|\cos \tilde{\alpha}| > 0.9$ at 68% CL. In the limit $\cos \tilde{\alpha} \rightarrow 1$, there are three possible surviving decay channels: $H^+ \rightarrow W^+ \gamma$, $H^+ \rightarrow H f_u \bar{f}_d$ and, when kinematically allowed, $H^+ \rightarrow A f_u \bar{f}_d$.

For all three cases we set $\lambda_{hH^+H^-} = \lambda_{HH^+H^-} = 1$ and vary $\cos \tilde{\alpha} \in [0.9, 0.99]$. In Fig. 7.6 we show the H^\pm branching ratios (top-left) and total decay width (bottom-right) when $M_H = 140$ GeV and $M_A > M_W + M_Z$ (first case). To illustrate the other two possibilities, we set $(M_H, M_A) = (140, 150)$ GeV (Fig. 7.6, top-right) and $(M_H, M_A) = (150, 140)$ GeV (Fig. 7.6, bottom-left). The total H^\pm decay widths for these two last configurations are very similar to the first one.

The H^\pm decay into an on-shell h boson has a global relative suppression factor of $\tan^2 \tilde{\alpha}$ with respect to the decay into an on-shell H and $\sin^2 \tilde{\alpha}$ with respect to the decay into an on-shell A . Therefore, when $h f_u \bar{f}_d$ competes with $H f_u \bar{f}_d$, the later one dominates as $\cos \tilde{\alpha} \rightarrow 0.99$ (Fig. 7.6, upper-left). When all three channels compete, the decay rate into the heaviest scalar boson grows the slowest and, therefore, brings a sub-dominant contribution to the branching ratios.

7.4.1.4 Fourth Scenario

In this last scenario we are going to set the mass of the heavy CP-even scalar to $M_H = 125$ GeV; therefore, the LHC bounds translate into $|\sin \tilde{\alpha}| > 0.9$ at 68% CL. The mass of the light CP-even scalar will be set to $M_h = 90$ GeV. As for the CP-odd one, we will consider three possible values: $M_A = 150, 140$ and 110 GeV.

In order to safely avoid the stringent constraints on light scalar masses from LEP [67, 68], we need to have very suppressed decay and production channels. In our particular case with $\zeta_f = 0$, CP-conserving potential, and $M_A > M_h$

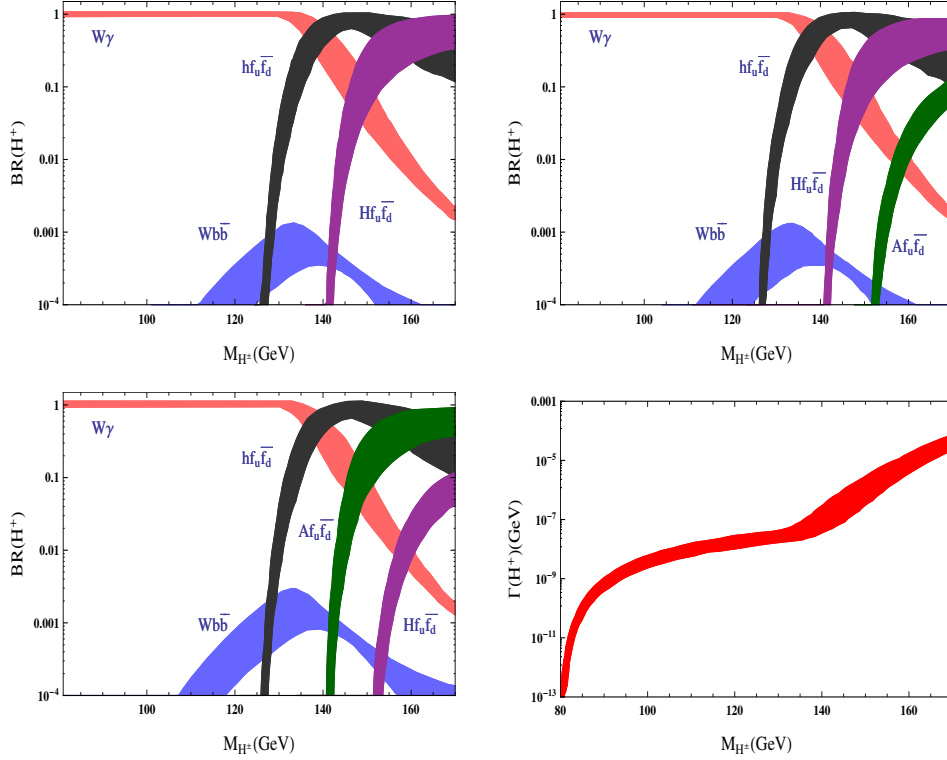


Figure 7.6: Charged-Higgs branching ratios as functions of M_{H^\pm} , for $\lambda_{hH^+H^-} = \lambda_{HH^+H^-} = 1$, $\cos \tilde{\alpha} \in [0.9, 0.99]$, $M_H = 140$ GeV, $M_A > M_W + M_Z$ (top-left); $(M_H, M_A) = (140, 150)$ GeV (top-right) and $(M_H, M_A) = (150, 140)$ GeV (bottom-left). The total decay width for the first case is also shown (bottom-right).

(therefore the decays $h \rightarrow AA$ and $h \rightarrow AZ$ are forbidden), we have the simple relation $\Gamma_h = \cos^2 \tilde{\alpha} \Gamma_h^{\text{SM}}$. Here Γ_h is the total decay rate of the light CP-even scalar boson with $M_h < M_H = 125$ GeV, and Γ_h^{SM} the corresponding decay rate in the SM for a Higgs boson with the same mass M_h . The $\cos^2 \tilde{\alpha}$ suppression factor is common to all allowed $h \rightarrow f\bar{f}$ decay modes, and cancels out in the branching ratios. The same suppression factor appears in the LEP production rate, so that the signal strengths, relative to the SM, are then given by

$$\mu_X^h \equiv \frac{\sigma(e^+e^- \rightarrow Zh) \text{Br}(h \rightarrow X)}{\sigma(e^+e^- \rightarrow Zh)_{\text{SM}} \text{Br}(h \rightarrow X)_{\text{SM}}} = \cos^2 \tilde{\alpha}, \quad (7.27)$$

with $X = b\bar{b}$ and $\tau^+\tau^-$. Thus, we have a global suppression factor $\cos^2 \tilde{\alpha}$. The LEP constraints from the $\tau^+\tau^-$ channel, which are the strongest ones in our case, can then be avoided by setting $\cos^2 \tilde{\alpha} \approx 0.02$ ($\sin \tilde{\alpha} \approx 0.99$). The OPAL collaboration has also performed a decay-mode-independent search for a light neutral scalar and found the upper limits $\cos^2 \tilde{\alpha} < 0.1$ (1) for $M_h < 19$ (81) GeV [67], which are weaker (in our case).

It is worth mentioning that in (7.27) we have ignored the charged-Higgs contribution to the $h \rightarrow \gamma\gamma$ decay rate. If however, we choose to enhance it through the H^\pm loop contribution, it would only further suppress the fermionic branching ratios, weakening the bound on $\sin \tilde{\alpha}$.

With all this being said, we set $\sin \tilde{\alpha} = 0.99$. In Fig. 7.7 we plot the H^\pm branching ratios for $M_A = 150$ (top-left) and 140 GeV (top-right), taking $\lambda_{hH^+H^-} = \lambda_{HH^+H^-}$. In both plots we can observe that, when kinematically allowed, the tree-level $H^+ \rightarrow hf_u\bar{f}_d$ decay dominates. In this case, this decay no longer has a suppression factor as its partial width is proportional to $\sin^2 \tilde{\alpha} \sim 1$. The suppression factor appears now in the $Hf_u\bar{f}_d$ decay mode with a partial decay width proportional to $\cos^2 \tilde{\alpha}$. This is why, when $M_A \sim M_H$, the decay into an on-shell A boson dominates over the decay into an on-shell H . Both A and H contributions are, however, very suppressed due to their heavy masses. It is also worth mentioning that a small variation of M_A can produce a significant change (roughly, one order of magnitude) in $\text{Br}(H^+ \rightarrow Af_u\bar{f}_d)$, as can be seen in Fig. 7.7 (top-left and top-right).

For the last case we set M_A to 110 GeV. The perturbativity bounds on neutral scalar couplings to a pair of charged Higgses, for the considered region of the charged Higgs mass, are roughly given by $|\lambda_{\varphi_i^0 H^+ H^-}| \leq 5$ (here $\varphi_i^0 = h, H$) [14]. In order to see the impact of these two parameters on the H^\pm branching ratios, we will vary both independently in this region. The result, shown in Fig. 7.7 (bottom-left), is that $W\gamma$ and $hf_u\bar{f}_d$ compete, even after crossing the h production threshold. Since M_A is lighter than in the previous two cases, the $H^+ \rightarrow Af_u\bar{f}_d$ branching ratio can also reach higher values. The total decay rate for this configuration is also shown in Fig. 7.7 (bottom-right).

As we have seen, in the four proposed scenarios, the configuration of the H^\pm branching ratios depends very sensitively on the chosen parameters. However, we can draw some important conclusions. There are only a few decay channels to be analysed and the largest decay widths are the tree-level ones, corresponding to the on-shell production of scalar bosons. Thus, the number of decay channels decreases as the number of neutral scalar bosons that are heavier than the charged Higgs (*i.e.*, $M_{\varphi_i^0} > M_{H^\pm}$) increases. The $W\gamma$ decay mode can bring sizeable

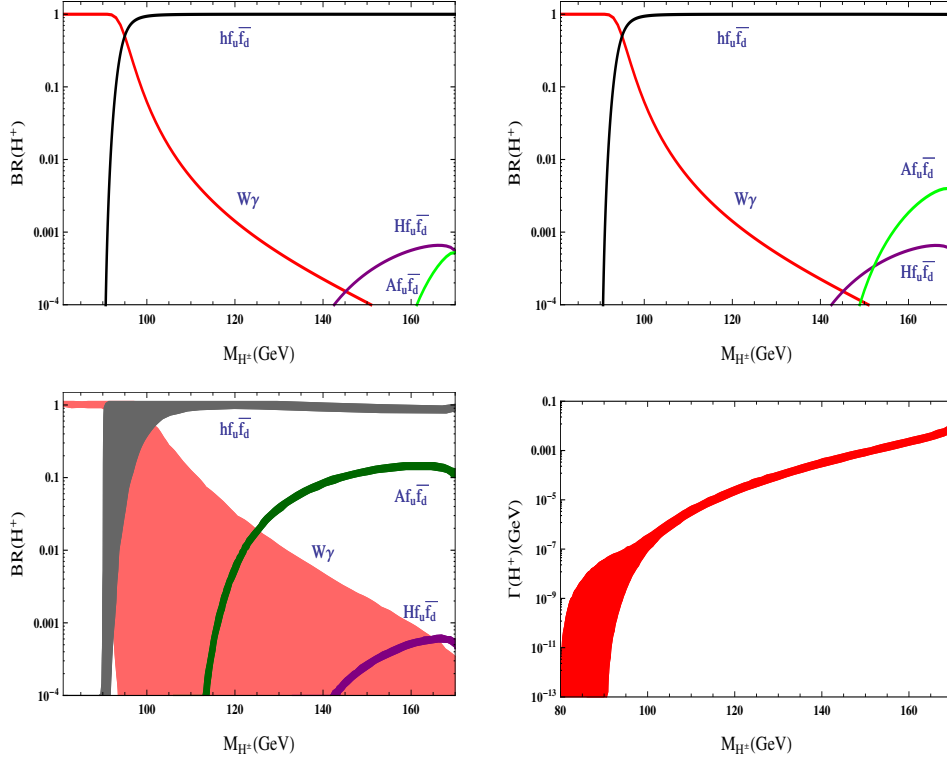


Figure 7.7: Charged-Higgs branching ratios as functions of M_{H^\pm} , for $\sin \tilde{\alpha} = 0.99$ and $M_h = 90$ GeV. The trilinear couplings are set to $\lambda_{hH^+H^-} = \lambda_{HH^+H^-} = 1$, with $M_A = 150$ GeV (top-left) and $M_A = 140$ GeV (top-right), and $\lambda_{hH^+H^-}, \lambda_{HH^+H^-} \in [-5, 5]$ with $M_A = 110$ GeV (bottom-left). The total decay width (bottom-right) for the last case is also shown.

contributions below and close to the on-shell production threshold of a scalar boson. Short after this threshold is reached, as M_{H^\pm} grows, the $H^+ \rightarrow W^+\gamma$ branching ratio rapidly decreases. As we have shown, the $H^+ \rightarrow W^+b\bar{b}$ decay can dominate over $H^+ \rightarrow W^+\gamma$ in some cases, depending on the values of the $\lambda_{\varphi_i^0 H^+ H^-}$ couplings. If a fermiophobic charged Higgs is finally discovered in this mass range, the precise values of its mass and branching ratios would provide priceless information about all other parameters. The masses of the remaining scalars would also be highly constrained by the electroweak oblique parameters. These constraints were used in our second scenario, because they put an upper bound on M_H ; we did not mention them in the other cases, since they do not bring

additional constraints. The mean lifetime of a fermiophobic charged scalar is short, ranging from 10^{-11} to 10^{-23} s, making its direct detection very compelling at the LHC.

7.4.2 Production cross sections

In order to estimate the total hadronic cross sections for the various production channels, we need to convolute the partonic cross sections with the corresponding parton distribution functions (PDFs). Here we will use the MSTW set [69]. Moreover, we will compute the cross sections at the NLO; *i.e.*, including the LO QCD corrections, for which simple analytical expressions can be obtained [70, 71]. For the $q_u\bar{q}_d \rightarrow H^+\varphi_i^0$ associated production, the $\mathcal{O}(\alpha_s)$ contributions simply correspond to the QCD corrections to the Drell-Yan process $q_u\bar{q}_d \rightarrow W^*$, integrating over the virtuality of the W boson. As for the H^+W^- associated production, the needed QCD corrections can be easily extracted from the SM Higgs production channels $q\bar{q} \rightarrow h$ and $gg \rightarrow h$. At the LHC, $gg \rightarrow H^+W^-$ production dominates over $q\bar{q} \rightarrow H^+W^-$. For typical LHC hadronic center-of-mass energies, *i.e.*, $\sqrt{s} \sim 14$ TeV, the latter only corresponds at LO to a few percent of the total $pp \rightarrow H^+W^-$ cross section, so we can safely neglect it. The detailed expressions of the hadronic cross sections and the QCD corrections are given in appendices 7.C and 7.D. In order to estimate the theoretical uncertainty of the QCD enhancement factor $K \equiv \sigma_{NLO}/\sigma_{LO}$, we vary the factorization (μ_F) and renormalization (μ_R) scales for σ_{NLO} , keeping both scales fixed at their central value $\mu_F = \mu_R = \hat{s}$ for σ_{LO} .

When one of the intermediate scalar bosons reaches its on-shell kinematical region, one needs to estimate also its total decay rate. The explicit expressions for the tree-level scalar decay rates are presented in appendix 7.B.

7.4.2.1 $H^+\varphi_i^0$ associated production

Assuming the most general scalar potential, the LO partonic cross section, given in Eq. (7.18), is proportional to the combination of rotation matrix elements $R^2 \equiv (\mathcal{R}_{i2}^2 + \mathcal{R}_{i3}^2)$. We take away the explicit dependence on the scalar-potential parameters, plotting in Fig. 7.8 (left) the ratio $\sigma(pp \rightarrow H^+\varphi_i^0)/R^2$ at $\sqrt{s} = 14$ TeV, as a function of M_{H^\pm} , for different values of $M_{\varphi_i^0}$ which can be interpreted as the mass of any of the three neutral scalars of the theory.

As expected, the cross section reaches higher values for lower scalar masses. The most interesting case is of course $M_{\varphi_i^0} = 125$ GeV, which could constitute a very good detection channel, since we already know that there is one scalar with

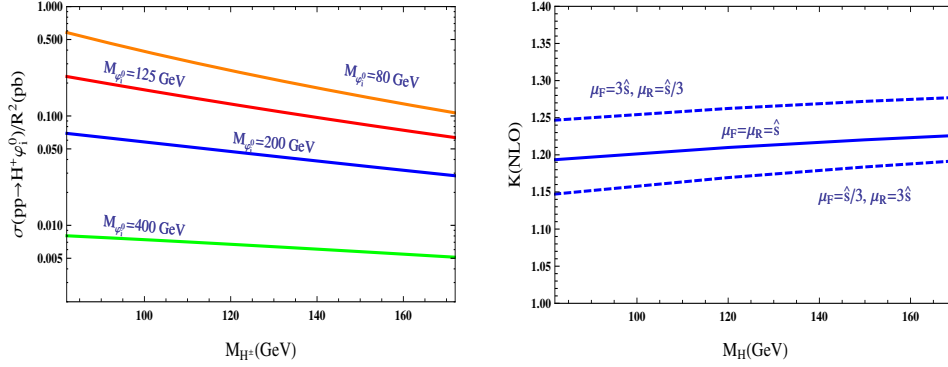


Figure 7.8: LO production cross section $\sigma(pp \rightarrow H^+ \varphi_i^0)/R^2$ at $\sqrt{s} = 14$ TeV (left), as function of M_{H^\pm} , for different values of $M_{\varphi_i^0}$. The QCD K factor is shown (right) for $M_{\varphi_i^0} = 125$ GeV and different choices of μ_R and μ_F

that mass. If we consider φ_i^0 to be the light CP-even scalar of the theory, the cross section is suppressed by a factor $R^2 = \sin^2 \tilde{\alpha}$. The measurement of this production channel can be experimentally challenging due to the small value of the cross section.

QCD corrections provide a mild enhancement of the cross section. The resulting QCD K factor is shown in Fig. 7.8 (right), for $M_{\varphi_i^0} = 125$ GeV and different choices of μ_R and μ_F . Its central value is around 1.2, similarly to other cross sections of the Drell-Yan type.

7.4.2.2 H^+W^- associated production

For this specific production channel we are going to consider two alternative possibilities: we can either identify the 125 GeV boson with the lightest CP-even scalar h , or with the heaviest one H . In the first case ($M_h = 125$ GeV), the scalar H can be heavy enough to reach the on-shell region and, therefore, it is necessary to regulate the propagator pole with its total decay width. In the second case ($M_H = 125$ GeV), both M_h and M_H are below the H^+W^- production threshold for the whole considered range of charged Higgs masses. Therefore, there is no need to regulate the h and H poles (assuming their total decay widths to be small).

A) $M_h = 125$ GeV.

Let us first estimate the size of the H decay width for three representative values of M_H (150, 200 and 400 GeV) and different choices for the cubic scalar couplings. The CP-odd mass M_A will always be taken within the 68% CL range allowed by the oblique parameters. In the following discussion, we set $\cos \tilde{\alpha} = 0.9$ and ignore the loop-induced decays $H \rightarrow gg$ and $H \rightarrow \gamma\gamma$, which are suppressed by a $\sin^2 \tilde{\alpha}$ factor with respect to the SM.

For $M_H = 150$ GeV, the H boson does not reach the on-shell region (its mass is below the H^+W^- threshold) and its total decay width is in principle not needed to regulate the propagator pole. However, Γ_H can induce sizeable effects for small M_A and large values of the cubic coupling λ_{HAA} . This is shown in Fig. 7.9 (upper-left). When $M_A > M_H/2$, the H width is small because its only relevant tree-level decays are $H \rightarrow b\bar{b}$, WW and ZZ . However, extra decay channels like $H \rightarrow AA$ or $H \rightarrow AZ$ are open when one allows A to be light. This possibility is exemplified in the figure, taking $M_A = 50$ GeV and $\lambda_{HAA} = 0$ (therefore $H \rightarrow AZ$ is the only extra channel), and also for $|\lambda_{HAA}| = 0.1, 1$ and 5. The width Γ_H varies roughly from around 10^{-3} up to 100 GeV for the considered parameter configurations.

Let us now consider $M_H = 200$ GeV. If the CP-odd boson satisfies $M_A > M_H - M_Z \approx 110$ GeV, then the channels $H \rightarrow AA, AZ$ are closed. The open decay channels are $H \rightarrow b\bar{b}, WW, ZZ$ as before, plus two extra ones: $H \rightarrow H^\pm W^\mp$ (up to $M_{H^\pm} \approx 120$ GeV) and $H \rightarrow H^+H^-$ (up to $M_{H^\pm} = 100$ GeV). When kinematically allowed (and if $|\lambda_{HH^+H^-}|$ is not too small), the decay into two charged scalars is the dominating channel. There is also a sizeable contribution from $H \rightarrow H^\pm W^\mp$ when this decay mode is open. The predicted values of Γ_H are shown in Fig. 7.9 (upper-right) for different values of $|\lambda_{HH^+H^-}|$. If we take instead $M_A = 50$ GeV, the channels $H \rightarrow AA, AZ$ open. The H decay width is shown for this configuration in Fig. 7.9 (lower-left), as a function of the charged Higgs mass, taking $|\lambda_{HAA}| = 0, 5$ and $|\lambda_{HH^+H^-}| = 0, 5$. The total H decay width obviously increases with increasing values of $|\lambda_{HAA}|$ and $|\lambda_{HH^+H^-}|$. In the considered range of cubic couplings, Γ_H can vary between 1 and 200 (70) GeV when $H \rightarrow H^+H^-$ is allowed (forbidden, $M_{H^\pm} > M_H/2$).

Taking a heavier mass $M_H = 400$ GeV, the electroweak oblique parameters imply very stringent restrictions on M_A : the only value that roughly satisfies these constraints for the whole considered range of the charged Higgs mass is $M_A = 140$ GeV. For this configuration, all the channels we have considered before are kinematically allowed. Besides, there is an extra one, the decay into two light CP-even scalars $H \rightarrow hh$. Thus, we have three unknown couplings $\lambda_{HAA}, \lambda_{Hhh},$

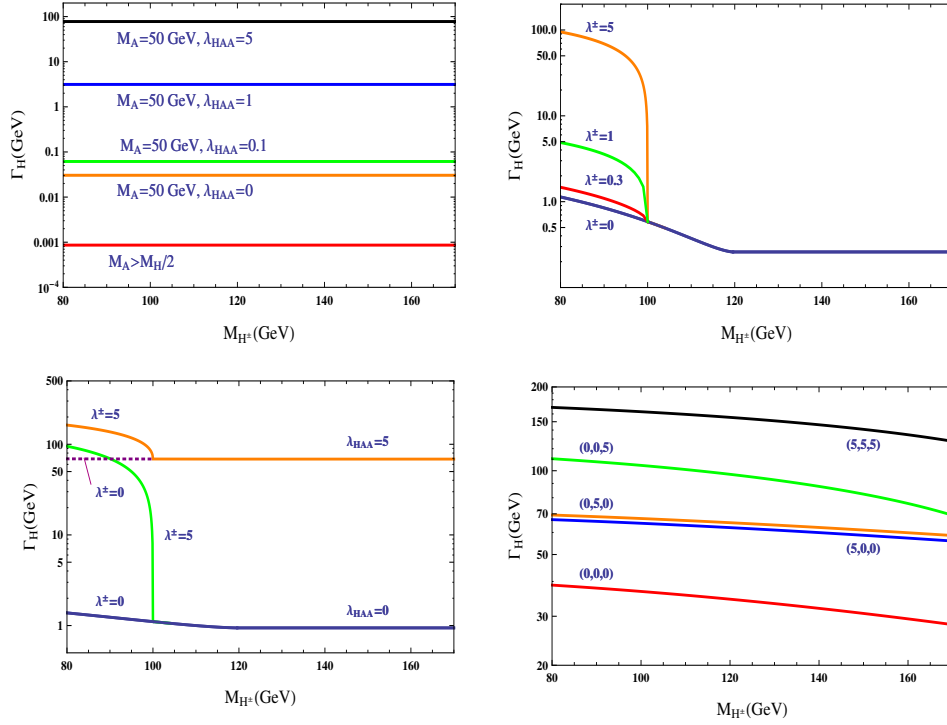


Figure 7.9: Total H decay rate as a function of M_{H^\pm} for a) $M_H = 150$ GeV with different values of M_A and $|\lambda_{HAA}|$ (top-left), b) $M_H = 200$ GeV and $M_A > M_H - M_Z$ with different values of $\lambda^\pm \equiv |\lambda_{HH+H-}|$ (top-right), c) $M_H = 200$ GeV and $M_A = 50$ GeV with different values of $|\lambda_{HH+H-}|$ and $|\lambda_{HAA}|$ (bottom-left), and d) $M_H = 400$ GeV and $M_A = 140$ GeV with different values for the set of couplings $(|\lambda_{HAA}|, |\lambda_{Hhh}|, |\lambda_{HH+H-}|)$ (bottom-right).

and λ_{HH+H-} . The lower-right panel in Fig. 7.9 shows the resulting values of Γ_H , taking $(|\lambda_{HAA}|, |\lambda_{Hhh}|, |\lambda_{HH+H-}|) = (0, 0, 0), (5, 0, 0), (0, 5, 0), (0, 0, 5),$ and $(5, 5, 5)$. The total H decay rate grows from around 30 GeV when the three cubic scalar couplings are zero, up to approximately 150 GeV when their values are $(5, 5, 5)$.

Fig. 7.10 (left) shows the predicted LO production cross sections at $\sqrt{s} = 14$ TeV, for representative values of M_H and Γ_H , which cover the range of possibilities we have just discussed: $(M_H, \Gamma_H) = (150, 10^{-3}), (150, 50), (200, 1), (200, 80), (400, 30),$ and $(400, 150)$ GeV. The cross section is very small when both CP-even scalars are off-shell. For $M_H = 150$ GeV, $\sigma(pp \rightarrow H^+W^-)$ is roughly smaller

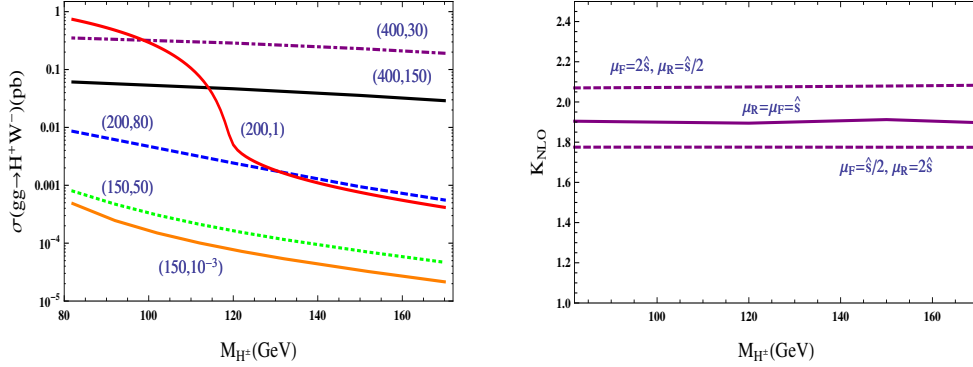


Figure 7.10: LO production cross section $\sigma(pp \rightarrow H^\pm W^\mp)$ at $\sqrt{s} = 14$ TeV (left), as a function of M_{H^\pm} , for $M_h = 125$ GeV, $\cos \tilde{\alpha} = 0.9$ and different values for the pair (M_H, Γ_H) in GeV. The QCD K factor is shown (right) for $(M_H, \Gamma_H) = (400, 30)$ GeV and different choices of μ_R and μ_F .

than 10^{-3} pb. With $M_H = 200$ GeV and a large decay width $\Gamma_H = 80$ GeV, the cross section stays below 10^{-2} pb; however, with a smaller width $\Gamma_H = 1$ GeV, the cross section is enhanced by approximately two orders of magnitude (three orders of magnitude with respect to the previous cases), in the region where M_H is on-shell ($M_{H^\pm} \lesssim 120$ GeV).

The most interesting case is when $M_H = 400$ GeV, because the cross section gets enhanced by the on-shell H pole, reaching higher values around 0.1 pb. The QCD K factor for this H mass and $\Gamma_H = 30$ GeV is given in Fig. 7.10 (right), and it is practically constant in the whole range of M_{H^\pm} ; it approximately corresponds to the K factor for the production of a SM Higgs with a 400 GeV mass. Its central value is around 1.9. A very similar K factor is obtained for $\Gamma_H = 150$ GeV, although with a smaller cross section.

Thus, a heavy H boson would be the most favourable situation from the experimental point of view, with production cross sections between 10^{-2} and 1 pb at $\sqrt{s} = 14$ TeV, depending on the value of Γ_H , which are potentially measurable at the LHC. As we have seen, they are increased by a factor of ≈ 2 by the NLO QCD corrections. For the other configurations both CP-even scalars are off-shell and the value of the cross section decreases by a few orders of magnitude, which results pretty challenging for the LHC, if not impossible. Nonetheless, these small values could turn out to be measurable in the future if the LHC luminosity is increased by a factor of 10, as planned for its High-Luminosity option.

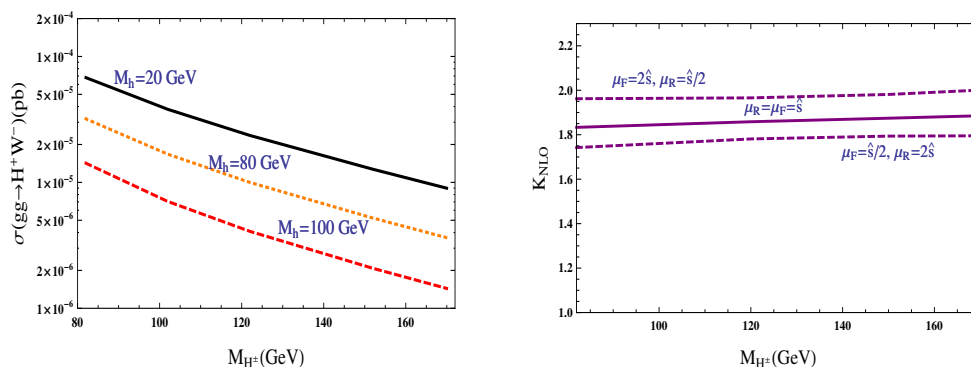


Figure 7.11: LO production cross section $\sigma(pp \rightarrow H^+ W^-)$ at $\sqrt{s} = 14$ TeV (left), as a function of M_{H^\pm} , for $M_H = 125$ GeV, $\sin \tilde{\alpha} = 0.99$ and $M_h = 20, 80, 100$ GeV. The NLO QCD K factor (right) is shown for $M_h = 20$ GeV and different choices of μ_R and μ_F .

B) $M_H = 125$ GeV.

In this case both CP-even neutral scalars are off-shell and their decay widths can be neglected (assuming they are small). The scalar mixing angle must be small enough to avoid the LEP constraints, thus we take $\sin \tilde{\alpha} = 0.99$, as we have done before in the analysis of branching ratios. The mass of the light scalar will be set to $M_h = 20, 80$ and 100 GeV. The predicted LO production cross sections at $\sqrt{s} = 14$ TeV are shown in Fig. 7.11 (left). For the chosen values of M_h , they range in between 10^{-5} and 10^{-6} pb. These values are extremely small and lay below the experimental sensitivity attainable in the near future. This scenario is thus, the most challenging experimentally. The computed K factor, Fig 7.11 (right), has a similar value to the one obtained in the previous scenario.

7.5 Conclusions

The recent discovery of a Higgs-like boson has confirmed the existence of a scalar sector, which so far seems compatible with the SM predictions. As it is widely known, an enlarged scalar sector is not forbidden by the symmetries of the electroweak theory, and there exists a broad range of possibilities satisfying all experimental constraints. The direct discovery of another scalar particle would represent a major break-through in particle physics, opening a window into a new high-energy dynamics and providing priceless information on which type of

extension, amongst many theoretical models of the scalar sector, is preferred by Nature.

Here we have focused on a particular 2HDM scenario, characterized by a fermiophobic charged Higgs, which would have evaded all experimental searches performed until now. It is a quite predictive case, since all Yukawa couplings are determined by the mixing among the neutral scalars. We have assumed a CP-conserving scalar potential and have restricted our analysis to the range $M_{H^\pm} \in [M_W, M_W + M_Z]$, so that only a few decay modes are kinematically open. We have presented detailed formulae for the loop-induced decay $H^+ \rightarrow W^+ \gamma$, which becomes very relevant in this mass region, and for the tree-level three-body decays of the charged scalar. We have analyzed the parameter space of the model, in order to characterize the possible values of the H^\pm decay width and branching ratios, taking into account the constraints from LHC, LEP and flavour data.

The two most important production channels for a fermiophobic charged scalar have been investigated, including NLO QCD corrections: the associated production with either a neutral scalar or a charged W ; *i.e.*, $q_u \bar{q}_d \rightarrow H^+ \varphi_i^0$ and $gg \rightarrow H^+ W^-$. The predicted cross sections are small in most of the parameter space, making the experimental search challenging, but they become very sizeable ($\geq 10^{-3}$ pb) for large values of the mass of the heavy neutral scalar H . In some extreme cases, cross sections between 0.1 and 1 pb are obtained. Thus, the detection of a fermiophobic H^\pm at the LHC seems plausible in the near future. The interesting features of this possible scenario should encourage specific experimental searches for such a particle in the LHC data.

7.A Scalar Potential

In the Higgs basis, the most general scalar potential takes the form

$$\begin{aligned}
 V = & \mu_1 \Phi_1^\dagger \Phi_1 + \mu_2 \Phi_2^\dagger \Phi_2 + \left[\mu_3 \Phi_1^\dagger \Phi_2 + \mu_3^* \Phi_2^\dagger \Phi_1 \right] + \lambda_1 \left(\Phi_1^\dagger \Phi_1 \right)^2 \\
 & + \lambda_2 \left(\Phi_2^\dagger \Phi_2 \right)^2 + \lambda_3 \left(\Phi_1^\dagger \Phi_1 \right) \left(\Phi_2^\dagger \Phi_2 \right) + \lambda_4 \left(\Phi_1^\dagger \Phi_2 \right) \left(\Phi_2^\dagger \Phi_1 \right) \\
 & + \left[\left(\lambda_5 \Phi_1^\dagger \Phi_2 + \lambda_6 \Phi_1^\dagger \Phi_1 + \lambda_7 \Phi_2^\dagger \Phi_2 \right) \left(\Phi_1^\dagger \Phi_2 \right) + \text{h.c.} \right]. \quad (7.28)
 \end{aligned}$$

The hermiticity of the potential requires all parameters to be real except μ_3 , λ_5 , λ_6 and λ_7 ; thus, there are 14 real parameters. The minimization conditions

$\langle 0|\Phi_1^T(x)|0\rangle = \frac{1}{\sqrt{2}}(0, v)$ and $\langle 0|\Phi_2^T(x)|0\rangle = \frac{1}{\sqrt{2}}(0, 0)$ impose the relations

$$\mu_1 = -\lambda_1 v^2, \quad \mu_3 = -\frac{1}{2}\lambda_6 v^2. \quad (7.29)$$

The potential can then be decomposed into a quadratic term plus cubic and quartic interactions

$$V = -\frac{1}{4}\lambda_1 v^4 + V_2 + V_3 + V_4. \quad (7.30)$$

The mass terms take the form

$$\begin{aligned} V_2 &= M_{H^\pm}^2 H^+ H^- + \frac{1}{2}(S_1, S_2, S_3) \mathcal{M} \begin{pmatrix} S_1 \\ S_2 \\ S_3 \end{pmatrix} \\ &= M_{H^\pm}^2 H^+ H^- + \frac{1}{2}M_h^2 h^2 + \frac{1}{2}M_H^2 H^2 + \frac{1}{2}M_A^2 A^2, \end{aligned} \quad (7.31)$$

with

$$M_{H^\pm}^2 = \mu_2 + \frac{1}{2}\lambda_3 v^2 \quad (7.32)$$

and

$$\mathcal{M} = \begin{pmatrix} 2\lambda_1 v^2 & v^2 \lambda_6^R & -v^2 \lambda_6^I \\ v^2 \lambda_6^R & M_{H^\pm}^2 + v^2 \left(\frac{\lambda_4}{2} + \lambda_5^R\right) & -v^2 \lambda_5^I \\ -v^2 \lambda_6^I & -v^2 \lambda_5^I & M_{H^\pm}^2 + v^2 \left(\frac{\lambda_4}{2} - \lambda_5^R\right) \end{pmatrix}, \quad (7.33)$$

where $\lambda_i^R \equiv \text{Re}(\lambda_i)$ and $\lambda_i^I \equiv \text{Im}(\lambda_i)$. The symmetric mass matrix \mathcal{M} is diagonalized by an orthogonal matrix \mathcal{R} , which defines the neutral mass eigenstates:

$$\mathcal{M} = \mathcal{R}^T \mathcal{M}_D \mathcal{R}, \quad \varphi^0 = \mathcal{R} S, \quad (7.34)$$

where we have introduced the shorthand matrix notation

$$\mathcal{M}_D \equiv \begin{pmatrix} M_h^2 & 0 & 0 \\ 0 & M_H^2 & 0 \\ 0 & 0 & M_A^2 \end{pmatrix}, \quad \varphi^0 \equiv \begin{pmatrix} h \\ H \\ A \end{pmatrix}, \quad S \equiv \begin{pmatrix} S_1 \\ S_2 \\ S_3 \end{pmatrix}. \quad (7.35)$$

Since the trace remains invariant, the masses satisfy the relation

$$M_h^2 + M_H^2 + M_A^2 = 2 M_{H^\pm}^2 + v^2 (2 \lambda_1 + \lambda_4) . \quad (7.36)$$

The minimization conditions allow us to trade the parameters μ_1 and μ_3 by v and λ_6 . The freedom to rephase the field Φ_2 implies, moreover, that only the relative phases among λ_5 , λ_6 and λ_7 are physical; but only two of them are independent. Therefore, we can fully characterize the potential with 11 parameters: v , μ_2 , $|\lambda_{1,\dots,7}|$, $\arg(\lambda_5 \lambda_6^*)$ and $\arg(\lambda_5 \lambda_7^*)$. Four parameters can be determined through the physical scalar masses [14]. The matrix equation

$$(\mathcal{M} \mathcal{R}^T - \mathcal{R}^T \mathcal{M}_D) = 0 \quad (7.37)$$

relates the scalar masses and mixings. Summing the second row with $(-i)$ times the third row, one obtains the identity (imaginary parts included):

$$v^2 \lambda_6 \mathcal{R}_{i1} + \left[M_{H^\pm}^2 - M_{\varphi_i^0}^2 + v^2 \left(\frac{\lambda_4}{2} + \lambda_5 \right) \right] (\mathcal{R}_{i2} - i \mathcal{R}_{i3}) + 2i v^2 \lambda_5 \mathcal{R}_{i3} = 0 . \quad (7.38)$$

This proves in full generality that

$$\begin{aligned} (\mathcal{R}_{i2} - i \mathcal{R}_{i3}) \frac{M_{\varphi_i^0}^2 - M_{H^\pm}^2}{v^2} &= (\mathcal{R}_{i2} - i \mathcal{R}_{i3}) \left(\frac{\lambda_4}{2} + \lambda_5 \right) + 2i \mathcal{R}_{i3} \lambda_5 + \mathcal{R}_{i1} \lambda_6 \\ &= \lambda_{H+G^- \varphi_i^0} . \end{aligned} \quad (7.39)$$

Taking instead the first row, one gets:

$$(2\lambda_1 v^2 - M_{\varphi_i^0}^2) \mathcal{R}_{i1} + v^2 \lambda_6^R \mathcal{R}_{i2} - v^2 \lambda_6^I \mathcal{R}_{i3} = 0 , \quad (7.40)$$

which generalizes the usual relation determining $\tan \tilde{\alpha}$ in the CP-conserving limit ($\mathcal{R}_{13} = \mathcal{R}_{23} = 0$). It also proves that the following identity holds in general

$$\frac{M_{\varphi_i^0}^2}{v^2} \mathcal{R}_{i1} = 2R_{i1} \lambda_1 + i \mathcal{R}_{i3} \lambda_6 + (\mathcal{R}_{i2} - i \mathcal{R}_{i3}) \lambda_6^R = \lambda_{G+G^- \varphi_i^0} . \quad (7.41)$$

Here, similarly to Eq. (7.6), we have parametrized the Goldstone terms of V_3 in the form

$$\left(v \lambda_{H+G^- \varphi_i^0} H^+ G^- \varphi_i^0 + \text{h.c.} \right) + v \lambda_{G+G^- \varphi_i^0} G^+ G^- \varphi_i^0 \subset V_3 . \quad (7.42)$$

These identities generalize the ones from [72], that are valid only in the CP-conserving limit of the scalar potential. They turn out to be very useful if one works in R_ξ gauges with a fully general potential.

Using again Eq. (7.40), the orthogonality of \mathcal{R} implies:

$$\begin{aligned} \sum_i \mathcal{R}_{i1}^2 M_{\varphi_i^0}^2 &= 2\lambda_1 v^2, & \sum_i \mathcal{R}_{i1} \mathcal{R}_{i2} M_{\varphi_i^0}^2 &= \lambda_6^R v^2, \\ \sum_i \mathcal{R}_{i1} \mathcal{R}_{i3} M_{\varphi_i^0}^2 &= -\lambda_6^I v^2. \end{aligned} \quad (7.43)$$

Eq. (7.38) gives the additional orthogonality relations.

$$\sum_i \mathcal{R}_{i1} (\mathcal{R}_{i2} - i\mathcal{R}_{i3}) M_{\varphi_i^0}^2 = \lambda_6 v^2, \quad (7.44)$$

$$\sum_i \mathcal{R}_{i2} (\mathcal{R}_{i2} - i\mathcal{R}_{i3}) M_{\varphi_i^0}^2 = M_{H^\pm}^2 + v^2 \left(\frac{\lambda_4}{2} + \lambda_5 \right), \quad (7.45)$$

$$i \sum_i \mathcal{R}_{i3} (\mathcal{R}_{i2} - i\mathcal{R}_{i3}) M_{\varphi_i^0}^2 = M_{H^\pm}^2 + v^2 \left(\frac{\lambda_4}{2} - \lambda_5 \right). \quad (7.46)$$

The first identity reproduces in complex form the last two real equations in (7.43). Separating the real and imaginary parts of the last two relations, one gets:

$$\sum_i \mathcal{R}_{i2}^2 M_{\varphi_i^0}^2 = M_{H^\pm}^2 + v^2 \left(\frac{\lambda_4}{2} + \lambda_5^R \right), \quad (7.47)$$

$$\sum_i \mathcal{R}_{i3}^2 M_{\varphi_i^0}^2 = M_{H^\pm}^2 + v^2 \left(\frac{\lambda_4}{2} - \lambda_5^R \right), \quad (7.48)$$

$$\sum_i \mathcal{R}_{i2} \mathcal{R}_{i3} M_{\varphi_i^0}^2 = -v^2 \lambda_5^I. \quad (7.49)$$

7.A.1 Inert 2HDM

Imposing a discrete \mathcal{Z}_2 symmetry such that all SM fields remain invariant under a \mathcal{Z}_2 transformation, while

$$\Phi_1 \rightarrow \Phi_1, \quad \Phi_2 \rightarrow -\Phi_2, \quad (7.50)$$

one makes the second scalar doublet *inert*: linear interactions of Φ_2 with the SM fields are odd under a \mathcal{Z}_2 transformation, and thus forbidden [48, 49]. In particular, Φ_2 is fermiophobic. This inert scalar doublet can only interact with

the other fields through quadratic couplings. The lightest neutral component of Φ_2 is then a very good candidate for dark matter.

The \mathcal{Z}_2 symmetry implies a significant simplification of the scalar potential, because all terms with an odd number of Φ_2 fields vanish: $\mu_3 = \lambda_6 = \lambda_7 = 0$. Moreover, making an appropriate rephasing of Φ_2 , λ_5 can be taken real. Therefore, the neutral mass matrix (7.33) becomes diagonal and there is no mixing among the neutral scalars ($\mathcal{R} = I$). The neutral scalar masses are given by:

$$\begin{aligned} M_h^2 &= 2\lambda_1 v^2, & M_H^2 &= M_{H^\pm}^2 + \left(\frac{\lambda_4}{2} + \lambda_5\right) v^2, \\ M_A^2 &= M_{H^\pm}^2 + \left(\frac{\lambda_4}{2} - \lambda_5\right) v^2. \end{aligned} \quad (7.51)$$

7.B Heavy neutral Higgs decay rates

In this section we are going to write down the tree-level on-shell two-body dominant decay rates of a heavy neutral Higgs. All the formulae presented here are, as in section 7.3, completely general (no assumptions are made on the Higgs potential and the A2HDM Yukawa structure is assumed). The decay rate of a neutral scalar to a pair of massive fermions is given by:

$$\begin{aligned} \Gamma(\varphi_i^0 \rightarrow f\bar{f}) &= \frac{N_c^f m_f^2 M_{\varphi_i^0}}{8\pi v^2} \left(1 - \frac{4m_f^2}{M_{\varphi_i^0}^2}\right)^{3/2} \\ &\times \left[\text{Re}(y_f^{\varphi_i^0})^2 + \text{Im}(y_f^{\varphi_i^0})^2 \left(1 - \frac{4m_f^2}{M_{\varphi_i^0}^2}\right)^{-1} \right], \end{aligned} \quad (7.52)$$

where N_c^f is 1 for leptons and 3 for quarks. The decay into two gauge bosons reads ($V = W, Z$)

$$\begin{aligned} \Gamma(\varphi_i^0 \rightarrow VV) &= \mathcal{R}_{i1}^2 \frac{M_{\varphi_i^0}^3 \delta_V}{32\pi v^2} \left(1 - \frac{4M_V^2}{M_{\varphi_i^0}^2}\right)^{1/2} \\ &\times \left(1 - \frac{4M_V^2}{M_{\varphi_i^0}^2} + \frac{12M_V^4}{M_{\varphi_i^0}^4}\right), \end{aligned} \quad (7.53)$$

with $\delta_Z = 1$ and $\delta_W = 2$. Other channels that can bring important contributions are $\varphi_i^0 \rightarrow \varphi_j^0 \varphi_j^0$ and $\varphi_i^0 \rightarrow H^+ H^-$. The corresponding decay widths are given by

$$\Gamma(\varphi_i^0 \rightarrow \varphi_j^0 \varphi_j^0) = \frac{v^2 \lambda_{\varphi_i^0 \varphi_j^0 \varphi_j^0}^2}{32 \pi M_{\varphi_i^0}} \left(1 - \frac{4M_{\varphi_j^0}^2}{M_{\varphi_i^0}^2}\right)^{1/2}, \quad (7.54)$$

$$\Gamma(\varphi_i^0 \rightarrow H^+ H^-) = \frac{v^2 \lambda_{\varphi_i^0 H^+ H^-}^2}{16 \pi M_{\varphi_i^0}} \left(1 - \frac{4M_{H^\pm}^2}{M_{\varphi_i^0}^2}\right)^{1/2}, \quad (7.55)$$

where, for the charged Higgs interaction Lagrangian we have used the parametrization given in (7.6) and we have parametrized the cubic interaction of the neutral Higgs fields as

$$\mathcal{L}_{\varphi_i^0 \varphi_j^0 \varphi_j^0} = -\frac{v}{2} \lambda_{\varphi_i^0 \varphi_j^0 \varphi_j^0} \varphi_i^0 \varphi_j^0 \varphi_j^0. \quad (7.56)$$

Explicit expressions for these couplings can be found in [14]. Here we didn't consider the off-shell $\varphi_i^0 \rightarrow \varphi_j^{0*} \varphi_j^{0*}$ decay mode because in addition to its kinematical suppression it also depends on the unknown parameter $\lambda_{\varphi_i^0 \varphi_j^0 \varphi_j^0}$ and would not bring useful information. The last two processes that must be taken into account are $\varphi_i^0 \rightarrow \varphi_j^0 Z$ and $\varphi_i^0 \rightarrow H^+ W^-$. We have

$$\Gamma(\varphi_i^0 \rightarrow \varphi_j^0 Z) = (\mathcal{R}_{i3} \mathcal{R}_{j2} - \mathcal{R}_{i2} \mathcal{R}_{j3})^2 \frac{1}{16 \pi v^2 M_{\varphi_i^0}^3} \times \lambda^{3/2}(M_{\varphi_i^0}^2, M_{\varphi_j^0}^2, M_Z^2), \quad (7.57)$$

$$\Gamma(\varphi_i^0 \rightarrow H^+ W^-) = (\mathcal{R}_{i2}^2 + \mathcal{R}_{i3}^2) \frac{1}{16 \pi v^2 M_{\varphi_i^0}^3} \times \lambda^{3/2}(M_{\varphi_i^0}^2, M_{H^\pm}^2, M_W^2). \quad (7.58)$$

Again, the scalar couplings to gauge bosons are taken from [14].

7.C QCD corrections to $pp \rightarrow H^+ \varphi_i^0$

For the $H^+ \varphi_i^0$ associated production, we write the LO hadronic cross section as

$$\sigma_{\text{LO}} = \int_{\tau_0}^1 d\tau \int_{\tau}^1 \frac{dx}{x} \sum_{q_u, \bar{q}_d} \left[q_u(x, \mu_F) \bar{q}_d(\tau/x, \mu_F) + \bar{q}_d(x, \mu_F) q_u(\tau/x, \mu_F) \right] \times \hat{\sigma}_{\text{LO}}(\hat{s} = \tau s), \quad (7.59)$$

where we have introduced the shorthand notation $\hat{\sigma}_{\text{LO}} \equiv \hat{\sigma}(q_u \bar{q}_d \rightarrow H^+ \varphi_i^0)$, for the partonic cross section given in Eq. (7.18). As usual, the partonic invariant-mass \hat{s} must be expressed as a fraction of the hadronic center-of-mass energy s , that is $\hat{s} = \tau s$. The lower integration limit is given by $\tau_0 = (M_{H^\pm} + M_{\varphi_i^0})^2/s$. The PDFs $q_i(x, \mu_F)$, for a given quark flavour ‘i’, depend on the momentum fraction x and the factorization scale μ_F .

The NLO cross section, that includes first-order QCD corrections, can be cast in the simple form [70, 71]

$$\sigma_{\text{NLO}} = \sigma_{\text{LO}} + \Delta\sigma_{q\bar{q}} + \Delta\sigma_{qg}, \quad (7.60)$$

where $\Delta\sigma_{q\bar{q}}$ and $\Delta\sigma_{qg}$ are given by

$$\begin{aligned} \Delta\sigma_{q\bar{q}} &= \frac{\alpha_s(\mu_R)}{\pi} \int_{\tau_0}^1 d\tau \int_{\tau}^1 \frac{dx}{x} \sum_{q_u, \bar{q}_d} \\ &\times \left[q_u(x, \mu_F) \bar{q}_d(\tau/x, \mu_F) + \bar{q}_d(x, \mu_F) q_u(\tau/x, \mu_F) \right] \\ &\times \int_{\tau_0/\tau}^1 dz \hat{\sigma}_{\text{LO}}(\tau s z) \omega_{q\bar{q}}(z), \end{aligned} \quad (7.61)$$

$$\begin{aligned} \Delta\sigma_{qg} &= \frac{\alpha_s(\mu_R)}{\pi} \int_{\tau_0}^1 d\tau \int_{\tau}^1 \frac{dx}{x} \sum_{q_u, \bar{q}_d} \left[q_u(x, \mu_F) g(\tau/x, \mu_F) + g(x, \mu_F) q_u(\tau/x, \mu_F) \right. \\ &\left. + \bar{q}_d(x, \mu_F) g(\tau/x, \mu_F) + g(x, \mu_F) \bar{q}_d(\tau/x, \mu_F) \right] \\ &\times \int_{\tau_0/\tau}^1 dz \hat{\sigma}_{\text{LO}}(\tau s z) \omega_{qg}(z), \end{aligned} \quad (7.62)$$

with μ_R the renormalization scale and

$$\begin{aligned}\omega_{q\bar{q}}(z) &= -P_{qq}(z) \log\left(\frac{\mu_F^2}{\tau s}\right) \\ &\quad + \frac{4}{3} \left[\left(\frac{\pi^2}{3} - 4\right) \delta(1-z) + 2(1+z^2) \left(\frac{\log(1-z)}{1-z}\right)_+ \right], \\ \omega_{qg}(z) &= -\frac{1}{2} P_{qg}(z) \log\left(\frac{\mu_F^2}{(1-z)^2 \tau s}\right) + \frac{1}{8} [1 + 6z - 7z^2].\end{aligned}\quad (7.63)$$

The Altarelli-Parisi splitting functions P_{qq} and P_{qg} are given by

$$P_{qq}(z) = \frac{4}{3} \left[\frac{1+z^2}{(1-z)_+} + \frac{3}{2} \delta(1-z) \right], \quad P_{qg}(z) = \frac{1}{2} [z^2 + (1-z)^2], \quad (7.64)$$

where F_+ is the ‘+’ distribution defined as $F_+(x) = F(x) - \delta(1-x) \int_0^1 dx' F(x')$, and

$$\int_a^1 dz g(z) \left(\frac{f(z)}{1-z}\right)_+ \equiv \int_a^1 dz (g(z) - g(1)) \frac{f(z)}{1-z} - g(1) \int_0^a dz \frac{f(z)}{1-z}. \quad (7.65)$$

7.D QCD corrections to $pp \rightarrow H^+W^-$

The LO hadronic production cross section for the dominant gluon-fusion channel (in the heavy top-mass approximation) can be cast in the simple form

$$\sigma_{\text{LO}} = \int_{\tau_0}^1 d\tau \int_{\tau}^1 \frac{dx}{x} g(x, \mu_F) g(\tau/x, \mu_F) \hat{\sigma}_{\text{LO}}(\hat{s} = \tau s), \quad (7.66)$$

where $\hat{\sigma}_{\text{LO}}$ stands for the partonic cross section $\hat{\sigma}(gg \rightarrow H^+W^-)$, given in Eq. (7.21), and $\tau_0 = (M_{H^\pm} + M_W)^2/s$. At the NLO, the cross section can be written as [70, 71]

$$\sigma_{\text{NLO}} = \sigma_{\text{LO}} + \Delta\sigma_{gg}^{\text{virt}} + \Delta\sigma_{gg} + \Delta\sigma_{q\bar{q}} + \Delta\sigma_{qg}, \quad (7.67)$$

where:

$$\Delta\sigma_{gg}^{\text{virt}} = \frac{\alpha_s(\mu_R)}{\pi} \int_{\tau_0}^1 d\tau \int_{\tau}^1 \frac{dx}{x} g(x, \mu_F) g(\tau/x, \mu_F) \hat{\sigma}_{\text{LO}}(\tau s) \omega_{gg}^{\text{virt}}, \quad (7.68)$$

$$\begin{aligned} \Delta\sigma_{gg} &= \frac{\alpha_s(\mu_R)}{\pi} \int_{\tau_0}^1 d\tau \int_{\tau}^1 \frac{dx}{x} g(x, \mu_F) g(\tau/x, \mu_F) \\ &\quad \times \int_{\tau_0/\tau}^1 \frac{dz}{z} \hat{\sigma}_{\text{LO}}(\tau s z) \omega_{gg}(z), \end{aligned} \quad (7.69)$$

$$\begin{aligned} \Delta\sigma_{gq} &= \frac{\alpha_s(\mu_R)}{\pi} \int_{\tau_0}^1 d\tau \int_{\tau}^1 \frac{dx}{x} \sum_{q, \bar{q}} \\ &\quad \times \left[q(x, \mu_F) g(\tau/x, \mu_F) + g(x, \mu_F) q(\tau/x, \mu_F) \right. \\ &\quad \left. + \bar{q}(x, \mu_F) g(\tau/x, \mu_F) + g(x, \mu_F) \bar{q}(\tau/x, \mu_F) \right] \\ &\quad \times \int_{\tau_0/\tau}^1 \frac{dz}{z} \hat{\sigma}_{\text{LO}}(\tau s z) \omega_{gq}(z), \end{aligned} \quad (7.70)$$

$$\begin{aligned} \Delta\sigma_{q\bar{q}} &= \frac{\alpha_s(\mu_R)}{\pi} \int_{\tau_0}^1 d\tau \int_{\tau}^1 \frac{dx}{x} \sum_{q, \bar{q}} \\ &\quad \times \left[q(x, \mu_F) \bar{q}(\tau/x, \mu_F) + \bar{q}(x, \mu_F) q(\tau/x, \mu_F) \right] \\ &\quad \times \int_{\tau_0/\tau}^1 \frac{dz}{z} \hat{\sigma}_{\text{LO}}(\tau s z) \frac{32}{27} (1-z)^3, \end{aligned} \quad (7.71)$$

with the functions $\omega_{gg}^{\text{virt}}$, ω_{gg} and ω_{gq} given by

$$\begin{aligned} \omega_{gg}^{\text{virt}} &= \pi^2 + \frac{11}{2} + \frac{33 - 2N_f}{6} \log\left(\frac{\mu_R^2}{\tau s}\right), \\ \omega_{gg} &= -z P_{gg}(z) \log\left(\frac{\mu_F^2}{\tau s}\right) - \frac{11}{2} (1-z)^3 + 12 \left(\frac{\log(1-z)}{1-z}\right)_+ \\ &\quad - 12 z (2-z+z^2) \log(1-z), \\ \omega_{gq} &= -\frac{z}{2} P_{gq}(z) \log\left(\frac{\mu_F^2}{\tau s (1-z)^2}\right) - 1 + 2z - \frac{1}{3} z^2, \end{aligned} \quad (7.72)$$

where P_{gg} and P_{gq} are the Altarelli-Parisi splitting functions

$$\begin{aligned} P_{gg}(z) &= 6 \left[\left(\frac{1}{1-z} \right)_+ + \frac{1}{z} - 2 + z(1-z) \right] + \frac{33 - 2N_f}{6} \delta(1-z), \\ P_{gq}(z) &= \frac{4}{3} \frac{1 + (1-z)^2}{z}. \end{aligned} \tag{7.73}$$

Acknowledgements

This work has been supported in part by the Spanish Government and ERDF funds from the EU Commission [Grants FPA2011-23778 and CSD2007-00042 (Consolider Project CPAN)] and by Generalitat Valenciana under Grant No. PROMETEOII/2013/007. The work of V.I. is supported by the Spanish Ministry MINECO through the FPI grant BES-2012-054676.

BIBLIOGRAPHY

- [1] ATLAS Collaboration, *Observation of a new particle in the search for the Standard Model Higgs boson with the ATLAS detector at the LHC*, Phys. Lett. B **716** (2012) 1 [arXiv:1207.7214 [hep-ex]].
- [2] ATLAS Collaboration, *Measurements of Higgs boson production and couplings in diboson final states with the ATLAS detector at the LHC*, Phys. Lett. B **726** (2013) 88 [arXiv:1307.1427 [hep-ex]].
- [3] ATLAS Collaboration, *Search for the $b\bar{b}$ decay of the Standard Model Higgs boson in associated (W/Z)H production with the ATLAS detector*, ATLAS-CONF-2013-079 (July 19, 2013).
- [4] ATLAS Collaboration, *Combined coupling measurements of the Higgs-like boson with the ATLAS detector using up to 25 fb^{-1} of proton-proton collision data*, ATLAS-CONF-2013-034 (March 13, 2013);
- [5] CMS Collaboration, *Observation of a new boson at a mass of 125 GeV with the CMS experiment at the LHC*, Phys. Lett. B **716** (2012) 30 [arXiv:1207.7235 [hep-ex]].
- [6] CMS Collaboration, *Observation of a new boson with mass near 125 GeV in pp collisions at $\sqrt{s} = 7$ and 8 TeV*, JHEP **06** (2013) 081 [arXiv:1303.4571 [hep-ex]].
- [7] CMS Collaboration, *Measurements of the properties of the new boson with a mass near 125 GeV*, CMS-PAS-HIG-13-005 (April 17, 2013).
- [8] CDF and D0 Collaborations, *Evidence for a particle produced in association with weak bosons and decaying to a bottom-antibottom quark pair in Higgs boson searches at the Tevatron*, Phys. Rev. Lett. **109** (2012) 071804 [arXiv:1207.6436 [hep-ex]].
- [9] CDF and D0 Collaborations, *Higgs Boson Studies at the Tevatron*, Phys. Rev. D **88** (2013) 052014 [arXiv:1303.6346 [hep-ex]].

-
- [10] J. F. Gunion, H. E. Haber, G. L. Kane and S. Dawson, *The Higgs Hunter's Guide*, Front. Phys. **80** (2000) 1.
- [11] G. C. Branco, P. M. Ferreira, L. Lavoura, M. N. Rebelo, M. Sher and J. P. Silva, *Theory and phenomenology of two-Higgs-doublet models*, Phys. Rept. **516** (2012) 1 [arXiv:1106.0034 [hep-ph]].
- [12] A. Celis, V. Ilisie and A. Pich, *Towards a general analysis of LHC data within two-Higgs-doublet models*, JHEP **1312** (2013) 095 [arXiv:1310.7941 [hep-ph]].
- [13] V. Ilisie, *Constraining the two-Higgs doublet models with the LHC data*, PoS (EPS - HEP 2013) **286** [arXiv:1310.0931 [hep-ph]].
- [14] A. Celis, V. Ilisie and A. Pich, *LHC constraints on two-Higgs doublet models*, JHEP **1307** (2013) 053 [arXiv:1302.4022 [hep-ph]].
- [15] A. Pich and P. Tuzón, *Yukawa Alignment in the Two-Higgs-Doublet Model*, Phys. Rev. D **80** (2009) 091702 [arXiv:0908.1554 [hep-ph]].
- [16] M. Jung, A. Pich and P. Tuzón, *Charged-Higgs phenomenology in the Aligned two-Higgs-doublet model*, JHEP **1011** (2010) 003 [arXiv:1006.0470 [hep-ph]].
- [17] M. Jung, A. Pich and P. Tuzón, *The $B \rightarrow X_s \gamma$ Rate and CP Asymmetry within the Aligned Two-Higgs-Doublet Model*, Phys. Rev. D **83** (2011) 074011 [arXiv:1011.5154 [hep-ph]].
- [18] M. Jung, X.-Q. Li and A. Pich, *Exclusive radiative B-meson decays within the aligned two-Higgs-doublet model*, JHEP **1210** (2012) 063 [arXiv:1208.1251 [hep-ph]].
- [19] A. Celis, M. Jung, X.-Q. Li and A. Pich, *Sensitivity to charged scalars in $B \rightarrow D^{(*)} \tau \nu_\tau$ and $B \rightarrow \tau \nu_\tau$ decays*, JHEP **1301** (2013) 054 [arXiv:1210.8443 [hep-ph]].
- [20] M. Jung and A. Pich, *Electric Dipole Moments in Two-Higgs-Doublet Models*, JHEP **1404** (2014) 076 [arXiv:1308.6283 [hep-ph]].
- [21] X.-Q. Li, J. Lu and A. Pich, *$B_{s,d}^0 \rightarrow \ell^+ \ell^-$ Decays in the Aligned Two-Higgs-Doublet Model*, [arXiv:1404.5865 [hep-ph]].

- [22] A. Pich, *The Physics of the Higgs-like Boson*, EPJ Web Conf. **60** (2013) 02006 [arXiv:1307.7700 [hep-ph]].
- [23] O. Deschamps, S. Descotes-Genon, S. Monteil, V. Niess, S. T’Jampens and V. Tisserand, *The Two Higgs Doublet of Type II facing flavour physics data*, Phys. Rev. D **82** (2010) 073012 [arXiv:0907.5135 [hep-ph]].
- [24] A. Barroso, P. M. Ferreira, R. Santos, M. Sher and J. P. Silva, *2HDM at the LHC - the story so far*, arXiv:1304.5225 [hep-ph].
- [25] B. Grinstein and P. Uttayarat, *Carving Out Parameter Space in Type-II Two Higgs Doublets Model*, JHEP **1306** (2013) 094 [arXiv:1304.0028 [hep-ph]].
- [26] O. Eberhardt, U. Nierste and M. Wiebusch, *Status of the two-Higgs-doublet model of type II*, JHEP **1307** (2013) 118 [arXiv:1305.1649 [hep-ph]].
- [27] C. -Y. Chen, S. Dawson and M. Sher, *Heavy Higgs Searches and Constraints on Two Higgs Doublet Models*, Phys. Rev. D **88** (2013) 015018 [arXiv:1305.1624 [hep-ph]];
- [28] N. Craig, J. Galloway and S. Thomas, *Searching for Signs of the Second Higgs Doublet*, arXiv:1305.2424 [hep-ph].
- [29] B. Coleppa, F. Kling and S. Su, *Constraining Type II 2HDM in Light of LHC Higgs Searches*, JHEP **1401** (2014) 161 [arXiv:1305.0002 [hep-ph]].
- [30] J. Shu and Y. Zhang, *Impact of a CP Violating Higgs: from LHC to Baryogenesis*, Phys. Rev. Lett. **111** (2013) 091801 [arXiv:1304.0773 [hep-ph]].
- [31] C. -W. Chiang and K. Yagyu, *Implications of Higgs boson search data on the two-Higgs doublet models with a softly broken Z_2 symmetry*, JHEP **1307** (2013) 160 [arXiv:1303.0168 [hep-ph]].
- [32] M. Krawczyk, D. Sokolowska, P. Swaczyna and B. Swiezewska, *Constraining Inert Dark Matter by $R_{\gamma\gamma}$ and WMAP data*, JHEP **1309** (2013) 055 [arXiv:1305.6266 [hep-ph]].
- [33] B. Swiezewska and M. Krawczyk, *Diphoton rate in the Inert Doublet Model with a 125 GeV Higgs boson*, Phys. Rev. D **88** (2013) 035019 [arXiv:1212.4100 [hep-ph]].

-
- [34] B. Swiezewska, *Yukawa independent constraints for Two Higgs Doublet Models with a 125 GeV Higgs boson*, Phys. Rev. D **88** (2013) 055027, Erratum: Phys. Rev. D **88** (2013) 119903 [arXiv:1209.5725 [hep-ph]].
- [35] M. Krawczyk, D. Sokolowska, P. Swaczyna and B. Swiezewska, *Higgs $\rightarrow \gamma\gamma, Z\gamma$ in the Inert Doublet Model*, Acta Phys. Pol. B **44** (2013) 2163 [arXiv:1309.7880 [hep-ph]].
- [36] G. Belanger, B. Dumont, U. Ellwanger, J. F. Gunion and S. Kraml, *Global fit to Higgs signal strengths and couplings and implications for extended Higgs sectors*, Phys. Rev. D **88** (2013) 075008 [arXiv:1306.2941 [hep-ph]].
- [37] R. Enberg, J. Rathsman and G. Wouda, *Higgs properties in a softly broken Inert Doublet Model*, JHEP **1308** (2013) 079 [arXiv:1304.1714 [hep-ph]].
- [38] G. C. Dorsch, S. J. Huber and J. M. No, *A strong electroweak phase transition in the 2HDM after LHC8*, JHEP **1310** (2013) 029 [arXiv:1305.6610 [hep-ph]].
- [39] G. C. Dorsch, S. Huber, K. Mimasu and J. M. No, *Echoes of the Electroweak Phase Transition: Discovering a second Higgs doublet through $A_0 \rightarrow H_0 Z$* , arXiv:1405.5537 [hep-ph].
- [40] G. Bhattacharyya, D. Das and A. Kundu, *Feasibility of light scalars in a class of two-Higgs-doublet models and their decay signatures*, arXiv:1402.0364 [hep-ph].
- [41] W. Altmannshofer, S. Gori and G. D. Kribs, *A Minimal Flavor Violating 2HDM at the LHC*, Phys. Rev. D **86** (2012) 115009 [arXiv:1210.2465 [hep-ph]].
- [42] S. Chang, S. K. Kang, J. -P. Lee, K. Y. Lee, S. C. Park and J. Song, *Two Higgs doublet models for the LHC Higgs boson data at $\sqrt{s} = 7$ and 8 TeV*, arXiv:1310.3374 [hep-ph].
- [43] K. Cheung, J. S. Lee and P. -Y. Tseng, *Higgcision in the Two-Higgs Doublet Models*, JHEP **1401** (2014) 085 [arXiv:1310.3937 [hep-ph]].
- [44] R. Enberg, J. Rathsman and G. Wouda, *Higgs phenomenology in the Stealth Doublet Model*, arXiv:1311.4367 [hep-ph].

- [45] ATLAS Collaboration, *Search for charged Higgs bosons decaying via $H^+ \rightarrow \tau\nu$ in top quark pair events using pp collision data at $\sqrt{s} = 7$ TeV with the ATLAS detector*, JHEP **1206** (2012) 039 [arXiv:1204.2760 [hep-ex]]; ATLAS-CONF-2013-090 (August 25, 2013).
- [46] ATLAS Collaboration, *Search for a light charged Higgs boson in the decay channel $H^+ \rightarrow c\bar{s}$ in $t\bar{t}$ events using pp collisions at $\sqrt{s} = 7$ TeV with the ATLAS detector*, Eur. Phys. J. C **73** (2013) 2465 [arXiv:1302.3694 [hep-ex]].
- [47] CMS Collaboration, *Search for a light charged Higgs boson in top quark decays in pp collisions at $\sqrt{s} = 7$ TeV*, JHEP **1207** (2012) 143 [arXiv:1205.5736 [hep-ex]].
- [48] E. Ma, *Utility of a Special Second Scalar Doublet*, Mod. Phys. Lett. A **23** (2008) 647 [arXiv:0802.2917 [hep-ph]];
- [49] E. Ma, *Verifiable radiative seesaw mechanism of neutrino mass and dark matter*, Phys. Rev. D **73** (2006) 077301 [hep-ph/0601225].
- [50] Q.-H. Cao, E. Ma, and G. Rajasekaran, *Observing the Dark Scalar Doublet and its Impact on the Standard-Model Higgs Boson at Colliders*, Phys. Rev. D **76** (2007) 095011 [arXiv:0708.2939 [hep-ph]].
- [51] R. Barbieri, L. J. Hall and V. S. Rychkov, *Improved naturalness with a heavy Higgs: An Alternative road to LHC physics*, Phys. Rev. D **74** (2006) 015007 [hep-ph/0603188].
- [52] L. Lopez Honorez, E. Nezri, J. F. Oliver and M. H. G. Tytgat, *The Inert Doublet Model: An Archetype for Dark Matter*, JCAP **0702** (2007) 028 [hep-ph/0612275].
- [53] C. Arina, F.-S. Ling, and M. H. Tytgat, *IDM and iDM or The Inert Doublet Model and Inelastic Dark Matter*, JCAP **0910** (2009) 018 [arXiv:0907.0430 [hep-ph]].
- [54] L. Lopez Honorez and C. E. Yaguna, *The inert doublet model of dark matter revisited*, JHEP **1009** (2010) 046 [arXiv:1003.3125 [hep-ph]].
- [55] L. Lopez Honorez and C. E. Yaguna, *A new viable region of the inert doublet model*, JCAP **1101** (2011) 002 [arXiv:1011.1411 [hep-ph]].
- [56] E. M. Dolle and S. Su, *The Inert Dark Matter*, Phys. Rev. D **80** (2009) 055012 [arXiv:0906.1609 [hep-ph]].

- [57] A. Arhrib, Y.-L. S. Tsai, Q. Yuan and T.-C. Yuan, *An Updated Analysis of Inert Higgs Doublet Model in light of the Recent Results from LUX, PLANCK, AMS-02 and LHC*, JCAP **1406** (2014) 030 [arXiv:1310.0358 [hep-ph]].
- [58] I. F. Ginzburg, K. A. Kanishev, M. Krawczyk and D. Sokolowska, *Evolution of Universe to the present inert phase*, Phys. Rev. D **82** (2010) 123533 [arXiv:1009.4593 [hep-ph]].
- [59] N. Cabibbo, *Unitary Symmetry and Leptonic Decays*, Phys. Rev. Lett. **10** (1963) 531.
- [60] M. Kobayashi and T. Maskawa, *CP Violation in the Renormalizable Theory of Weak Interaction*, Prog. Theor. Phys. **49** (1973) 652.
- [61] T. Hermann, M. Misiak and M. Steinhauser, $\bar{B} \rightarrow X_s \gamma$ in the Two Higgs Doublet Model up to Next-to-Next-to-Leading Order in QCD, JHEP **1211** (2012) 036 [arXiv:1208.2788 [hep-ph]].
- [62] T. Abe, J. Hisano, T. Kitahara and K. Tobioka, *Gauge invariant Barr-Zee type contributions to fermionic EDMs in the two-Higgs doublet models*, JHEP **1401** (2014) 106 [arXiv:1311.4704 [hep-ph]].
- [63] J.F. Gunion, G.L. Kane and J. Wudka, *Search techniques for charged and neutral intermediate-mass Higgs Bosons*, Nucl. Phys. B **299** (1988) 231.
- [64] S. Raychaudhuri, *Detection of charged Higgs bosons through the rare decay $H^+ \rightarrow W^+ \gamma$* , Phys. Lett. B **297** (1992) 159.
- [65] A. Arhrib, R. Benbrik and M. Chabab, *Charged Higgs Bosons decays $H^\pm \rightarrow W^\pm(\gamma, Z)$ revisited*, J. Phys. G **34** (2007) 907 [hep-ph/0607182].
- [66] J. Hernández-Sánchez, M. A. Pérez, G. Tavares-Velasco and J. J. Toscano, *Decay $H^+ \rightarrow W^+ \gamma$ in a nonlinear R_ξ -gauge*, Phys. Rev. D **69** 095008 [hep-ph/0402284].
- [67] OPAL Collaboration, *Decay mode independent searches for new scalar bosons with the OPAL detector at LEP*, Eur. Phys. J. C **27** (2003) 311 [hep-ex/0206022].
- [68] LEP Working Group for Higgs boson searches and ALEPH and DELPHI and L3 and OPAL Collaborations, *Search for the standard model Higgs boson at LEP*, Phys. Lett. B **565** (2003) 61 [hep-ex/0306033].

-
- [69] A. D. Martin, W. J. Stirling, R. S. Thorne and G. Watt, *Parton distributions for the LHC*, Eur. Phys. J. C **63** (2009) 189-285 [arXiv:0901.0002 [hep-ph]].
- [70] S. Dawson, S. Dittmaier and M. Spira, *Neutral Higgs-Boson Pair Production at Hadron Colliders: QCD Corrections*, Phys. Rev. D **58** (1998) 115012 [hep-ph/9805244].
- [71] A. Djouadi, *The Anatomy of Electro-Weak Symmetry Breaking. I: The Higgs boson in the Standard Model*, Phys. Rept. **457** (2008) 1-216 [hep-ph/0503172].
- [72] J. F. Gunion and H. E. Haber, *The CP-conserving two-Higgs-doublet model: the approach to the decoupling limit*, Phys. Rev. D **67** 075019 [hep-ph/0207010].

8. NEW BARR-ZEE CONTRIBUTIONS TO $(g - 2)_\mu$ IN TWO-HIGGS-DOUBLET MODELS

Victor Ilisie

IFIC, Universitat de València – CSIC, Apt. Correus 22085, E-46071 València, Spain

Journal of High Energy Physics: JHEP 04(2015)077, arXiv: 1502.04199

Abstract: We study the contribution of new sets of two-loop Barr-Zee type diagrams to the anomalous magnetic moment of the muon within the two-Higgs-doublet model framework. We show that some of these contributions can be quite sizeable for a large region of the parameter space and can significantly reduce, and in some cases even explain, the discrepancy between the theoretical prediction and the experimentally measured value of this observable. Analytical expressions are given for all the calculations performed in this work.

8.1 Introduction

Now that a SM-like Higgs particle has been experimentally discovered [1–5], the possibility of an enlarged scalar sector becomes very plausible. In this analysis we are going to use the anomalous magnetic moment of the muon as a probe for new physics and study new contributions to this observable within the two-Higgs-doublet model (2HDM) framework. The anomalous magnetic moment of the muon has been extensively analysed within the Standard Model (SM) and its numerous extensions. Even if the SM prediction still suffers from large theoretical uncertainties (mostly hadronic and electroweak) it is a nice place to look for new physics. The latest result for the discrepancy between the SM prediction and the experimental measured value is given by [6–28]

$$\Delta a_\mu^{exp} \equiv a_\mu^{exp} - a_\mu^{SM} = 262(85) \times 10^{-11}. \quad (8.1)$$

Here we will study the two-loop Barr-Zee type [29] contributions to Δa_μ that have not been analysed previously within the 2HDM. We show that some of these diagrams can bring rather sizeable contributions for a quite large region of the parameter space and therefore can reduce the value of the difference between theory and experiment given by (8.1). We also show that other sets of these type of diagrams bring small contributions and can be safely discarded. For the calculations we use the most generic Higgs potential and the generic Yukawa structure of the aligned two-Higgs-doublet model (A2HDM) [30]. Thus, we also re-examine the classical Barr-Zee type diagrams [6, 7, 31–42] expressing their contributions in terms of the three independent complex alignment parameters $\zeta_{u,d,l}$. All the results are given in analytical form. The phenomenological analysis is made assuming a CP-conserving Lagrangian. However, all the generic formulae given in this work can be used for future, and more complete, analyses without assuming CP-conservation. Additional constraints coming from the flavour sector and global fits to the LHC data are also taken into account [43–52].

In the first part of this paper, section 8.2, we present the relevant features of the A2HDM. In section 8.3 we present the one-loop results in terms of the generic A2HDM parameters. In section 8.4 we present the classical two-loop Barr-Zee results and the calculation of the new sets of this type of diagrams that can potentially bring sizeable contributions to the anomalous magnetic moment. Section 8.5 is dedicated to the phenomenological analysis for the CP-conserving case and the presentation of the relevant contributions. Finally, we conclude in section 8.6 with a brief summary of our results. One appendix is also given, with technical details for the calculation of a particular set of Barr-Zee type diagrams.

8.2 The Aligned Two-Higgs-Doublet Model

The 2HDM extends the SM with a second scalar doublet of hypercharge $Y = \frac{1}{2}$. It is convenient to work in the so-called Higgs basis (Φ_1, Φ_2) , where only one doublet acquires a vacuum expectation value:

$$\Phi_1 = \begin{bmatrix} G^+ \\ \frac{1}{\sqrt{2}}(v + S_1 + iG^0) \end{bmatrix}, \quad \Phi_2 = \begin{bmatrix} H^+ \\ \frac{1}{\sqrt{2}}(S_2 + iS_3) \end{bmatrix}, \quad (8.2)$$

where G^\pm and G^0 denote the Goldstone fields. Thus, Φ_1 plays the role of the SM scalar doublet with $v = (\sqrt{2}G_F)^{-1/2} = 246$ GeV. The physical scalar spectrum contains five degrees of freedom: two charged fields $H^\pm(x)$ and three neutral scalars $\varphi_i^0(x) = \{h(x), H(x), A(x)\}$, which are related with the S_i fields through an orthogonal transformation $\varphi_i^0(x) = \mathcal{R}_{ij}S_j(x)$. The form of the \mathcal{R} matrix is fixed by the scalar potential, which determines the neutral scalar mass matrix and the corresponding mass eigenstates. A detailed discussion is given in [43–45]. In general, the CP-odd component S_3 mixes with the CP-even fields $S_{1,2}$ and the resulting mass eigenstates do not have a definite CP quantum number. If the scalar potential is CP symmetric this admixture disappears; in this particular case, $A(x) = S_3(x)$ and

$$\begin{pmatrix} h \\ H \end{pmatrix} = \begin{bmatrix} \cos \tilde{\alpha} & \sin \tilde{\alpha} \\ -\sin \tilde{\alpha} & \cos \tilde{\alpha} \end{bmatrix} \begin{pmatrix} S_1 \\ S_2 \end{pmatrix}. \quad (8.3)$$

Performing a phase redefinition of the neutral CP-even fields, we can fix the sign of $\sin \tilde{\alpha}$. In this work we adopt the conventions $M_h \leq M_H$ and $0 \leq \tilde{\alpha} \leq \pi$, so that $\sin \tilde{\alpha}$ is positive.

The most generic Yukawa Lagrangian with the SM fermionic content gives rise to FCNCs because the fermionic couplings of the two scalar doublets cannot be simultaneously diagonalized in flavour space. The non-diagonal neutral couplings can be eliminated by requiring the alignment in flavour space of the Yukawa matrices [30]; *i.e.*, the two Yukawa matrices coupling to a given type of right-handed fermions are assumed to be proportional to each other and can, therefore, be diagonalized simultaneously. The three proportionality parameters ς_f ($f = u, d, l$) are arbitrary complex numbers and introduce new sources of CP violation.

In terms of the fermion mass-eigenstate fields, the Yukawa interactions of the A2HDM read [30]

$$\begin{aligned} \mathcal{L}_Y = & -\frac{\sqrt{2}}{v} H^+ \left\{ \bar{u} \left[\varsigma_d V M_d \mathcal{P}_R - \varsigma_u M_u^\dagger V \mathcal{P}_L \right] d + \varsigma_l \bar{\nu} M_l \mathcal{P}_R l \right\} \\ & - \frac{1}{v} \sum_{\varphi_i^0, f} y_f^{\varphi_i^0} \varphi_i^0 \left[\bar{f} M_f \mathcal{P}_R f \right] + \text{h.c.}, \end{aligned} \quad (8.4)$$

where $\mathcal{P}_{R,L} \equiv \frac{1 \pm \gamma_5}{2}$ are the right-handed and left-handed chirality projectors, M_f the diagonal fermion mass matrices and the couplings of the neutral scalar fields are given by:

$$y_{d,l}^{\varphi_i^0} = \mathcal{R}_{i1} + (\mathcal{R}_{i2} + i \mathcal{R}_{i3}) \varsigma_{d,l}, \quad y_u^{\varphi_i^0} = \mathcal{R}_{i1} + (\mathcal{R}_{i2} - i \mathcal{R}_{i3}) \varsigma_u^*. \quad (8.5)$$

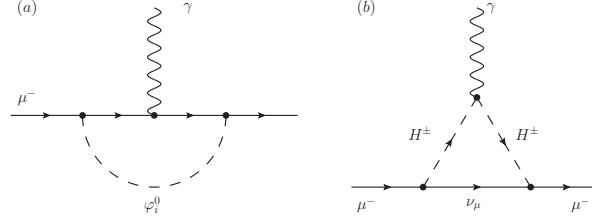
The usual models with natural flavour conservation, based on discrete \mathcal{Z}_2 symmetries, are recovered for particular (real) values of the couplings ς_f [30]. The coupling of a single neutral scalar with a pair of gauge bosons takes the form ($V = W, Z$)

$$g_{\varphi_i^0 VV} = \mathcal{R}_{i1} g_{hVV}^{\text{SM}}, \quad (8.6)$$

which implies $g_{hVV}^2 + g_{HVV}^2 + g_{AVV}^2 = (g_{hVV}^{\text{SM}})^2$. Thus, the strength of the SM Higgs interaction is shared by the three 2HDM neutral bosons. In the CP-conserving limit, the CP-odd field decouples while the strength of the h and H interactions is governed by the corresponding $\cos \tilde{\alpha}$ and $\sin \tilde{\alpha}$ factors. Again, for further details about the interaction Lagrangian as well as the Higgs potential, needed for the calculations in this work, see [43–45].

8.3 One-loop contribution

At the one-loop level, the contribution of the 2HDM extension of the SM to the anomalous magnetic moment of the muon is given by the two well-known diagrams shown in Fig. 8.1. The explicit expressions for these contributions, in terms of the most generic Higgs potential and the A2HDM Yukawa structure, are given by

Figure 8.1: *One-loop contribution to Δa_μ in two-Higgs-doublet models.*

$$\Delta a_\mu^{(a)} = \frac{m_\mu^2}{8\pi^2 v^2} \sum_i \frac{m_\mu^2}{M_{\varphi_i^0}^2} \left[\text{Re}(y_i^{\varphi_i^0})^2 \int_0^1 dx \frac{x^2(2-x)}{(m_\mu^2/M_{\varphi_i^0}^2)x^2 - x + 1} + \text{Im}(y_i^{\varphi_i^0})^2 \int_0^1 dx \frac{-x^3}{(m_\mu^2/M_{\varphi_i^0}^2)x^2 - x + 1} \right], \quad (8.7)$$

for the neutral Higgses and

$$\Delta a_\mu^{(b)} = \frac{m_\mu^2}{8\pi^2 v^2} \left(\frac{m_\mu^2}{M_{H^\pm}^2} \right) |S_l|^2 \int_0^1 dx \frac{x^2(1-x)}{(m_\mu^2/M_{H^\pm}^2)x(1-x) - x}, \quad (8.8)$$

for the charged Higgs. These contributions have been previously analysed in [6, 31, 36, 53–56].

It's a known fact that the two-loop Bar-Zee type diagrams dominate over the one-loop contributions. The two loop contributions have a loop suppression factor of (α/π) but also have an enhancement factor of (M^2/m_μ^2) , where M stands for the mass of heavy particles running in one of the loops: M_{H^\pm} , m_t , $M_{\varphi_i^0}$, etc. This last factor usually dominates over the first one. Furthermore, in the usual \mathcal{Z}_2 models, there is an extra enhancement (suppression) factor from $\tan \beta$ ($\cot \beta$) for some diagrams. In the aligned model there is a lot more freedom to independently enhance or suppress any contribution through the alignment parameters ς_f . We shall see next, that for somewhat large values of these parameters, there are new Barr-Zee contributions that have never been taken into account, and can bring quite sizeable contributions to $(g-2)_\mu$.

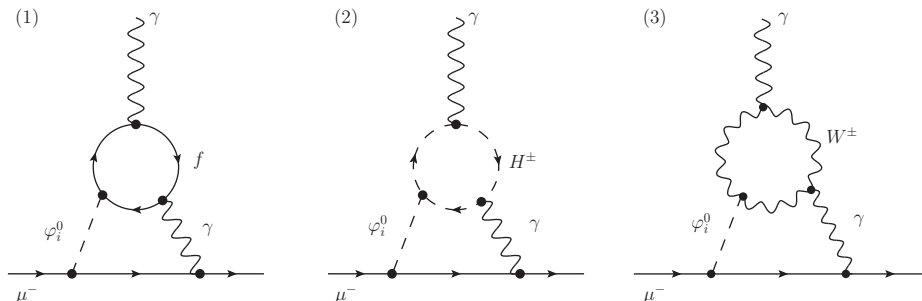


Figure 8.2: *Two-loop Barr-Zee type (with an internal photon) contribution to Δa_μ in two-Higgs-doublet models.*

8.4 Two-loop contribution

The Barr-Zee type contributions with an internal photon, *i.e.*, Fig. 8.2, diagrams (1) and (2), have been extensively analysed within the 2HDM and also in minimal super-symmetry (MSSM) framework [6, 7, 31–42]. Diagram (3) from Fig. 8.2 is also of the Barr-Zee type and could, in principle bring important contributions. Given that the coupling to a pair of gauge bosons of the recently discovered scalar particle is close to the SM prediction [43], one expects the contributions from the remaining scalars to be somewhat suppressed (by a factor \mathcal{R}_{i1}). However, we shall see that this statement is not correct, and that this contribution is quite sizeable.

Similar contributions to the ones shown in Fig. 8.2, but with the internal photon replaced by a Z boson have been also analysed in the literature [33]. These contributions have a relative suppression factor of order 10^{-2} . This factor is in part due to the vectorial couplings of Z to leptons, which are the only ones that survive for both scalar and pseudo-scalar bosons [33], and in part from the Z propagator which introduces a new mass scale M_Z . Therefore we will ignore these contributions in our present analysis.

This is, pretty much, the summary of all the mechanisms that are usually considered in the literature. However, there is no reason a priori to discard other similar Barr-Zee contributions with a charged Higgs H^\pm substituting the neutral scalars φ_i^0 , and a W boson substituting the internal photon¹. These diagrams are illustrated in Fig. 8.3. On one hand, one expects a relative suppression factor with respect to the contributions of the diagrams from Fig. 8.2 due to the propagator

¹Similar contributions, however, with sfermionic loops within the MSSM framework have been previously analysed in [57].

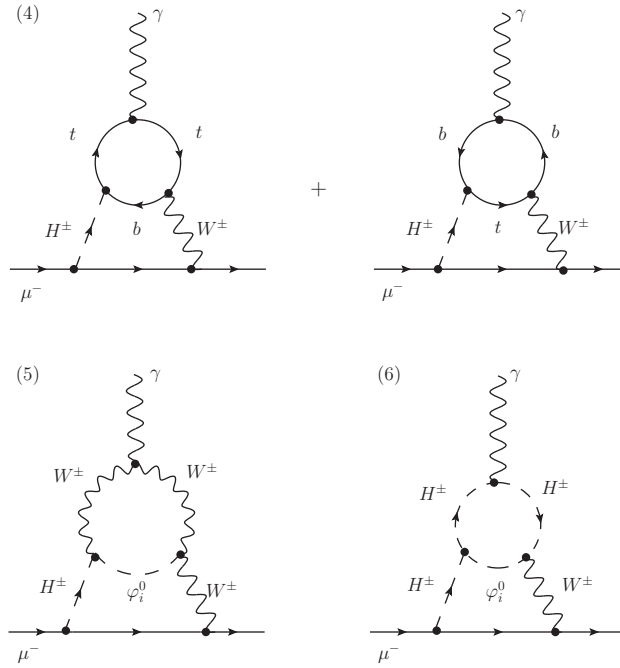


Figure 8.3: Two-loop Barr-Zee type (with a charged Higgs and an internal W boson) contribution to Δa_μ in two-Higgs-doublet models.

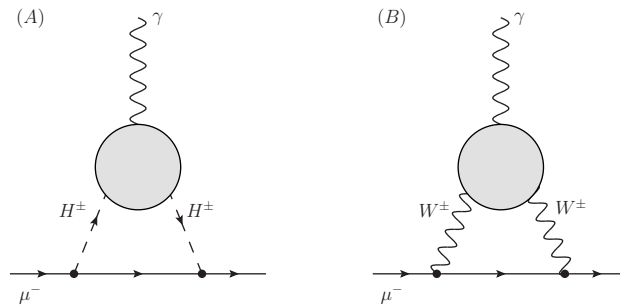


Figure 8.4: Generic two-loop Barr-Zee type contributions, with two internal charged Higgses (left) and two internal W bosons (right), to Δa_μ in two-Higgs-doublet models.

of the W boson (note that in this case we don't have the additional suppression factor due to the gauge boson couplings to leptons, as in the Z case). On the other hand, one must also expect to be able to re-enhance these contributions with the ς_f (or $\tan\beta$) parameters, and therefore, obtain sizeable contributions at least in some regions of the parameter space.

In this analysis we shall calculate the contribution from these new diagrams and demonstrate, that in fact, all of these new sets can bring rather sizeable contributions to the anomalous magnetic moment of the muon in a quite large region of the parameter space. For completeness we shall also present the classical two-loop results in terms of the most generic Higgs potential and in terms of the generic Yukawa texture of the A2HDM.

Before moving on to the next section and presenting the analysis, there are a couple of related cases that are worth discussing. They are shown in Fig. 8.4, where the grey circles stand for the same loop contributions as in Fig. 8.3 (excluding the fermionic loops for diagram (B) which is just a pure SM contribution). The contribution from the first case (A), will have a relative suppression factor m_μ^2/M_W^2 with respect to the contributions of diagrams from Fig. 8.3 so we can safely discard it. The contribution coming from the second set, Fig. 8.4 (B), does not have this suppression factor, thus we can expect, at least in principle, a rather sizeable effect. Details of the the full calculation of this last set of diagrams, together with other technical details are given in appendix 8.A. Roughly one obtains a contribution of $\mathcal{O}(10^{-11})$ which is rather small and we shall not include it in this analysis.

Next we move on to the analysis of the set of diagrams shown in Fig. 8.3 which is the main goal of our paper.

8.4.1 Gauge invariant effective vertices

The calculation of the two-loop Barr-Zee type diagrams can be separated in two parts. We will first calculate the $\varphi_i^0 - \gamma\gamma$ and $H^+ - \gamma W^+$ one-loop effective vertices and obtain analytical and rather simple expressions. With these expressions, the calculation of the second loop becomes quite trivial. The effective vertices can be written in a generic gauge-invariant transverse form:

$$i\Gamma^{\mu\nu} = i(g^{\mu\nu}k \cdot q - k^\mu q^\nu) S + i\epsilon^{\mu\nu\alpha\beta} k_\alpha q_\beta \tilde{S}, \quad (8.9)$$

where q^μ is the momentum of the incoming real photon and k^ν is the momentum of the out-going virtual gauge boson (see Fig. 8.5), and where S and \tilde{S} are scalar form factors. In order to obtain this expression we have considered the

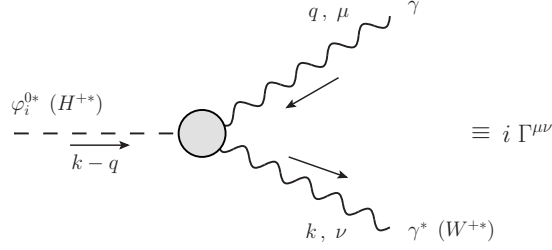


Figure 8.5: Feynman rule for the gauge-invariant one loop effective vertices $\varphi_i^0 - \gamma\gamma$ and $H^+ - W^+\gamma$.

most generic Lorentz structure for the $\Gamma^{\mu\nu}$ vertex, and we have imposed the electromagnetic current conservation $q_\mu \Gamma^{\mu\nu} = 0$. All terms proportional to q^μ have also been eliminated as they cancel when contracted with the polarization vector of the photon. As the W boson is off-shell, in the actual calculation of the effective vertex there will also appear some other Lorentz structures than the ones shown in (8.9). However in some cases, these gauge-dependent contributions vanish when calculating the second loop or they are cancelled by some other non Barr-Zee terms, as it is nicely shown in [58]. If this was not the case, when summing the proper non Barr-Zee contributions to the gauge dependent Barr-Zee terms, the result must be gauge independent. As the gauge dependence from the Barr-Zee terms is cancelled by other sub-dominant topologies, we also expect this contribution to be sub-dominant. Therefore, we shall discard these terms in our analysis.

The gauge independent contribution from each set represented by the generic topologies in Fig. 8.2 and Fig. 8.3 is transverse by itself, *i.e.*, of the form given in (8.9); we can therefore decompose the results into eight separate contributions. For the $\varphi_i^0 - \gamma\gamma$ effective vertex $S = S_{(1)} + S_{(2)} + S_{(3)}$ and $\tilde{S} = \tilde{S}_{(1)}$; as for the $H^+ - \gamma W^+$ vertex we have $S = S_{(4)} + S_{(5)} + S_{(6)}$ and $\tilde{S} = \tilde{S}_{(6)}$. Note that the only contributions to the $\epsilon^{\mu\nu\alpha\beta} k_\alpha q_\beta$ structure come from the fermionic loops. Furthermore, one can adopt our strategy from [45], and further simplify the calculations of $S_{(j)}$ by only considering the terms that contribute to the structure $k^\mu q^\nu$.

It is worth mentioning the following technical detail. When performing the calculations for the first loop, after introducing the Feynman parametrization and after integrating over the four-momentum, one obtains a denominator similar to

$$[k^2 x(x-1) + M_a^2 x + M_b^2(1-x) + k \cdot q 2yx(1-x)]^{-1}, \quad (8.10)$$

where $M_{a,b}$ are the masses of *heavy* particles running in the loop, *i.e.*, M_W , m_t , M_{H^\pm} , etc. It is a very common assumption that the photon is “soft” so one can ignore the $k \cdot q$ term as a good approximation. This term, in fact, can be safely ignored without making any assumptions on the “softness” of the photon. Keeping track of this term, one can observe that it simply vanishes when calculating the second loop integral. However, this happens accidentally for diagrams (1) to (6); for the $WW\gamma$ effective vertices calculated in appendix 8.A, this is not always the case. Thus, having checked that these terms play no role in our present case, we will discard them already at the one-loop level in order to give simpler and more elegant expressions for the form factors $S_{(i)}$ and $\tilde{S}_{(i)}$. After performing the four-momentum loop integral we obtain the following expressions for the scalar form-functions

$$S_{(1)} = \sum_{i,f} \frac{\alpha m_f^2}{\pi v} Q_f^2 N_C^f \operatorname{Re}(y_f^{\varphi_i^0}) \int_0^1 dx \frac{2x(1-x) - 1}{k^2 x(1-x) - m_f^2}, \quad (8.11)$$

$$\tilde{S}_{(1)} = \sum_{i,f} \frac{\alpha m_f^2}{\pi v} Q_f^2 N_C^f \operatorname{Im}(y_f^{\varphi_i^0}) \int_0^1 dx \frac{1}{k^2 x(1-x) - m_f^2}, \quad (8.12)$$

$$S_{(2)} = \sum_i \frac{\alpha v}{2\pi} \lambda_{\varphi_i^0 H^+ H^-} \int_0^1 dx \frac{x(x-1)}{k^2 x(1-x) - M_{H^\pm}^2}, \quad (8.13)$$

for the $\varphi_i^0 - \gamma\gamma$ vertices with a fermionic or a charged Higgs loop, in agreement with [41]. As for the third diagram, we find

$$S_{(3)} = \sum_i \frac{\alpha}{2\pi v} \mathcal{R}_{i1} \int_0^1 dx \frac{M_W^2 x(3x(4x-1) + 10) - M_{\varphi_i^0}^2 x(1-x)}{k^2 x(1-x) - M_W^2}. \quad (8.14)$$

The new gauge-invariant scalar form factors coming from diagrams (4) to (6) are given by:

$$S_{(4)} = \frac{\alpha N_C |V_{tb}|^2}{2\pi v s_w} \int_0^1 dx \times \frac{[Q_t x + Q_b(1-x)] [\varsigma_u m_t^2 x^2 - \varsigma_d m_b^2 (1-x)^2]}{k^2 x(1-x) - m_b^2 (1-x) - m_t^2 x}, \quad (8.15)$$

$$\begin{aligned} \tilde{S}_{(4)} = & i \frac{\alpha N_C |V_{tb}|^2}{2\pi v s_w} \int_0^1 dx \\ & \times \frac{[Q_t x + Q_b(1-x)] [-\varsigma_u m_t^2 x + \varsigma_d m_b^2(x-1)]}{k^2 x(1-x) - m_b^2(1-x) - m_t^2 x}, \end{aligned} \quad (8.16)$$

$$\begin{aligned} S_{(5)} = & \frac{\alpha}{4\pi v s_w} \sum_i \mathcal{R}_{i1} (\mathcal{R}_{i2} - i\mathcal{R}_{i3}) \int_0^1 dx x^2 \\ & \times \frac{(M_{H^\pm}^2 + M_W^2 - M_{\varphi_i^0}^2)(1-x) - 4M_W^2}{k^2 x(1-x) - M_W^2 x - M_{\varphi_i^0}^2(1-x)}, \end{aligned} \quad (8.17)$$

$$\begin{aligned} S_{(6)} = & \frac{\alpha v}{4\pi s_w} \sum_i \lambda_{\varphi_i^0 H^+ H^-} (\mathcal{R}_{i2} - i\mathcal{R}_{i3}) \int_0^1 dx \\ & \times \frac{x^2(x-1)}{k^2 x(1-x) - M_{H^\pm}^2 x - M_{\varphi_i^0}^2(1-x)}, \end{aligned} \quad (8.18)$$

with $s_w \equiv \sin \theta_w$, and θ_w the weak mixing angle.

8.4.2 Contributions to Δa_μ

Using the effective vertices from the previous section for calculating the second loop, ignoring suppressed terms proportional to higher powers of m_μ^2/M^2 (with M a *heavy* mass) in the numerator and the muon mass in the denominator, we obtain the various contributions to the anomalous magnetic moment of the muon. The first two contributions are the well known classical results [6, 7, 31–41]

$$\begin{aligned} \Delta a_\mu^{(1)} = & \sum_{i,f} \frac{\alpha m_\mu^2}{4\pi^3 v^2} N_C^f Q_f^2 \left[\text{Re}(y_f^{\varphi_i^0}) \text{Re}(y_l^{\varphi_i^0}) \mathcal{F}^{(1)}\left(\frac{m_f^2}{M_{\varphi_i^0}^2}\right) \right. \\ & \left. + \text{Im}(y_f^{\varphi_i^0}) \text{Im}(y_l^{\varphi_i^0}) \tilde{\mathcal{F}}^{(1)}\left(\frac{m_f^2}{M_{\varphi_i^0}^2}\right) \right], \end{aligned} \quad (8.19)$$

$$\Delta a_\mu^{(2)} = \sum_i \frac{\alpha m_\mu^2}{8\pi^3 M_{\varphi_i^0}^2} \text{Re}(y_l^{\varphi_i^0}) \lambda_{\varphi_i^0 H^+ H^-} \mathcal{F}^{(2)}\left(\frac{M_{H^\pm}^2}{M_{\varphi_i^0}^2}\right). \quad (8.20)$$

The third contribution simply reads

$$\Delta a_\mu^{(3)} = \sum_i \frac{\alpha m_\mu^2}{8\pi^3 v^2} \operatorname{Re}(y_l^{\varphi_i^0}) \mathcal{R}_{i1} \mathcal{F}^{(3)}\left(\frac{M_W^2}{M_{\varphi_i^0}^2}\right). \quad (8.21)$$

As for the new contributions, given by the last three sets in Fig. 8.3, their contributions are given by

$$\begin{aligned} \Delta a_\mu^{(4)} &= \frac{\alpha m_\mu^2 N_C |V_{tb}|^2}{32\pi^3 s_w^2 v^2 (M_{H^\pm}^2 - M_W^2)} \int_0^1 dx \left[Q_t x + Q_b(1-x) \right] \\ &\quad \times \left[\operatorname{Re}(\varsigma_d \varsigma_l^*) m_b^2 x(1-x) + \operatorname{Re}(\varsigma_u \varsigma_l^*) m_t^2 x(1+x) \right] \\ &\quad \times \left[\mathcal{G}\left(\frac{m_t^2}{M_{H^\pm}^2}, \frac{m_b^2}{M_{H^\pm}^2}\right) - \mathcal{G}\left(\frac{m_t^2}{M_W^2}, \frac{m_b^2}{M_W^2}\right) \right], \end{aligned} \quad (8.22)$$

$$\begin{aligned} \Delta a_\mu^{(5)} &= \frac{\alpha m_\mu^2}{64\pi^3 s_w^2 v^2 (M_{H^\pm}^2 - M_W^2)} \sum_i \operatorname{Re} \left[\varsigma_l^* \mathcal{R}_{i1} (\mathcal{R}_{i2} - i\mathcal{R}_{i3}) \right] \\ &\quad \times \int_0^1 dx x^2 \left[(M_{H^\pm}^2 + M_W^2 - M_{\varphi_i^0}^2)(1-x) - 4M_W^2 \right] \\ &\quad \times \left[\mathcal{G}\left(\frac{M_W^2}{M_{H^\pm}^2}, \frac{M_{\varphi_i^0}^2}{M_{H^\pm}^2}\right) - \mathcal{G}\left(1, \frac{M_{\varphi_i^0}^2}{M_W^2}\right) \right], \end{aligned} \quad (8.23)$$

$$\begin{aligned} \Delta a_\mu^{(6)} &= \frac{\alpha m_\mu^2}{64\pi^3 s_w^2 (M_{H^\pm}^2 - M_W^2)} \sum_i \operatorname{Re} \left[\varsigma_l^* (\mathcal{R}_{i2} - i\mathcal{R}_{i3}) \right] \lambda_{\varphi_i^0 H^+ H^-} \\ &\quad \times \int_0^1 dx x^2 (x-1) \left[\mathcal{G}\left(1, \frac{M_{\varphi_i^0}^2}{M_{H^\pm}^2}\right) - \mathcal{G}\left(\frac{M_{H^\pm}^2}{M_W^2}, \frac{M_{\varphi_i^0}^2}{M_W^2}\right) \right]. \end{aligned} \quad (8.24)$$

We can also consider the contribution from a lepton and a neutrino loop by replacing $Q_t \rightarrow 0$, $m_t \rightarrow 0$, $Q_b \rightarrow -1$, $m_b \rightarrow m_l$, $\varsigma_d \rightarrow \varsigma_l$ and $\varsigma_u \rightarrow 0$ in (8.22) and where m_l is the mass of the considered lepton. However, these contributions turn out to be very suppressed due to the smallness of the lepton masses and we shall ignore them in our present analysis. The needed loop functions are given

by:

$$\mathcal{F}^{(1)}(\omega) = \frac{\omega}{2} \int_0^1 dx \frac{2x(1-x) - 1}{\omega - x(1-x)} \ln \left(\frac{\omega}{x(1-x)} \right), \quad (8.25)$$

$$\tilde{\mathcal{F}}^{(1)}(\omega) = \frac{\omega}{2} \int_0^1 dx \frac{1}{\omega - x(1-x)} \ln \left(\frac{\omega}{x(1-x)} \right), \quad (8.26)$$

$$\mathcal{F}^{(2)}(\omega) = \frac{1}{2} \int_0^1 dx \frac{x(x-1)}{\omega - x(1-x)} \ln \left(\frac{\omega}{x(1-x)} \right), \quad (8.27)$$

$$\mathcal{F}^{(3)}(\omega) = \frac{1}{2} \int_0^1 dx \frac{x[3x(4x-1) + 10]\omega - x(1-x)}{\omega - x(1-x)} \ln \left(\frac{\omega}{x(1-x)} \right), \quad (8.28)$$

and

$$\mathcal{G}(\omega^a, \omega^b) = \frac{\ln \left(\frac{\omega^a x + \omega^b (1-x)}{x(1-x)} \right)}{x(1-x) - \omega^a x - \omega^b (1-x)}. \quad (8.29)$$

8.5 Phenomenology

In the present analysis we neglect possible CP-violating effects; *i.e.*, we consider a CP-conserving scalar potential and real alignment parameters ζ_f . The fermionic couplings of the neutral scalar fields are then given, in units of the SM Higgs couplings, by

$$\begin{aligned} y_f^h &= \cos \tilde{\alpha} + \zeta_f \sin \tilde{\alpha}, & y_{d,l}^A &= i \zeta_{d,l}, \\ y_f^H &= -\sin \tilde{\alpha} + \zeta_f \cos \tilde{\alpha}, & y_u^A &= -i \zeta_u, \end{aligned} \quad (8.30)$$

and the couplings to a pair of gauge bosons (8.6) are simply ($\kappa_V^{\varphi_i^0} \equiv g_{\varphi_i^0 V V} / g_{h V V}^{\text{SM}}$, $V = W, Z$)

$$\begin{aligned} \kappa_V^h &= \mathcal{R}_{11} = \cos \tilde{\alpha}, & \kappa_V^H &= \mathcal{R}_{21} = -\sin \tilde{\alpha}, \\ \kappa_V^A &= \mathcal{R}_{31} = 0. \end{aligned} \quad (8.31)$$

We shall separate the phenomenological analysis in two parts. For the first part we will analyse the individual contributions from the various $\Delta a_\mu^{(i)}$ factors for different coupling and mass configurations. As for the second part we shall sum all these contributions choosing a few relevant scenarios compatible with collider and flavour bounds and also with constraints from the oblique parameters. Also, we will identify the lightest CP-even Higgs with h and take $M_h = 125$ GeV for the whole analysis.

8.5.1 Individual $\Delta a_\mu^{(i)}$ contributions

As we know from global fits to the LHC data, the Yukawa couplings of the discovered scalar boson are SM-like, however with quite large experimental errors. The coupling of h to two gauge bosons is constrained by $|\cos \tilde{\alpha}| > 0.8$ at 95% CL [43]. Here we shall always take the positive solution, $\cos \tilde{\alpha} > 0$ (flipping the sign of $\cos \tilde{\alpha}$ leads to an equivalent solution with a sign flip of the couplings ζ_f). Choosing the positive solution for $\cos \tilde{\alpha}$, the top Yukawa coupling must also be positive. We shall vary it in the range $y_u^h \in [0.8, 1.2]$. As we know, at least for now, there is no experimental sensitivity to the relative sign of the down-type or leptonic Yukawas with respect to the up-type Yukawas. Therefore we shall be less restrictive with the $y_{d,l}^h$ couplings and allow them to vary in the range $y_{d,l}^h \in [-1.5, 1.5]$. As for the alignment parameters, we will vary them as follows: $-1 < \zeta_u < 1$ compatible with all flavour constraints and direct charged Higgs searches [43] for a broad range of the charged Higgs mass, and $-50 < \zeta_{d,l} < 50$ to safely avoid the non-perturbative regime. We shall also vary y_f^H in the same regions as the ζ_f parameters (in the limit $\cos \tilde{\alpha} \rightarrow 1$ we obtain $y_f^H = \zeta_f$). The remaining parameters are the couplings of the neutral scalars to a pair of charged Higgses. In order to safely satisfy the perturbativity bounds [44] for a broad range of M_{H^\pm} , we will impose $|\lambda_{\varphi_i^0 H^+ H^-}| < 5$.

The one-loop well known contribution from the various scalars are shown in Fig. 8.6. The contribution of h is small and positive for the whole considered range of the coupling $|y_l^h|$. The contribution of H is also positive and, its contribution can be of some significance only for large values of $|y_l^H|$ and small values of M_H simultaneously. The contribution of the CP-odd scalar is negative and it is only relevant for large values of $|\zeta_l|$ and low values of its mass, similar to the previous case. As for the charged Higgs contribution, it is always negative and very small, thus irrelevant, at the one loop level.

The two-loop results are presented next. The contribution of h , associated with a top-quark loop, to $\Delta a_\mu^{(1)}$ is shown in Fig. 8.7 (top-left). It is positive

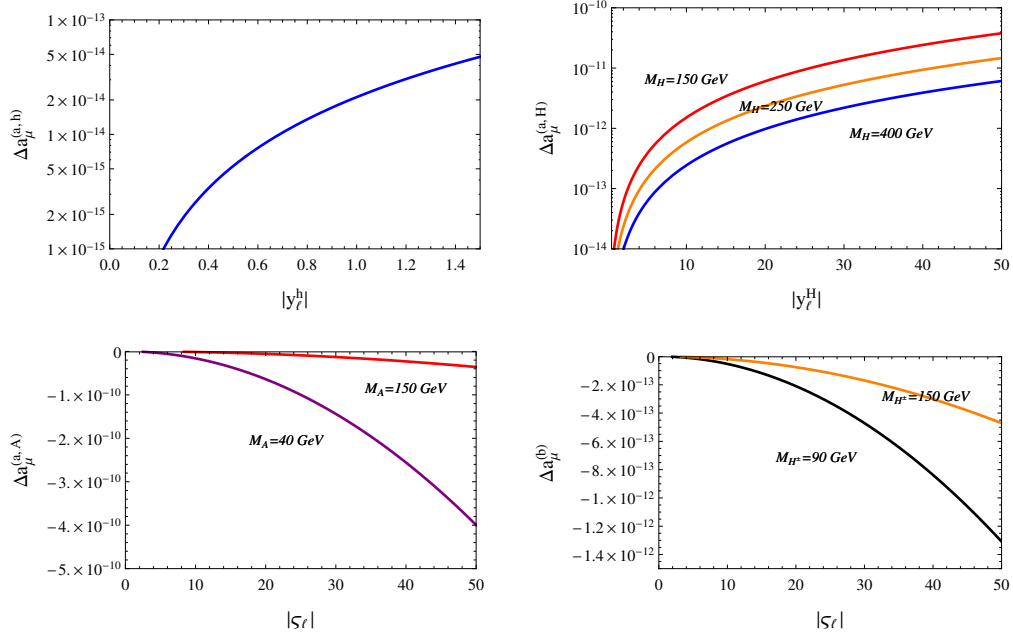


Figure 8.6: One-loop scalar contributions to Δa_μ as functions their couplings to fermions from h (top-left), H (top-right), A (bottom-left) and H^\pm (bottom-right).

for $y_l^h y_u^h < 0$. The contribution of the same scalar h associated with bottom and tau loops is much smaller, of $\mathcal{O}(10^{-13})$ or less for the whole considered parameter space, and is not shown here. The contribution of H for different mass configurations and for different fermionic loops is also shown in Fig. 8.7. This contribution is proportional to the y_l^H coupling which can be large. Thus it turns out to be non-negligible even for the sub-dominant bottom-quark and tau-lepton loops. The top-quark loop contribution can be large for all considered mass settings as long as y_l^H is large, and it is positive for $y_l^H y_u^H < 0$, as we can observe in Fig. 8.7 (top-right). The bottom-quark loop contribution can be additionally enhanced by the coupling y_d^H , thus, it can overcome the mass suppression. This contribution is positive for $y_l^H y_d^H < 0$, see Fig. 8.7 (bottom-left). Similar considerations about the enhancement factor $(y_l^H)^2$ can be made for the tau-lepton part, however this contribution is always negative, as shown in the bottom-right panel of Fig. 8.7.

The contribution of the CP-odd scalar to $\Delta a_\mu^{(1)}$ is probably the most interesting yet. It has been extensively analysed in previous works [6, 7, 31–37]. For low values of its mass and large values of $s_{d,l}$ it can reach values within or close to

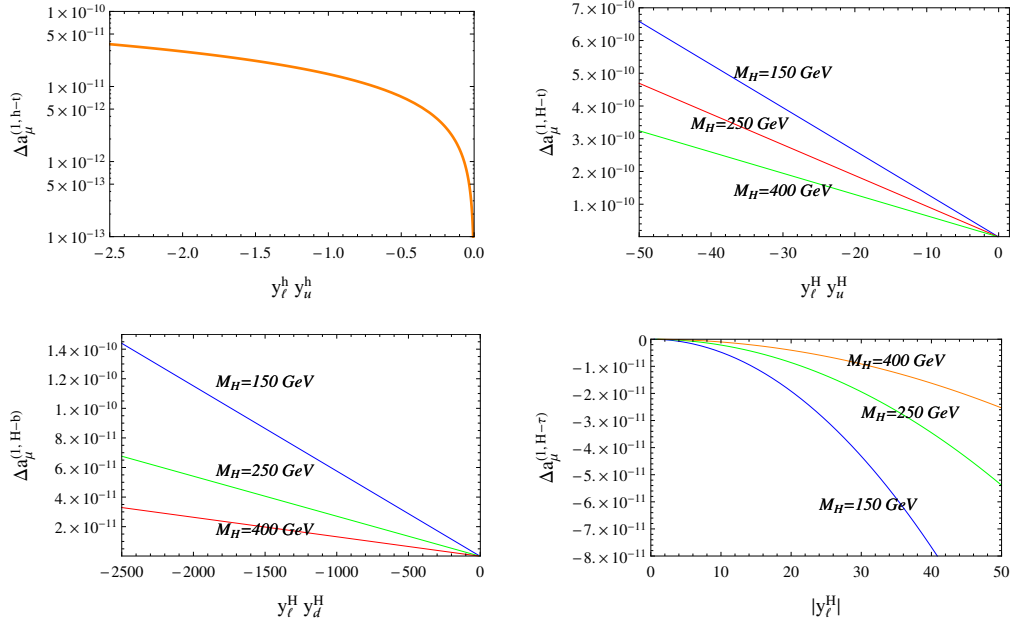


Figure 8.7: Contributions to $\Delta a_\mu^{(1)}$ from h (top-left) and H (top-right) with an associated top-quark loop, and from H with an associated bottom-quark (bottom-left) and tau-lepton (bottom-right) loop, as functions of their couplings to fermions.

the two-sigma region of Δa_μ^{exp} , as it is plotted in Fig. 8.8. Its value is positive for $s_u s_l < 0$ ($s_d s_l > 0$) for the top (bottom) quark loop contribution and is always positive for the tau loop contribution. This last case is not shown. It is worth mentioning, however that the tau loop contribution is somewhat larger than the (absolute value of the) bottom contribution. Even if the tau-lepton has a relative mass suppression, the bottom-quark has a charge suppression that is in general larger.

For $\Delta a_\mu^{(2)}$ we only have two possible contributions, from h and H (in the CP-conserving limit the vertex AH^+H^- vanishes [44]). The contribution of the light scalar h is relatively small for the whole considered parameter space, Fig. 8.9 (left) and that is due to the fact that $y_l^h \in [-1.5, 1.5]$ whereas y_l^H can be much larger. The contribution of H can be quite large depending on the configuration of the masses (M_{H^\pm} , M_H) (GeV). It reaches its largest value for low masses of both M_{H^\pm} and M_H and large values of the product of the couplings $y_l^H \lambda_{HH^+H^-}$. However, even for lower values of the couplings but with low masses (or large

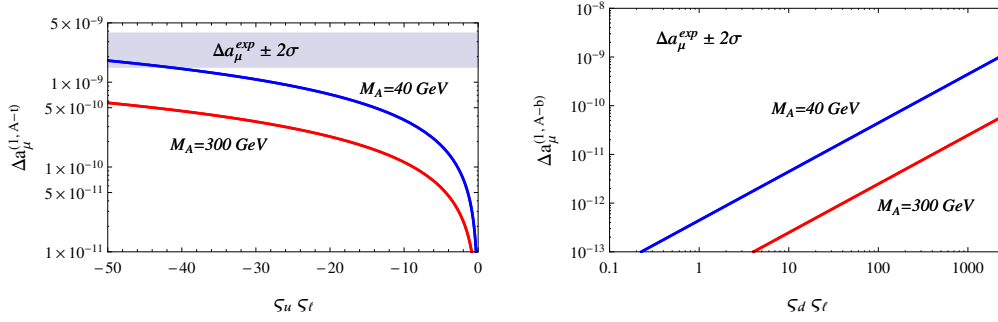


Figure 8.8: Contributions to $\Delta a_\mu^{(1)}$ from the CP-odd scalar A , associated with a top-quark (left) and bottom-quark (right) loop, as functions its couplings to fermions.

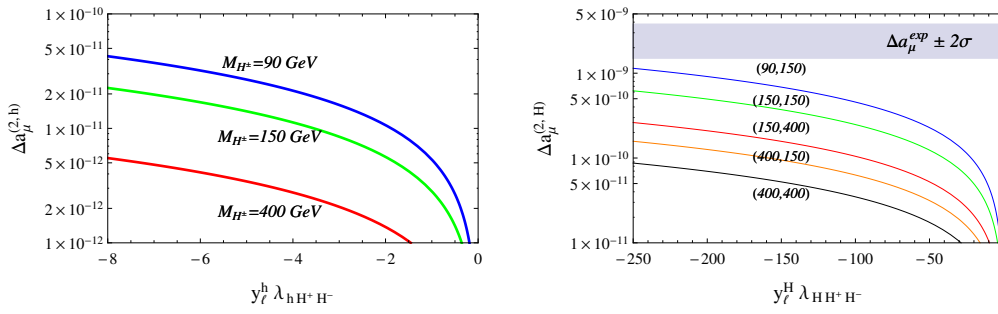


Figure 8.9: Contributions to $\Delta a_\mu^{(2)}$ from $\varphi_i^0 = h, H$ as functions of the product of the couplings $y_l^{\varphi_i^0} \lambda_{\varphi_i^0 H^+ H^-}$ for various charged Higgs masses (left) and for various configurations of (M_{H^\pm}, M_H) (GeV) (right).

masses and large couplings) the contribution can be non-negligible. For details see Fig. 8.9 (right).

The next contribution we focus on is $\Delta a_\mu^{(3)}$. The contribution from the light scalar is small, of $\mathcal{O}(10^{-11})$ or less (after subtracting the SM), therefore we can safely neglect it. The H contribution however, is non-negligible. It reaches higher values (and it is positive) for low values of M_H and large positive values of the product $\mathcal{R}_{21} y_l^H (= \sin^2 \tilde{\alpha} - \varsigma_l \sin \tilde{\alpha} \cos \tilde{\alpha})$ as it is plotted in Fig. 8.10 (left). As we have already mentioned before, this diagram should not be neglected, as it can introduce sizeable effects for some regions of the parameter space.

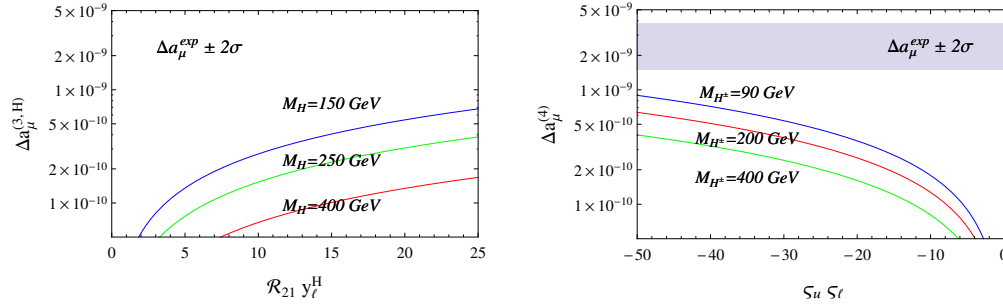


Figure 8.10: Contribution to $\Delta a_\mu^{(3)}$ from H (left) as function of the product of the couplings $\mathcal{R}_{21} y_t^H$ for various mass configurations. Two-loop dominant contribution from the top-bottom quark loops to $\Delta a_\mu^{(4)}$ (right).

Now we move on to the analysis of the charged Higgs contributions of the Barr-Zee type diagrams (Fig. 8.3), which is the main goal of this paper. It is obvious from Fig. 8.10 (right) that the $\Delta a_\mu^{(4)}$ contribution is non-negligible for a large region of the parameter space, except for very small values of the product $|\zeta_u \zeta_t|$. For a charged Higgs with a low mass, say 90 GeV, and large negative values of $\zeta_t \zeta_u$ this contribution alone can explain around 35 % of the measured discrepancy. This looks very appealing, because with the exception of a very light CP-odd scalar, the previous contributions cannot reach such large values. For the plot shown in Fig. 8.10 (right) we have chosen $\zeta_d = 0$. However, a variation of ζ_d in its allowed interval $[-50, 50]$ only produces a shift in the plotted values of order 10^{-12} or less. This is obviously due to a relative suppression factor m_b^2/m_t^2 and therefore this contribution can be safely ignored.

Last, contributions $\Delta a_\mu^{(5)}$ and $\Delta a_\mu^{(6)}$ are shown in Fig. 8.11 and Fig. 8.12. They are a little bit smaller, however they can reach values up to 10^{-10} . Again this happens, for small mass configurations and large values of the corresponding couplings. We can see in Fig. 8.11 that both h and H contributions can be very similar, however, they cannot be simultaneously positive (if the product of the three couplings $\zeta_l \mathcal{R}_{i1} \mathcal{R}_{i2}$ is chosen positive for one scalar, for the other must necessarily be negative). On the other hand, both h and H contributions from $\Delta a_\mu^{(6)}$ can be simultaneously positive, and of similar value. Thus, when summed up they can play an important role in the total value of Δa_μ .

We have proven thus, that these new Barr-Zee contributions must not be ignored, as they might sizeably modify the theoretical prediction for this observable within the 2HDM framework.

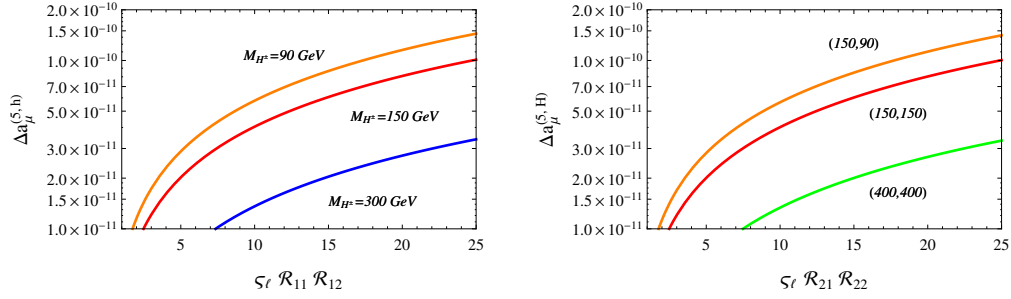


Figure 8.11: Contributions to $\Delta a_\mu^{(5)}$ from $\varphi_i^0 = h, H$ as functions of the product of the couplings $\varsigma_l \mathcal{R}_{i1} \mathcal{R}_{i2}$ for various charged Higgs masses (left) and for various configurations of (M_H, M_{H^\pm}) (GeV) (right).

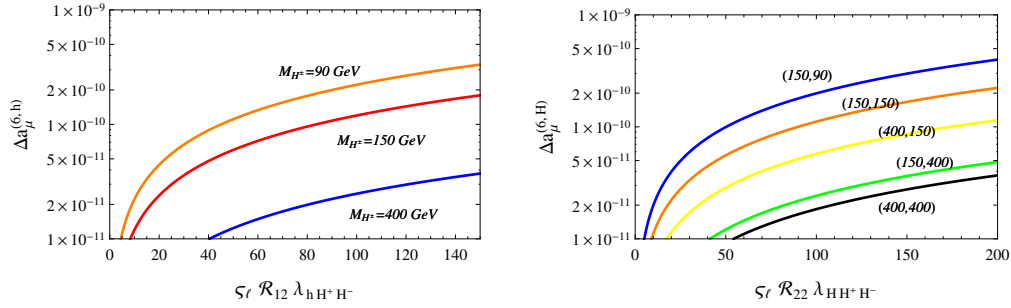


Figure 8.12: Contributions to $\Delta a_\mu^{(6)}$ from $\varphi_i^0 = h, H$ as functions of the product of the couplings $\varsigma_l \mathcal{R}_{i2} \lambda_{\varphi_i^0 H^+ H^-}$ for various charged Higgs masses (left) and for various configurations of (M_H, M_{H^\pm}) (GeV) (right).

8.5.2 Total contribution to $(g - 2)_\mu$

Thus, we have seen that the dominant contributions of the new Bar-Zee type diagrams come from the mechanisms (3) (Fig. 8.2) and (4) (Fig. 8.3). All the other *new* contributions are sub-dominant. Now, it is interesting to put all these results together, and show the total effect on Δa_μ for a few relevant scenarios. In Fig. 8.13 (left panel) we show Δa_μ as a function of ς_l for positive values of this coupling and for a few scenarios given by $\cos \tilde{\alpha} = 0.9$, $\varsigma_u = -0.8$, $\varsigma_d = -20$, $M_h = 125$ GeV, $\lambda_{hH^+H^-} = 0$, $\lambda_{hH^+H^-} = -5$. The masses (in GeV) of the remaining scalars are chosen the following way: $M_H = M_{H^\pm} = M_A = 250$ (lower orange curve), 150 (middle blue curve), $M_H = M_{H^\pm} = 150$ and $M_A = 50$ (upper green curve). Similar to the previous case, but this time for negative values of ς_l , in the right

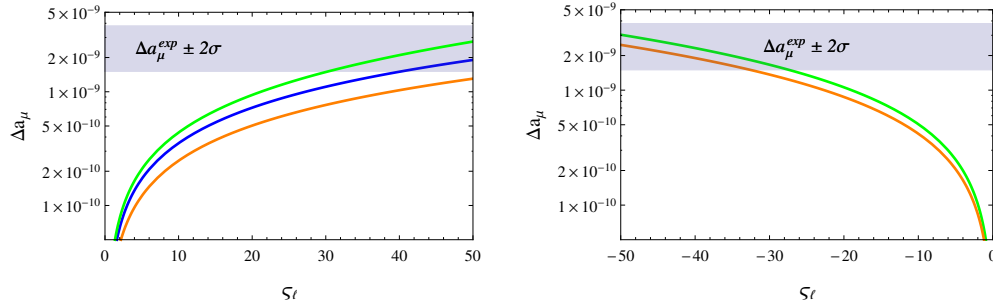


Figure 8.13: Total Δa_μ contribution as a function of ς_l for different coupling and mass configurations.

panel we have chosen the following parameter configuration: $\cos \tilde{\alpha} = 0.9$, $\varsigma_u = 0.8$, $\varsigma_d = 2$, $M_h = 125$ GeV, $\lambda_{hH^+H^-} = 0$, $\lambda_{hH^+H^-} = 5$ and $M_H = M_{H^\pm} = 250$ GeV and $M_A = 40$ GeV (upper green curve) or $M_H = M_{H^\pm} = 350$ GeV and $M_A = 50$ GeV (lower orange curve). As expected, from the analysis of the various $\Delta a_\mu^{(i)}$ individual contributions, one obtains a significant contribution for low masses of the scalars (especially for low M_A) and large couplings. We can also observe that in some cases we do not need the maximum allowed value of $|\varsigma_l|$ in order to reach the two-sigma region of Δa_μ^{exp} ; a value around $|\varsigma_l| \sim 30$ might just be enough.

8.6 Conclusions

It is a common belief that only a restrained number of diagrams, namely (1) and (2) from Fig. 8.2, can significantly contribute to Δa_μ in 2HDMs and in most of the previous analyses [6, 7, 31–37], a CP-odd scalar in the low-mass range is enough to explain, or reduce, the discrepancy between theory and experiment. In this work we have shown that the extra degrees of freedom of the A2HDM given by the ς_f parameters, can also explain this discrepancy in some region of the parameter space, and if not, they can significantly reduce it in most cases. We have also seen that the W loop contribution associated with a heavy scalar H (diagram (3) from Fig. 8.2) can bring important contributions even if it has a global suppression factor \mathcal{R}_{21} . This contribution is positive for negative values of ς_l . The most interesting case is, however, the fermionic loop contribution (diagrams (4) from Fig. 8.3) with the dominant part given by the top-quark. The last two diagrams (5) and (6) are also interesting, as they can sum up to an $\mathcal{O}(10\%)$ of the total contribution. Also, we have seen that not all of these

new contributions can be made simultaneously positive, however the total Δa_μ is positive for most parameter configurations.

A highly interesting scenario, that we defer for future work, is to consider CP-violating effects. The imaginary part of the parameters of the potential and especially of the Yukawa sector might be able to bring somewhat sizeable effects.

8.A $WW\gamma$ effective vertex contribution to $(g - 2)_\mu$

In this section we present the explicit calculation of the contributions from Fig. 8.4 (B) to $(g - 2)_\mu$. The 2HDM contributions to the one-loop $WW\gamma$ effective vertex are shown in Fig. 8.14, where last diagram stands for the one-loop renormalization counter-term. For this calculation we have followed the renormalization prescription described in [59]. Following this prescription one does not need to renormalize the gauge-fixing Lagrangian. Thus, we simply worked in the Feynman gauge [44]. Working in this gauge, one also needs to take into account $WG^\pm\gamma$ (Fig. 8.15) and $G^\pm G^\mp\gamma$ effective vertices. The last set ($G^\pm G^\mp\gamma$) will give rise to contributions to the anomalous magnetic moment that will have a relative suppression factor of m_μ^2/M_W^2 (just as in case (A) of Fig. 8.4 for the $H^\pm H^\mp\gamma$ effective vertex), and therefore will not be taken into account.

The one-loop counterterms for the needed $WW\gamma$ and $WG\gamma$ vertices are given by

$$i \Gamma_\delta^{\rho\mu\nu} = i e \Gamma^{\rho\mu\nu} \delta_W, \quad i \Gamma_\delta^{\mu\nu} = i e g^{\mu\nu} \frac{1}{2} (\delta_W + \delta_{G^\pm} + \delta_M), \quad (8.32)$$

where $i e \Gamma^{\rho\mu\nu}$ is the tree-level $WW\gamma$ vertex and where we have defined the G^\pm , W^μ and M_W^2 renormalization constants as

$$Z_W = 1 + \delta_W, \quad Z_{G^\pm} = 1 + \delta_{G^\pm}, \quad Z_M = 1 + \delta_M. \quad (8.33)$$

The needed W and G^\pm self-energy diagrams needed for the calculation of these counter-terms are shown in Fig. 8.16. As we can see, no tadpole diagrams are present. At one-loop level, using the renormalization prescription from [59], tadpole diagrams do not contribute to the W mass renormalization. On the other hand, they do not contribute to the wave-function renormalization either as they do not generate any four-momentum dependence. Thus, for our present calculation we need not to worry about tadpoles.

One last technical issue is the $W - G^\pm$ mixing that occurs at one-loop level. The gauge fixing Lagrangian cancels exactly the tree-level mixing between the

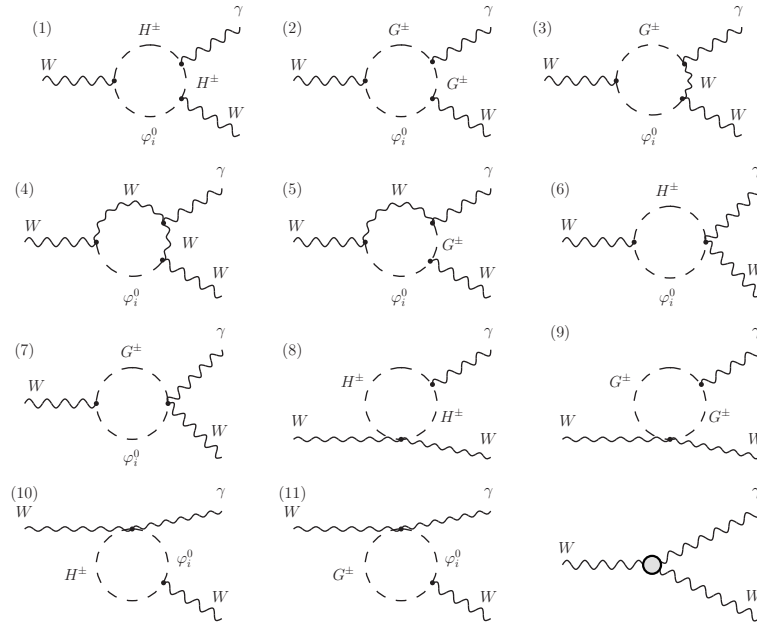


Figure 8.14: One-loop contributions to the $WW\gamma$ effective vertex. The last diagram stands for the one-loop counter-term.

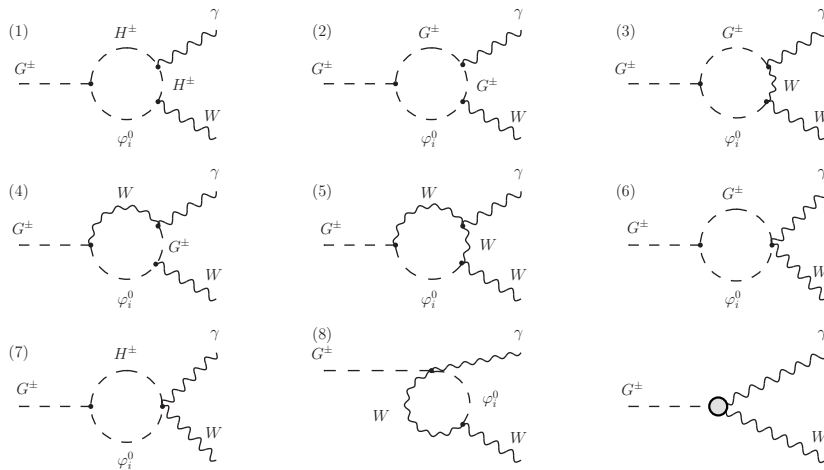


Figure 8.15: One-loop contributions to the $WG^\pm\gamma$ effective vertex. The last diagram stands for the one-loop counter-term.

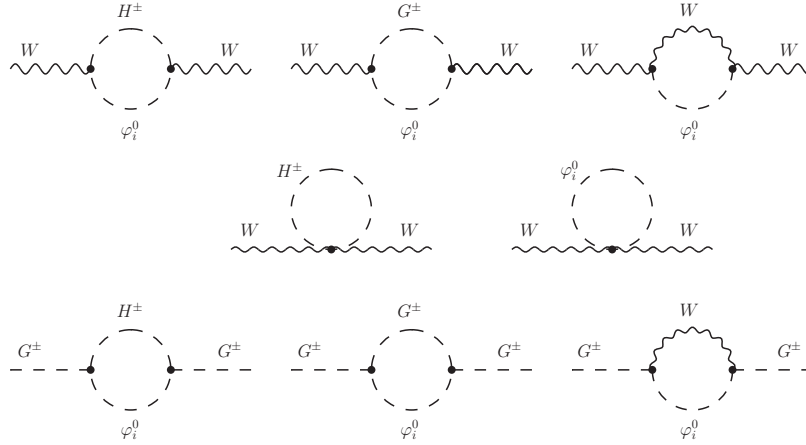


Figure 8.16: One-loop W self energy diagrams needed for the vector boson wave-function and mass renormalization, and G^\pm self-energy diagrams needed for the charged Goldstone boson wave-function renormalization.

$$\begin{aligned}
 & \partial^\mu \partial^\nu \left[\text{Wavy } W_\mu \text{ --- } \text{Grey Circle} \text{ --- } \text{Wavy } W_\nu \right] + M_W^2 \left[\text{Dashed } G^\pm \text{ --- } \text{Grey Circle} \text{ --- } \text{Dashed } G^\pm \right] \\
 & + M_W \partial^\mu \left[\text{Wavy } W_\mu \text{ --- } \text{Grey Circle} \text{ --- } \text{Dashed } G^\pm \right] + M_W \partial^\mu \left[\text{Dashed } G^\pm \text{ --- } \text{Grey Circle} \text{ --- } \text{Wavy } W_\mu \right] = 0
 \end{aligned}$$

Figure 8.17: One-loop doubly contracted Ward identity. The grey circles stand for the one-loop self energies.

gauge and Goldstone bosons generated by the covariant derivatives. This mixed term, when renormalizing the Lagrangian is in fact, counter-term for the $W - G^\pm$ self-energies, as it is nicely explained in [59]. For this calculation, however, we don't need to worry about this mixture. As we are going to ignore the propagator corrections, and these corrections are related to the $W - G^\pm$ mixing through the Ward identities (for example the doubly contacted identity shown diagrammatically in Fig. 8.17), we are also going to ignore the one-loop mixing in order to preserve these identities.

Using the on-shell scheme, working in $D = 4 + 2\epsilon$ dimensions ($\epsilon < 0$), the expression for δ_W reads $\delta_W = \delta_W^{(1)} + \delta_W^{(2)} + \delta_W^{(3)}$, with:

$$\delta_W^{(1)} = \frac{M_W^2}{v^2} \sum_i |\mathcal{R}_{i2} + \mathcal{R}_{i3}|^2 \frac{\mu^{2\epsilon}}{(4\pi)^2} \left(\frac{1}{3\hat{\epsilon}} + \int_0^1 dx \, 2x(1-x) \ln \frac{a^2(M_W^2)}{\mu^2} \right), \quad (8.34)$$

$$\delta_W^{(2)} = \frac{M_W^2}{v^2} \sum_i \mathcal{R}_{i1}^2 \frac{\mu^{2\epsilon}}{(4\pi)^2} \left(\frac{1}{3\hat{\epsilon}} + \int_0^1 dx \, 2x(1-x) \ln \frac{\bar{a}^2(M_W^2)}{\mu^2} \right), \quad (8.35)$$

$$\delta_W^{(3)} = -\frac{4M_W^4}{v^2} \sum_i \mathcal{R}_{i1}^2 \frac{1}{(4\pi)^2} \int_0^1 dx \, \frac{x(1-x)}{\bar{a}^2(M_W^2)}. \quad (8.36)$$

in agreement with [60]. The wave function renormalization counter-term for the charged Goldstone boson is given by $\delta_{G^\pm} = \delta_{G^\pm}^{(1)} + \delta_{G^\pm}^{(2)} + \delta_{G^\pm}^{(3)}$ with:

$$\delta_{G^\pm}^{(1)} = -\frac{1}{(4\pi)^2} \sum_i |\mathcal{R}_{i2} + \mathcal{R}_{i3}|^2 \frac{(M_{\varphi_i^0}^2 - M_{H^\pm}^2)^2}{v^2} \int_0^1 dx \, \frac{x(1-x)}{a^2(M_W^2)}, \quad (8.37)$$

$$\delta_{G^\pm}^{(2)} = -\frac{1}{(4\pi)^2} \sum_i \mathcal{R}_{i1}^2 \frac{M_{\varphi_i^0}^4}{v^2} \int_0^1 dx \, \frac{x(1-x)}{\bar{a}^2(M_W^2)}, \quad (8.38)$$

$$\begin{aligned} \delta_{G^\pm}^{(3)} = & -\frac{\mu^{2\epsilon}}{(4\pi)^2} \frac{M_W^2}{v^2} \sum_i \mathcal{R}_{i1}^2 \left[\frac{2}{\hat{\epsilon}} + \frac{1}{6} + \int_0^1 dx \, (3x^2 - 6x + 4) \ln \frac{\bar{a}^2(M_W^2)}{\mu^2} \right. \\ & \left. + \int_0^1 dx \, \frac{x(x-1)}{\bar{a}^2(M_W^2)} (M_W^2(3x^2 - 8x + 6) + 2xM_{\varphi_i^0}^2) \right]. \end{aligned} \quad (8.39)$$

Last, the W mass counter-term is given by $\delta_M = \delta_M^{(1)} + \delta_M^{(2)} + \delta_M^{(3)} + \delta_M^{(4)} + \delta_M^{(5)}$ with:

$$\begin{aligned} \delta_M^{(1)} = & \frac{1}{v^2} \frac{\mu^{2\epsilon}}{(4\pi)^2} \sum_i |\mathcal{R}_{i2} + \mathcal{R}_{i3}|^2 \left[\left(\frac{1}{\hat{\epsilon}} - 1 \right) (M_{H^\pm}^2 + M_{\varphi_i^0}^2 - \frac{1}{3} M_W^2) \right. \\ & \left. + \int_0^1 dx \, 2a^2(M_W^2) \ln \frac{a^2(M_W^2)}{\mu^2} \right], \end{aligned} \quad (8.40)$$

$$\delta_M^{(2)} = \frac{1}{v^2} \frac{\mu^{2\epsilon}}{(4\pi)^2} \sum_i R_{i1}^2 \left[\left(\frac{1}{\hat{\epsilon}} - 1 \right) (M_{\varphi_i^0}^2 + \frac{2}{3} M_W^2) + \int_0^1 dx \, 2\bar{a}^2(M_W^2) \ln \frac{\bar{a}^2(M_W^2)}{\mu^2} \right], \quad (8.41)$$

$$\delta_M^{(3)} = -\frac{4M_W^2}{v^2} \frac{\mu^{2\epsilon}}{(4\pi)^2} \sum_i R_{i1}^2 \left[\frac{1}{\hat{\epsilon}} + \int_0^1 dx \, \ln \frac{\bar{a}^2(M_W^2)}{\mu^2} \right], \quad (8.42)$$

$$\delta_M^{(4)} = -\frac{2M_{H^\pm}^2}{v^2} \frac{\mu^{2\epsilon}}{(4\pi)^2} \left[\frac{1}{\hat{\epsilon}} + \ln \frac{M_{H^\pm}^2}{\mu^2} - 1 \right], \quad (8.43)$$

$$\delta_M^{(5)} = -\frac{\mu^{2\epsilon}}{(4\pi)^2} \sum_i \frac{M_{\varphi_i^0}^2}{v^2} \left[\frac{1}{\hat{\epsilon}} + \ln \frac{M_{\varphi_i^0}^2}{\mu^2} - 1 \right]. \quad (8.44)$$

Here we have defined $1/\hat{\epsilon} \equiv 1/\epsilon + \gamma_E - \ln(4\pi)$. The functions $a^2(p^2)$ and $\bar{a}^2(p^2)$ are given by:

$$a^2(p^2) = -p^2 x(1-x) + M_{\varphi_i^0}^2 x + M_{H^\pm}^2 (1-x), \quad (8.45)$$

$$\bar{a}^2(p^2) = -p^2 x(1-x) + M_{\varphi_i^0}^2 x + M_W^2 (1-x). \quad (8.46)$$

Now, we move on and present the expressions for the one-loop $WW\gamma$ effective vertices from Fig. 8.14. The considered kinematics and the assigned Lorentz indices for this process are $W^+(k-q, \rho) + \gamma(q, \mu) \rightarrow W^+(k, \nu)$. Discarding all terms proportional to q^μ , the first and second diagrams give:

$$i \Gamma_{(1)}^{\rho\mu\nu} = i \frac{e}{(4\pi)^2} \frac{M_W^2}{v^2} \mu^{2\epsilon} \sum_i |\mathcal{R}_{i2} + \mathcal{R}_{i3}|^2 \left[-\frac{1}{3\hat{\epsilon}} \Gamma^{\rho\mu\nu} + \int_0^1 dx \int_0^1 dy \, J_{(a)}^{\rho\mu\nu} 2(1-x) \ln \frac{a_x^2}{\mu^2} + \int_0^1 dx \int_0^1 dy \, \frac{J_{(b)}^{\rho\mu\nu}}{k^2 - M_x^2 - 2y k \cdot q} \right], \quad (8.47)$$

$$\begin{aligned}
i \Gamma_{(2)}^{\rho\mu\nu} = & i \frac{e}{(4\pi)^2} \frac{M_W^2}{v^2} \mu^{2\epsilon} \sum_i \mathcal{R}_{i1}^2 \left[-\frac{1}{3\hat{\epsilon}} \Gamma^{\rho\mu\nu} \right. \\
& + \int_0^1 dx \int_0^1 dy J_{(a)}^{\rho\mu\nu} 2(1-x) \ln \frac{\bar{a}_x^2}{\mu^2} \\
& \left. + \int_0^1 dx \int_0^1 dy \frac{J_{(b)}^{\rho\mu\nu}}{k^2 - \bar{M}_x^2 - 2y k \cdot q} \right]. \quad (8.48)
\end{aligned}$$

Again, $\Gamma^{\rho\mu\nu}$ is the tree-level vertex function and it is given by

$$\Gamma^{\rho\mu\nu} = g^{\mu\nu}(-k-q)^\rho + g^{\mu\rho}(2q-k)^\nu + g^{\nu\rho}(2k-q)^\mu. \quad (8.49)$$

The sum of diagrams (3), (4) and (5) gives

$$\begin{aligned}
i \Gamma_{(3+4+5)}^{\rho\mu\nu} = & -i \frac{e}{(4\pi)^2} \frac{M_W^4}{v^2} \sum_i \mathcal{R}_{i1}^2 \int_0^1 dx \int_0^1 dy \frac{1}{x} \\
& \times \frac{-2 g^{\mu\nu} Q^\rho - 2 g^{\mu\rho} J^\nu + 4 J_{(c)}^{\rho\mu\nu}}{k^2 - \bar{M}_x^2 - 2y k \cdot q}. \quad (8.50)
\end{aligned}$$

With diagram (6) we have to be specially careful. Its explicit expression reads

$$\begin{aligned}
i \Gamma_{(6)}^{\rho\mu\nu} = & i \frac{e}{(4\pi)^2} \frac{M_W^2}{v^2} g^{\mu\nu} (k^\rho - q^\rho) \mu^{2\epsilon} \sum_i |\mathcal{R}_{i2} + i\mathcal{R}_{i3}|^2 \\
& \times \int_0^1 dx (2x-1) \left(\frac{1}{\hat{\epsilon}} + \ln \frac{b_x^2}{\mu^2} \right). \quad (8.51)
\end{aligned}$$

Integrating over x , the pole and the μ -dependence vanish. We are left with a logarithm that depends on the four momentum and that we need to integrate in the second loop. Using the expansion ($\delta \ll 1$)

$$\ln A = \frac{1}{\delta} (A^\delta - 1) + O(\delta), \quad (8.52)$$

we can write the previous expression as

$$\begin{aligned}
i \Gamma_{(6)}^{\rho\mu\nu} = & i \frac{e}{(4\pi)^2} \frac{M_W^2}{v^2} g^{\mu\nu} (k^\rho - q^\rho) \frac{(-1)^\delta}{\delta} \sum_i |\mathcal{R}_{i2} + i\mathcal{R}_{i3}|^2 \\
& \times \int_0^1 dx \frac{(2x-1) x^\delta (1-x)^\delta}{(k^2 - M_x^2 - 2k \cdot q)^{-\delta}}, \quad (8.53)
\end{aligned}$$

and use the Feynman parametrization

$$\frac{1}{A_1^{-\delta} A_2 A_3 A_4} = \frac{\Gamma(3-\delta)}{\Gamma(-\delta)} \int_0^1 dx_1 \int_0^{1-x_1} dx_2 \int_0^{1-x_1-x_2} dx_3 x_1^{-\delta-1} \times \frac{1}{(x_1 A_1 + x_2 A_2 + x_3 A_3 + (1-x_1-x_2-x_3) A_4)^{3-\delta}}, \quad (8.54)$$

in order to solve the second loop (taking the limit $\delta \rightarrow 0$ at the end of the calculation). We obtain a similar expression for diagram (7):

$$i \Gamma_{(7)}^{\rho\mu\nu} = i \frac{e}{(4\pi)^2} \frac{M_W^2}{v^2} g^{\mu\nu} (k^\rho - q^\rho) \frac{(-1)^\delta}{\delta} \sum_i \mathcal{R}_{i1}^2 \times \int_0^1 dx \frac{(2x-1) x^\delta (1-x)^\delta}{(k^2 - \bar{M}_x^2 - 2k \cdot q)^{-\delta}}. \quad (8.55)$$

Contributions (8) and (9) vanish as their expressions are terms proportional to q^μ . Finally, diagrams (10) and (11) read

$$i \Gamma_{(10)}^{\rho\mu\nu} = i \frac{e}{(4\pi)^2} \frac{M_W^2}{v^2} g^{\mu\rho} k^\nu \mu^{2\epsilon} \sum_i |\mathcal{R}_{i2} + i\mathcal{R}_{i3}|^2 \times \int_0^1 dx (2x-1) \left(\frac{1}{\hat{\epsilon}} + \ln \frac{\bar{c}_x^2}{\mu^2} \right), \quad (8.56)$$

$$i \Gamma_{(11)}^{\rho\mu\nu} = i \frac{e}{(4\pi)^2} \frac{M_W^2}{v^2} g^{\mu\rho} k^\nu \mu^{2\epsilon} \sum_i \mathcal{R}_{i1}^2 \times \int_0^1 dx (2x-1) \left(\frac{1}{\hat{\epsilon}} + \ln \frac{\bar{c}_x^2}{\mu^2} \right), \quad (8.57)$$

which can be treated exactly as diagrams (6) and (7). The previously introduced tensorial functions are given by:

$$J_{(a)}^{\rho\mu\nu} = g^{\mu\rho} ((1-2x)k^\nu + 2y(x-1)q^\nu) + g^{\mu\nu} ((1-2x)k^\rho + (2(x-1)y+1)q^\rho) - 2x g^{\nu\rho} k^\mu, \quad (8.58)$$

$$J_{(b)}^{\rho\mu\nu} = -2k^\mu ((2x-1)k^\nu - 2y(x-1)q^\nu) ((1-2x)k^\rho + (2(x-1)y+1)q^\rho), \quad (8.59)$$

$$J_{(c)}^{\rho\mu\nu} = g^{\mu\rho} ((xy-y+2)q^\nu - xk^\nu) - g^{\mu\nu} (xk^\rho + q^\rho(y-xy+1)) + 2x g^{\nu\rho} k^\mu, \quad (8.60)$$

and,

$$\begin{aligned} Q^\rho &= k^\rho (1-2x) + q^\rho (2xy - 2y + 1), \\ J^\nu &= k^\nu (1-2x) + q^\nu 2y(x-1). \end{aligned} \quad (8.61)$$

The scalar functions are given by:

$$\begin{aligned} a_x^2 &= -x(1-x)(k^2 - M_x^2 - 2y k \cdot q), \\ \bar{a}_x^2 &= -x(1-x)(k^2 - \bar{M}_x^2 - 2y k \cdot q), \\ b_x^2 &= -x(1-x)(k^2 - M_x^2 - 2k \cdot q), \\ \bar{b}_x^2 &= -x(1-x)(k^2 - \bar{M}_x^2 - 2k \cdot q), \\ c_x^2 &= -x(1-x)(k^2 - M_x^2), \\ \bar{c}_x^2 &= -x(1-x)(k^2 - \bar{M}_x^2), \end{aligned} \quad (8.62)$$

with

$$M_x^2 = \frac{M_{\varphi_i^0}^2}{1-x} + \frac{M_{H^\pm}^2}{x}, \quad \bar{M}_x^2 = \frac{M_{\varphi_i^0}^2}{1-x} + \frac{M_W^2}{x}. \quad (8.63)$$

Next we present the $G^\pm W \gamma$ effective vertices from Fig. 8.15. The kinematics and Lorentz indices are given by $G^+(k-q) + \gamma(q, \mu) \rightarrow W^+(k, \nu)$. Thus, the one-loop expressions are:

$$\begin{aligned} i \Gamma_{(1)}^{\mu\nu} &= -i \frac{e}{(4\pi)^2} M_W \mu^{2\epsilon} \sum_i |\mathcal{R}_{i2} + i\mathcal{R}_{i3}|^2 \frac{M_{\varphi_i^0}^2 - M_{H^\pm}^2}{v^2} \left[g^{\mu\nu} \frac{1}{\hat{\epsilon}} + \right. \\ &\quad \left. + \int_0^1 dx \int_0^1 dy \left(2g^{\mu\nu} (1-x) \ln \frac{a_x^2}{\mu^2} - \frac{2K^{\mu\nu}}{k^2 - M_x^2 - 2y k \cdot q} \right) \right], \end{aligned} \quad (8.64)$$

$$\begin{aligned} i \Gamma_{(2)}^{\mu\nu} &= -i \frac{e}{(4\pi)^2} M_W \mu^{2\epsilon} \sum_i \mathcal{R}_{i1}^2 \frac{M_{\varphi_i^0}^2}{v^2} \left[g^{\mu\nu} \frac{1}{\hat{\epsilon}} + \right. \\ &\quad \left. + \int_0^1 dx \int_0^1 dy \left(2g^{\mu\nu} (1-x) \ln \frac{\bar{a}_x^2}{\mu^2} - \frac{2K^{\mu\nu}}{k^2 - \bar{M}_x^2 - 2y k \cdot q} \right) \right], \end{aligned} \quad (8.65)$$

$$i \Gamma_{(3)}^{\mu\nu} = -i \frac{e}{(4\pi)^2} M_W \sum_i \mathcal{R}_{i1}^2 \frac{M_{\varphi_i^0}^2}{v^2} \int_0^1 dx \int_0^1 dy \frac{1}{x} \frac{2M_W^2 g^{\mu\nu}}{k^2 - \bar{M}_x^2 - 2y k \cdot q}, \quad (8.66)$$

$$i \Gamma_{(4)}^{\mu\nu} = i \frac{e}{(4\pi)^2} \frac{M_W^3}{v^2} \mu^{2\epsilon} \sum_i \mathcal{R}_{i1}^2 \left[g^{\mu\nu} \frac{1}{2\hat{\epsilon}} + \int_0^1 dx \int_0^1 dy \left(g^{\mu\nu} (1-x) \ln \frac{\bar{a}_x^2}{\mu^2} + \frac{(2-x)}{x} \frac{K^{\mu\nu}}{k^2 - \bar{M}_x^2 - 2y k \cdot q} \right) \right], \quad (8.67)$$

$$i \Gamma_{(5)}^{\mu\nu} = i \frac{e}{(4\pi)^2} \frac{M_W^3}{v^2} \mu^{2\epsilon} \sum_i \mathcal{R}_{i1}^2 \left[-g^{\mu\nu} \left(\frac{3}{2\hat{\epsilon}} + 1 \right) + \int_0^1 dx \int_0^1 dy \left(3g^{\mu\nu} (x-1) \ln \frac{\bar{a}_x^2}{\mu^2} + \frac{2}{x} \frac{G^{\mu\nu}}{k^2 - \bar{M}_x^2 - 2y k \cdot q} \right) \right], \quad (8.68)$$

$$i \Gamma_{(6)}^{\mu\nu} = i \frac{e}{(4\pi)^2} M_W g^{\mu\nu} \mu^{2\epsilon} \sum_i \mathcal{R}_{i1}^2 \frac{M_{\varphi_i^0}^2}{v^2} \left(\frac{1}{\hat{\epsilon}} + \int_0^1 dx \ln \frac{\bar{b}_x^2}{\mu^2} \right), \quad (8.69)$$

$$i \Gamma_{(7)}^{\mu\nu} = i \frac{e}{(4\pi)^2} M_W g^{\mu\nu} \mu^{2\epsilon} \sum_i |\mathcal{R}_{i2} + \mathcal{R}_{i3}|^2 \times \frac{M_{\varphi_i^0}^2 - M_{H^\pm}^2}{v^2} \left(\frac{1}{\hat{\epsilon}} + \int_0^1 dx \ln \frac{b_x^2}{\mu^2} \right), \quad (8.70)$$

$$i \Gamma_{(8)}^{\mu\nu} = i \frac{e}{(4\pi)^2} g^{\mu\nu} \frac{2M_W^3}{v^2} \mu^{2\epsilon} \sum_i \mathcal{R}_{i1}^2 \left(\frac{1}{\hat{\epsilon}} + \int_0^1 dx \ln \frac{\bar{c}_x^2}{\mu^2} \right). \quad (8.71)$$

The tensorial functions are given by:

$$K^{\mu\nu} = k^\mu ((2x-1)k^\nu - 2y(x-1)q^\nu), \quad (8.72)$$

$$G^{\mu\nu} = g^{\mu\nu} (k^2 x(x-2) - 2(x-1)(xy-y-1)k \cdot q) + k^\mu ((x-1)(xy+2y-4)q^\nu - x(x-2)k^\nu). \quad (8.73)$$

All other functions are the same as previously. Note, that for the previous expressions of the one-loop effective vertices, we have maintained the $k \cdot q$ structure in the denominator (in contrast to the $H^\pm W \gamma$ effective vertices) because here, in some cases, this structure does contribute to the final result.

Inserting all these expressions into the second loop we finally obtain the expression for the total contribution to the anomalous magnetic moment of the

muon. Subtracting the SM contributions we have

$$\Delta a_\mu = \frac{\alpha}{128 \pi^2 s_w^2} \frac{m_\mu^2}{v^2} \int_0^1 dx \times \left(\sum_i \mathcal{R}_{i1}^2 \mathcal{A} - \mathcal{A}_{\text{SM}} + \sum_i |\mathcal{R}_{i2} + i\mathcal{R}_{i3}|^2 \mathcal{B} + \mathcal{C} \right), \quad (8.74)$$

with the functions \mathcal{A} , \mathcal{B} and \mathcal{C} given by:

$$\begin{aligned} \mathcal{A} = & \frac{7}{3} x(1-x) \ln \frac{\bar{a}^2(M_W^2)}{M_W^2} - \frac{(2x^2 - 3x + 2) M_{\varphi_i^0}^2}{2x(M_W^2 - \bar{M}_x^2)} \\ & + \frac{6(x-1) \bar{M}_x^2 + (-12x^2 + 30x - 55) M_W^2}{6(M_W^2 - \bar{M}_x^2)} \\ & + \frac{M_{\varphi_i^0}^2 \ln(\bar{M}_x^2/M_W^2)}{2x M_W^2 (M_W^2 - \bar{M}_x^2)^2} \left(\bar{M}_x^4 x(2x-1) - 2M_W^4 + 4M_W^2 \bar{M}_x^2 x(1-x) \right) \\ & + \frac{\ln(\bar{M}_x^2/M_W^2)}{6x (M_W^2 - \bar{M}_x^2)^2} \left(\bar{M}_x^4 x(16x-9) + M_W^4 (8x-42) \right. \\ & \quad \left. + 2M_W^2 \bar{M}_x^2 (-6x^3 + 10x^2 - 30x + 21) \right) \\ & + \frac{x(1-x)}{4M_W^2 \bar{a}^2(M_W^2)} \left(M_W^4 (3x^2 - 8x - \frac{50}{3}) + 2x M_W^2 M_{\varphi_i^0}^2 - M_{\varphi_i^0}^4 \right), \quad (8.75) \end{aligned}$$

$$\begin{aligned} \mathcal{B} = & \frac{7}{3} x(1-x) \ln \frac{a^2(M_W^2)}{M_W^2} + \frac{1}{2} (2x-1) \frac{M_x^2 - 2M_W^2(x-1)}{M_W^2 - M_x^2} \\ & + \frac{(M_{\varphi_i^0}^2 - M_{H^\pm}^2)(3-2x)}{2(M_W^2 - M_x^2)} - \frac{(M_{\varphi_i^0}^2 - M_{H^\pm}^2)^2 x(1-x)}{4M_W^2 a^2(M_W^2)} \\ & + \frac{M_x^2 \ln(M_x^2/M_W^2)}{6(M_W^2 - M_x^2)^2} \left(M_W^2 2x(7-6x) + M_x^2(10x-9) \right) \\ & + \frac{(M_{\varphi_i^0}^2 - M_{H^\pm}^2) M_x^2 \ln(M_x^2/M_W^2)}{2M_W^2 (M_W^2 - M_x^2)^2} \left(4M_W^2(1-x) + M_x^2(2x-1) \right) \end{aligned}$$

$$+ \frac{1}{4M_W^2} \left(2(1-x) M_{H^\pm}^2 \ln \frac{a^2(M_W^2)}{M_{H^\pm}^2} + 2x M_{\varphi_i^0}^2 \ln \frac{a^2(M_W^2)}{M_W^2} \right), \quad (8.76)$$

$$\begin{aligned} \mathcal{C} = \sum_i \left(-\frac{M_{\varphi_i^0}^2}{4M_W^2} \ln \frac{M_{\varphi_i^0}^2}{M_W^2} + \mathcal{R}_{i1}^2 \frac{1}{4} (-3x^2 + 4x - 6) \ln \frac{\bar{a}^2(M_W^2)}{\bar{a}_{\text{SM}}^2(M_W^2)} \right. \\ \left. + \mathcal{R}_{i1}^2 \frac{x M_{\varphi_i^0}^2}{2M_W^2} \ln \frac{\bar{a}^2(M_W^2)}{M_W^2} \right) - \frac{x M_\phi^2}{2M_W^2} \ln \frac{\bar{a}_{\text{SM}}^2(M_W^2)}{M_\phi^2} + \frac{1}{6}. \end{aligned} \quad (8.77)$$

All the functions that carry a SM sub-index are obtained from the original ones by replacing $M_{\varphi_i^0}$ with M_ϕ everywhere, where M_ϕ is the mass of the SM Higgs. The numerical values that we obtain for this contribution (for $M_{H,A,H^\pm} < 500$ GeV) are typically of $\mathcal{O}(10^{-11})$ both positive or negative, which is two orders of magnitude below $\Delta a_\mu^{\text{exp}}$, therefore we shall not take it into account in this analysis.

Acknowledgements

I am grateful to Antonio Pich for reviewing this manuscript and to Alejandro Celis for helpful comments. This work has been supported in part by the Spanish Government and ERDF funds from the EU Commission [Grants FPA2011-23778 and CSD2007-00042 (Consolider Project CPAN)] and by the Spanish Ministry MINECO through the FPI grant BES-2012-054676.

BIBLIOGRAPHY

- [1] ATLAS Collaboration, Phys. Lett. B **716** (2012) 1 [arXiv:1207.7214 [hep-ex]].
- [2] ATLAS Collaboration, Phys. Lett. B **726** (2013) 88 [arXiv:1307.1427 [hep-ex]]; ATLAS-CONF-2013-079 (July 19, 2013); ATLAS-CONF-2013-034 (March 13, 2013); David López Mateos talk at EPS 2013 for the ATLAS collaboration.
- [3] CMS Collaboration, Phys. Lett. B **716** (2012) 30 [arXiv:1207.7235 [hep-ex]].
- [4] CMS Collaboration, JHEP **06** (2013) 081 [arXiv:1303.4571 [hep-ex]]; CMS-PAS-HIG-13-005 (April 17, 2013).
- [5] CDF and D0 Collaborations, Phys. Rev. Lett. **109** (2012) 071804 [arXiv:1207.6436 [hep-ex]]; Phys. Rev. D **88** (2013) 052014 [arXiv:1303.6346 [hep-ex]].
- [6] A. Broggio, E. J. Chun, M. Passera, K. M. Patel and S. K. Vempati, JHEP **1411** (2014) 058 [arXiv:1409.3199 [hep-ph]].
- [7] L. Wang and X. F. Han, arXiv:1412.4874 [hep-ph].
- [8] T. Aoyama, M. Hayakawa, T. Kinoshita and M. Nio, Phys. Rev. Lett. **109** (2012) 111808 [arXiv:1205.5370 [hep-ph]].
- [9] A. Czarnecki, B. Krause and W. J. Marciano, Phys. Rev. D **52** (1995) 2619 [hep-ph/9506256].
- [10] A. Czarnecki, B. Krause and W. J. Marciano, Phys. Rev. Lett. **76** (1996) 3267 [hep-ph/9512369].
- [11] C. Gnendiger, D. Stöckinger and H. Stöckinger-Kim, Phys. Rev. D **88** (2013) 5, 053005 [arXiv:1306.5546 [hep-ph]].

-
- [12] F. Jegerlehner and A. Nyffeler, Phys. Rept. **477** (2009) 1 [arXiv:0902.3360 [hep-ph]].
- [13] M. Davier, A. Hoecker, B. Malaescu and Z. Zhang, Eur. Phys. J. C **71** (2011) 1515 [Erratum-ibid. C **72** (2012) 1874] [arXiv:1010.4180 [hep-ph]].
- [14] B. Krause, Phys. Lett. B **390** (1997) 392 [hep-ph/9607259].
- [15] J. Prades, E. de Rafael and A. Vainshtein, (Advanced series on directions in high energy physics. 20) [arXiv:0901.0306 [hep-ph]].
- [16] G. Colangelo, M. Hoferichter, M. Procura and P. Stoffer, JHEP **1409** (2014) 091 [arXiv:1402.7081 [hep-ph]].
- [17] G. Colangelo, M. Hoferichter, B. Kubis, M. Procura and P. Stoffer, Phys. Lett. B **738** (2014) 6 [arXiv:1408.2517 [hep-ph]].
- [18] T. Blum, S. Chowdhury, M. Hayakawa and T. Izubuchi, Phys. Rev. Lett. **114** (2015) 012001 [arXiv:1407.2923 [hep-lat]].
- [19] V. Pauk and M. Vanderhaeghen, Phys. Rev. D **90** (2014) 11, 113012 [arXiv:1409.0819 [hep-ph]].
- [20] A. Kurz, T. Liu, P. Marquard and M. Steinhauser, Phys. Lett. B **734** (2014) 144 [arXiv:1403.6400 [hep-ph]].
- [21] G. Colangelo, M. Hoferichter, A. Nyffeler, M. Passera and P. Stoffer, Phys. Lett. B **735** (2014) 90 [arXiv:1403.7512 [hep-ph]].
- [22] T. Blum, A. Denig, I. Logashenko, E. de Rafael, B. Lee Roberts, T. Teubner and G. Venanzoni, arXiv:1311.2198 [hep-ph].
- [23] K. Melnikov and A. Vainshtein, Springer Tracts Mod. Phys. **216** (2006) 1.
- [24] M. Davier and W. J. Marciano, Ann. Rev. Nucl. Part. Sci. **54** (2004) 115.
- [25] M. Passera, J. Phys. G **31** (2005) R75 [hep-ph/0411168].
- [26] M. Knecht, Lect. Notes Phys. **629** (2004) 37 [hep-ph/0307239].
- [27] G. W. Bennett *et al.* [Muon G-2 Collaboration], Phys. Rev. D **73** (2006) 072003 [hep-ex/0602035].
- [28] K. A. Olive *et al.* [Particle Data Group Collaboration], Chin. Phys. C **38** (2014) 090001.

-
- [29] S. M. Barr and A. Zee, Phys. Rev. Lett. **65** (1990) 21 [Erratum-ibid. **65** (1990) 2920].
- [30] A. Pich and P. Tuzón, Phys. Rev. D **80** (2009) 091702 [arXiv:0908.1554 [hep-ph]].
- [31] A. Dedes and H. E. Haber, JHEP **0105** (2001) 006 [hep-ph/0102297].
- [32] J. F. Gunion, JHEP **0908** (2009) 032 [arXiv:0808.2509 [hep-ph]].
- [33] D. Chang, W. F. Chang, C. H. Chou and W. Y. Keung, Phys. Rev. D **63** (2001) 091301 [hep-ph/0009292].
- [34] K. M. Cheung, C. H. Chou and O. C. W. Kong, Phys. Rev. D **64** (2001) 111301 [hep-ph/0103183].
- [35] M. Krawczyk, Acta Phys. Polon. B **33** (2002) 2621 [hep-ph/0208076].
- [36] F. Larios, G. Tavares-Velasco and C. P. Yuan, Phys. Rev. D **64** (2001) 055004 [hep-ph/0103292].
- [37] K. Cheung and O. C. W. Kong, Phys. Rev. D **68** (2003) 053003 [hep-ph/0302111].
- [38] A. Arhrib and S. Baek, Phys. Rev. D **65** (2002) 075002 [hep-ph/0104225].
- [39] S. Heinemeyer, D. Stockinger and G. Weiglein, Nucl. Phys. B **690** (2004) 62 [hep-ph/0312264].
- [40] O. C. W. Kong, hep-ph/0402010.
- [41] K. Cheung, O. C. W. Kong and J. S. Lee, JHEP **0906** (2009) 020 [arXiv:0904.4352 [hep-ph]].
- [42] L. Bian, T. Liu and J. Shu, arXiv:1411.6695 [hep-ph].
- [43] A. Celis, V. Ilisie and A. Pich, JHEP **1312** (2013) 095 [arXiv:1310.7941 [hep-ph]].
- [44] A. Celis, V. Ilisie and A. Pich, JHEP **1307** (2013) 053 [arXiv:1302.4022 [hep-ph]].
- [45] V. Ilisie and A. Pich, JHEP **1409** (2014) 089 [arXiv:1405.6639 [hep-ph]].
- [46] V. Ilisie, arXiv:1410.5164 [hep-ph].

- [47] V. Ilisie, PoS (EPS - HEP 2013) **286** [arXiv:1310.0931 [hep-ph]].
- [48] M. Jung, A. Pich and P. Tuzón, JHEP **1011** (2010) 003 [arXiv:1006.0470 [hep-ph]].
- [49] M. Jung, A. Pich and P. Tuzón, Phys. Rev. D **83** (2011) 074011 [arXiv:1011.5154 [hep-ph]].
- [50] A. Celis, M. Jung, X.-Q. Li and A. Pich, JHEP **1301** (2013) 054 [arXiv:1210.8443 [hep-ph]].
- [51] M. Jung and A. Pich, JHEP **1404** (2014) 076 [arXiv:1308.6283 [hep-ph]].
- [52] X.-Q. Li, J. Lu and A. Pich, arXiv:1404.5865 [hep-ph].
- [53] H. E. Haber, G. L. Kane and T. Sterling, Nucl. Phys. B **161** (1979) 493.
- [54] J. P. Leveille, Nucl. Phys. B **137** (1978) 63.
- [55] M. Krawczyk and J. Zochowski, Phys. Rev. D **55** (1997) 6968 [hep-ph/9608321].
- [56] F. S. Queiroz and W. Shepherd, Phys. Rev. D **89** (2014) 9, 095024 [arXiv:1403.2309 [hep-ph]].
- [57] C. H. Chen and C. Q. Geng, Phys. Lett. B **511** (2001) 77 [hep-ph/0104151].
- [58] T. Abe, J. Hisano, T. Kitahara and K. Tobioka, JHEP **1401** (2014) 106 [arXiv:1311.4704 [hep-ph], arXiv:1311.4704].
- [59] R. Santos and A. Barroso, Phys. Rev. D **56** (1997) 5366 [hep-ph/9701257].
- [60] M. Malinsky and J. Horejsi, Eur. Phys. J. C **34** (2004) 477 [hep-ph/0308247].

9. UPDATED FITS FROM RUN 1

In the following we shall present the updated analysis of some of the relevant parts of the studies and model fits performed in Chapters 5 and 6. The latest LHC combined analysis (at 7 and 8 TeV) from the Atlas and CMS collaborations [1] has been recently released and, as expected, the data are getting more and more precise. This obviously allows us to further constrain the parameter space of the A2HDM. However, the impact of the new data on the phenomenology of the fermiophobic charged Higgs (Chapter 7) and the analysis of the new contributions to $(g - 2)_\mu$ (Chapter 8) will not be affected, as these analyses were performed under very generic assumptions on the parameter space.

As we shall shortly see, the impact of the new data on the parameter space of the 2HDM will be somewhat sizeable when compared to the previous results, however the main conclusions will roughly, remain the same. In the following we shall present a comparison between the results with the *old* data [2–9] from Chapter 6, and the ones obtained with the *new* [1] LHC data (Fig. 9.1-9.4); CP conservation is assumed.

As one can immediately observe, the parameter space shrinks when including the new data. The already usual relative sign degeneracy for the y_d^h and y_l^h with respect to y_u^h coupling is obviously still present. Hopefully one could be able to discriminate among these four regions with more precise data and complementary flavour experiments.

The allowed regions for down-type Yukawa coupling are no longer connected (at 90% CL) as it can be observed in Fig. 9.1 and 9.2. In the same two figures one can also appreciate that the y_d^h isles are somewhat displaced inwards (toward the (0,0) origin) which reflects the fact that the data prefers values for these couplings that are mostly a little bit above their SM value or smaller.

Similar considerations can be made for the y_l^h coupling. The isles corresponding to the degenerate solutions are no longer connected either, thus, the allowed regions at 90% CL have also been quite significantly reduced. These isles, however, have not been displaced inwards by the new data, as in the previous case.

As for the up-type Yukawa, it roughly lives in the same domain (Figs.9.2-9.3), perhaps a bit reduced. Its relative sign with respect to the Higgs coupling to gauge bosons is still SM-like, just as in the *old* analysis. The possibility of

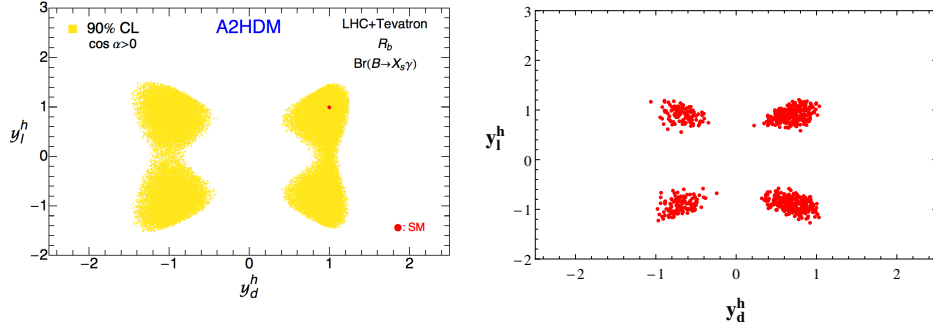


Figure 9.1: Allowed 90% CL regions in the $y_d^h - y_l^h$ plane from a global fit of the old LHC and Tevatron data (left) and of the latest ATLAS and CMS combination (right), together with the R_b and $\text{Br}(\bar{B} \rightarrow X_s \gamma)$ flavour constraints, within the CP-conserving A2HDM. The mass of the charged Higgs is varied within $M_{H^\pm} \in [80, 500]$ GeV and $\cos \tilde{\alpha} > 0$.

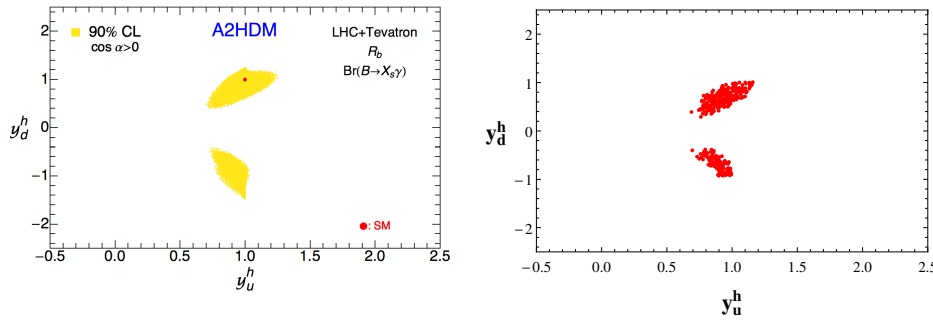
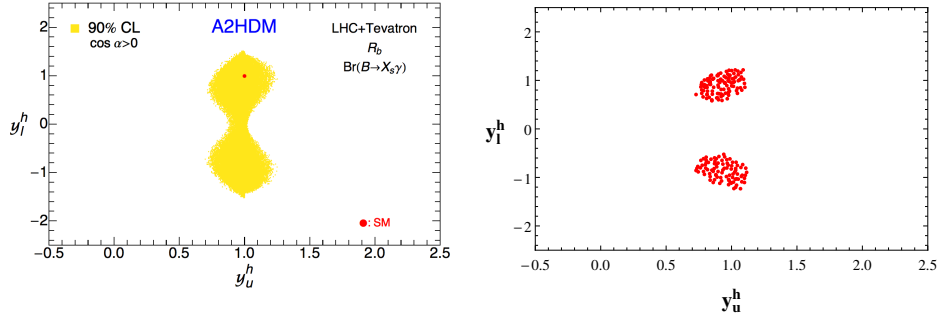
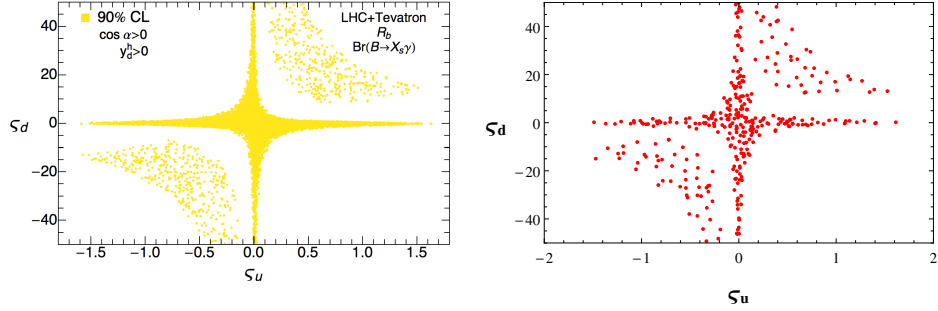


Figure 9.2: Same as in Fig. 9.1 for the $y_u^h - y_d^h$ plane.

having positive interference (non SM-like) between the W and top-quark loops for the $H \rightarrow \gamma\gamma$ decay was discarded, as the excess for the experimental value of the signal strength for this channel decreased sizeably.

Finally, the strong correlation in the $\zeta_u - \zeta_d$ plane, which is due to the flavour constraints, mainly $b \rightarrow s\gamma$, is obviously still present. As the LHC Higgs data provides (for now) information mainly on the Yukawa parameter space, roughly speaking one can always find values for the $\zeta_{d,l}$ parameters that satisfy this correlation. We would be able to significantly reduce this region (in half) when disentangling the sign degeneracy among the Yukawas, or on the contrary, if we are able to reduce this parameter space with more and more precise flavour data,

Figure 9.3: Same as in Fig.9.1 for the $y_u^h - y_l^h$ plane.Figure 9.4: Same as in Fig.9.1 for the $s_u - s_d$ plane.

we might be able to solve the Yukawa sign puzzle. An experimental upper bound on $|\cos \tilde{\alpha}|$ could also do the trick. Remember that the Yukawa couplings in the CP-conserving regime are given by

$$y_f^h = \cos \tilde{\alpha} + \zeta_f \sin \tilde{\alpha}, \quad (9.1)$$

thus as $\cos \tilde{\alpha} \rightarrow 1$ all information on the alignment parameters ζ_f is lost. An upper bound on $|\cos \tilde{\alpha}|$ would then prevent such loss and would significantly help us reduce the parameter space if the bound is sufficiently precise.

With all this being said, we can conclude that this last release of combined data between the two experimental collaborations has helped us to improve a little bit our phenomenological analysis and we can only hope for more of this to come in the next years. Generic conclusions as well as a brief summary of the relevant results of this Thesis will be given next.

BIBLIOGRAPHY

- [1] ATLAS-CONF-2015-044; CMS-PAS-HIG-15-002
- [2] ATLAS Collaboration, Phys. Lett. B **716** (2012) 1 [arXiv:1207.7214 [hep-ex]].
- [3] ATLAS Collaboration, Phys. Lett. B **726** (2013) 88 [arXiv:1307.1427 [hep-ex]]; ATLAS-CONF-2013-079 (July 19, 2013); ATLAS-CONF-2013-034 (March 13, 2013); David López Mateos talk at EPS 2013 for the ATLAS collaboration.
- [4] CMS Collaboration, Phys. Lett. B **716** (2012) 30 [arXiv:1207.7235 [hep-ex]].
- [5] CMS Collaboration, JHEP **06** (2013) 081 [arXiv:1303.4571 [hep-ex]]; CMS-PAS-HIG-13-005 (April 17, 2013).
- [6] CDF and D0 Collaborations, Phys. Rev. Lett. **109** (2012) 071804 [arXiv:1207.6436 [hep-ex]]; Phys. Rev. D **88** (2013) 052014 [arXiv:1303.6346 [hep-ex]].
- [7] ATLAS Collaboration, Phys. Lett. B **726** (2013) 120 [arXiv:1307.1432 [hep-ex]].
- [8] CMS Collaboration, Phys. Rev. Lett. **110** (2013) 081803 [arXiv:1212.6639 [hep-ex]].
- [9] D0 Collaboration, D0 Note 6387-CONF (July 22, 2013).

CONCLUSIONS

The discovery of the scalar boson with mass around 125 GeV has certainly opened the gate to a new era. The Standard Model seems to work perfectly and the spontaneous symmetry breaking mechanism is no longer a fairy tale. However, there is lots of room, and also need, for new physics, as many fundamental questions remain open. Nevertheless, all Standard Model extensions must fulfil all precision fits and experimental bounds on the new particles and interactions introduced by these models. In this work we have studied two types of such extensions, both of them related to the Higgs sector.

Quantum Chromodynamics postulates that gluons belong to the adjoint representation (of dimension 8) of the $SU(3)_C$ colour group and that quarks and antiquarks belong to the fundamental representation (of dimension 3). There is, as we have mentioned, no fundamental principle that forbids the existence of fermions belonging to higher representations. We have seen that, both the running of the strong coupling and the collider data put severe constraints on any type of new strongly-interacting fermions coupling to the Higgs boson. In fact, we can conclude that such QCD particles could only exist provided that their masses do not originate in the SM Higgs mechanism, as they would extremely enhance the Higgs boson production cross section, in contrast with the already measured cross section.

For the second part we have extensively analysed the Two-Higgs-Doublet Model extension of the SM. In the first two chapters dedicated to the 2HDM (Chapters 5 and 6), we have studied the implications of the LHC data on the allowed scalar spectrum both in the CP-violating and the CP-conserving cases, as well as the particular limits based on discrete \mathcal{Z}_2 symmetries. The current data are so far compatible with the SM Higgs hypothesis however, at the time (Paper II, Chapter 5), there was a slight excess in the diphoton channel observed by both experimental collaborations. This channel is particularly interesting due to the fact that the decay of the Higgs into two photons occurs at the one-loop level and it is thus, sensitive to new charged particles that couple directly to the Higgs or to flipped sign (with respect to the SM) Yukawa couplings, or even complex Yukawas. We have analysed all these possibilities. We have also fitted the collider data on the Higgs signal strengths from the ATLAS, CMS, CDF

and DØ collaborations, within our framework. Even with large experimental uncertainties, interesting conclusions can be obtained regarding the preferred regions in the parameter space of the model. The possibility that a CP-even and a CP-odd Higgs bosons have quasi-degenerate masses near 125 GeV was also tested. The excess in the $\gamma\gamma$ channel can occur in this case due to the contributions from both scalars.

In Chapter 6 we extended the analysis from the previous paper and updated the bounds with the latest LHC and Tevatron data. We also discussed the role of electroweak precision observables and took into account flavour constraints ($B \rightarrow X_s\gamma$, $Z \rightarrow b\bar{b}$, etc.) to further restrict the parameter space. The Higgs coupling to vector bosons is found to be very close to the SM limit, implying an upper bound on the heavy CP-even Higgs coupling to vector bosons. The flipped-sign solution for the top-quark Yukawa coupling, which was preferred by the fit in the previous analysis (Chapter 5) (with the data released before Moriond 2013) in order to explain the excess in the $\gamma\gamma$ channel was found to be excluded at 90% CL. A sign degeneracy in the determination of the bottom and tau Yukawa couplings however remains.

We have also considered experimental searches for additional Higgs bosons at the LHC especially for a charged Higgs. Regarding the charged Higgs searches at colliders, its decays into a $c\bar{b}$ pair and three-body decays $H^+ \rightarrow t^*\bar{b} \rightarrow W^+b\bar{b}$ were found to have sizable decay rates in some regions of the allowed parameter space. Future searches for a light charged Higgs at the LHC in hadronic final states should take these possibilities into account.

By the time the present work was completed new experimental data were available from the ATLAS and CMS collaborations regarding the Higgs boson signal strengths. Therefore, we have added an additional chapter, Chapter 9, with updates of some of the relevant bounds on the parameter space of the model. As the data are getting more precise, our model gets further constrained. However, roughly speaking, the main conclusions remain the same. We have seen that the main effect after including the new data, is that the parameter space visibly shrinks, and that the isles formed by allowed regions of the down-type Yukawa couplings are no longer connected (at 90% CL) and they are slightly displaced towards the (0,0) origin. Roughly speaking, these Yukawas prefer regions where their values are just a little bit above their SM value or smaller. The bound on the Higgs coupling (normalized to the SM) to a pair of WW bosons remains the same $|\cos\tilde{\alpha}| > 0.8$ at 90% CL. The degeneracy of the sign of the down-type and leptonic Yukawas (with respect to the up-type coupling) is still there and we might just be able to disentangle it with much more precise collider data

on the Higgs signal strengths and with also more precise complementary flavour results. Perhaps what we are missing are some new observables sensitive to this relative sign, that might just do the job. Lacking the direct detection of new extra particles, the proof of a *wrong sign* Yukawa coupling would definitely prove the existence of beyond SM physics and would give us some hints on where the new particles might be *hiding*.

The next chapter (7) was dedicated to the study of the phenomenology of a fermiophobic charged Higgs (that does not couple to fermions at tree level). As all experimental bounds are evaded trivially we have analysed the corresponding relevant decays and production channels. We have focused our study on a light fermiophobic H^\pm with mass in the range $M_{H^\pm} \in [M_W, M_W + M_Z]$, where only a few decays are possible. The dominant production channels are found to be: associated production with either a W^\mp boson or a neutral scalar; NLO QCD corrections have been included. Also, we have taken into account the constraints from LHC, LEP and the flavour sector. The predicted cross sections are small in most of the parameter space, thus making the experimental searches challenging. However, they become sizeable ($\geq 10^{-3}$ pb) for large values of M_H (the mass of the heavy neutral scalar). Some special cases give rise to cross sections between 0.1 and 1 pb. The analysis presented here should encourage experimental searches for such a particle at the LHC.

In Chapter 8 we have analysed the anomalous magnetic moment of the muon and the contribution to this observable from new sets of two-loop Barr-Zee type diagrams. We have also presented the one and two-loop classical results in terms of the generic A2HDM parameters and the generic scalar potential. Analytical results are always given together with details of the calculation. Contrary to the common belief that only a restrained number of diagrams (the classical Barr-Zee diagrams) can significantly contribute to this observable, we have shown that these new contributions can be quite large in some regions of the parameter space, and that they can significantly reduce, and in some cases even explain, the discrepancy between the theoretical prediction and the experimentally measured value of $(g - 2)_\mu$.

These last two analyses, are minimally affected by the new released experimental data by the LHC collaborations, as they were performed under very generic assumptions on the parameter space.

ACKNOWLEDGEMENTS

I would like to thank my supervisor for all the time invested in me and in my work, for all his patience and clear vision. Thanks for sharing that with me. I would also like to thank Jorge Portolés and German Rodrigo for their help. Many thanks to my colleague Alejandro Celis, for a fruitful collaboration in two of the papers of this work. Also many thanks to Sébastien Descotes-Genon for a warm welcoming and stay at Université Paris Sud, for introducing me to the realm of angular observables. I would like to thank all my family, especially my dear wife Carmen and my parents Nusa and Nicu for their infinite patience and support that helped me get here. Last, but not least, I would like to thank all my friends and colleagues Antonio, Sebastián, Eleonora, María-José, Sandra and many more, for so many coffees that kept me awake all this time, and for cheering me up when I was upset with my loop diagrams.

This work has been supported in part by the Spanish Government and ERDF funds from the EU Commission [Grants FPA2011-23778, FPA2014-53631-C2-1-P and CSD2007-00042 (Consolider Project CPAN)] and by the Spanish Ministry MINECO through the FPI grant BES-2012-054676.

